



The  
University  
Of  
Sheffield.

**The University of Sheffield**

Faculty of Engineering

Department of Materials Science and Engineering

---

---

**Development of  
emulsion templated matrices and  
their use in tissue engineering applications**

---

---

**Betül ALDEMİR DİKİCİ**

*A thesis submitted in fulfilment of the requirements for the degree of*

*Doctor of Philosophy*

Submitted: June 2020



# Abstract

---

Tissue Engineering (TE) aims to devise solutions for the healing of critical defects which cannot heal naturally, within the host tissue. In a typical TE approach, biodegradable scaffolds are used to fill the defect site to provide temporary mechanical support and to serve as a three-dimensional substrate for cell attachment and proliferation. These TE scaffolds need to have a highly interconnected porous architecture to enable cell infiltration, nutrient flow, and integration of the material within the host tissue. To date, various scaffold fabrication routes have been reported. However, recently, emulsion templating has gained particular attention as a scaffold fabrication technique due to its ability to introduce (i) up to 99% porosity, (ii) high interconnectivity, and high tunability. The technique is briefly based on the preparation of emulsion composed of at least two immiscible liquids where one phase is dispersed in the other phase and solidification of the continuous phase of the emulsion and removal of the internal phase. Fabrication of emulsion templated matrices made of a wide range of synthetic and natural polymers have been reported. However, polycaprolactone (PCL)-based emulsion templated substrates have previously been shown to be challenging to formulate due to the high viscosity of the polymer, which limits the efficient mixing of the two phases within the emulsion.

In this study, tetramethacrylate functionalised PCL (4PCLMA) was synthesised, and photocurable PCL-based Polymerised High Internal Phase Emulsions (PolyHIPes) were developed. The effect of diluting solvent volume and composition on the stability of HIPes and morphology of PolyHIPes was studied in depth. Following the

development of the formulation of PCL PolyHIPEs using a solvent blend of chloroform and toluene and their initial cytotoxicity test were conducted. Then, the suitability of PCL PolyHIPEs to be used as a dental membrane (BM) was tested. Bilayer BM was developed by combining electrospinning and emulsion templating techniques. Impact of air plasma treatment of PolyHIPEs on cell viability and cell penetration was investigated. Results showed that PCL electrospun layer was capable of limiting cell infiltration at least for four weeks while the morphology of the PCL PolyHIPEs allows infiltration of bone cells through the pores. Especially, cell infiltration was significantly higher in air plasma treated PolyHIPEs. *Ex ovo* chick chorioallantoic membrane (CAM) assay showed that the pore structure of PolyHIPEs allows blood vessel growth through the pores.

PCL PolyHIPE-based multiscale porous scaffolds were also fabricated by combining emulsion templating with additive manufacturing. In this study, PCL-based emulsions were prepared and transferred into the syringe of the pneumatic extrusion printer, and scaffolds were printed and cured simultaneously by the integrated LED of the printer. This multi-step fabrication route is a promising way to develop scaffolds with more complex shapes using three-dimensional data of the defect site. To increase the biological performance of the polymeric multiscale porous scaffolds, they were decorated with *in vitro* generated bone extracellular matrix (ECM). Briefly, bone cells were grown on PCL PolyHIPEs, and a decellularisation procedure was applied to remove the genetic material and create a biohybrid scaffold. The presence of bone ECM, which is mainly composed of collagen and mineral, was shown to improve the osteogenic performance of PolyHIPE scaffolds *in vitro* and enhance the angiogenic performance *in vivo*. In addition, a higher degree of cell infiltration and a higher

number of blood vessels within the macropores was observed in biohybrid scaffolds compared to PolyHIPEs.

To summarise, 4PCLMA was used as a novel biomaterial with an emulsion templating as a scaffold fabrication technique, to produce highly tunable scaffolds, demonstrating that emulsion templated 4PCLMA is a promising candidate to be used for tissue engineering applications.



*This thesis is dedicated*

- *to joys of the moments of exploring the little secrets of*

*the perfect engineering of mother nature,*

- *and to you! This is the fruit of four years of my life for you to exploit.*



# Acknowledgements

---

*“The road is beautiful, not to arrive.”*

I would like to thank people and organisations, all of whom have an impact on my PhD journey. This lovely journey would not be the same without your fantastic touches.

First of all, I gratefully acknowledge the Turkish Ministry of National Education for my PhD fellowship; this research would not be possible without their financial support.

I would like to express my sincere thanks to my first supervisor, Dr Frederik Claeysens, for always being such a supportive supervisor and providing freedom in my research. There is no day that I did not amaze to your patience. I learnt from you that there is always an alternative way of doing things. I am grateful to my second supervisor, Prof Gwendolen Reilly, for your insightful thoughts and comments. Without our meetings in which you two were like a good cop and bad cop and suggesting opposing approaches to almost each and every research problem, this journey would not have been achievable.

I would like to thank Prof Neil Cameron and Prof Michael S Silverstein for their great contributions to the field of emulsion templating that guide me to better understand this lovely technique to a great extent.

I also would like to thank Dr Marco Domingos and Dr Ilida Ortega Asencio for accepting to join my journey as my PhD Viva examiners. Thanks to my first year and second year Viva assessors; Prof Sheila MacNeil, Prof Ihtesham U Rehman, Dr Nicola Green, and Dr

Michael Z Trikić for the fruitful discussions that helped me to look from different perspectives. Dr Chris Holland for letting me use mechanical testing machine and rheometer in his laboratory, Dr Andreas Koepfel for training me for mechanical test device, Dr Anthony Bullock for training me for various cell culture applications and isolating human dermal fibroblasts used in this thesis, Dr Colin Sherborne for his kind helps on PolyHIPEs and for being always there for interesting discussions, Dr Jonathan Field for his help on the synthesis of polycaprolactone and training me on stereolithography set-up, Dr Robert Owen and Dr Liam Boyle, for their help on the culture of MLO-A5s and hES-MPs, Dr Gabriella Kakonyi for providing technical support on contact angle measurements, Dr Le Ma for her help on scanning electron microscopy, Dr Sandra van Meurs for her help on Nuclear magnetic resonance spectroscopy, Robert Hanson for his help on gel permeation chromatography. I would like to thank MSc and MEng students that I have mentored, for helping me to improve my teaching skills.

I also thank all members of the big Kroto family and especially the researchers that I have shared this journey, and I have enjoyed their company; Dr Mehri Behbehani, Iris Cristina Becerril Rodrigue, Dr Jose R Aguilar Cosme, Dr Hossein Bahmaee, Colin Sherborne, Dr Kat Murray, Dr Jonathan Field, Dr Caroline Taylor, Sarina Chand, Dr Samand Pashneh-Tala, Dr Sabiniano Román, Dr Robert Owen, Dr Liam Boyle, Dr Thomas Paterson, Dr George Bullock, Dr Marcela Garcia, Dr Naşide Mangır, Dr Raj K Kampa, Alejandra A Penuelas, Fer Velazquez de la Paz (Maria), Ana Maria Sandoval, David H Ramos Rodriguez, Sarah Shafaat, Tuğba Cebe, and Enes Durgut.

My lovely friend, Alev Sönmez, thanks for your friendship over 15 years and your heart-melting, lovely postcards. Thanks to Merve Şaşmaz, Zaliqe Keskin, Afra Demirci,

Çağrı Çavdarođlu, Suat Sabuncuođlu, and to many other beloved friends from Turkey, the UK, and the USA for being a part of this journey by their support and lovely energies.

I would like to thank Battelle Memorial Institute for awarding me Dr Jeff Wadsworth-Battelle Fellowship to undertake a period of my research study at Massachusetts Institute of Technology (MIT). I would like to thank Prof Elazer Edelman and Prof Mercedes Balcells-Camps for hosting me as a visiting PhD student in their laboratories at MIT. Thanks to all the colleagues in these labs and especially Dr Shirin Issa Bhaloo for helping me to adapt to a new lab. I am grateful to Prof Sarah Langridge, Neil Lowrie, Lisa Cocking, and Stephen Birch for their support and help on this visit.

I would like to thank Dr Levent Efe, the medical and anatomical artist, for inspiring me with his amazing artwork and for sharing his valuable experiences on medical illustration with his pupils.

My dearie family, Nurten Aldemir, Metin Aldemir, and Ozan Aldemir; benim can ailem, öncelikle bana açık fikirli, aydınlık bir ailede büyüme fırsatı verdiğiniz için teşekkür ediyorum. Şartlar ne olursa olsun, en büyük destekçim olduğunuz için size minnettarım. İyi ki varsınız. My parent in-laws, Gülgün Topçu and Selahittin Dikici, bu yolculuktaki sonsuz desteğiniz için teşekkür ederim.

I owe my deepest gratitude to my dearest life-partner, colleague, best friend, Serkan Dikici; I cannot find words that can express my appreciation to you. Thanks for being you and being there with all your unconditional love, endless support, and patience throughout the entire journey.

... And finally, Dear Life, thanks for being kind to me!



# Academic Outputs

## Honours & Awards

---

- (2020)** Doctoral Researcher Awards 2020 (DRA 2020), Category: Engineering Sciences, 1<sup>st</sup> Place
- (2020)** Medical Illustration Competition of Inonu University, 1<sup>st</sup> Place
- (2019)** BITEG 21<sup>th</sup> Annual White Rose Work in Progress Meeting, Best Poster Presentation
- (2019)** Nature Reviews Cover Image Competition, Nature Reviews Rheumatology, Winner
- (2019)** Engineering Researcher Symposium, Poster of the year, Winner
- (2019)** University of Sheffield, 2019 Image Competition, Category: Biomaterials, Winner
- (2019)** University of Sheffield, Faculty of Engineering Photography Competition, Category: The Future of Engineering, Winner
- (2019)** Battelle - Jeff Wadsworth Visiting Research Fellowship
- (2019)** Armourers & Brasiers Travel Grant (October)
- (2019)** Armourers & Brasiers Travel Grant (April)
- (2019)** Learned Society Travel Grant, University of Sheffield
- (2018)** BITEG 20<sup>th</sup> Annual White Rose Work in Progress Meeting, Best Oral Presentation
- (2018)** Early Career Colloid Meeting 2018, Poster Prize Winner

## Publications

---

### From PhD Thesis

**Aldemir Dikici, B.;** Reilly, G.C.; Claeysens, F., (2020), “Boosting the osteogenic and angiogenic performance of multiscale porous polycaprolactone scaffolds by *in vitro* generated extracellular matrix decoration”, ACS Appl. Mater. Interfaces., 12 (11), 12510-12524. <https://doi.org/10.1021/acsami.9b23100>.

**Aldemir Dikici, B.\*;** Dikici, S.\*; Reilly, G.C.; MacNeil, S.; Claeysens, F., (2019), “A novel bilayer polycaprolactone membrane for guided bone regeneration: combining electrospinning and emulsion templating”, Materials (Basel), 12, 2643. <https://doi.org/10.3390/ma12162643>.

**Aldemir Dikici, B.;** Sherborne, C.; Reilly, G.C.; Claeysens, F., (2019), “Emulsion templated scaffolds manufactured from photocurable polycaprolactone”, Polymer (Guildf), 175, 243–254. <https://doi.org/10.1016/j.polymer.2019.05.023>.

**Aldemir Dikici, B.;** Claeysens, F., (2020) “Basic principles of emulsion templating and its use as an emerging manufacturing method of tissue engineering scaffolds”, Front. Bioeng. Biotechnol., 8. <https://doi.org/10.3389/fbioe.2020.00875>

### From Side Projects

Dikici, S.\*; **Aldemir Dikici, B.\*;** Issa Bhaloo, S.; Balcells, M.; Edelman, E.; MacNeil, S., Reilly, G.C.; Sherborne, C.; Claeysens, F., (2020), “Assessment of the angiogenic potential of 2-deoxy-D-ribose using a novel *in vitro* 3D dynamic model in comparison with established *in vitro* assays”, Front. Bioeng. Biotechnol., 7 (451), 1–20. <https://doi.org/10.3389/fbioe.2019.00451>.

Mangir, N.; **Aldemir Dikici, B.;** Chapple, C.R.; MacNeil, S., (2019), “Landmarks in vaginal mesh development: polypropylene mesh for treatment of SUI and POP”, Nat. Rev. Urol. 2019, 16 (11), 675–689. <https://doi.org/10.1038/s41585-019-0230-2>.

(\*co-first authors)

## Oral Presentations

---

**Aldemir Dikici, B.;** Reilly, G.C.; Claeysens, F., (2019), “Can the biological performance of 3D printed synthetic polymeric scaffolds be boosted by *in vitro* generated extracellular matrix decoration?”, BioMedEng2019, London, UK.

**Aldemir Dikici, B.;** Reilly, G.C.; Claeysens, F., (2019), “Boosting biological performance of multiscale porous scaffolds by *in vitro* generated extracellular matrix decoration”, TERMIS European Chapter Meeting, Rhodes, Greece.

**Aldemir Dikici, B.;** (2019), “You want your missing tooth back? Start by winning the competition against your gum tissue!”, Engineering Researcher Symposium (ERS) , Sheffield, UK.

**Aldemir Dikici, B.;** Reilly, G.C.; Claeysens, F., (2018), “Enhancing biological performance of multiscale porous scaffolds by *in vitro* generated extracellular matrix decoration”, BITEG 20th Annual White Rose Work In Progress Meeting, Sheffield, UK, (Best oral presentation).

**Aldemir Dikici, B.;** Dikici, S.\*; Reilly, G.C.; MacNeil, S.; Claeysens, F., (2018), “Scientific&medical illustration: worth a thousand words”, International Eurasian Conference on Science, Engineering and Technology, Ankara, Turkey.

**Aldemir Dikici, B.;** Reilly, G.C.; Claeysens, F., (2018), “Improving biological performance of 3DP multiscale porous polymer scaffolds by *in vitro* generated extracellular matrix”, International Eurasian Conference on Science, Engineering and Technology, Ankara, Turkey.

## Poster Presentations

---

**Aldemir Dikici, B.;** Reilly, G.C.; Claeysens, F., (2019), “Boosting the osteogenic and angiogenic performance of 3D printed synthetic scaffolds by *in vitro* generated extracellular matrix decoration”, BITEG 21th Annual White Rose Work In Progress Meeting, Sheffield, UK.

**Aldemir Dikici, B.;** Dikici, S.\*; Reilly, G.C.; MacNeil, S.; Claeysens, F., (2019), “A novel bifunctional membrane for guided bone regeneration: combining electrospinning and emulsion templating”, BITEG 21th Annual White Rose Work In Progress Meeting, Sheffield, UK (Best poster presentation).

**Aldemir Dikici, B.;** Reilly, G.C.; Claeysens, F., (2019), “Development of emulsion templated scaffolds manufactured from photocurable polycaprolactone”, TERMIS European Chapter Meeting, Rhodes, Greece.

**Aldemir Dikici, B.;** Dikici, S.\*; Reilly, G.C.; MacNeil, S.; Claeysens, F., (2019), “Bifunctional guided bone regeneration membrane: combining electrospinning and emulsion templating”, BioMedEng2019, London, UK.

**Aldemir Dikici, B.;** (2019), “Additive manufactured multiscale porous scaffolds with enhanced biological performance for tailor-made bone repair”, Engineering Researcher Symposium (ERS), Sheffield, UK (Poster of the year).

**Aldemir Dikici, B.;** Claeysens, F., (2018), “Effect of porogenic solvents on morphology of emulsion templated scaffolds made of polycaprolactone, Early Career Colloid Meeting, Sheffield, UK (Poster Prize Winner).

**Aldemir Dikici, B.;** Reilly, G.C.; Claeysens, F., (2018), “Photocurable emulsion templated scaffolds made of solely polycaprolactone methacrylate”, BITEG 20th Annual White Rose Work In Progress Meeting, Sheffield, UK.

**Aldemir Dikici, B.;** Reilly, G.C.; Claeysens, F., (2018), “Effect of *in vitro* Generated Extracellular Matrix on Osteogenic Potential of Additive Manufactured Multiscale Porous Hybrid Scaffolds”, 2018 TERMIS World Congress, Kyoto, Japan.

## **Collaborative Visit**

---

**Visiting PhD Student,** Massachusetts Institute of Technology, Harvard-MIT Biomedical Engineering Center, Massachusetts, United States of America, February 2019-July 2019.



# Table of Contents

---

<b>Abstract</b> .....	<b>iii</b>
<b>Dedication</b> .....	<b>vi</b>
<b>Acknowledgements</b> .....	<b>ix</b>
<b>Academic Outputs</b> .....	<b>xiii</b>
Honours & Awards .....	xiii
Publications .....	xiv
Oral Presentations .....	xv
Poster Presentations.....	xvi
Collaborative Visit.....	xvii
<b>Table of Contents</b> .....	<b>xix</b>
<b>List of Abbreviations</b> .....	<b>xxiii</b>
<b>List of Figures</b> .....	<b>xxvii</b>
<b>List of Tables</b> .....	<b>xxxvii</b>
<b>CHAPTER 1</b> .....	<b>39</b>
<b>Introduction</b> .....	<b>39</b>
1.1. Thesis outline .....	39
1.2. Literature review: emulsion templating as an emerging manufacturing method of tissue engineering scaffolds.....	42
1.2.1. Introduction.....	43
1.2.2. Mechanism of emulsion templating and the terminology .....	48
1.2.3. Characteristics of emulsion templated scaffolds.....	50
1.2.4. Development of the emulsion templated scaffolds .....	55

1.2.5. PolyHIPEs in TE applications.....	95
1.2.6. Where are we currently? .....	106
1.2.7. Conclusion and prospective outlook .....	109
1.3. Research Aim and Objective.....	111
<b>CHAPTER 2.....</b>	<b>115</b>
<b>Emulsion templated scaffolds manufactured from photocurable polycaprolactone.....</b>	<b>115</b>
2.1. Introduction.....	116
2.2. Experimental.....	120
2.2.1. Materials.....	120
2.2.2. Synthesis of 4PCLMA .....	121
2.2.3. Preparation and characterisation of 4PCLMA PolyHIPEs .....	123
2.2.4. Statistical analysis.....	132
2.3. Results and Discussion.....	132
2.3.1. Synthesis and characterisation of the photocurable 4PCLMA .....	132
2.3.2. Diluent solvent type and amount affect the 4PCLMA PolyHIPE morphology	134
2.3.3. Morphology of 4PCLMA PolyHIPE affects the mechanical properties .....	146
2.3.4. 4PCLMA PolyHIPEs can support the attachment, growth, and infiltration of HDFs .....	148
2.4. Conclusions.....	151
2.5. Supporting information .....	151
<b>CHAPTER 3.....</b>	<b>155</b>
<b>A novel bilayer polycaprolactone membrane for guided bone regeneration: combining electrospinning and emulsion templating.....</b>	<b>155</b>
3.1. Introduction.....	156
3.2. Experimental.....	160
3.2.1. Materials.....	160

3.2.2. Manufacturing of the PCL PolyHIPE, PCL electrospun, and bilayer membrane .....	161
3.2.3. Morphological, mechanical and surface characterisation.....	166
3.2.4. Biological assessment.....	167
3.2.5. Statistical analysis.....	172
3.3. Results and Discussion .....	173
3.3.1. Manufacturing and characterisation of the PCL PolyHIPE layer.....	173
3.3.2. Assessment of the metabolic activity of MLO-A5s on PCL PolyHIPE and the cellular infiltration through PCL PolyHIPE layer .....	175
3.3.3. Assessment of the extracellular matrix (ECM) deposition of MLO-A5s on PCL PolyHIPE layer .....	178
3.3.4. Assessment of the performance of PCL PolyHIPE for supporting blood vessel ingrowth using ex-ovo CAM assay.....	180
3.3.5. Assessment of solvent compositions in terms of their ability to form the nanofibrous structure.....	182
3.3.6. Manufacturing and characterisation of the PCL bilayer barrier membrane	185
3.3.7. Assessment of the metabolic activity of HDFs on PCL electrospun layer and the ability of the PCL electrospun layer to act as a cell barrier.....	189
3.4. Conclusions .....	191
<b>CHAPTER 4 .....</b>	<b>193</b>
<b>Boosting the osteogenic and angiogenic performance of multiscale porous polycaprolactone scaffolds by <i>in vitro</i> generated extracellular matrix decoration .....</b>	<b>193</b>
4.1. Introduction.....	194
4.2. Experimental .....	198
4.2.1. Materials.....	198
4.2.2. Manufacturing and characterisation of the multiscale porous PCL scaffolds	199
4.2.3. Manufacturing of the biohybrid scaffolds via <i>in vitro</i> generated ECM matrix deposition on multiscale porous PCL scaffolds.....	204
4.2.4. Cellularisation of the biohybrid scaffolds with mesenchymal progenitors	206
4.2.5. Biological characterisation of PCL-only and biohybrid scaffolds .....	207

4.2.6. Statistical analysis.....	212
4.3. Results and Discussion.....	212
4.3.1. Synthesis and characterisation of the photocurable PCL.....	212
4.3.2. Fabrication of multiscale porous PCL scaffolds by a combination of emulsion templating and 3D printing.....	214
4.3.3. Generation of the biohybrid scaffolds and evaluation of their biological activity.....	219
4.4. Conclusions.....	229
<b>CHAPTER 5.....</b>	<b>231</b>
<b>Overall conclusion and future work.....</b>	<b>231</b>
<b>CHAPTER 6.....</b>	<b>235</b>
<b>pArt of science.....</b>	<b>235</b>
6.1. Introduction.....	235
6.2. Medical and Scientific Illustration .....	235
6.3. False Coloured SEM Images.....	238
6.4. Conclusion.....	242
<b>REFERENCES.....</b>	<b>243</b>

# List of Abbreviations

---

<b>2D</b>	2 dimensional
<b>3D</b>	3 dimensional
<b>4PCL</b>	4-arm hydroxyl-terminated polycaprolactone
<b>4PCLMA</b>	4-arm polycaprolactone methacrylate
<b>AA2P</b>	Ascorbic acid 2-phosphate
<b>AIBN</b>	Azobisisobutyronitrile
<b>ALP</b>	Alkaline phosphatase
<b>AM</b>	Additive manufacturing
<b>ANOVA</b>	Analysis of variance
<b>APS</b>	Ammonium persulfate
<b>AR</b>	Alizarin red
<b>ARS</b>	Alizarin red solution
<b>BAPO</b>	Phenyl bis(2,4,6 - trimethyl benzoyl) - phosphine oxide
<b>BM</b>	Barrier membrane
<b>BMP-2</b>	Bone morphogenetic protein 2
<b>BPO</b>	Benzoyl peroxide
<b>BSA</b>	Bovine serum albumin
<b>CAM</b>	Chick chorioallantoic membrane
<b>CSTR</b>	Controlled stirred-tank reactor
<b>CTAB</b>	Cetyltrimethylammonium bromide
<b>DAPI</b>	4',6-diamidino-2-phenylindole
<b>DBM</b>	Demineralised bone matrix
<b>DCE</b>	Dichloroethane
<b>DCM</b>	Dichloromethane
<b>dH<sub>2</sub>O</b>	Deionised water
<b>DMEM</b>	Dulbecco's Modified Eagle Media
<b>DMF</b>	Dimethylformamide
<b>DNA</b>	Deoxyribonucleic acid
<b>DPEHA</b>	Dipentaerythritol penta/hexa-acrylate
<b>DVB</b>	Divinylbenzene

<b>ECM</b>	Extracellular matrix
<b>EDD</b>	Embryonic development day
<b>EDX</b>	Energy Dispersive X-Ray Analysis
<b>EHA</b>	2-Ethylhexyl acrylate
<b>ENR</b>	Enrofloxacin
<b>FA</b>	Formaldehyde
<b>FCS</b>	Fetal calf serum
<b>FDA</b>	Food and Drug Administration
<b>FITC</b>	Fluorescein isothiocyanate
<b>FRP</b>	Free radical polymerisation
<b>FT</b>	Freezing and thawing
<b>GBR</b>	Guided bone regeneration membranes
<b>GPC</b>	Gel permeation chromatography
<b>GTR</b>	Guided tissue regeneration
<b>H&amp;E</b>	Haematoxylin & Eosin
<b>HA</b>	Hydroxyapatite
<b>HCl</b>	Hydrochloric acid
<b>HDDA</b>	1,6-hexanediol diacrylate
<b>HDF</b>	Human dermal fibroblast
<b>hES-MPs</b>	Human mesenchymal progenitor cells
<b>hFGF</b>	Human fibroblastic growth factor
<b>HIPE</b>	High internal phase emulsion
<b>HLB</b>	Hydrophile-lipophile balance
<b>HMDS</b>	Hexamethyldisilazane
<b>hMSCs</b>	Human mesenchymal stem cells
<b>hNPCs</b>	Human neural progenitor cells
<b>hPSC-NPCs</b>	Embryonic stem cell-derived neural precursor cells
<b>IBOA</b>	Isobornyl acrylate
<b>IMS</b>	Industrial methylated spirit
<b>iPSC</b>	Induced pluripotent stem cell
<b>KPS</b>	Potassium persulfate
<b>MAAn</b>	Methacrylic anhydride
<b>MDD</b>	Medical Device Directive
<b>MDR</b>	Medical Device Regulations
<b>MLO-A5</b>	Murine long bone osteocytes
<b>MMA</b>	Methyl methacrylate

<b>MTT</b>	3-[4, 5-dimethylthiazol-2-yl]-2, 5 diphenyl tetrazolium bromide
<b>NASA</b>	National Aeronautics and Space Administration
<b>NMR</b>	Nuclear magnetic resonance
<b>NRES</b>	National Research Ethics Service
<b>OB</b>	Osteoblast
<b>OCT-TFM</b>	Optimum cutting temperature tissue freezing medium
<b>OM</b>	Osteogenic media
<b>PBS</b>	Phosphate buffer saline
<b>PCL</b>	Polycaprolactone
<b>PCL-DI</b>	PCL-diisocyanate
<b>PCL-TI</b>	PCL-triisocyanate
<b>PCR</b>	Polymerase chain reaction
<b>PDMS</b>	Polydimethylsiloxane
<b>PEG</b>	Poly(ethylene glycol)
<b>PEGDA</b>	PEG diacrylate
<b>PFDA</b>	Propylene fumarate diacrylate
<b>PFDMA</b>	Polypropylene fumarate dimethacrylate
<b>PFPA</b>	Pentafluorophenyl acrylate
<b>PG</b>	PicoGreen
<b>PGPR</b>	Polyglycerol polyricinoleate
<b>PHBV</b>	Poly(3-hydroxybutyrate-co-3-hydroxyvalerate)
<b>PI</b>	Photoinitiator
<b>PLA</b>	Poly(lactic acid)
<b>PLGA</b>	Poly(lactic-co-glycolic acid)
<b>PNIPAM</b>	Poly(N-isopropylacrylamide)
<b>PolyHIPE</b>	Polymerised internal phase emulsion
<b>PolyLIPE</b>	Polymerised low internal phase emulsion
<b>PolyMIPE</b>	Polymerised medium internal phase emulsions
<b>PPF</b>	Polypropylene fumarate
<b>PS</b>	Penicillin/streptomycin
<b>PTFE</b>	Polytetrafluoroethylene
<b>PVA</b>	Polyvinyl alcohol
<b>RDH</b>	Rhomboidal dodecahedron
<b>RGD</b>	Arginine-glycine-aspartate
<b>ROP</b>	Ring-opening polymerisation
<b>RR</b>	Resazurin reduction

<b>RT</b>	Room temperature
<b>SEM</b>	Scanning electron microscopy
<b>SM</b>	Supplemented media
<b>SR</b>	Sirius red
<b>SRS</b>	Sirius red solution
<b>STL</b>	Standard tessellation language
<b>TA</b>	Triton and ammonia
<b>TCP</b>	Tissue culture plates
<b>TE</b>	Tissue engineering
<b>TEM</b>	Transmission electron microscopy
<b>THF</b>	Tetrahydrofuran
<b>TMA</b>	Trimethylaniline
<b>TMPTA</b>	Trimethylolpropane triacrylate
<b>TRITC</b>	Tetramethylrhodamine
<b>UTS</b>	Ultimate tensile strength
<b>UV</b>	Ultraviolet
<b><math>\alpha</math>-MEM</b>	Minimum Essential Alpha Medium
<b><math>\beta</math>GP</b>	Beta-glycerolphosphate

# List of Figures

---

**Figure 1.1:** Significance of the interconnectivity on scaffold design. (A) Scaffolds are 3D substrates that are implanted to the defect site to guide tissue regeneration. (B) Low interconnectivity limits cell infiltration due to blind (labelled with \*) and inaccessible (labelled with #) pores, while higher interconnectivity provides enhanced permeability and cell penetration. (C) Scanning electron microscope image of the emulsion templated scaffold (polycaprolactone PolyHIPE) that shows tissue infiltration through the interconnected pores of the scaffold (cross-section).  
.....44

**Figure 1.2:** Fabrication steps of the Polymerised High Internal Phase Emulsion (PolyHIPE). (A, B) The gradual addition of the internal phase into the continuous phase while the system is mixed, (C) polymerisation of the high internal phase emulsion (HIPE), D. 2D projection of PolyHIPE, (E-G) the formation of the pores and windows, and H. scanning electron microscope image of the PolyHIPE.....45

**Figure 1.3:** Historical landmarks in emulsion templating in terms of material development and its use in tissue engineering applications (a. [20], b. [27], c. [28,29], d. [30], e. [31,32], f. [1], g. [33], h. [34], i. [35], j. [36], k. [37], l. [38], m. [39,40], n. [41], o. [42], p. [13]).  
.....46

**Figure 1.4:** (A) The number of publications on emulsion templating in tissue engineering (TE) and other areas. Data generated using “tissue engineering” and “emulsion templating” for the navy portion, “emulsion templating” for the whole. (B) The number of publications between 1900-2019 (Data obtained on 22 Nov 2019) for various scaffold fabrication methods. Data generated using –the name of the manufacturing route- and “tissue engineering” as a search term. (C) The number of papers published on emulsion templating in TE in the given years. Data generated using “emulsion templating” and “tissue engineering” as a search term. Web of science was used as a search platform, and keywords were searched in all the fields.  
.....47

**Figure 1.5:** (A) Closest packing density of the solid spheres (non-deformed) (74.048%) where each sphere touches twelve other spheres. (B) The transition from sphere to rhomboidal dodecahedron (RDH) by the gradual flattening of the touching points. (C) The geometry of the basic RDH. (Improved images were recreated using Ref [27] as a guide). ..... 49

**Figure 1.6:** Derivation of the statistical correction factor that is applied for adjusting the underestimation of the exact diameter of the pore size.  $R$ , an actual radius of the pore and  $r$ , the radius of the circular section at a distance of  $h$  from the centre of the pore. .... 53

**Figure 1.7:** (Top) Steps of manufacturing of the emulsion templated substrates, (Bottom) commonly seen relations of the characteristics of HIPEs and PolyHIPEs and some of the process conditions. (Orange arrows indicate one-way reciprocal proportionality, brown arrows indicate one-way direct proportionality. For example, an increase in the porosity of PolyHIPEs (or internal phase volume of HIPEs –characteristic of HIPEs and PolyHIPEs corresponds to each other) reduces the density of PolyHIPEs and increases the emulsion viscosity). References for the relations; (a-i) [91–93], (a-g) [70,85,86], (a-e) [72], (a-c) [64,72], (a-b) [65,70], (a-f) [45], (b-g) [42,66,70], (c-i) [94], (c-g) [42,87–89], (c-f) [45], (d-b) [50], (d-n) [45], (e-g) [72], (h-c) [42], (h-n) [42], (h-i) [95], (j-i) [94,96], (j-c) [38,94,97], (j-n) [96], (k-h) [42], (k-f) [45,73], (k-n) [42,69], (l-c) [38], (l-f) [98], (m-h) [42], (m-n) [69], (m-c) [69,97,99], (m-d) [69], (m-f) [100]. ..... 56

**Figure 1.8:** Emulsions can be stabilised either by surfactants or particles. (A) The positioning of the surfactant molecules in o/w or w/o emulsions and type of surfactants. (B) The positioning of the particles on the water-oil interface of either in o/w or w/o emulsions depending on the degree of wettability of the particles by these phases. .... 61

**Figure 1.9:** (A) Positioning of the crosslinker between linear polymer chains. As an example; (B) formation of polystyrene chain from styrene monomers and crosslinking of polystyrene chains using the crosslinker, divinylbenzene. .... 66

**Figure 1.10:** Setups of various fabrication routes of emulsion templated scaffolds (Aa, Ba, Ca, Da, Ea, Fa), and scanning electron microscopy images of these scaffolds (Ab, Bb, Cb, Db, Eb, Fb). (Original images were cropped, and scale bars were added to enhance the figures). Images Ab, Bb, Cb, and Fb are adapted from [186], [70], [75], and [97] respectively, under The Creative Commons License. Image Db was adapted with permission from [38], Copyright 2011 American Chemical Society. Image Eb was adapted with permission from [213], Copyright 2017 American Chemical Society. ....78

**Figure 1.11:** Commonly used synthetic polymers to prepare emulsion templated matrices.....83

**Figure 1.12:** The hierarchical structure of bone.....99

**Figure 1.13:** Hybrid PolyHIPE scaffolds with multiple layers: (A) emulsion templating combined with electrospinning for development of membrane for guided bone regeneration, (B) PolyHIPEs with two different morphologies, (C) 3D printing of drug-loaded and drug-free HIPEs selectively, and (D) emulsion templating combined with electrospinning in a tubular form for the development of in vitro angiogenesis model. Images A and D were reproduced with permission from ref [13] and [186] respectively, under The Creative Commons License. Image B was adapted with permission from [269] Copyright 2015 John Wiley and Sons. Image C was adapted with permission from, [146] Copyright 2017 American Chemical Society..... 103

**Figure 1.14:** (A) False coloured scanning electron microscopy (SEM) image of human dermal fibroblasts on PCL PolyHIPE [42] (scale bar: 250  $\mu\text{m}$ ), (B) H&E image of L929 fibroblasts on thiolene PolyHIPE [107] (scale bar: 200  $\mu\text{m}$ ), (C) confocal microscopy image of MG63 bone cells on EHA:IBOA PolyHIPE (DAPI and Phalloidin-FITC) [133] (scale bar: 500  $\mu\text{m}$ ), (D) SEM image of murine long-bone osteocytes (MLO-A5s) on PCL PolyHIPE [13] (scale bar: 100  $\mu\text{m}$ ), (E) confocal microscopy image of mouse bone mesenchymal stem cells (mBMSCs) on PCL PolyHIPE (Calcein-AM stained)[146] (scale bar: 200  $\mu\text{m}$ ), (F) confocal microscopy image of human embryonic stem cell-derived mesenchymal progenitor cells (hES-MPs) on EHA:IBOA PolyHIPE (DAPI and Phalloidin-FITC) [97] (scale bar: 200  $\mu\text{m}$ ),

(G) confocal microscopy image of hES-MPs on EHA PolyHIPE (DAPI and Phalloidin-TRITC) [70] (scale bar: 200  $\mu\text{m}$ ), (H) fluorescent microscopy image of human aortic endothelial cells (HAECs) on PCL PolyHIPE (Phalloidin-TRITC) [186] (scale bar: 200  $\mu\text{m}$ ), (I) SEM image of mix nerve cells (extracted from mice retina) on dextran PolyHIPE [108] (scale bar: 10  $\mu\text{m}$ ), (J) fluorescent microscopy image of cardiac muscle cells (H9c2s) on polyacrylamide PolyHIPE (DAPI) [276], (K) SEM image of human articular chondrocytes on polyester PolyHIPE [140] (scale bar: 5  $\mu\text{m}$ ), (L) PCL PolyHIPE on chick chorioallantoic membrane (CAM) [13] (scale bar: 10 mm), (M) H&E image of PCL PolyHIPE on CAM at day 14 (green arrow indicates the blood vessel on the CAM itself; yellow arrows indicate the blood vessels in PCL PolyHIPE [13] (scale bar: 100  $\mu\text{m}$ ), (N) in vitro bone ECM decorated 3D printed PCL PolyHIPE on CAM [75] (scale bar: 2 mm), (O) H&E image of in vitro bone ECM decorated 3D printed PCL PolyHIPE on CAM at day 14 (black arrows indicate the blood vessels) [75] (scale bar: 100  $\mu\text{m}$ ). Images were reproduced with permission from the indicated references. Images A, C, D, F, G, H, K were adapted from [42], [133], [13], [97], [70], [186], [140], respectively, L and M were adapted from [13], N and O were adapted from [75], under The Creative Commons License. The image B was adapted with permission from [107], Copyright 2015 Royal Society of Chemistry. Image E was adapted with permission from [146], Copyright 2017 American Chemical Society. The image I was adapted with permission from [108], Copyright 2005 John Wiley and Sons. Image J was adapted with permission from [276], Copyright 2015 Royal Society of Chemistry.

..... 108

**Figure 2.1:** (A) Air plasma machine used in this study, (B) PolyHIPEs during air plasma treatment, (C) parameters used for air plasma treatment. .... 128

**Figure 2.2:** A. (i) Synthesis of 4PCL from the monomers via ring-opening polymerisation, (ii) methacrylate functionalisation of the hydroxyl end groups (4PCLMA), B. Chemical structure diagram and proton NMR spectrum of 4PCL and 4PCLMA and the relative assignments. Hydrogen environments in the polymer are labelled a-j..... 133

**Figure 2.3:** SEM micrograph of A. NS, B. 4PCLMA PolyHIPE composition prepared using chloroform as a diluting solvent, C. SEM images of each 4PCLMA PolyHIPE composition prepared using toluene as a diluting solvent (scale bar: 100µm). B. The viscosity of the oil phase components without any solvent (n=4). ..... 138

**Figure 2.4:** A. SEM images of C/T:60/40, C/T:80/20 and C/T:100/0; polymerised A. Right after preparation of HIPE, B. 5 days after preparation (scale bars: 100µm). ..... 146

**Figure 2.5:** Mechanical properties of C/T:60/40, C/T:80/20 and C/T:100/0 A.Elastic modulus, B. Ultimate tensile strength, C. Percentage elongation at failure (\*: p<0.05, ns: no significant difference, n=3). ..... 147

**Figure 2.6:** A. Biological assessment of 4PCLMA PolyHIPE scaffolds. A. Resazurin reduction assay results which show the cellular metabolic activity of HDSs for 7 days on PolyHIPE scaffolds (ANOVA, multiple comparisons, ns, 0.05>p, \*,+,# , p ≤ 0.05, n=3), B. SEM images of 4-day cultured HDFs on C/T:60/40, C/T:80/20, C/T:100/0 and Alvetex®, respectively (top view). SEM images were false-coloured for clear visibility of the cells on the scaffold surface. (yellow: scaffold, turquoise: cells (Scale bars: 50µm) C. H&E stain of a section of 4PCLMA PolyHIPE groups after 7 days of cell culture (scale bar: 250µm). ..... 149

**Figure 2.7:** The processing steps of pore size calculation, from left to right: the SEM image was imported into Adobe Photoshop CS6, using the ellipse tool pores are framed in a new layer, the image is saved as a black and white 8-bit tiff file, the file is converted into a binary image, the area of each pore was calculated. .... 152

**Figure 2.8:** Average pore sizes and pore size distributions of 4PCLMA PolyHIPEs prepared by using single solvents of either chloroform or toluene. .... 152

**Figure 2.9:** Average pore sizes and pore size distributions of 4PCLMA PolyHIPEs prepared by using solvent blends of chloroform and toluene. .... 153

**Figure 2.10:** 4PCLMA PolyHIPE compositions whose oil phases were diluted with (A.0.25 mL, B. 0.40 mL, C. 0.55 mL, and D. 0.70 mL) toluene prepared without surfactant (scale bar: 500 µm). ..... 153

- Figure 2.11:** A. Viscosity changes with changing solvent ratios of chloroform and toluene in the solvent blend (n=4), B. Macro images of emulsions once prepared and 5 days after preparation (scale bar: 5mm), C. SEM image of the bottom of the cured emulsion 5 days later, which shows separation at the bottom of the bottle (scale bar: 1mm)..... 153
- Figure 2.12:** Average pore sizes and pore size distributions of HIPE compositions which were prepared by using solvent blends of chloroform and toluene (samples were cross-linked 5 days later for stability tests)..... 154
- Figure 2.13:** Original SEM images of 4-day cultured fibroblasts on C/T:60/40, C/T:80/20, C/T:100/0 and Alvetex®, respectively (scale bar: 250µm)..... 154
- Figure 3.1:** Summary of the manufacturing process of the bilayer membrane. (A) Synthesis of 4-arm hydroxyl-terminated PCL and methacrylate terminalisation reaction (B) PCL PHIPE preparation process, (C) the polymerisation of PCL HIPEs to obtain PCL PolyHIPE and slicing the samples, (D) air plasma treatment of PCL PolyHIPE, (E) electrospinning of PCL on 250 µm thick PCL PolyHIPE layer, (F) Final representation of the bilayer BM..... 164
- Figure 3.2:** SEM images of the top surfaces PCL PolyHIPEs cured in contact with; (A) air, (B) glass, and (C) PDMS sheet. (D) SEM image of the transverse section of PCL PolyHIPEs. (E) Pore size and window size distributions of the inner section. (F) Contact angle measurements of a water droplet on PCL PolyHIPE before and after air plasma treatment (n=3)..... 174
- Figure 3.3:** (A) Metabolic activity of MLO-A5s cultured on P-, P+ PCL PolyHIPEs, and TCP for 4 weeks. SEM images of the top surfaces of (B) P+ and (C) P- PCL PolyHIPEs cultured MLO-A5s on for 4 weeks (Scale bar represents 500 µm). (D) H&E and Alizarin Red, and (E) Fluorescent staining of MLO-A5s cultured on P+ and P- PCL PolyHIPEs for 1 week and 4 weeks (Scale bar represents 250 µm, blue: DAPI, red: Phalloidin TRITC)..... 177
- Figure 3.4:** (A) Assessment of calcium and collagen deposition of MLO-A5s after 7, 14, 21 and 28-day culture on PCL PolyHIPE by using Alizarin Red and Sirius Red,

respectively. (B) Scanning electron microscopy images of the surface, and (C, D, E) the cross-section of PCL PolyHIPE cultured with MLO-A5s for 28 days in supplemented media..... 179

**Figure 3.5:** Chick embryos in a petri dish on (A) embryonic development day 3 and (B) embryonic development day 7 (Scale bar represents 10 mm). (C) PCL PolyHIPE on CAM at day 14 (Scale bar represents 2 mm). (D) H&E images of PCL PolyHIPE on CAM at day 14 (Green arrow indicates the blood vessel on CAM itself; yellow arrows indicate the blood vessels in PCL PolyHIPE. Scale bar represents 100  $\mu$ m). ..... 181

**Figure 3.6:** Morphological characterisation of the electrospun PCL fibres, where polymer solutions were prepared with different solvents. SEM image of PCL electrospun prepared by dissolving PCL in (A) acetone (100), (B) acetone:chloroform (30:70), (C) DCM:methanol (90:10), (D) chloroform:DMF (70:30). The graphs show (E) the fibre diameter and (F) the pore size distributions, respectively. Yellow scale bars represent 20 $\mu$ m..... 183

**Figure 3.7:** SEM images of (A) 250  $\mu$ m sectioned PCL PolyHIPE layer, (B) 20 minutes PCL electrospun on PCL PolyHIPE, (C) 40 minutes PCL electrospun on PCL PolyHIPE, (D) Higher magnification SEM image showing the border of two layers. Macro images of the bilayer PCL BM to show the suitability of the design for (E-F) stretching in different axes, (G-H) bending, (I) space making, and (J) side view of the BM to show the integration of the two layers..... 187

**Figure 3.8:** Mechanical properties of the BM under dry and wet conditions. (A) Representative stress-strain curves, (B) Elastic modulus, (C) UTS of the BMs under dry and wet conditions (\*\* $p \leq 0.001$ , ns  $p \geq 0.05$ ,  $n = 3$ ). ..... 188

**Figure 3.9:** Evaluation of the biocompatibility and the barrier properties of the bilayer BM. The metabolic activity of the HDFs growing on PCL electrospun layer from day 1 to day 28 is given in the graph (\*\* $p \leq 0.001$ , \*\* $p \leq 0.01$ , \* $p \leq 0.05$ ,  $n = 3$ ). Histological images demonstrate the barrier properties of the PCL electrospun layer over 4 weeks. Dotted line indicates the boundary of the two layers (Scale bar represents 200  $\mu$ m). ..... 190

**Figure 4.1:** Manufacturing routes of the multiscale porous photocurable polycaprolactone (PCL) scaffolds (step1, 2) and multiscale porous biohybrid scaffolds (step 1-3). (1) Preparation of the emulsion made of photocurable PCL and water, (2) the transfer of the PCL-based high internal phase emulsion (HIPE) into the syringe, pressure-assisted 3D printing and simultaneous cross-linking, and (3) the culture of bone cells on PCL-only scaffold to be decellularised and generation of the biohybrid scaffolds..... 199

**Figure 4.2:** Isometric view of (A) the 3D design of the tetragonal prism (10x10x1.4 mm, .stl) and (B) the layer-by-layer design of the scaffold. (C) Top view of a single layer and (D) complete model of the layer-by-layer design..... 202

**Figure 4.3:** Steps of the morphometric quantification of angiogenesis; (A) macro-image as captured, (B) improved image using Photoshop, (C) drawn discernable blood vessels, (D) exported blood vessel layer from Photoshop, (E) binary and inverted image in Image J, (F) analysed image using Angiotool..... 211

**Figure 4.4:** The synthesis scheme of 4-arm photocurable polycaprolactone: (A-B) monomer and initiator were used for the synthesis of hydroxyl-terminated 4-arm polycaprolactone (4PCL). (B-C). 4PCL was methacrylated. (D) Schematic demonstration of the photocured (UV-crosslinked) network showing a building block made of 4PCLMA. (E) <sup>1</sup>H NMR spectrum of 4PCL, 4PCLMA and relative assignments. Dark grey region: peaks of the hydroxyl group, light yellow regions: peaks of the methacrylate group, which only showed up after methacrylation reaction while they are absent in 4PCL..... 213

**Figure 4.5:** (A) Viscosity of the polycaprolactone (PCL)-based high internal phase emulsion (HIPE) prepared to be used in the printing process. (B) 3D printing and simultaneous cross-linking of PCL HIPE. (C) Morphological characterisation ( $n_{\text{macropore}}=20$ ,  $n_{\text{strut}}=20$  and  $n_{\text{micropore}}=50$ ) and (D) micropore size distribution of the scaffolds in terms of the diameter frequency and the volume frequency. ... 215

**Figure 4.6:** SEM micrographs (A-D) multiscale porous PCL-only scaffolds immediately after manufacture, (E-G) after 1-week of MLO-A5 culture, (H-J) after 4-weeks of MLO-A5 culture, (K-M) after the decellularisation process (biohybrid scaffold), (N-

P) after 4-weeks of the culture of hES-MPs on the biohybrid scaffolds. First column macro view of the scaffold, the second column shows the single pore, and the third column shows the microsurface of the scaffold at different stages of the experiment. All the images were captured from the top view..... 218

**Figure 4.7:** (A) Cell seeding efficiency of MLO-A5s on multiscale porous PCL-only scaffolds (n=5). (B) Metabolic activity (n=5), (C) mineral, and (D) collagen deposition of MLO-A5s on multiscale porous PCL-only scaffolds and TCP as control over 28 days (n=3,\*: p<0.05, p>0.5; ns: not significant)..... 220

**Figure 4.8:** (A) Comparison of the various decellularisation techniques in terms of remaining DNA content (n=3), (B) Calcium and collagen content of the scaffolds cultured with MLOs for 4 weeks (blue) and scaffolds that are decellularised (purple) (n=3, p>0.05; ns: not significant), (C) EDX spectrum of the decellularised scaffold showing the peaks of carbon (C), phosphorus (P), calcium (Ca), and oxygen (O), (D, E) SEM images of the decellularised scaffolds in lower and higher magnifications, respectively (top-view). (F-I) EDX elemental mapping of Ca (red) and P (green) ..... 222

**Figure 4.9:** (A) Seeding efficiencies of human embryonic stem cell-derived mesenchymal progenitor cells (hES-MPs) on polycaprolactone (PCL) -only and biohybrid scaffolds (n=6), (B) the metabolic activity (n=6), (C) mineral (n=3), and (D) collagen deposition of hES-MPs on PCL-only, biohybrid scaffolds, and on tissue culture plate (TCP) as a control in 28 days culture (n=3) (\*: p<0.05, \*\*\*\*: p<0.001, ns: not significant)..... 224

**Figure 4.10:** Evaluation of the angiogenic potential of polycaprolactone (PCL)-only, PCL-only populated with murine long bone osteocyte cells (MLO-A5s), and biohybrid scaffolds using chick chorioallantoic membrane (CAM) assay; (A-C) Macro images were taken on embryonic development day 14, (D-F) quantification of the number of blood vessels, total vessel length and the total number of junctions. (n=4, \*: p<0.05, \*\*: p<0.01, \*\*\*: p<0.005, \*\*\*\*: p<0.001, ns: not significant), (G-O) histological evaluation of the scaffolds isolated from CAM (Black arrows indicate the blood vessels). ..... 228

- Figure 6.1:** Power of an illustration to simplify the scene. Intraoperative photograph (A) and illustration (B) of the entrapped ulnar nerve by flexor carpi ulnaris tendon. Intraoperative photograph (C) and illustration (D) of the release of nerve loop from flexor carpi ulnaris tendon. a. the ulnar nerve, b. flexor carpi ulnaris tendon, c. main trunk, d. ulnar artery, e. pisiform bone. Image reprinted from [514] with the kind permission of the Journal of Neurosurgery Publishing Group..... 236
- Figure 6.2:** The medical illustration showing the anatomical features of pelvic floor created for the study published in Nature Reviews Urology [15]..... 237
- Figure 6.3:** Graphical abstract figure drawn for the research presented in Chapter 3, published on Materials [13]..... 238
- Figure 6.4:** Semi-automated false SEM colouring. Cellulose–fibre–epoxy composite SEM sample images. (A) Image after marking with colours on monochrome SEM image and (B) after false colourisation. Black arrows show the inaccuracy in the detection of the edges. Images are adapted from [517] with the kind permission of John Wiley and Sons..... 239
- Figure 6.5:** Recreation. (Top) Original scanning electron microscopy image and (Bottom) False scanning electron microscopy image of 4 days culture of human dermal fibroblasts on polycaprolactone PolyHIPE scaffold. Winners of Department of Materials Science and Engineering 2019 Image Competition, in the category of Biomaterials, and The University of Sheffield, Faculty of Engineering Photography Competition, category of The Future of Engineering..... 240
- Figure 6.6:** Dali’s Crumpet. (Top) Original scanning electron microscopy image and (Bottom) False scanning electron image the cross-section of polycaprolactone PolyHIPE scaffold which has different morphologies inside and outside. Although this heterogeneity can be a problem to be solved for scaffold engineering, this false coloured scanning electron microscope image reminds Dali’s “Persistence of Memory” and crumpets. .... 241

# List of Tables

---

<b>Table 1.1:</b> Commonly used surfactants in HIPEs of various polymer systems.....	62
<b>Table 1.2:</b> Parameters that affect the fibre morphology of the electrospun meshes [205]. .....	76
<b>Table 1.3:</b> Advantages of disadvantages of the fabrication routes of emulsion templated scaffolds .....	79
<b>Table 1.4:</b> Various functionalisation strategies for PolyHIPE scaffolds from the literature. .....	91
<b>Table 2.1:</b> Composition details of 4PCLMA PolyHIPE groups which were prepared by using no solvent or single solvent of chloroform or toluene.....	137
<b>Table 2.2:</b> Details of compositions of 4PCL PolyHIPE prepared by using solvent blends of chloroform and toluene. ....	145
<b>Table 4.1:</b> Design and processing parameters of the scaffolds.....	203



# CHAPTER 1

---

## Introduction

### 1.1. Thesis outline

This thesis describes the development of emulsion templated matrices made of photocurable polycaprolactone (PCL) and their use in tissue engineering (TE) applications.

Chapter 1 is a literature review that approaches the emulsion templating technique as a scaffold manufacturing route. Chapter 2 explains the development process of emulsion templated matrices made of solely photocurable PCL. In Chapter 3, these matrices were fabricated in membrane form and tested to be used as a guided bone regeneration membrane. In the next chapter, PCL-based emulsions were used as printing ink, and multiscale porous scaffolds were fabricated, combining additive manufacturing with emulsion templating techniques. Additionally, these 3D printed scaffolds were decorated with bone cell-derived extracellular matrix to increase the biological performance of the PCL-based synthetic scaffolds, creating 'biohybrid' scaffolds. In Chapter 5, the overall conclusion and future work of this study are discussed. Finally, in Chapter 6, I explain and discuss the development of artistic visual materials with various techniques for better communication in science.

Chapters 1-4 of this thesis are the published/submitted articles in peer-reviewed journals. The numbering of the figures, tables, and the headings of the papers were

revised for the continuity of the thesis. Minor revisions were applied to published work for better clarification or amendment where necessary. The sections of “Acknowledgements” and “References” of all papers were combined and presented in relevant sections of the thesis.

The candidate confirms that the work submitted is her own, except where work which has formed part of jointly authored publications has been included. The contribution of the candidate and the other authors to this work has been explicitly indicated below.

### **Chapter 1:** Published Review Article

---

**Basic principles of emulsion templating and its use as an emerging manufacturing method of tissue engineering scaffolds**, Aldemir Dikici, B.; Claeysens, F., (2020), *Frontiers Bioengineering and Biotechnology*, 8. <https://doi.org/10.3389/fbioe.2020.00875>

*Author contributions:* BAD performed the review and wrote the manuscript. FC provided feedback and edited the manuscript.

### **Chapter 2:** Published Research Article

---

**Emulsion templated scaffolds manufactured from photocurable polycaprolactone**, Aldemir Dikici, B.; Sherborne, C.; Reilly, G.C.; Claeysens, F., (2019), *Polymer (Guildf)*, 175, 243–254.

<https://doi.org/10.1016/j.polymer.2019.05.023>.

*Author contributions:* BAD was the key contributor to experimental design, analysis, acquisition, and interpretation of data, statistical analysis, and drafting of this paper. CS performed the additional experiments asked by the reviewers; gel fraction analysis, density, and porosity measurements, as the main author BAD was in abroad for a collaborative project.

CS, GR, and FC contributed with their supervision, critical revision, and editing of the manuscript.

### **Chapter 3:** Published Research Article

---

**A Novel Bilayer Polycaprolactone Membrane for Guided Bone Regeneration: Combining Electrospinning and Emulsion Templating**, Aldemir Dikici, B.; Dikici, S.; Reilly, G.C.; MacNeil, S.; Claeysens, F., (2019), *Materials (Basel)*, 12, 2643.

<https://doi.org/10.3390/ma12162643>.

*Author contributions:* BAD and SD were co-first authors in this paper. While BAD was responsible for the experimental design, analysis, acquisition, and interpretation of data, statistical analysis of the experiments related with the emulsion templated layer, and chick chorioallantoic membrane assay, SD was responsible from the experiments related with the electrospun layer and mechanical testing of the membrane. SM, GR, and FC contributed with their supervision, critical revision, and editing of the manuscript. The final manuscript was improved by comments from all the co-authors.

### **Chapter 4:** Published Research Article

---

**Boosting the osteogenic and angiogenic performance of multiscale porous polycaprolactone scaffolds by *in vitro* generated extracellular matrix decoration**, Aldemir Dikici, B.; Reilly, G.C.; Claeysens, F., (2020), *ACS Appl. Mater. Interfaces.*, 12 (11), 12510-12524.

<https://doi.org/10.1021/acsami.9b23100>.

*Author contributions:* BAD was the key contributor to experimental design, analysis, acquisition, and interpretation of data, statistical analysis, and drafting of this paper. GR and FC contributed with their supervision, critical revision and editing of the manuscript.

## **1.2. Literature review: emulsion templating as an emerging manufacturing method of tissue engineering scaffolds**

### ***Abstract***

Tissue engineering (TE) aims to regenerate critical size defects, which cannot heal naturally, by using highly porous biodegradable matrices called TE scaffolds. There are various manufacturing techniques commonly used to fabricate TE scaffolds. However, in most cases, they do not provide materials with a highly interconnected pore design. Thus, emulsion templating is a promising and convenient route for the fabrication of matrices with up to 99% porosity and high interconnectivity. These matrices have been used for various applications for decades. Although this polymer structuring technique is older than TE itself, the use of polymerised internal phase emulsions (PolyHIPEs) in TE is relatively new compared to other scaffold manufacturing techniques. To date, a number of excellent reviews on emulsion templating have been published by the pioneers of this field in order to explain the chemistry behind this technique and potential areas of use of the emulsion templated structures. This particular review focusses on the key points of how emulsion templated scaffolds can be fabricated for different TE applications. Accordingly, we first explain the basics of emulsion templating and characteristics of PolyHIPE scaffolds. Then, we discuss the role of each ingredient in the emulsion and the impact of the compositional changes and process conditions on the characteristics of PolyHIPEs. Afterwards, current fabrication methods of PolyHIPE scaffolds and polymerisation routes are detailed, and the functionalisation strategies that can be used to improve the biological activity of

PolyHIPE scaffolds are discussed. Finally, the applications of PolyHIPEs on soft and hard TE as well as *in vitro* models and drug delivery in the literature are summarised.

### **1.2.1. Introduction**

Tissue and organ failure is one of the most frequent, inevitable major public health problems due to congenital health issues, traumas, diseases, and the increasing average age of the population [1,2]. Tissue Engineering (TE) aims to devise solutions to restore or to improve the functions of injured/diseased parts of the host tissue which cannot heal naturally [3,4]. TE utilizes porous matrices that are called scaffolds to fill the defect site. Scaffolds serve as a guide for tissue regeneration as a three-dimensional substrate for cell attachment, proliferation, infiltration, and they also provide temporary mechanical support [5,6] (Figure 1.1A). There are five essential requirements that an ideal scaffold should have [3,7]; (i) biocompatibility, not causing any adverse effect at any level, from cellular activity to molecular signalling, on cells/tissues when they are in contact [7,8], (ii) biodegradability, degrading over time *in vivo* to create a space for newly forming tissues, (iii) having appropriate surface chemistry to allow cellular attachment, proliferation and differentiation, (iv) having similar mechanical properties with the native tissue not to inhibit tissue formation due to excessive deformation [7,9], and (v) the morphology is a key feature that affects both biological and mechanical efficiency of the scaffolds. Scaffolds need to have a porous architecture with high interconnectivity to enable cell infiltration, nutrient flow, and integration of the material within the host tissue (Figure 1.1B).

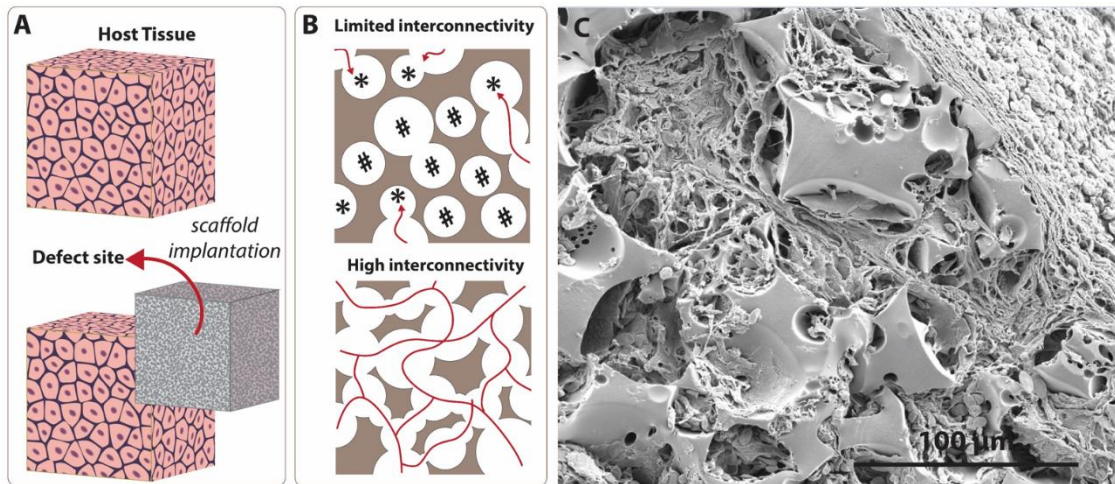


**Figure 1.1:** Significance of the interconnectivity on scaffold design. (A) Scaffolds are 3D substrates that are implanted to the defect site to guide tissue regeneration. (B) Low interconnectivity limits cell infiltration due to blind (labelled with \*) and inaccessible (labelled with #) pores, while higher interconnectivity provides enhanced permeability and cell penetration. (C) Scanning electron microscope image of the emulsion templated scaffold (polycaprolactone PolyHIPE) that shows tissue infiltration through the interconnected pores of the scaffold (cross-section).

To date, various scaffold manufacturing techniques such as gas foaming [10,11], porogen leaching [10,12], electrospinning [13–16], and additive manufacturing (AM) [17,18] have been widely used to introduce porosity into TE scaffolds. Recently, emulsion templating has gained particular attention as a scaffold fabrication technique due to its three main advantages; providing (i) high porosity (up to 99% [19]), (ii) high interconnectivity (Figure 1.1C), and (iii) high tunability. The technique is briefly based on two basic steps; the preparation of emulsion composed of at least two immiscible liquids where one phase is dispersed in the other phase and solidification of the continuous phase of the emulsion (the phase that liquid droplets dispersed in). These biphasic emulsion systems can be either water-in-oil (w/o) or oil-in-water (o/w) depending on the positioning of the lipophilic (non-polar, fat-loving, oil) and hydrophilic (polar, water-loving, water) phases. In this process, droplets of dispersed

phase behave like templates, and they are removed following solidification to obtain porous matrices (Figure 1.2).

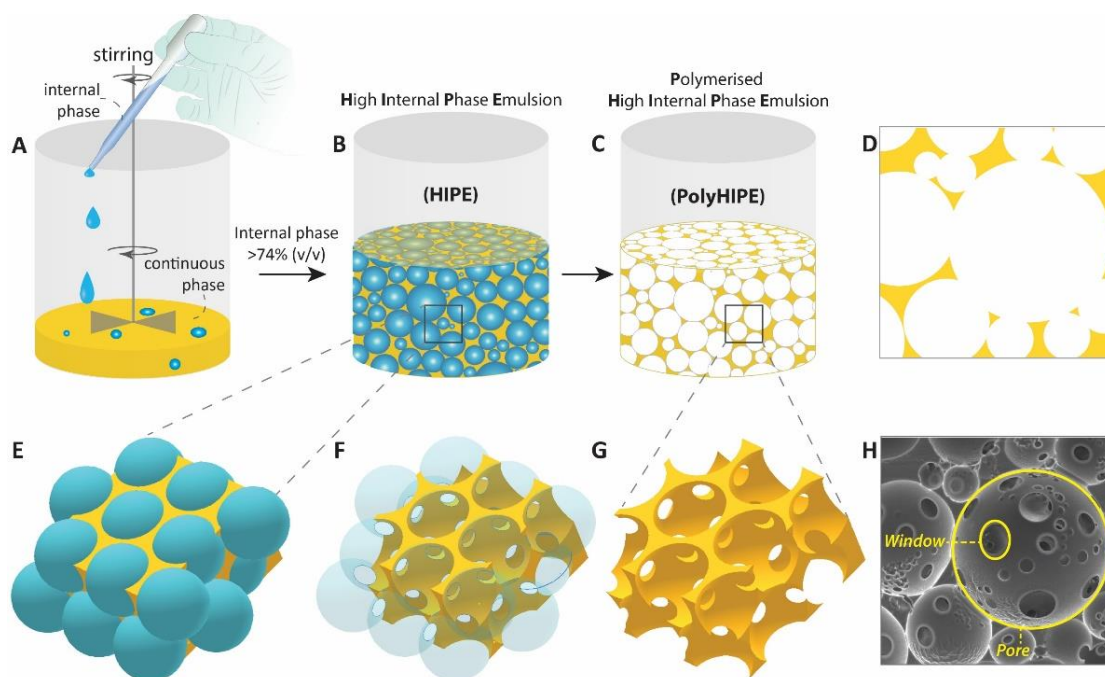


**Figure 1.2:** Fabrication steps of the Polymerised High Internal Phase Emulsion (PolyHIPE). (A, B) The gradual addition of the internal phase into the continuous phase while the system is mixed, (C) polymerisation of the high internal phase emulsion (HIPE), (D) 2D projection of PolyHIPE, (E-G) the formation of the pores and windows, and H. scanning electron microscope image of the PolyHIPE.

Although emulsion templating has been mentioned as a relatively new scaffold manufacturing route in recent publications, the birth of the term ‘emulsion templating’ in the literature is older than TE itself (Figure 1.3); it dates back to the late 1950s [20] where it was defined in a patent. Many other patents -including one by National Aeronautics and Space Administration (NASA)- followed up the development of emulsion templated polymers for different applications such as oil absorbents [21] and 3D shaped porous objects with smooth surfaces [22]. Over the years, emulsion templated matrices have been used in various other areas such as; catalyst supports

[23], separation columns [24], solid-phase synthesis [25], and substrates for electrodes [26].

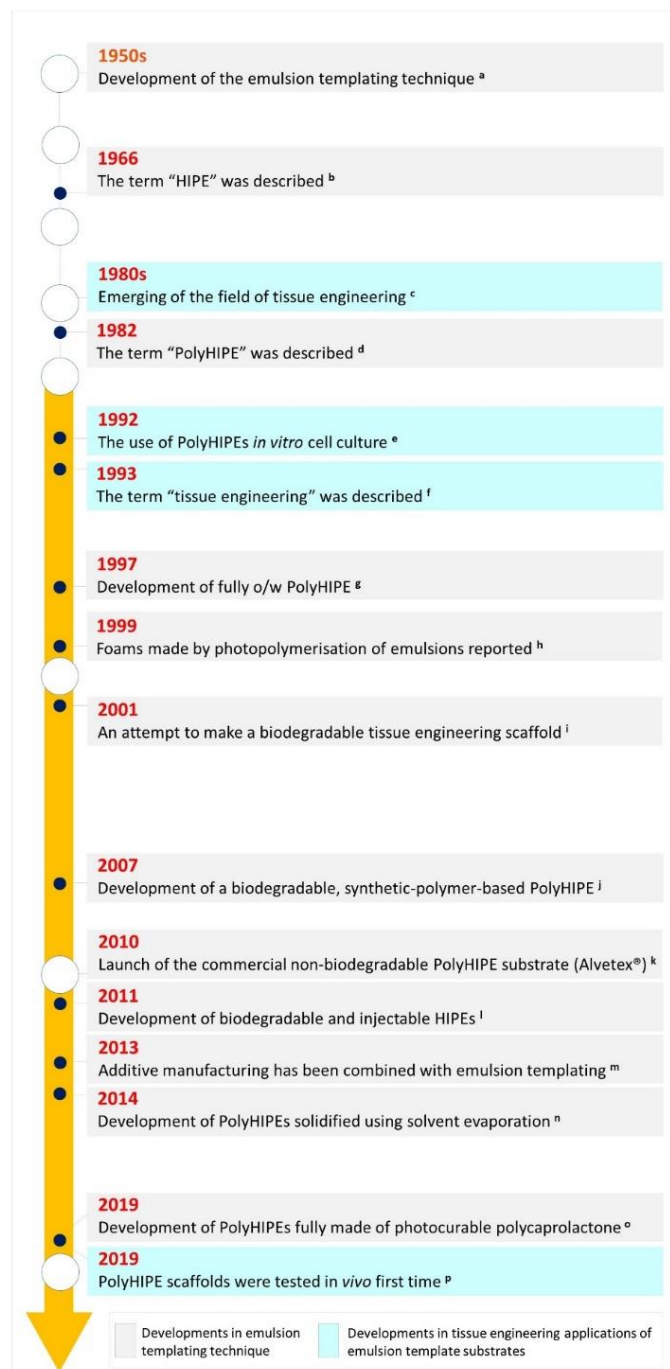


**Figure 1.3:** Historical landmarks in emulsion templating in terms of material development and its use in tissue engineering applications (a. [20], b. [27], c. [28,29], d. [30], e. [31,32], f. [1], g. [33], h. [34], i. [35], j. [36], k. [37], l. [38], m. [39,40], n. [41], o. [42], p. [13]).

Studies on the use of emulsion templating for the manufacturing of 3D substrates for cell culture applications is relatively new; it dates back to the early 1990s [31,32,43,44]. That is most likely why the number of TE-related studies is not more than 6% of the total number of all reported applications about emulsion templating (Figure 1.4A). Emulsion templating also has the lowest number of reports within TE applications when compared with other well-known scaffold manufacturing techniques (Figure 1.4B). However, there has been an increasing trend in the number of publications on emulsion templating in the last years, and almost 40% of emulsion templating in TE papers have been published in the last three years (Figure 1.4C).

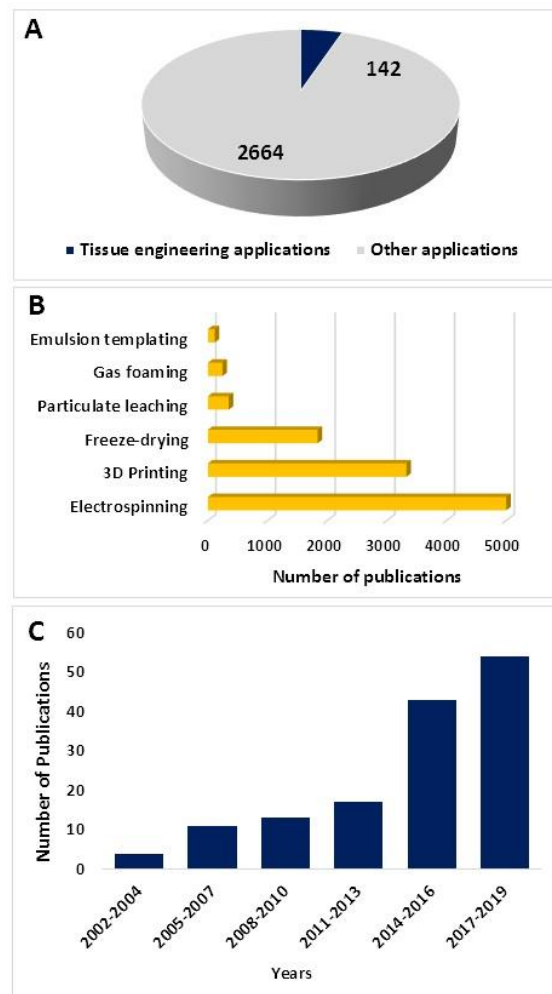


**Figure 1.4:** (A) The number of publications on emulsion templating in tissue engineering (TE) and other areas. Data generated using “tissue engineering” and “emulsion templating” for the

*navy portion, "emulsion templating" for the whole. (B) The number of publications between 1900-2019 (Data obtained on 22 Nov 2019) for various scaffold fabrication methods. Data generated using -the name of the manufacturing route- and "tissue engineering" as a search term. (C) The number of papers published on emulsion templating in TE in the given years. Data generated using "emulsion templating" and "tissue engineering" as a search term. Web of science was used as a search platform, and keywords were searched in all the fields.*

Development of the emulsion templated scaffolds requires a multidisciplinary approach that combines knowledge and experience from chemistry, materials science, and TE. To date, there has been a number of significant reviews from the pioneers of the field of emulsion templating in the literature [45–50]. These reviews comprehensively cover the chemistry and material science behind this technique and briefly summarise all of the potential usage areas of emulsion templating. Accordingly, in this review, we aimed to approach emulsions templating as solely a scaffold fabrication technique. We summarised the basics of emulsion templating by reviewing the literature and determined a road map for researchers that would like to explore this advantageous technique in their TE applications.

### **1.2.2. Mechanism of emulsion templating and the terminology**

One of the most favourable features of emulsion templated scaffolds is the tunability of their porosity by simply increasing the internal phase volume. In the literature, emulsions that have at least 74.048% internal phase volume are defined as High Internal Phase Emulsions (HIPes). The value of 74.048% is the densest possible monodispersed sphere packing density, according to Kepler Conjecture [51]. In 1966, Lissant reported that beyond 74.048%, monodispersed water droplets are deformed into polyhedrons as the touching points become flattened (Figure 1.5) [27].

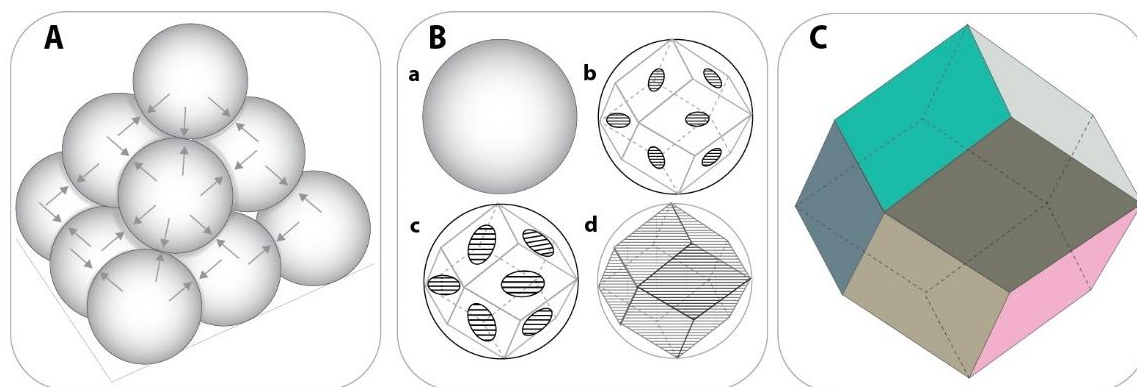


**Figure 1.5:** (A) Closest packing density of the solid spheres (non-deformed) (74.048%) where each sphere touches twelve other spheres. (B) The transition from sphere to rhomboidal dodecahedron (RDH) by the gradual flattening of the touching points. (C) The geometry of the basic RDH. (Improved images were recreated using Ref [27] as a guide).

This situation applies in monodispersed solid spheres, and already in 1907 Spencer Pickering questioned the validity of this value for liquid spheres as liquid droplets in emulsion are in reality not uniform but are polydisperse [52]. Additionally, in emulsions, liquid droplets are not actually in contact; there is a thin wall separating the droplets from each other. That's why, even the maximum packing density for mono-disperse, non-deformed liquid droplets would be less than the maximum packing density of the solid spheres (<74.048%). Indeed, the requirement for the revised definition of HIPEs has also been reflected recently by other researchers [42,53,54]. However, herein, we use the commonly recognised definition of HIPEs.

Although emulsion polymerisation has previously been described in the literature [55,56] the term “Polymerised High Internal Phase Emulsion (PolyHIPE)” appeared in the literature the first time in 1982 to define porous structures formed following solidification of the HIPEs [30]. Emulsion templated matrices with various internal phase volumes; PolyHIPEs (~74-99% [57]), Polymerised Medium Internal Phase Emulsions (PolyMIPEs) (20–65% [27]) and Polymerised Low Internal Phase

Emulsions (PolyLIPes) (<20% [27]) have been reported in the literature. However, in this review, we mainly focused on PolyHIPEs unless otherwise stated.

In terminology, it is important to comprehend the difference between HIPEs and PolyHIPEs. HIPEs can be further processed until the gelation point to change their droplet size and viscosity, but PolyHIPEs are the solid matrices that are made of solely the continuous phase, and they are obtained by the polymerisation of HIPEs. The cavities formed after removal of the internal phase being defined as “pores”, “cells”, or “voids”. The throats connect the adjacent pores to each other are defined as “interconnects” or “windows” (Figure 1.2). The formation of these interconnects has been reported to be due to the rupture of the thin polymer films between neighbouring pores during the polymerisation [58]. Depending on the presence and absence of interconnects, PolyHIPEs are categorised as “open cellular” and “closed cellular”, respectively.

### **1.2.3. Characteristics of emulsion templated scaffolds**

Although the emulsion templating technique itself is easy to apply, due to the high tunability of the process, there are many parameters that need to be controlled for the precise engineering of characteristics of the matrices (detailed in Section 1.2.4). In this section, we covered the characteristics of HIPEs and PolyHIPEs that can be controlled for specific applications.

#### **1.2.3.1. Morphological characteristics**

Internal phase volume is the main factor determining the porosity of emulsion templated scaffolds. However, the volume of the internal phase does not always correspond to the porosity of PolyHIPE scaffolds. In our recent study, the porosity of

PolyHIPEs prepared using 82% internal phase volume was measured at around 70%. This is likely because of 15–20% shrinkage of these scaffolds in each dimension during crosslinking and drying [42]. This is corroborated by other studies, for example, Chen et al. also reported the lesser extent of porosity than the internal phase volume due to the same reason [59]. This could be a problem for the clinic when defect matching scaffolds are needed. Thus, for more accurate design of the scaffolds, the degree of shrinkage can be calculated accurately, and it can be taken into account during the design process. Also, especially in dentistry, there are some approaches to overcome the polymerisation shrinkage [60].

Thus, the porosities of the PolyHIPEs can be calculated using Equation 1 [42,61,62], where  $\rho_{\text{PolyHIPE}}$  is the PolyHIPE density and  $\rho_{\text{wall}}$  is the density of PolyHIPE wall. The measured density of the bulk polymer is used for the density of the wall.

$$\% \text{ Porosity} = \left(1 - \frac{\rho_{\text{PolyHIPE}}}{\rho_{\text{wall}}}\right) \times 100 \quad (1)$$

It is also important to note that emulsion templated scaffolds mostly shrink in a dry state [63]. Thus, densities and accordingly, the porosities are different at their wet and dry conditions. However, for TE scaffolds, we believe that the porosity in the wet state is more relevant as the scaffolds are introduced into a fluid-rich environment of the body.

Higher volume of the internal phase causes a reduction in the pore size as tighter packing of the droplets is needed [64]. Typically, the average pore size and window size ranges of PolyHIPEs are 1-150  $\mu\text{m}$  and 0.2-50  $\mu\text{m}$ , respectively [57,65]. Mercury porosimetry and nitrogen adsorption methods are effective tools to characterise the

structural and physical features of PolyHIPEs [66]. The use of micro-computed tomography (micro-CT) for microstructural characterisation of PolyHIPEs has also been reported [67,68]

Another commonly used method is measuring the pore and window sizes using scanning electron microscopy (SEM) images of the cross-section of the PolyHIPEs. However, when the scaffolds are sectioned, pores are not ideally bisected; they are sectioned from a random distance ( $h$ ) from the centre (Figure 1.6). Thus, as we can only measure the radius of the circular section at a distance of  $h$  from the centre of the pore ( $r$ ) rather than the exact pore radius ( $R$ ), a statistical correction factor should be applied to the measured average pore size [66]. The relationship between  $R$ ,  $r$ , and  $h$  can be expressed using Equation 2.

$$R^2 = h^2 + r^2 \quad (2)$$

The value of  $h$  can be between 0 to  $R$ , depending on the position of the sectioning. By replacing an average value for  $h$ ;  $R/2$ , in Equation 2,  $R/r$  can be found  $2/\sqrt{3}$  as a correction factor that is applied to the measured diameter for adjusting the underestimation of the exact diameter.

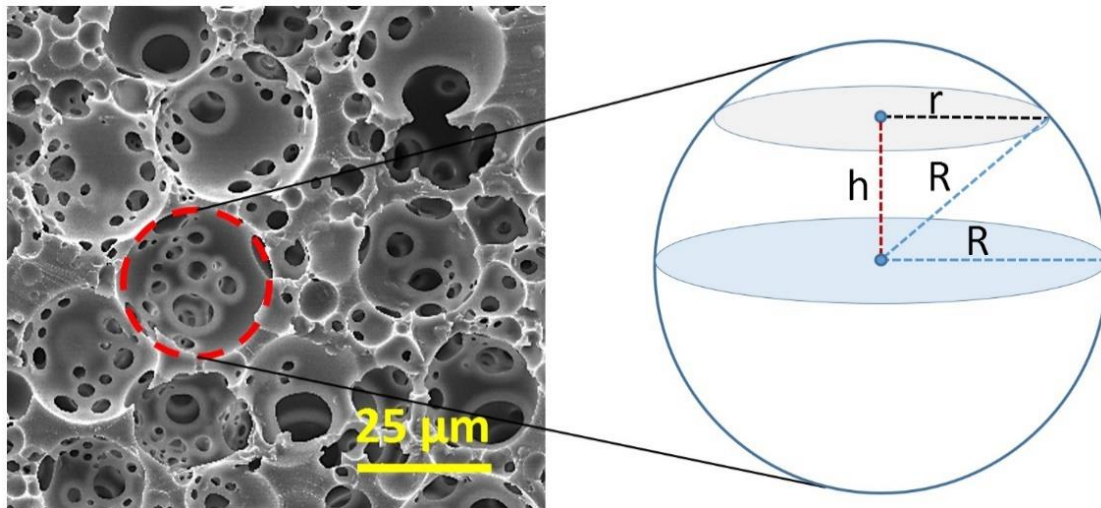


**Figure 1.6:** Derivation of the statistical correction factor that is applied for adjusting the underestimation of the exact diameter of the pore size.  $R$ , an actual radius of the pore and  $r$ , the radius of the circular section at a distance of  $h$  from the centre of the pore.

The degree of interconnectivity of PolyHIPEs is calculated by dividing the average window size to average pore size ( $d/D$ ) [42,69] however, as this number does not give any indication about the number of windows, an alternative definition termed the degree of openness, is suggested to be calculated by dividing open surface to total surface (Equation 3) [50,70].

$$\text{Degree of openness} = \frac{\text{Open surface area of the pore (area of the windows)}}{\text{Total surface area of the pore}} \quad (3)$$

### 1.2.3.2. Physical characteristics

PolyHIPEs are defined as low-density polymeric foams with typical densities of around  $0.1 \text{ g/cm}^3$  [71]. This value can be lowered with higher porosity and a higher degree of openness, and it has a direct effect on the mechanical properties of the matrices [72]. PolyHIPEs are also characterised with the low surface area due to the openness on the cavities. While increasing internal phase volume reduces the surface area dramatically

[45], the addition of porogenic solvents can increase the surface area up to 690 m<sup>2</sup>/g. PolyHIPEs with significantly higher surface area (up to 2000 m<sup>2</sup>/g) can be obtained using the hyper-crosslinking approach [73,74].

### **1.2.3.3. Rheological characteristics**

HIPEs are viscous emulsions, and they have a mayonnaise-like consistency with yellowish-white colour due to the light refraction difference between the oil and water phase. They exhibit shear-thinning behaviour which is a favourable characteristic for them to be used in extrusion-based fabrication methods [75–77]. Sears et al. reported that viscosity of methacrylate-based emulsions are less than 10 Pa.s at a shear rate of 50 s<sup>-1</sup>, and that is low enough to be printed via extrusion printer [76]. The viscosity of HIPEs depends on the viscosities of the internal and continuous phases, droplet size and the internal phase volume [78–81]. Anisa et al. showed that viscosity of w/o crude oil emulsion increases from 152.69 cP to 493.16 cP when the average droplet diameter reduced from 60.34 μm to 15.82 μm [78]. Yield stress, the minimum critical stress value that needs to be applied to the materials to start the flow [82,83], and thixotropic recovery rate, the rate that the material returns its original viscosity when the force is removed [84], are other critical rheological parameters that need to be considered, especially when the extrusion-based printing or injecting will be used as a fabrication technique.

### **1.2.3.4. Mechanical characteristics**

The mechanical features of PolyHIPEs can be tailored to a large extent by tuning other parameters such as the composition, porosity, and pore size of the PolyHIPE. Although high porosity is desired for better cell infiltration in TE scaffolds, there is an indirect relationship between porosity and mechanical properties [70,85,86]. Larger pore size

increases the Young's Modulus of the PolyHIPeS [42,87,88] probably due to the thicker struts between the pores [89]. The higher degree of interconnectivity results in a larger open area within the walls, and it leads to lower structural integrity [42,66].

#### **1.2.4. Development of the emulsion templated scaffolds**

Emulsion templated scaffolds are fabricated by following a multi-step route before they are used in TE applications (Figure 1.7); (i) development of the emulsions by optimisation of their composition and emulsification conditions, (ii) structuring the emulsions, (iii) applying the appropriate solidification method, and (iv) post-processes which include improving the functionality of the scaffolds, purification and sterilisation.

##### **1.2.4.1. Preparation of HIPeS**

There are at least three essential ingredients that need to be used to make HIPeS; (i) a continuous phase (polymer phase), (ii) an internal phase, and (iii) a stabiliser (although there are a limited number of studies on the development of stabiliser-free HIPeS [90]). In addition to these core elements of the HIPeS, additional ingredients may be required to be added into the inner or/and into the continuous phase of the emulsion.

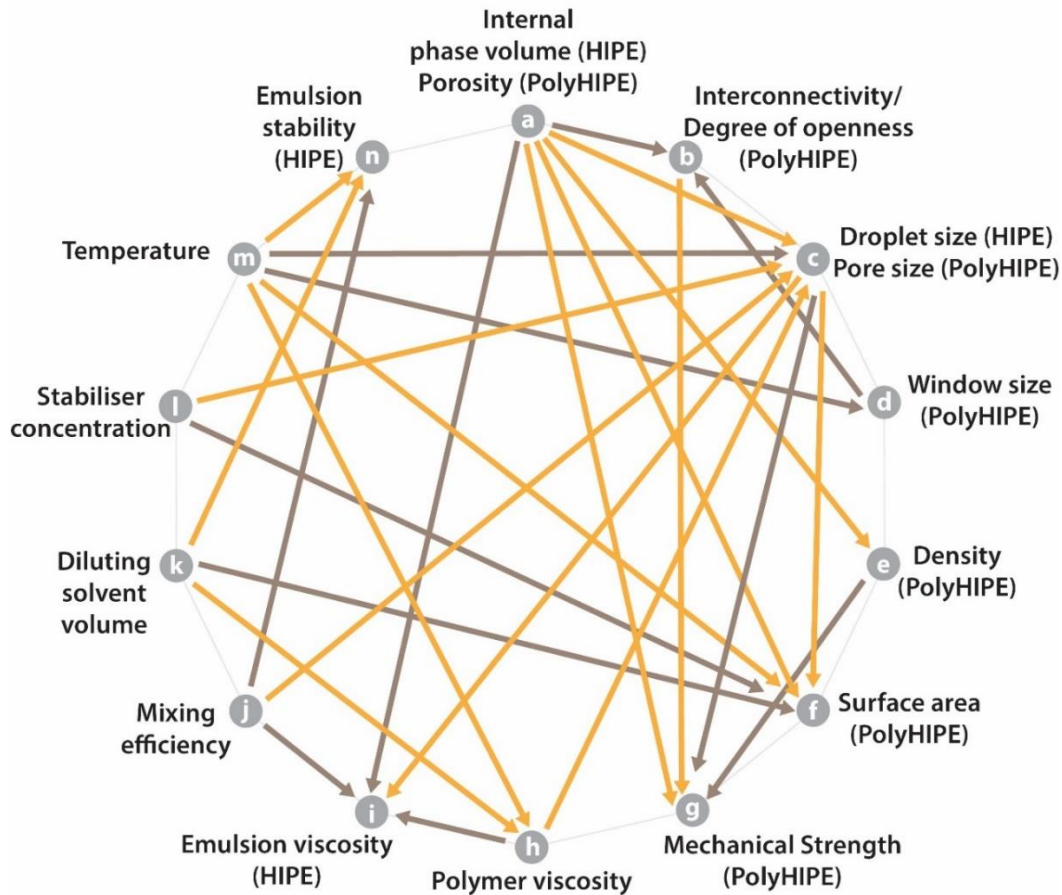
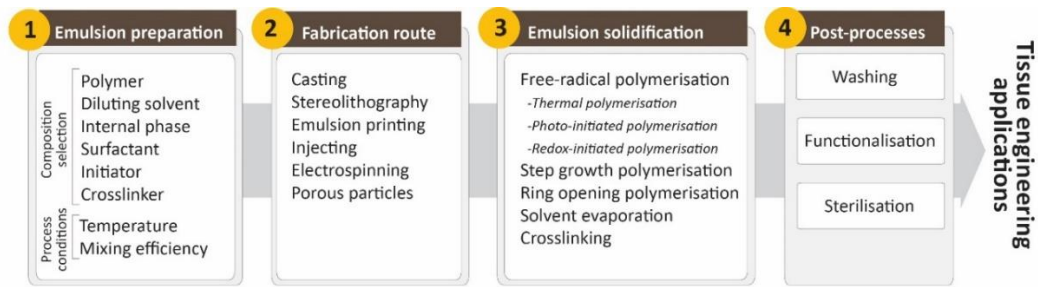


**Figure 1.7:** (Top) Steps of manufacturing of the emulsion templated substrates, (Bottom) commonly seen relations of the characteristics of HIPEs and PolyHIPEs and some of the process conditions. (Orange arrows indicate one-way reciprocal proportionality, brown arrows indicate one-way direct proportionality. For example, an increase in the porosity of PolyHIPEs (or internal phase volume of HIPEs –characteristic of HIPEs and PolyHIPEs corresponds to each other) reduces the density of PolyHIPEs and increases the emulsion viscosity). References for the relations; (a-i) [91–93], (a-g) [70,85,86], (a-e) [72], (a-c) [64,72], (a-b) [65,70], (a-f) [45], (b-g) [42,66,70], (c-i) [94], (c-g) [42,87–89], (c-f) [45], (d-b) [50], (d-n) [45], (e-g) [72], (h-c) [42], (h-n) [42], (h-i) [95], (j-i) [94,96], (j-c) [38,94,97], (j-n) [96], (k-h) [42], (k-f) [45,73], (k-n) [42,69], (l-c) [38], (l-f) [98], (m-h) [42], (m-n) [69], (m-c) [69,97,99], (m-d) [69], (m-f) [100].

#### **1.2.4.1.1. Formulation of the continuous phase**

The selection of the monomeric or oligomeric pre-polymer for the continuous phase of the PolyHIPEs is the fundamental basis to formulating emulsion templated structures with pre-determined properties and will be discussed in Section 1.2.4.3. The pre-polymer is typically formulated with a number of additives (i.e. solvent, stabiliser and initiator) to form the continuous phase, which will be discussed in this section.

#### **1.2.4.1.2. Diluting solvents**

Pre-polymers used in the emulsification process may be in solid-state or in liquid phase with high viscosity. During the mixing of the two immiscible phases, although the high viscosity of the continuous phase increases the kinetic stability of the emulsion, it needs to be low enough to enable efficient mixing of the two phases [36,101]. In order to reduce the viscosity of the oil phase, either the temperature of the system can be increased (Figure 1.7), or polymers can be diluted with the solvents that are called diluting or porogenic solvents as they are removed after polymerisation. After removal, these matrices shrink up to 50% [102]. Also, the addition of diluting solvents may provide additional nanoscale porosity on the walls of the PolyHIPEs [103].

Diluent type [42] and volume [36,42] plays a critical role in the characteristics of HIPEs and PolyHIPEs. While water and phosphate buffer saline (PBS) are commonly used to dilute the continuous phase of the o/w emulsions [90], more apolar solvents (with less solubility in water) such as; toluene [36,42,104,105], chloroform [42], tetrahydrofuran (THF) [106], dichloromethane (DCM), and dichloroethane (DCE) [107] are used as diluents in w/o emulsions.

Recently, we have shown the impact of absence/presence, volume and the type of diluting solvents on the stability of polycaprolactone (PCL) HIPEs and the morphology of PCL PolyHIPEs [42]. Increasing the volume of the diluent enhances the limit of the maximum internal phase volume that can be incorporated into the emulsion. However, a further increase in the solvent volume from a certain point reduces stability HIPE [42]. Thus, there is a narrow range that a stable emulsion can be formed. The viscosity should be low enough to enable mixing of the two phases, but high enough to form a stable emulsion.

#### **1.2.4.1.3. Internal phase (dispersed phase)**

While the internal phase of w/o emulsions is most dominantly composed of water, in reversed emulsions (o/w), more apolar liquids, often toluene [65,108,109] form the internal phase. Selection of the internal phase composition and the volume is another factor that has an impact on the properties of HIPEs and PolyHIPEs. Krajnc et al. tested toluene, chlorobenzene, DCM, and chloroform as the internal phases for acrylic acid PolyHIPEs (o/w), and reported that only the emulsions prepared with toluene resulted in a stable emulsion [109].

There are some salts such as sodium sulphate ( $\text{Na}_2\text{SO}_4$ ), calcium chloride ( $\text{CaCl}_2$ ), sodium chloride ( $\text{NaCl}$ ) [110], and potassium iodide ( $\text{KI}$ ) that are included in the internal phase of the w/o emulsions to increase stability [111,112]. Opawale et al. showed that  $\text{NaCl}$  affects the surfactant adsorption and the emulsions interfacial elasticity, which play a crucial role in emulsion stability [113]. However, the intensity of the impact depends on the type of surfactant used [114].  $\text{CaCl}_2$  was reported to increase emulsion stability by preventing Oswald ripening [38]. Similarly, potassium

sulphate ( $K_2SO_4$ ) was also reported to increase the rigidity of the interface between two-phase [115–117].

Opposed to abovementioned applications that attempt to increase the stability of the emulsions, there are some approaches to reduce emulsion stability on purpose to enable an increase of the pore size of the PolyHIPE. Magnesium sulphate ( $MgSO_4$ ) has been reported to reduce the surfactant adsorption and increases the droplet size within the emulsion [118]. Also, chemicals that are partially soluble in both phases of the emulsion such as poly(ethylene glycol) (PEG) [69] and THF [45,69,119,120] reduce emulsion stability and are included in the internal phase of the w/o emulsions to increase pore size.

#### **1.2.4.1.4. Stabilisers**

The coexistence of two immiscible liquids in the emulsion composition causes high surface tension at the interfaces of these liquids. The droplets of the inner phase coalesce gradually to reduce the surface area, and this process ends up inevitably as phase separation. Stabilising agents, surfactants and Pickering particles, reduce the interfacial tension by stabilising the oil-water interface.

##### **1.2.4.1.4.1. Surfactant stabilisation**

The surfactant is an amphiphilic compound that its head is water-soluble, and the tail is oil-soluble (Figure 1.8). Surfactants create a continuous film around the inner phase, act as a barrier between two phases, reduce the interfacial tension, and stabilise the emulsions. There are various types of surfactants available, and they are classified as non-ionic, anionic, cationic, and amphoteric, depending on the charge of the

hydrophilic head (Figure 1.8A). The surfactant choice [35,38,102] and concentration [42] play an important role in emulsion stability and PolyHIPE morphology.

When there is no surfactant used in the water and oil system, the type of emulsion depends on the volume of the phase. The higher volume phase will be the continuous phase. In the presence of surfactants, according to the Bancroft rule [121], the phase that the surfactant is predominantly dissolved in forms the continuous phase. Specifically, while oil-soluble surfactants tend to form w/o emulsions, water-soluble surfactants are suitable for o/w emulsions [122].

Although the selection of the best working surfactant has been empirical, the quantitative classification of the surfactants, hydrophile-lipophile balance (HLB) classification described by Griffing, gives an insight for the initial surfactant choice [123,124]. The HLB value varies between 0 to 20, and the value is in direct correlation with the hydrophilicity of the surfactant [125]. While surfactants with low HLB values are good for w/o emulsions, surfactants with high HLB values are more suitable for o/w emulsions [125].

The HLB value of a surfactant is not always a sole determining factor for emulsion stability, which depends on various parameters such as the selection of the monomer and solvent, emulsification temperature, and absence/presence of the electrolyte [125]. Indeed, many researchers reported that just HLB is not enough on its own to select a suitable surfactant for emulsion systems [35,38].

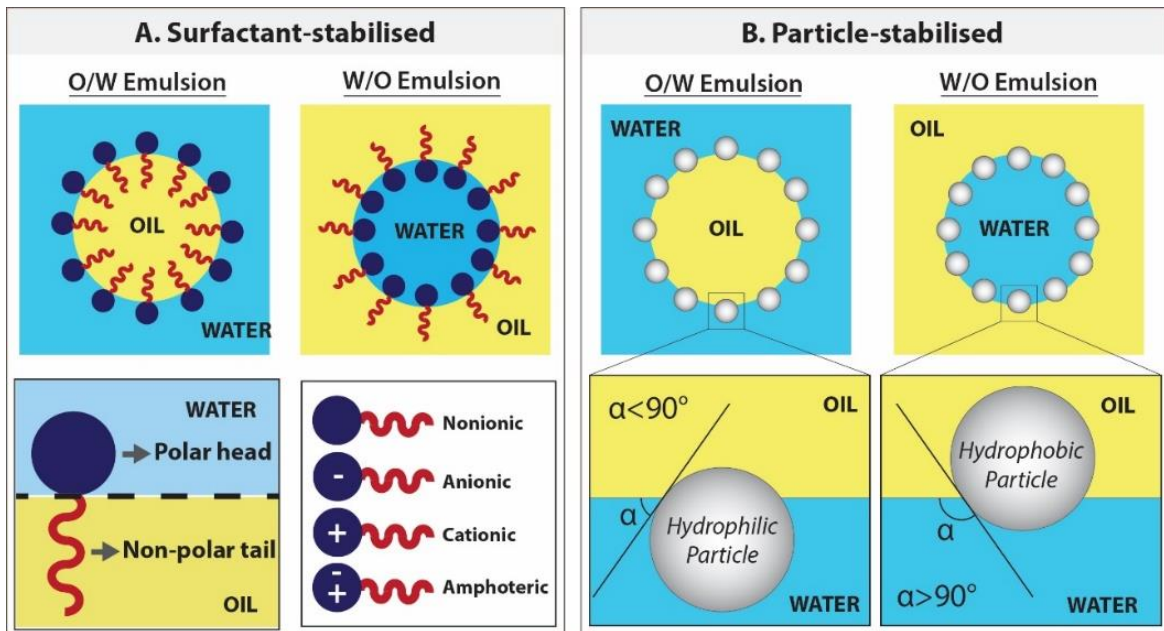


**Figure 1.8:** Emulsions can be stabilised either by surfactants or particles. (A) The positioning of the surfactant molecules in o/w or w/o emulsions and type of surfactants. (B) The positioning of the particles on the water-oil interface of either in o/w or w/o emulsions depending on the degree of wettability of the particles by these phases.

W/o emulsions are mostly stabilised using oil-soluble nonionic surfactants [46]. Span 80, Hypermer 246, and polyglycerol polyricinoleate (PGPR) are the most widely used surfactants for w/o HIPEs (Table 1.1). However, Zhang at al. replaced the non-ionic surfactant with cationic surfactant for divinylbenzene (DVB)-styrene HIPEs and reported the formation of PolyHIPEs with higher pore volumes than the ones prepared using non-ionic surfactants [126]. The concentration of the surfactants used in the preparation of HIPEs is generally in the range of 1-30% (w/w) (of the monomer). Higher surfactant concentration results in smaller average pore size and more uniform pore size distribution [38].

Surfactants are commonly intended not to react with the monomer, and they are removed from the PolyHIPE composition following polymerisation. However, the use

of reactive block copolymer surfactants in HIPE composition is also reported [127]. As they covalently attach to the PolyHIPE surface, surfactant removal is not needed.

**Table 1.1:** Commonly used surfactants in HIPEs of various polymer systems.

Emulsion type	Emulsifier	HLB/ Type	Polymer	Ref.
w/o	Polyglycerol polyricinoleate (PGPR)	~3 [128]	1,6-diisocyanatohex-ane and Polycaprolactone triol	[106]
		Nonionic	Propylene fumarate Dimethacrylate	[38,57,129]
	Sorbitan monooleate (Span 80)	4.3 [130] Nonionic	Propylene fumarate (diacrylate)	[36]
			Styrene/divinylbenzene	[119,131]
			2-Ethylhexyl acrylate (EHA) and isobornyl acrylate (IBOA)	[63]
	Hypermer 246	5-6 [132] Nonionic	2-Ethylhexyl acrylate (EHA) and isobornyl acrylate (IBOA)	[39,70,133,134]
			Thiolene	[135,136]
			Polycaprolactone	[13,42]
	Brij-58	15.7 [137] Nonionic	Polycaprolactone	[138]
	Pluronic L121	1 [139] Nonionic	Tetrakis-3-mercaptopropionate and divinyladipate	[140]
Cetyltrimethylammonium bromide (CTAB)	10 [141] Cationic	Styrene/divinylbenzene	[126]	
o/w	Triton X-405	17.9 [142] Nonionic	Alginate methacrylate	[143,144]
			Dextran	[145]
			Dextran-b-PolyNIPAAm (Poly(N-isopropylacrylamide))	
			Gelatin methacrylate	[65,108]
			Pullulan methacrylate	[108]
			Dextran methacrylate	[108]
			Alginate	[144]
			Acrylic acid	[109]

#### *1.2.4.1.4.2. Pickering particle stabilisation*

The emulsion can also be stabilised using solid particles (micro or nanoparticles), and these surfactant-free emulsions are defined as Pickering emulsions [146,147]. As in surfactant stabilised emulsions, the pore size of the particle stabilised emulsions can be adjusted by changing the particle concentration [148].

The principle behind the stabilisation mechanism of Pickering emulsions lays on the wettability of the particles by oil and the water phases. These particles position at the interface and need to be absorbed by both phases to some extent. The particles are more adsorbed in the phase that they are wetted more, and this defines their positioning in the interface (Figure 1.8B). While water wetted particles forms o/w emulsions, oil-wetted particles can stabilise w/o emulsions [149–151]. The particles that are not wetted by one of these phases disperse in the phase they are wetted and fail to stabilise the emulsion.

Hydroxyapatite (HA) is the most widely used particles used for stabilisation of Pickering HIPEs. Interestingly it is reported to be used both o/w [148] and w/o [41,152,153] HIPEs. Hu et al. used nano-HA to stabilise PCL HIPEs [154] and in their follow-up study, Yang et al. claimed that emulsions stabilised using silica nanoparticles have a higher viscosity than the emulsions stabilised by HA particles [146]. Starch nanoparticles [155] and gelatin nanoparticles [156] are the other alternative particles used for the stabilisation of the Pickering o/w and w/o emulsions, respectively.

#### *1.2.4.1.5. Initiators*

Initiators are chemical compounds that react with the monomers. They form intermediate compounds that can be linked with other monomers and propagate to

form the polymer chains. Initiators can be included either into the inner or continuous phase of the emulsions, and the locus of initiation has been shown to have a significant effect on porous structures [147].

Ammonium persulfate (APS) [38] and potassium persulfate (KPS) [115,117,157] are water-soluble oxidising agents that are used as redox initiators in radical crosslinking of the macromer chains. They have been reported to be introduced into the water phase of the styrene [158,159], dextran, [148] or polypropylene fumarate (PPF) [36,38] HIPEs with the concentration of 1-5% w/v of the aqueous phase.

Benzoyl peroxide (BPO) is an oil-soluble redox initiator also used for polymerisation of PPF HIPEs. Robinson et al. showed that initiator selection has a great impact on PolyHIPE morphology [57]. While PPF PolyHIPEs prepared using APS as an initiator resulted in closed cellular structure, BPO included PolyHIPEs exhibited open cellular structure. Also, the concentration of the redox initiator has shown to have an impact on the curing time of HIPEs and on the mechanical properties of PolyHIPEs [129]. 2,2'-Azobisisobutyronitrile (AIBN) is another oil-soluble initiator. It has been reported to be introduced into the continuous phase of styrene [160] and the internal phase of gelatin HIPEs [65] for thermal polymerisation.

Photoinitiators are the molecules that create reactive species when exposed to light, and they are included in the composition of the HIPEs that will be polymerised via photo-initiation. In the photoinitiator selection process, the critical parameter is that the absorption band of the photoinitiator should overlap with the emission spectrum of the light source [161]. 2,4,6-Trimethylbenzoyl phosphine oxide/2-hydroxy-2-methyl propiophenone blend [13,42,107,162] and phenyl bis(2,4,6-trimethyl benzoyl)-phosphine oxide (BAPO) [76] are widely used photoinitiators in photo-

polymerisation of HIPEs. Photoinitiators are mostly used in HIPE compositions at a concentration range of 0.2-10% (w/w) of the polymer. The concentration of the photoinitiator that is included in the composition of the photocurable resins is reported to have an effect on the rheological properties of the monomer and its gelation time [163]. Interestingly, there are very few studies that investigate the photoinitiator type and concentration on the characteristics of PolyHIPEs [164]. Also, photopolymerisation kinetics has been shown to be affected by the photopolymerisation temperature and the intensity of the light source [165,166]. In most cases, higher temperature and light intensity has been reported to increase the polymerisation rate [166–168].

#### **1.2.4.1.6. Crosslinker (crosslinking agent)**

Crosslinkers are the precursors with at least two reactive ends to connect primary polymer chains by forming intermolecular linkages (Figure 1.9A). Using an external crosslinking agent increases the degree of crosslinking of the polymer phase, and it improves the stiffness of the materials [157]. The most known crosslinker is DVB that is used in the composition of styrene HIPEs [131,169,170] (Figure 1.9B, C). Christenson et al. used propylene fumarate diacrylate (PFDA) as a crosslinker for PPF HIPEs and showed that crosslinker concentration has an impact on the emulsion stability of HIPEs and on the morphology of PolyHIPEs [36]. Nalawade verified this finding on hydrogel-based HIPEs [171]. Trimethylolpropane triacrylate (TMPTA) is also widely used crosslinker for 2-ethyl hexyl acrylate (EHA) and isobornyl acrylate (IBOA) PolyHIPEs [70,133].

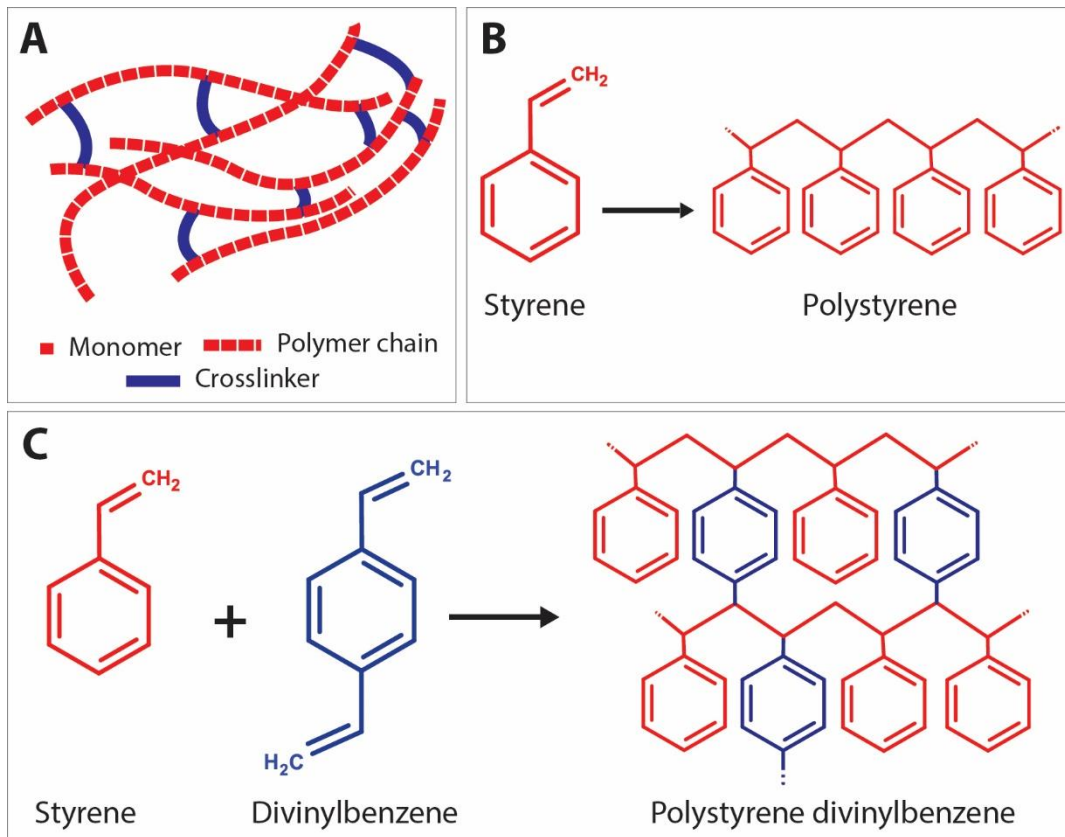


**Figure 1.9:** (A) Positioning of the crosslinker between linear polymer chains. As an example; (B) formation of polystyrene chain from styrene monomers and crosslinking of polystyrene chains using the crosslinker, divinylbenzene.

#### 1.2.4.1.7. Temperature

The most dramatic effect of the temperature is on the viscosity of the oil phase that also affects the viscosity and the stability of the emulsion. The viscosity of the polymer and the temperature are inversely proportional to each other as shown in Equation 6 where  $\eta$  is the viscosity of the polymer,  $T$  is the temperature,  $A$  and  $B$  are the material constants;

$$\eta = Ae^{\frac{B}{T}} \quad (4)$$

Also, according to Stoke's equation (Equation 7), the viscosity of the polymer and the velocity of the droplet ( $v$ ) are inversely proportional [172];

$$v = D^2 \Delta\rho g / 18n \quad (5)$$

$D$  is the droplet diameter under gravitational force,  $\Delta\rho$  is the density difference between water and oil phase,  $n$  is the viscosity of the oil phase, and  $g$  is the gravitational force. Consequently, the increasing temperature reduces the oil phase viscosity, and this increases the speed of droplets of the inner phase and creates a bigger pore size [64,97,173]. Further increase in the temperatures can lead to emulsion separation due to the increased mobility of the droplets [69,99]. Although some studies increase the temperatures in a controlled manner to increase the pore size, moderate temperatures are more favourable as they create comparatively more stable emulsions.

To investigate the effect of higher temperature on PolyHIPEs, researchers use different setups. Caldwell et al. showed that increasing the temperature of the inner phase from 23 °C to 80 °C increased the pore sizes up to 2-fold [99]. Akay et al. heated the whole mixing system using a stainless steel vessel with a heating jacket [131].

#### **1.2.4.1.8. Efficiency of mixing**

In the conventional emulsification route, the internal phase is introduced into the continuous phase dropwise while the system is mixed continuously. There are various mixing methods reported; such as over-head stirrer [99,107,135], magnetic stirrer [13,42], mechanical shaking [146], speed mixer [38,57,129], vortex [19], homogeniser [152], and shaking by hand [153]. The type of mixing route is reported to have an effect on the maximum internal phase volume that could be incorporated into the emulsion [19]. Effect of stirring speed on the characteristics of HIPEs has been reported by many groups [38,64,97]. Higher mixing speeds commonly result in smaller pore sizes.

Bokhari et al. revealed that the way of adding inner phase into the continuous phase (syringe pump or dropping funnel) also influences the emulsion stability, the pore size distribution of the droplets, and the reproducibility [173]. Another emulsification route; the multiple emulsion method, combines and mixes all the components from the oil and water phase together. But as the emulsion prepared using this method forms gradually, the system needs to be stirred until the PolyHIPE forms [19].

Apart from the parameters mentioned above, it is also important to note that, every parameter that affects the energy input for the droplet breakup; such as mixing time, the batch volume of the emulsion, materials and the diameter of the emulsification container, and the magnetic stirrer/paddle size (where relevant) directly affects the mixing efficiency of the emulsion and will have an impact on the final morphology. Keeping these parameters constant between batches helps the consistency and reproducibility of the PolyHIPEs.

#### **1.2.4.2. HIPEs to PolyHIPEs**

##### **1.2.4.2.1. *Emulsion solidification approaches***

###### **1.2.4.2.1.1. *Free-radical polymerisation***

PolyHIPEs based on many popular polymers, such as; acrylates, methacrylates, and styrenes are synthesised using free radical polymerisation (FRP) [48]. The type of the initiator (Section 1.2.4.1.5) used in the emulsion composition determines one of the following initiation routes of FRP; (i) thermal-initiated polymerisation, (ii) photo-initiated polymerisation, and (iii) redox-initiated polymerisation.

The earliest examples of the PolyHIPEs (the 1980s) were based on thermal polymerisation [174,175]. In this process, an emulsion mixture that contains thermal

initiator is exposed to heat in an oven or in a heat bath for 6-48 hours for the polymerisation. The temperature is often kept quite high (60-70 °C [36,102,115,159,173]) to decompose the initiator into radicals thermally. Exceptionally, polypropylene fumarate dimethacrylate (PFDMA) HIPEs can be polymerised at 37 °C [38,57]. Also, by the use of a catalyst, the polymerisation temperatures can be reduced [176].

In photo-initiated polymerisation, emulsions are prepared using photosensitive materials as a continuous phase and photoinitiators are exposed to light to be able to generate free-radicals and initiate the polymerisation. This method has many advantages over thermal-induced polymerisation; polymerisation takes place at room temperature (RT) just in seconds to minutes depending on the sample size. Photopolymerisation is an efficient polymerisation route, especially in relatively small samples, as ultraviolet (UV) penetration depth can be limited in a larger volume of emulsions. Photo-initiated polymerisation of the emulsions, specifically HIPEs, were described in patents in 1986 [177] and 1999 [34], respectively. A more detailed experimental procedure of photo-initiated polymerisation of HIPEs was reported in 2006 by Pierre et al. [63]. However, recently, a number of studies about the development of PolyHIPEs based on photocurable materials such as thiolene [107], meth(acrylates) of PCL [13,42] or gelatin [178] have increased the potential applications. Redox-initiated polymerisation, which uses reducing and oxidising agents, is also another FRP route used in the polymerisation of HIPEs [129].

#### *1.2.4.2.1.2. Step growth (condensation) polymerisation*

Integration of step-growth polymerisation into the emulsion templating process has been successfully implemented in polyurethane PolyHIPEs [106]. It is synthesised

using diisocyanate and PCL triol, and the reaction of a diisocyanate with water produced urea groups and carbon dioxide (CO<sub>2</sub>). The bubbles of generated CO<sub>2</sub> created additional porosity into PolyHIPE structure.

#### *1.2.4.2.1.3. Ring-opening polymerisation*

Development of PolyHIPEs by ring-opening polymerisation (ROP) of cyclic monomers is a relatively new route of polymerisation HIPEs.  $\epsilon$ -caprolactone and L-lactide are the most widely used monomers in this approach [179–183]. One of the most important advantages of this technique is the elimination of diluting solvents from the emulsion composition due to the low viscosity of the cyclic monomers. Catalyst concentration is the deterministic factor of the rate and the degree of polymerisation. The polymerisation temperatures and the polymerisation durations vary between 37 °C to 120 °C and 6 hours to overnight, respectively.

#### *1.2.4.2.1.4. Solvent evaporation*

Although the term PolyHIPE refers to polymerised emulsions, recently polylactic acid (PLA), PCL, polylactic-co-glycolic acid (PLGA) PolyHIPEs solidified without polymerisation have been reported [41,138,146,152,153,184,185]. This process is based on dissolving the non-functional, linear, high molecular weight polymer in an appropriate diluting solvent, then emulsification, and finally solidification of HIPEs via solvent evaporation. As high molecular weight polymers are commercially available, this process does not require polymer synthesis or functionalisation steps. PolyHIPEs can be fabricated either with moulding or 3D printing. The main disadvantages of this technique are the long solidification process (24-48 hours) [146], and the requirement

of development of emulsions with high stability that would keep the shape until solidification.

#### *1.2.4.2.1.5. Crosslinking*

Crosslinking of PolyHIPEs as a solidification approach can be either ionic, thermal or enzymatic. Alginate PolyHIPEs has been synthesised using calcium ions [143,144]. This reversible gelation can be de-cross-linked using sodium citrate. Solidification of gelatin HIPEs using enzymatic crosslinking also has been reported [178]. In another study, gelatin PolyHIPEs has been obtained by physically thermal-crosslinking at 4 °C [90].

#### **1.2.4.2.2. Fabrication routes**

##### *1.2.4.2.2.1. Casting (moulding)*

The earliest examples of PolyHIPE scaffolds were fabricated using the casting technique (Figure 1.10Aa). This technique is the easiest way of manufacturing PolyHIPE scaffolds with almost no additional technical equipment requirement. Silicone [13,42,140,186], polyvinyl chloride [102], polytetrafluoroethylene [119,120,187], glass [158], polypropylene [188], polycarbonate centrifuge tubes [69,189], and aluminium [38] are some of the materials reported to be used to create moulds for the fabrication of PolyHIPE scaffolds. Recently, we have shown that mould material has a significant impact on the morphology of the contact surface of PolyHIPEs which have fully or partially closed cellular morphology [13]. Similar to our finding, the influence of the mould material on PolyHIPE morphology and HIPE stability has also been reported previously by Cameron et al. [45].

In order to avoid the closed-pores on the surface of the PolyHIPEs, the moulded PolyHIPE blocks are typically sectioned using various methods and benefit from the open porous cross-sectional surface. Vibratomes [13,160] and microtomes [173] allow precise micro-scale thick scaffolds to be obtained. Additionally, tabletop precision saws [57,190,191], and scalpels/razor blades [13,42,99] have been used cut monoliths to millimetre scale sections.

Casting enables the manufacturing of scaffolds in a wide range of shapes and sizes, depending on the mould design [186,192–194]. Recently, Dikici et al. reported the fabrication of the PolyHIPEs in tubular form by designing a re-usable tubular silicone mould system that, HIPE can be injected into, polymerised and recovered easily (Figure 1.10Ab) [186]. Also, sacrificial polymer beads made of PDMS [193] or alginate [194] have been incorporated into emulsion composition prior to polymerisation in a mould to simply introduce multiscale porosity to PolyHIPEs.

#### *1.2.4.2.2. Vat polymerisation*

Fabrication of TE scaffolds using AM techniques gained huge attention in the last decades due to various advantages of the AM such as enabling the manufacture of complex shapes using a broad range of materials, high reproducibility and providing control on the exterior architecture of the scaffolds. However, manufacturing of pores less than 20  $\mu\text{m}$  using the current AM techniques remains a challenge [195]. Alternatively, combining emulsion templating with AM techniques such as vat polymerisation or material extrusion enables the fabrication of well-defined multiscale porous complex scaffolds.

Vat polymerisation is a laser-based fabrication method that selectively polymerises photo-sensitive liquid resin layer-by-layer by use of a laser. During the process, light is formed by static or dynamic masking and exposed to the top or bottom of a thin layer of a photocurable monomer, once a layer of the resin cured, the stage moves and the surface is recoated with the monomer, and the process is repeated. The schematic diagram of vat polymerisation is given in Figure 1.10Ba. It provides higher accuracy compared to other AM technologies [39,196,197]. Emulsions with low viscosity are preferable to be able to provide enough spreading on the z-stage while the building chamber is moving in the z-axis. Advantages and disadvantages of stereolithography over other manufacturing techniques of emulsion templated scaffolds have been reported in Table 1.3.

Johnson et al. reported the 3D defined complex structures of PolyHIPEs made of EHA:IBOA using micro-stereolithography up to 30  $\mu\text{m}$  accuracy [39]. Exactly on the same date, Sušec et al. reported the development of stable photocurable thiolene HIPEs that can be used to produce PolyHIPEs using stereolithography [40]. Fabrication of EHA:IBOA PolyHIPEs via stereolithography in wood-pile structure has been reported many times for various TE applications (Figure 1.10Bb) [70,133,134]. However, manufacturing of EHA:IBOA PolyHIPEs cause the formation of surface skin that is characterised with the closed pore at the surface. In 2018, Sherborne et al. showed that the use of UV absorbers could reduce skin formation without causing any toxic effect on cells [162].

#### 1.2.4.2.2.3. *Material extrusion*

Material extrusion is another convenient AM route to combine with emulsion templating for the fabrication of multiscale scaffolds. This method is based on the

preparation of emulsions inks, filling the printing head reservoir with a required amount of the emulsion, and printing the emulsion in the designed 3D shape. Schematic of the setup is given in Figure 1.10. The material can be extruded via a filament-fed extruder, screw extruder or a syringe extruder. The syringe-type extruder can have either motor-driven plunger or pneumatic extruder. Nozzle size and printing speed are some of the parameters that have an impact on the final structure. There are two approaches used in this manufacturing technique; (i) simultaneous printing and solidification of the HIEs and (ii) printing HIEs and subsequent solidification. Only for the first approach, emulsions prepared from photocurable materials are needed. Otherwise, material extrusion is not limited to use of the photocurable resins as in vat polymerisation.

The shear-thinning nature and the high viscosity of HIEs make them good candidates to be used as inks for the 3D printing. It is essential to highlight the fact that emulsion viscosity is inversely proportional to the size distribution of the water droplets [78]. Thus, the viscosity of the emulsion should be high enough for successful printing of the emulsion and low enough for enabling the manufacturing of the scaffolds with a pore size range that allows cell infiltration. Recently, a few publications have reported the use of material extrusion for the fabrication of bone TE scaffolds [75,76,146]. Unlike vat polymerisation, material extrusion enables fabrication of heterogeneous structures made of emulsions in different composition by using different printing heads [154]. Advantages and disadvantages of the fabrication techniques have been reported in Table 1.3.

#### 1.2.4.2.2.4. *Injecting*

Although AM techniques are first to come to the mind to fabricate defect matching scaffolds, their use requires highly accurate imaging techniques to be able to create 3D custom-made models [188]. Alternatively, injectable materials that harden *in situ* can fill irregular shapes by minimal invasive delivery (Figure 1.10D), and they can also be used as a carrier for cells and other biological molecules [198–200].

The main prerequisites for the development of injectable emulsions are the elimination of the toxic solvents and enabling polymerisation at physiological temperatures. Thus, there are a limited number of materials that can be used to develop injectable HIPEs.

PPF HIPEs, discussed in detail in Section 1.2.4.3, have a suitable viscosity for injection from a syringe, and they can solidify at body temperature in 15 minutes. They have been shown to be stable for storage up to 6 months and to integrate into the host tissue successfully [57,129]. Moglia et al. also developed PCL-diisocyanate (PCL-DI) and PCL-triisocyanate (PCL-TI)-based injectable PolyMIPES without the use of any organic solvents, but curing time at 37 °C has been reported as 48 hours which limits their clinical applicability [188]. Zhou et al. reported injectable alginate PolyHIPEs (not HIPEs) [143]. Following the preparation of o/w HIPEs with methacrylate functionalised alginate, they were thermally set. It was shown that PolyHIPEs could be extruded from a needle by retaining its morphology and further crosslinked using calcium ions. Similarly, Oh et al. developed injectable poly(N-isopropylacrylamide) (PNIPAM) grafted gelatin PolyHIPEs [90].

#### 1.2.4.2.2.5. Electrospinning

Electrospinning is a versatile route for the fabrication of the fibres with varying diameters from nanometres to micrometres scale using a wide range of materials [13,15,186,201]. The system has three main components; high voltage power unit, material delivery unit, and fibre collection unit (the schematic illustration of the electrospinning setup is given in Figure 1.10E). The polymer solution is dispensed from the syringe using a syringe pump, and electrically charged jet of the polymer solution is created under high voltage. The polymer jet is elongated and collected on the collection unit [202]. Fibres in the nanometer scale to the micrometre scale can be fabricated using electrospinning. Final fibre morphology can be controlled via process parameters such as; flow rate, working distance, the diameter of the needle, voltage, temperature and properties of the polymer solution such as conductivity concentration, a viscosity (Table 1.2) [203,204].

**Table 1.2:** Parameters that affect the fibre morphology of the electrospun meshes [205].

	<b>Parameter</b>	<b>Effect on fibre morphology</b>
Process & Environmental parameters	Voltage ↑	Fibre diameter ↓
	Flow rate ↑	Fibre diameter ↑ Bead formation ↑
	Distance ↑	Fibre diameter ↑
	Needle diameter ↑	Fibre diameter ↑
	Temperature ↑	Fibre diameter ↓
Properties of the polymer solution	Solution concentration ↑	Fibre diameter ↑
	The conductivity of the polymer solution ↑	Fibre diameter ↓
	The viscosity of the polymer solution ↑	Fibre diameter ↑

There are many examples of electrospinning of emulsions in the literature [206–208], but a few studies reported the electrospinning of HIPEs. Samanta et al. reported the fabrication of the PCL electrospun fibres from HIPE [138]. Briefly, PCL (dissolved in toluene) and polyvinyl alcohol (PVA) (dissolved in water) were used for continuous and internal phases, respectively. They showed that increasing the continuous/internal phase ratio reduces the fibre diameter. The same group also reported the electrospinning of solvent-free Pickering PCL HIPEs [209].

#### *1.2.4.2.2.6. Porous particle manufacturing*

Microporous PolyHIPE particles can be applied to the defect site by injecting and used as substrates for controlled drug delivery [210,211]. They can be created using multiphasic emulsion systems that are mostly water-in-oil-in-water (w/o/w) emulsions. The easiest way of fabrication of porous particles is dropwise addition of w/o emulsion into the water while the system is stirred (controlled stirred-tank reactor (CSTR)). Although CSTR is practical and does not need a complicated setup, it only enables fabrication of polydisperse particles, and it does not provide an accurate control on particle size. Recently, microfluidic systems gained attention for the fabrication of porous particles due to providing high control over particle size. The process is briefly based on injecting w/o emulsion and water phase into the tubing system using syringe pumps (Figure 1.10F) [212]. Bead size can be controlled by changing the nozzle size, flow rates of the water phase and emulsion phase. Paterson et al. reported that microfluidics enables the manufacturing of the beads with narrower size distribution compared to particles fabricated using CSTR [97].

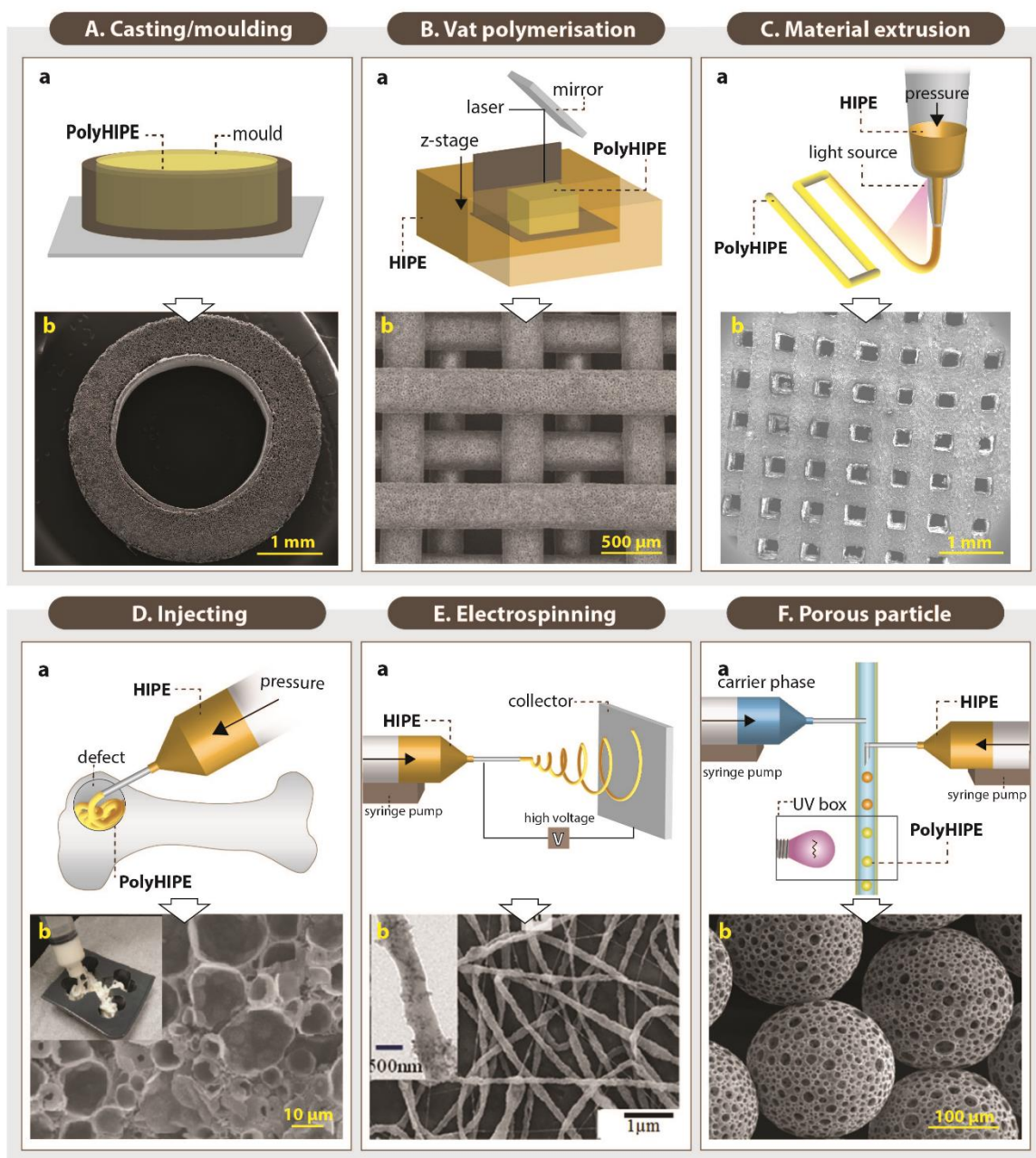


**Figure 1.10:** Setups of various fabrication routes of emulsion templated scaffolds (Aa, Ba, Ca, Da, Ea, Fa), and scanning electron microscopy images of these scaffolds (Ab, Bb, Cb, Db, Eb, Fb). (Original images were cropped, and scale bars were added to enhance the figures). Images Ab, Bb, Cb, and Fb are adapted from [186], [70], [75], and [97] respectively, under The Creative Commons License. Image Db was adapted with permission from [38], Copyright 2011 American Chemical Society. Image Eb was adapted with permission from [213], Copyright 2017 American Chemical Society.

**Table 1.3: Advantages of disadvantages of the fabrication routes of emulsion templated scaffolds**

	<b>Advantages</b>	<b>Disadvantages</b>
<b>Casting (Moulding)</b>	<ul style="list-style-type: none"> <li>▪ The easiest way of manufacturing PolyHIPE scaffolds</li> <li>▪ No additional technical equipment requirement</li> <li>▪ Enables the manufacturing of scaffold in a wide range of shapes and sizes</li> <li>▪ Can be used for all type of PolyHIPES</li> </ul>	<ul style="list-style-type: none"> <li>▪ Surface architecture is affected by mould material</li> <li>▪ Limited complexity of designs</li> <li>▪ Limited light penetration in photopolymerisation</li> </ul>
<b>Vat polymerisation</b>	<ul style="list-style-type: none"> <li>▪ Enables fabrication of complex shapes</li> <li>▪ Second-grade porosity can be introduced</li> <li>▪ Does not need sacrificial material</li> </ul>	<ul style="list-style-type: none"> <li>▪ Limited with photocurable material</li> <li>▪ The larger volume of the material requirement (to fill the tank)</li> <li>▪ Surface skin</li> <li>▪ Requires HIPES with low viscosity</li> <li>▪ The requirement of the 3D model</li> </ul>
<b>Material extrusion</b>	<ul style="list-style-type: none"> <li>▪ The small amount of material is sufficient</li> <li>▪ Not limited with the photocurable PolyHIPES</li> <li>▪ Can be combined with other materials</li> <li>▪ Second-grade porosity can be introduced</li> </ul>	<ul style="list-style-type: none"> <li>▪ Requires HIPES with high viscosity</li> <li>▪ Surface skin</li> <li>▪ Equipment coast</li> <li>▪ The sacrificial material can be needed for higher accuracy</li> <li>▪ The requirement of the 3D model</li> </ul>
<b>Injecting</b>	<ul style="list-style-type: none"> <li>▪ Can be used for complex shapes without need of the 3D model</li> <li>▪ Mild operation conditions</li> <li>▪ Enables minimal invasive delivery</li> </ul>	<ul style="list-style-type: none"> <li>▪ Limited choice of materials</li> </ul>
<b>Electrospinning</b>	<ul style="list-style-type: none"> <li>▪ Well-established method</li> <li>▪ High tunability</li> </ul>	<ul style="list-style-type: none"> <li>▪ Limited with the materials that can be solidified via solvent evaporation</li> </ul>
<b>Porous particle manufacturing</b>	<ul style="list-style-type: none"> <li>▪ Injectable</li> <li>▪ Suitable for drug delivery</li> </ul>	<ul style="list-style-type: none"> <li>▪ Limited with photocurable materials</li> <li>▪ Not suitable for large defects</li> </ul>

### **1.2.4.3. Monomers/macromers**

#### **1.2.4.3.1. Hydrophobic polymers for the fabrication of w/o PolyHIPEs**

##### *1.2.4.3.1.1. Non-degradable polymers*

The earliest studies about the development of emulsion templated substrates used styrene as a monomer [20,30–32,44]. In 1992, commercial styrene PolyHIPE microcarriers (provided by the company, Microporous Materials) tested with suspension-growing cell lines for the production of a therapeutic protein, and it was found advantageous as being sterilizable, cheap, and suitable for surface functionalisation [31,32]. In 1993, human endothelial cells were cultured on the same microcarriers for a similar purpose, and they reported that PolyHIPEs did not support cell growth [43]. Akay et al. have a patent on styrene/DVB PolyHIPEs as a cell growth media in 1998 [44]. Since then, styrene/DVB is also the highest reported PolyHIPE material in the literature.

The blend of acrylate-based monomers; EHA:IBOA is another commonly reported non-degradable material that is mostly solidified using photo-initiated polymerisation [63,97,133]. Owen et al. showed that PolyHIPEs prepared by changing the ratios of EHA or IBOA yield in varying mechanical properties (up to a 60-folds) [70,85].

##### *1.2.4.3.1.2. Degradable polymers*

**PCL:** As TE scaffolds are desired to be made of biodegradable materials, the development of biodegradable PolyHIPEs is important to satisfy the need of implantable TE constructs (Figure 1.11). PCL is the earliest biodegradable polymer that has been included in PolyHIPE composition. However, the development of HIPEs

made of PCL has been problematic over the years due to the high viscosity of the polymer, which limits the mixing of two phases during emulsion [104,115–117].

The earliest reported PolyHIPE made from PCL was created by copolymerisation of PCL diacrylate with non-degradable monomers [104]. Various diluting solvents were included in HIPE composition to reduce the viscosity of PCL [104–106]. Johnson et al. reported the incorporation of 76% PCL triacrylate into HIPE composition when DCE used as a porogenic solvent [107]. Recently, we have reported the manufacturing route of PolyHIPEs fully made of photocurable PCL tetra-methacrylate diluted by a solvent blend of chloroform and toluene [42]. Also, recently, the development of high molecular weight non-reactive PCL PolyHIPEs has been reported by solvent evaporation [138,146,153,184,185].

**PLA and PLGA:** PLA and its copolymer PLGA are widely used biomaterials for fabrication of TE scaffolds. In 2002, Busby et al. reported the development of thermal polymerised PLA diacrylate PolyHIPEs (PLA content up to 40%) by diluting the oil phase with methyl methacrylate (MMA) [102]. Also, synthesis PolyHIPEs based on PCL and PLA blends, without the use of any diluents, via opening polymerisation also has been reported [180]. Recently, Hu et al. reported the development of composite HA/PLA [152] and HA/PLGA [41] scaffolds by Pickering emulsion templating and solvent evaporation.

**PPF:** PPF, an unsaturated linear polyester, can be easily cured through double-bond on the backbone of the fumarate using various crosslinking agents [214]. It is commonly suggested to be cured by *in situ* crosslinking in the defect site [215]. Its degradation products are nontoxic monomers [214,216]. Due to its aforementioned advantages, it has been used in various biomedical applications, including TE scaffolds

and orthopaedic implants [217]. Fumarate-based PolyHIPEs (PPF [36], PFDA [36] and PFDMA [38]), are groups of the well-established biodegradable PolyHIPE compositions.

In 2007, Christenson et al. developed PPF PolyHIPEs that can be cured at 60 °C in 48 hours in the presence of PFDA as a crosslinker [36]. They showed the tunability of the material by changing PPF, PFDA and toluene concentrations. Later on, Moglia et al. reported the development of injectable solvent-free PFDMA PolyHIPE that can be cured at 37 °C [38]. However, the structures obtained exhibited closed cellular morphology. In 2014, Robinson et al. hypothesised that including an oil-soluble initiator into PFDMA PolyHIPE might induce organic phase initiation and this results in open porous monoliths. Indeed, they have used both an oil-soluble initiator; BPO and a water-soluble initiator, APS, and PolyHIPEs with BPO showed open-porosity. However, the curing time of the HIPEs was still long (overnight) for the ultimate aim of *in situ* crosslinking [57]. Moglia et al. used the redox initiated polymerisation rather than thermal initiation in order to reduce the curing time. They created two PolyHIPE compositions; one with benzoyl peroxide (BPO) as an initiator and other with trimethylaniline (TMA) as reducing agent and used a syringe with the double barrel for the injection of the emulsion and enabled polymerisation of HIPEs just in 15 minutes [129].

**Thiol (ene/yne):** Thiol(ene/yne) chemistry (also classified as click chemistry [218]) is the reaction between a thiol and an alk(ene/yne) to thioether. This high yield reaction has recently gained attraction in various applications, including the development of thiol(ene/yne) PolyHIPEs [99,107,135].

In 2011 Lovelady et al. reported the development of thiol(ene/yne) PolyHIPEs [135]. In the follow-up study, Caldwell et al. developed TMPTA and dipentaerythritol penta/hexa-acrylate (DPEHA)-based thiolene PolyHIPEs and showed the dependency of mechanical properties to monomer selection [99]. In 2015, Johnson et al. reported the development of photocurable PCL triacrylate thiolene PolyHIPEs with up to 95% interconnected porosity [107]. The degradation products have been shown to be non-toxic on fibroblasts up to a concentration of 0.1 mg/ml. Whitely et al. also developed thiolene PolyHIPEs made of tetra-functional thiol, pentaerythritol tetrakis-3-mercaptopropionate, and PFDMA [191], and they showed the hydrolytic and accelerated degradation profiles of these scaffolds.

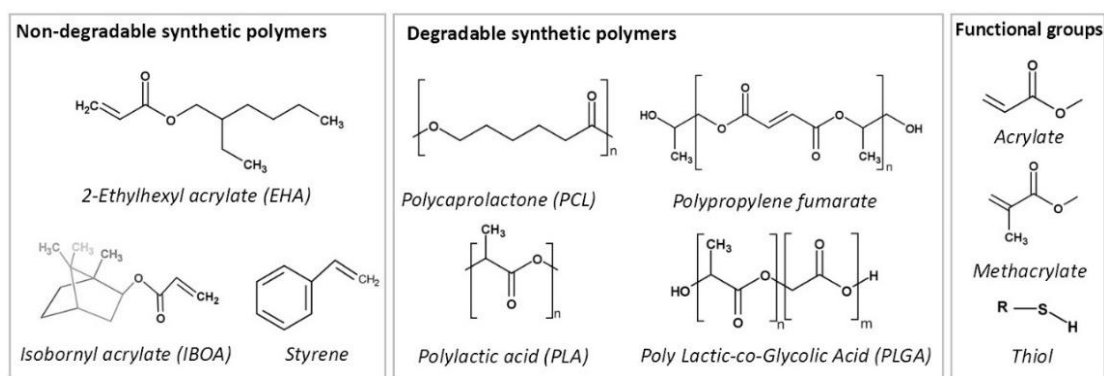


**Figure 1.11:** Commonly used synthetic polymers to prepare emulsion templated matrices.

#### 1.2.4.3.2. Hydrophilic polymers for the fabrication of o/w PolyHIPEs

In 1997, Naotaka Kitagawa described the development of hydrophilic PolyHIPEs [33]. Since then, a number of naturally derived polymers have been used to fabricate PolyHIPEs from o/w emulsions. These matrices have the advantages of being hydrophilic and biodegradable, often similar to extracellular matrix (ECM) components to be used as materials for the fabrication of TE scaffolds. However, they

have the disadvantages of having a high degree of batch-to-batch variability and comparably lower mechanical strength than synthetic counterparts [219,220].

Gelatin is one of the most common natural biopolymers used for the fabrication of TE scaffolds. As it is derived from collagen of skin, bone or tendon of animals, it is highly abundant and cost-effective [221]. In 2005, Barbetta et al. successfully developed gelatin-methacrylate PolyHIPEs with up to 95% internal phase using free-radical polymerisation [65]. Following this, they also reported the development polysaccharides; dextran and pullulan methacrylate PolyHIPEs [108]. They also developed gelatin PolyHIPEs that are solidified via enzymatic cross-linking [178]. Although PolyHIPEs obtained via free-radical polymerisation of gelatin exhibited better-defined morphology, enzymatically crosslinked PolyHIPEs were found less toxic on hepatocytes and showed an improved expression of adhesion proteins [178]. Oh et al. developed gelatin PolyHIPEs by grafting gelatin with poly(N-isopropylacrylamide) (PNIPAM). Due to the amphiphilic nature of gelatin-graft-PNIPAM as a continuous phase, they managed to incorporate an internal phase of up to 90% without the use of any surfactants [90]. Recently Yuan et al. reported the fabrication of gelatin PolyHIPEs with 92% porosity by two-step crosslinking and freeze-drying [222]. Alginate, a polysaccharide derived from seaweed, is another biomaterial that can be used to fabricate PolyHIPE scaffolds [143,144]. Krajnc et al. also reported the development of o/w HIPEs from a synthetic hydrophilic monomer, acrylic acid [109].

#### **1.2.4.4. Post-processes**

##### **1.2.4.4.1. *Improving the biomimetic behaviour of the PolyHIPE scaffolds***

The suitability of the morphology of PolyHIPE matrices to be used as TE scaffolds has been well-accepted. However, as PolyHIPEs are most commonly created using w/o emulsions, they are highly hydrophobic, and lack of functionality which limits their interaction with biological tissues [136]. Thus, starting from the early 2000s, researchers started to explore the ways of enhancing the biological activities of the PolyHIPE scaffolds using various methods such as chemical functionalisation [13], incorporation of the hydrophilic particles such as HA [131,134], incorporation of a single biologically active agent [136,223], or decoration PolyHIPEs with cell-derived *in vitro* generated ECM [75] (Table 1.4).

##### **1.2.4.4.1.1. *Chemical functionalisation***

The surface of the scaffolds can be modified to create functional groups that act as hooks for biomolecules and cells. Amines, hydroxyl, carbonyl, carboxyl, epoxy groups, and thiols are the functional groups generally used for improving cell interaction or enabling the incorporation of other biomacromolecules into the scaffolds [224]. A wide range of applications can be used for chemical functionalisation of PolyHIPEs [225]. There are two main approaches for chemical functionalisation of PolyHIPEs; (i) incorporating co-monomers with desired functionality into HIPE composition and (ii) post-functionalisation of PolyHIPEs. Although the first approach seems convenient as the functionality can be improved using a one-step route, incorporating hydrophilic monomers may cause destabilisation of the emulsion, results in bigger pores, and less well-defined morphology [226]. The second approach enables the introduction of functional groups without changing the morphology of the PolyHIPEs.

Hayward et al. incorporated acrylic acid into the water phase of the styrene/DVB/EHA PolyHIPE, and they verified the success of the carboxylic acid functionalisation by X-ray photoelectron spectroscopy, wettability analysis, and toluidin blue staining [189].

Post-polymerisation of thiol-acrylate PolyHIPEs has also been reported. During the polymerisation of thiol-acrylate, there are two competing addition reactions that occur; the first one is between thiols and acrylates, and the second one is between acrylates and acrylates. With a stoichiometric thiol to acrylate ratio, the occurrence of the second reaction will result in the presence of unreacted residual thiols. These can be used for further functionalisation using various reactions, such as thiol-ene click chemistry [227] or Michael addition reaction [223].

Plasma treatment is one of the most common and effective ways of post-functionalisation to promote hydrophilicity of the polymer surfaces by adding polar groups to the surface of the material without altering the bulk properties [228–232].

Owen et al. showed that both air and acrylic acid plasma treatment improved the attachment and proliferation of mesenchymal progenitors on acrylate-based PolyHIPEs, whereas untreated scaffolds did not support cell attachment [70,85].

Pakeyangkoon et al. reported that water contact angle on poly(styrene/ ethylene glycol dimethacrylate) PolyHIPE dramatically dropped and it improved attachment of fibroblast-like cells on PolyHIPEs [233]. Recently, we reported that air plasma treatment improved the wettability of highly hydrophobic polymer, PCL PolyHIPEs, and it enhanced infiltration of bone cells through PolyHIPE scaffolds [13].

#### 1.2.4.4.1.2. *Incorporation of ceramic particles*

Incorporating HA, a bioceramic that is present in native bone, forming about 70% of the matrix, within a scaffold is a common approach to improve the biocompatibility, osteoconductivity, and osteoinductivity of polymer-based bone TE scaffolds. Although emulsions are metastable systems that are readily destabilised by incorporation of additional particles, many researchers have managed to incorporate nano/micro HA particles into the various PolyHIPE compositions to improve the biological or mechanical properties of PolyHIPEs rather than using HA as Pickering particle.

HA is commonly included in HIPE composition before emulsification. It can be added either into the oil phase or into the water phase. Akay and Bokhari et al. incorporated commercially available HA into the water phase of the w/o PolyHIPEs to be able to locate the HA particles only on the surface of the pores. They showed that 0.5% HA (of the aqueous phase) incorporated DVB/styrene PolyHIPE increased the viability of cells, cell penetration into the scaffolds, and osteoblast differentiation *in vitro* [131,159]. Wang et al. incorporated 4-32% HA that was synthesised *in house* into the water phase of the EHA:IBOA PolyHIPE [134]. No pore size difference was observed between groups except that 32% HA incorporated HIPEs showed reduced stability and increased pore size. However, the tensile modulus of this group was increased more than 2-fold in comparison to the control group, probably due to having bigger pore sizes. Lee et al. incorporated (5-10%) HA and strontium-modified HA into PolyHIPE composition by adding it into the oil phase of the emulsion [187]. HA incorporation increased the pore size distribution with increasing concentration and significantly increased the compressive strength. Although it was incorporated into the oil phase, SEM/Energy Dispersive X-Ray Analysis (EDX) images showed the presence of HA

particles on the surface of the scaffolds as well. Incorporation of HA, particularly strontium-modified HA, increased cell adhesion and proliferation when compared to unmodified PolyHIPE. Similarly, Robinson et al. incorporated 2wt% calcium phosphate nanoparticles, 5wt% HA nanoparticles, and 15wt% demineralised bone matrix (DBM) particles into injectable PFDMA HIPEs [190]. Particles affected neither the emulsion stability nor the pore size of the PolyHIPEs. Similar to the results of Lee et al., although the particles were added into the oil phase of the emulsion, transmission electron microscopy (TEM) images showed the localisation of the particles on the surface unless they aggregated.

#### *1.2.4.4.1.3. Incorporation of biomolecules*

Incorporation of the biomolecules into the composition of PolyHIPE scaffolds requires moderate operation conditions in terms of temperature and solvents. Biomolecules such as peptides and ECM proteins can be either covalently attached to the surfaces or physically absorbed/coated to the PolyHIPEs.

Robinson et al. applied biologically inspired self-assembling peptide hydrogel into HA-doped styrene PolyHIPEs via cell seeding suspension. Osteoblast (OB) penetration depth and the alkaline phosphatase (ALP) activity have been shown to be increased in comparison with the control [159]. Hayman et al. used Poly-D-lysine and laminin coating on DVB/styrene PolyHIPEs and showed the advantages of Poly-D-lysine and laminin coating over only Poly-D-lysine coating in terms of increasing the mean neurite length [119,120]. Eissa et al. reported that fibronectin coating of thiolene PolyHIPEs significantly increased the attachment, proliferation and infiltration of primary human endometrial epithelial and stromal cells when compared to the uncoated PolyHIPEs [234].

Richardson et al. functionalised thiol-acrylate PolyHIPE scaffolds with covalent attachment of fibronectin using a two-step procedure. First, they functionalised PolyHIPEs with N-sulfosuccinimidyl-6-(4'-azido-2'-nitrophenylamino hexanoate (sulfo-SANPAH)), which is a photo-linker compound that enables conjugation of biomolecules to the surfaces, and then they further functionalised the surface by covalent attachment of fibronectin to sulfo-SANPAH molecule. An improved cell attachment and infiltration of human endometrial stromal cells have been found when compared to unmodified, just sulfo-SANPAH functionalised, and fibronectin-absorbed (physically) PolyHIPEs [136].

Ratcliffe et al. functionalised thiol-acrylate PolyHIPE using maleimide-derivatised cyclo-arginine-glycine-aspartate (RGD) peptide by benefiting from the reaction between the unreacted thiols in PolyHIPE and the maleimide. While non-functionalised scaffolds did not support attachment and proliferation of human embryonic stem cells, PolyHIPEs functionalised with RGD showed significantly higher proliferation and infiltration rate [223].

Hayward et al. incorporated pentafluorophenyl acrylate (PFPA) into the oil phase of the styrene HIPE to be able to conduct a coupling reaction between ester groups of PFPA and galactose afterwards, as hepatocytes are known to have specific receptors that bind to galactose. Hepatocytes have been shown to proliferate on the functionalised scaffold, and they showed significantly higher activity on galactose functionalised PolyHIPEs in terms of albumin synthesis compared to cells cultured on unmodified PolyHIPEs [160].

In our recent study, we decorated 3D printed PCL PolyHIPE scaffolds with *in vitro* cell generated bone ECM rather than a single biologically active agent [75]. This collagen

and mineral-rich ECM coating was shown to improve attachment and proliferation of human mesenchymal progenitor cells (hES-MPs). Both angiogenic and osteogenic activities of biohybrid scaffolds were found to be significantly higher than the activities of the non-coated PolyHIPes [75].

**Table 1.4:** Various functionalisation strategies for PolyHIPE scaffolds from the literature.

Approach	Monomer/macromer	Improvement	Results	Ref
Chemical functionalisation/ Incorporation of functional monomers	Styrene, divinylbenzene, and 2-Ethylhexyl acrylate	Incorporation of the monomer acrylic acid into the water phase of w/o emulsion	7.5% carboxylic acid functionality Increased wettability No adverse effect on cell attachment	[189]
Chemical functionalisation/ Post-functionalisation	Poly(styrene/ ethylene glycol dimethacrylate)	Air plasma treatment	Increased wettability Enhanced cell attachment	[233]
	2-Ethylhexyl acrylate and isobornyl acrylate	Air plasma or acrylic acid plasma treatment	Enhanced cell attachment and cellular metabolic activity	[70]
	Photocurable polycaprolactone	Air plasma treatment	Increased wettability Enhanced cell infiltration	[13]
Incorporation of ceramic particles	Styrene	Hydroxyapatite/internal phase	Higher cell viability, penetration and osteoblast differentiation	[131,159]
	2-Ethylhexyl acrylate and isobornyl acrylate	Hydroxyapatite/internal phase	Improved tensile modulus	[134]
	Thiol-acrylate	Hydroxyapatite and strontium-modified hydroxyapatite/ continuous phase	Improved cell adhesion and proliferation	[187]
	Poly fumarate dimethacrylate	Calcium phosphate, hydroxyapatite / demineralised bone matrix	Improved gene expression in some osteogenic markers	[190]
Incorporation of biomolecules	Styrene	Peptide coating (Physical)	Improved osteoblast penetration depth and the alkaline phosphatase activity	[159]
	Styrene	Poly-D-lysine & laminin coating (Physical)	Poly-D-lysine & laminin coating was found advantageous over only Poly-D-lysine	[119]
	Thiolene	Fibronectin coating (Physical)	Improved cell attachment, proliferation and infiltration	[234]
	Thiol-acrylate	Maleimide-derivatised RGD peptide attachment	Improved cell attachment and proliferation	[136]
	Photocurable polycaprolactone	<i>In vitro</i> cell-derived extracellular matrix deposition	Improved cell attachment and proliferation, Enhanced osteogenic and angiogenic activity	[75]
Chemical functionalisation/ Incorporation of functional monomers + Incorporation of biomolecules	Thiol-acrylate	Functionalisation with sulfo-SANPAH + Covalent fibronectin attachment	Improved cell attachment and infiltration	[136]
	Styrene	Incorporation of pentafluorophenyl acrylate into the oil phase of the HIPE + Galactose attachment	Higher albumin synthesis by hepatocytes	[160]



#### **1.2.4.4.2. Washing**

Following the fabrication of the emulsion templated scaffolds, typically a series of washing steps need to be applied to remove uncured material and residual surfactant. Insufficient washing of scaffolds may cause a toxic effect on cells. Also, they may give false colour changes on colourimetric cell viability assays such as MTT (3-[4, 5-dimethylthiazol-2-yl]-2, 5 diphenyl tetrazolium bromide) and resazurin reduction. The washing process can be conducted by either a series of manual soakings in selected solvents or using Soxhlet extractor.

The solubilities of the materials that need to be removed should be considered for the selection of the washing solvent. Acetone is one of the commonly used solvents for washing of PolyHIPE scaffolds due to the high solubility of a wide range of polymers in acetone [99,136,160]. In our recent studies, we have used methanol instead of acetone due to it being less toxic and less destructive to crosslinked monoliths [13,42]. There are also studies reported using different solvents such as isopropanol [159] or combinations of multiple solvents [109,143].

A limited number of studies have reported the effect of the washing method, duration and the choice of solvent on the features of PolyHIPE. Pakeyangkoon et al. showed that duration of solvent extraction has an impact on the surface area and mechanical properties of the PolyHIPEs [235]. While an extraction time of between 6-12 hours improves the surface area and mechanical properties compared to non-extracted samples, mechanical properties become poorer than control when the extraction time is longer than 12 hours.

#### **1.2.4.4.3. Sterilisation**

TE scaffolds should be free of contamination by living organisms such as bacteria and viruses for *in vitro* and *in vivo* tests and also for implantation to the human body. There are various methods used for this purpose, such as treatments with heat [236,237], gamma irradiation [236], UV [238], plasma [239,240], ethylene oxide [237,238], ethanol [240], and peracetic acid [237]. As the efficiency of the methods in terms of the degree of removal/inactivation of microorganism varies, it might be appropriate to clarify the difference between the terms of disinfection and sterilisation. While disinfection reduces the number of organisms present, this method cannot provide removal of all microorganisms, including spores. However, sterilisation indicates the removal of all kind of microorganisms including spores [241]. Most common sterilisation techniques in the clinics are ethylene oxide, gamma irradiation, and heat treatment. However, some of these methods have been found to cause compositional changes in the biomaterials [236,242,243].

Ethanol and UV treatment are commonly used for inactivation of the microorganisms on biomaterials for *in vitro* applications. However, ethanol treatment cannot inactivate bacteria spores, non-enveloped viruses, and prions. UV treatment works by damaging the DNA of microorganisms, and the major drawback of this technique is the limited penetration depth of UV. In addition, it was also found to be insufficient for inactivation of mycobacteria, bacteria spores, non-enveloped viruses, and prions. Thus, ethanol and UV treatments are categorised as medium level inactivation methods [242].

The sterilisation/disinfection method of the scaffolds should be selected by considering the material properties, application type, and experiment duration. Inactivation of microorganism on PolyHIPE scaffolds was commonly reported by using

ethanol [99,119,129,234]. There are also several studies that reported the use of UV irradiation [38,90], gamma-irradiation [146], electron-beam irradiation [154], and autoclave [140,193]. Future studies investigating the effect of sterilisation methods on physical, chemical, and mechanical properties of emulsion templated scaffolds are needed to establish a greater degree of understanding of this matter.

### **1.2.5. PolyHIPes in TE applications**

#### *1.2.5.1. In vitro models*

In 2018, 3.53 million procedures involving living animals were conducted in the United Kingdom, and 56% of these procedures were for basic research purposes [244]. Although animal models are the gold standard due to their better ability to mimic complex human physiology, the 3R approach, replacing, reducing and refining of animal-based tests, should also be considered where possible [245]. As an alternative to these *in vivo* platforms, the use of *in vitro* models has gained attention in various research areas such as; testing new drugs, studying diseases and monitoring of the natural behaviour of the cells at different scales [246]. *In vitro* models aim to mimic the natural environment of the cells isolated from the body in architectural, mechanical and biological aspects to be able to encourage cells to behave in a similar way as they would behave in their own niche *in vivo*.

Cells populated in 2D tissue culture plates (TCPs) are known not to be a good representative of the *in vivo* environment of the cells. Cells grown in 2D have shown to have flattened morphology opposed to their stretched 3D morphology *in vivo*, and they have been reported to have less similar gene expression profiles to that observed *in vivo* [247].

Non-degradable or slow-degrading 3D emulsion templated substrates are attractive *in vitro* test platforms due to their tunability in the physical and mechanical properties for different applications, ease of fabrication, reproducibility, and stability for long term experiments [234].

Styrene PolyHIPEs have been used as an *in vitro* platform by many researchers. Hayman et al. proposed the differentiation behaviour of human pluripotent stem cell-derived neurons to be studied *in vitro* on styrene PolyHIPEs [119,120]. Bokhari et al. showed that styrene PolyHIPEs showed better results over TCPs in terms of cell viability, ALP activity, and osteocalcin secretion of MG63 osteoblast-like cells, and better represents *in vivo* [173]. The same group also cultured hepatic carcinoma cells on polystyrene PolyHIPE and proposed this system to be used as *in vitro* platform to study toxicity and screening of drugs [248]. Similarly, Sun et al. used styrene PolyHIPEs as a 3D tissue model to study the cytotoxicity of cigarette smoke [249]. Polystyrene PolyHIPE is also commercially available (Alvetex®) on the market. Costello et al. developed a multi-layered skin equivalent on these scaffolds and suggested its use for disease modelling and testing of cosmetics' active compounds [250].

Non-degradable EHA and IBOA PolyHIPEs were also shown to support bone cell proliferation [133,162] and osteosarcoma growth [133], and they were suggested as an *in vitro* platform to study tumour tissue [133]. Eissa et al. proposed DPEHA and trimethylolpropane tris(3-mercaptopropionate) (trithiol) PolyHIPEs as an *in vitro* model that could mimic native human endometrial architecture and function [234].

Recently, Severn et al. revealed that functionalised thiolene PolyHIPEs are promising platforms to mimic the bone marrow niche [251]. Recently, Dikici et al. developed a 3D

dynamic *in vitro* model using tubular PCL PolyHIPEs combined with electrospun PCL tubes that can be used for the testing of angiogenic agents (Figure 1.14D) [186]. In the developed system, PCL PolyHIPE was found to be a suitable environment for comparison of the infiltration capacity of endothelial cells in response to different pro-angiogenic factors.

#### **1.2.5.2. PolyHIPEs as TE scaffolds**

Tissues in the body are subjected to various mechanical forces including compression, tension, torsion, and bending, and have some mechanical features such as; Young's modulus, toughness, elasticity, tensile, and compressive strength. These mechanical features vary depending on tissue type and function. Mechanical properties of the scaffolds are proposed to be required to match with the mechanical properties of the host tissue to avoid over/under mechanical loading and undesirable, heterogeneous stress distribution. Required Young's modulus of scaffolds has been reported to be in the range of 10–1500 MPa and 0.4–350 MPa for hard and soft tissues, respectively [9]. Also, cells can sense and respond to the mechanical forces in their microenvironments (mechanosensitivity). Thus, the elasticity of the surface that cells are attached is also known to affect cell behaviour, such as differentiation to specific phenotypes [252,253].

##### **1.2.5.2.1. PolyHIPEs for Hard TE**

###### *1.2.5.2.1.1. Basics of bone biology, anatomy and physiology*

Bone is a complex organ that has various roles in the human physiology such as; protecting internal organs, facilitating movement, housing bone marrow and progenitor cells, blood production, acting as mineral storage and homeostasis. The

bone ECM is composed of 60% inorganic component that is dominantly HA and 40% organic matrix which is predominantly collagen type I (90% of all proteins), trace amounts of collagen type III and V, and non-collagenous proteins such as proteoglycans, matrix proteins, cytokines and growth factors [254,255]. An adult skeleton has 206 bones and they classified by shape as long bone, short bone, flat bone, irregular bone and sesamoid bone. Long bones have a tubular shape with hollow shaft and end expanded for articulation with other bones, such as bones of arms and legs. Short bones are small, cuboidal bones and they present in ankles and wrists. Flat bone is plates of bone and often curved. Skull, mandible, ribs are categorised as flat bones. Irregular bones can be in various shapes, and sacrum and coccyx are examples for the irregular bones. Sesamoid bones are the round and oval nodules in a tendon [256].

Osseous tissue can be categorised as woven bone or lamellar bone depending on the organisation of the collagen fibrils (Figure 1. 12). Woven bone is immature bone and has disorganised collagen fibre orientation and forms during foetal development and tissue repair. On the other side, lamellar bone has highly organised collagen fibres and layered structure (lamellae).

The types of bone based on their macro-structure are cortical (compact) bone and trabecular (cancellous, spongy) bone. Cortical bone is the dense, solid outer shell of most of the bones in the body. Cancellous bone is the inside of the bone and has high porosity and made of open cellular, interconnecting rods. The surface of the bones is covered with the periosteum that is the outer membrane made of connective tissue.

The microarchitectures of cortical and trabecular bone are significantly different. The fundamental structural unit of the compact bone is osteon. It is composed of concentric cylindrical structures (Lamella) that surrounds the Haversian canal (Figure 1.12).

Osteons are connected to each other with Volkmann's canal. Both Haversian and Volkmann's canal hosts nerved and blood vessels. Lacunae are the small spaces between lamellae, and they hold osteocytes. Canaliculi is the fine branches of lacunae that enables communication of the osteocytes and transportation of waste and nutrients. The main microscopic difference between cortical and trabecular bone is that lamellae of the trabecular bone are not concentric and does not form osteons and vascular channels (Haversian channel) [257,258].

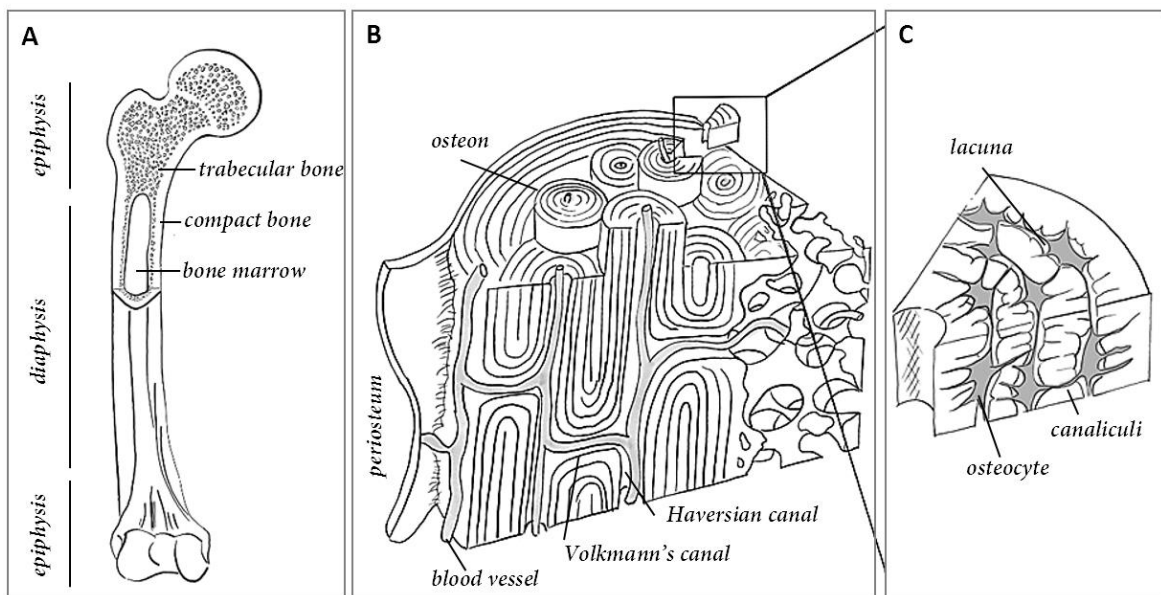


**Figure 1.12:** The hierarchical structure of bone.

There are four types of bone cells; osteoprogenitor cells, osteoblasts, osteocytes and osteoclasts. Osteoblasts are cuboidal cells that are generated from osteoprogenitor cells, and they are responsible for matrix production. They produce type I collagen and mineralised ECM by depositing HA crystals on collagen fibrils, and they show high ALP activity and also produce non-collagenous proteins. Osteocytes are terminally differentiated cells of the osteogenic lineage and the most abundant cells in bone. They are embedded in the bone matrix, and they are responsible for form maintaining the matrix and mineral haemostasis. Osteoclasts are multinucleated cells, they form from

hematopoietic stem cells, and they are responsible for the resorption of the bone by dissolving the mineralised matrix via acid and enzymatic breakdown of the collagen [259].

Bone is a metabolically active and highly dynamic organ. It remodels itself throughout life for its hemostasis, to form bone shape, to replace the woven bone with lamellar bone, for reorientate fibrils and trabeculae in a favourable direction for mechanical strength, as a response to loading (Wolf's Law), to repair the damage. This metabolic process is basically based on a bone deposition by osteoblast and bone resorption by osteoclasts. In this lifelong process, all of the bones are altered, and new bone replaces with the old bone. On the other side, bone modelling is the growth and development of the skeleton, and in this process, osteoblasts and osteoclasts are not necessarily coordinated. The gross shape of the bone is altered [260].

#### *1.2.5.2.1.2. Social, economic impact of bone defects*

There are various bone-related clinical problems such as; osteogenesis imperfecta (collagen), osteopetrosis (osteoclasts), Paget's disease (focal bone turnover), osteomalacia (mineralisation defect), rickets, primary bone cancers (osteosarcoma), secondary cancer (tumour metastasis), osteoarthritis, injuries and traumas [261]. They result in a variety of socio-economic issues. Bone is the second most commonly transplanted tissue after blood. More than two millions of bone grafting procedures are conducted every year, with an estimated cost of about USD 2.5 billion [262–264]. It is estimated that there will be more than 12 million bone fracture annually in the European Union by 2050 because of the increasing age of the population [265]. The market of bone graft substitutes and dental membranes is anticipated to rise from USD 419 million (2015) to USD 922.2 million by 2024 [266]. When the disadvantages of

autografts and allografts are considered (discussed in details in Section 4.1), the development of tissue-engineered scaffold-based bone grafts is crucial [267].

#### 1.2.5.2.1.3. Use of PolyHIPEs as bone graft

In hard TE, it is highly desirable to fabricate porous scaffolds with adequate strength and Young's Modulus. Thus, PolyHIPE scaffolds made from synthetic polymers are preferable over naturally sourced polymers for hard TE applications due to their comparatively higher mechanical strength.

Akay et al. showed the biocompatibility of HA incorporated DVB-styrene scaffolds up to 35 days using primary rat osteoblasts. They penetrated up to 1.4 mm, differentiated and formed mineralised matrix [131].

We have recently investigated the potential use of PCL PolyHIPE scaffolds for guided bone regeneration (Figure 1.13A) [13]. We showed that murine long-bone osteocytes (MLO-A5s) attached, proliferated and infiltrated throughout the interconnects of the PolyHIPE scaffolds. Suitability of the pores for blood vessel ingrowth was also shown using chick chorioallantoic membrane (CAM) assay (Figure 1.14L-O).

Moglia et al. developed injectable PFDMA PolyHIPEs with an average compressive modulus and strength of 33 MPa and 5 MPa, respectively, which showed up to 95% initial cytocompatibility with fibroblasts after 24 hours [38]. Whitely et al. have developed an *in situ* cell seeding approach for 3D printed PFDMA HIPEs to be used as a bone regeneration strategy [268]. They successfully showed the homogeneous seeding of human mesenchymal stem cells (hMSCs) all over the scaffold. HMSCs on scaffolds were mineralised and showed higher ALP activity compared to hMSCs on TCP.

Langford et al. reported the fabrication of bilayer thiol-acrylate PolyHIPEs made of two different HIPE compositions [269]. They obtained PolyHIPE structures with different morphologies and suggested their use as scaffolds for the tissues that require layered designs such as ligaments, tendons, and bone attachments (Figure 1.13B).

Naranda et al. developed thiolene PolyHIPEs for cartilage regeneration and showed that PolyHIPE scaffolds fully degraded with accelerated degradation and lost 55% of their weight in PBS in 4 weeks [140]. Young's modulus of the scaffolds was measured as 0.15 MPa as prepared and 0.18 MPa after 20-day culture of primary human chondrocytes on the scaffolds. Collagen type-II deposition and gene upregulation were shown using immunostaining and PCR, respectively.

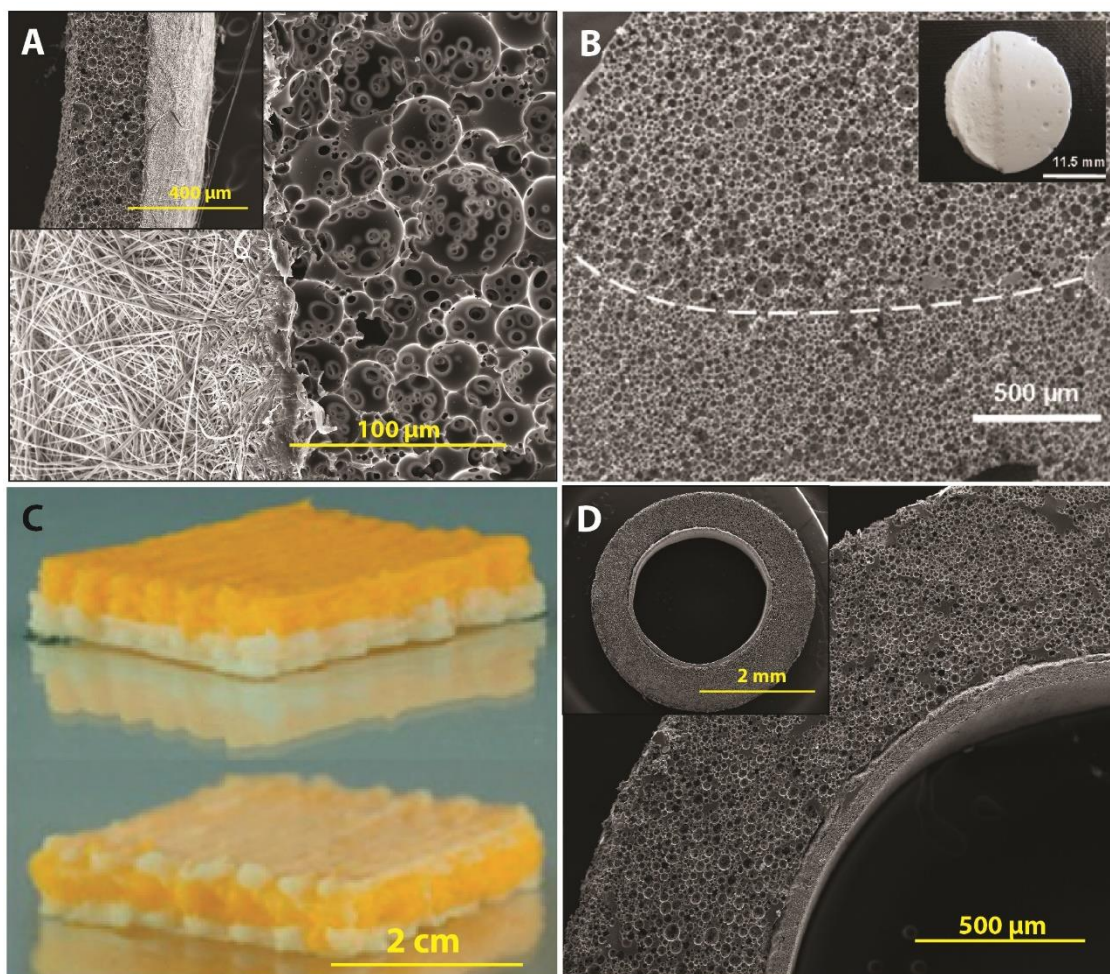


**Figure 1.13:** Hybrid PolyHIPE scaffolds with multiple layers: (A) emulsion templating combined with electrospinning for development of membrane for guided bone regeneration, (B) PolyHIPEs with two different morphologies, (C) 3D printing of drug-loaded and drug-free HIPEs selectively, and (D) emulsion templating combined with electrospinning in a tubular form for the development of *in vitro* angiogenesis model. Images A and D were reproduced with permission from ref [13] and [186] respectively, under The Creative Commons License. Image B was adapted with permission from [269] Copyright 2015 John Wiley and Sons. Image C was adapted with permission from, [146] Copyright 2017 American Chemical Society.

#### 1.2.5.2.2. PolyHIPEs for Soft TE

The two main components of soft tissues, such as skin, nerve, fascia, and blood vessels, are elastin and collagen, which both have very high water content [270]. Thus, hydrogels are preferable candidates to be used as scaffold materials for soft TE [271].

Barbetta et al. reported that dextran PolyHIPEs support penetration and colonisation of neurons into the inner cavities of the scaffold [108]. Murphy et al. showed that TMPTA, 1,6-hexanediol diacrylate (HDDA) and PEG diacrylate (PEGDA) thiolenes PolyHIPEs support proliferation, differentiation and infiltration of induced pluripotent stem cell (iPSC)-derived human neural progenitor cells (hNPCs) [272]. Especially thiolene polymerised PEGDA PolyHIPE was found to be a favourable substrate for hNPCs culture due to the similarity of its mechanical properties to the native human brain. Recently, they further explored the ability of laminin-coated PEGDA PolyHIPE for the culture of human-induced pluripotent stem cell- and embryonic stem cell-derived neural precursor cells (hPSC-NPCs) in 45-day culture period [273].

Luo et al. developed surfactant-free and solvent-free PolyHIPEs and showed the proliferation of fibroblasts and cardiac muscle cells on PVA PolyHIPE hydrogels [274]. Recently, we showed cell viability and attachment of human dermal fibroblasts (HDFs) on PCL PolyHIPEs in comparison with commercially available styrene PolyHIPE scaffolds [42]. SEM images of the HDFs suggested that the pore size of the PolyHIPEs have a profound effect on the orientation of the cells.

Moglia et al. developed injectable PCL PolyMIPES with 20-200 KPa and 4-60 KPa compressive moduli and strengths, respectively. They suggested their use for soft tissue regeneration and showed the initial cytocompatibility of PolyHIPEs with the activity of hMSC higher than 95% after 72 hours [188].

#### **1.2.5.2.3. Drug-releasing PolyHIPEs**

Controlled release of drugs and bioactive molecules is desired for accelerating tissue regeneration, controlling biological responses or inhibiting pathology. PolyHIPEs are good candidates to elute drugs in a controlled manner as the surface area of these

matrices can be precisely engineered. However, there is only a limited number of studies reporting PolyHIPE matrices as drug delivery tools.

Yang et al. incorporated enrofloxacin (ENR) solution (in DCM), a veterinary wide-spectrum antibiotic, into the oil phase of the PCL HIPEs [146]. They also showed the possibility of fabricating scaffolds using two different inks (drug-loaded and non-loaded) for the selective construction of drug-loaded parts (Figure 1.13C). Drug-loaded PolyHIPEs showed a rapid release profile with 80% and 98% release in 2.5 hours and 10 hours, respectively. Hu et al. dissolved ibuprofen, an anti-inflammatory drug, in the oil phase of PCL HIPE to create ibuprofen releasing PolyHIPE scaffolds [154]. Burst release of the drug (75-90% for various compositions) was observed within the first 8 hours. The release profile has been shown to be controllable by changing the concentration of the PCL. More research on the development of Ibuprofen-loaded PCL [275], PLGA [41], and PLA [152,275] Poly(HIPEs/MIPEs) has been reported by the same group. They also incorporated bovine serum albumin (BSA) into the water phase of the HA stabilised Pickering emulsions and showed that the release profile of BSA could be controlled by changing HA concentration in the composition [275].

All of these studies suggested promising results for the use of PolyHIPEs in drug delivery applications. The common characteristics of all the studies mentioned above were the inclusion of the drugs in the emulsion composition before emulsification, and the use of toxic solvents in the emulsion composition to dissolve the polymers. Although scaffolds were left under vacuum to remove the solvent after solidification, they did not include any washing step for the removal of any leftover uncured

materials or solvent as this step may also cause washout of the high amount of drugs from the scaffolds.

Moglia et al. developed bone morphogenetic protein 2 (BMP-2) releasing solvent-free ethylene glycol dimethacrylate PolyHIPE microspheres using w/o/w double emulsion system [210]. They reported that while the encapsulation efficiency of their system was up to 73%, this efficiency reduced to as low as 15% in the processes which required purification. In a follow-up study from the same group, they have shown the sustained release of BMP-2 over at least 14 days, and the retention of bioactivity was confirmed by osteogenic differentiation of OB cultured on these microspheres [211].

### **1.2.6. Where are we currently?**

To date, PolyHIPEs based on a wide variety of synthetic and natural materials have been developed, characterised, and tested *in vivo*. It is beyond doubt that we have gained a greater understanding of this formulation technique over the last decade. In addition to producing favourable 3D porosity, the development of surface functionalisation methods have further improved cell-material interactions of the emulsion templated matrices and increased the potential of PolyHIPEs to be used in the medical industry.

This extensively tunable fabrication technique has been used for the manufacture of TE scaffolds for various soft and hard tissues so far. The emulsion templated scaffolds have been demonstrated to support the *in vitro* growth of fibroblasts (Figure 1.14A, B) [42,107], bone cells (Figure 1.14C, D) [13,75,162], mesenchymal stem cells (Figure 1.14E) [188], mesenchymal progenitors (Figure 1.14F, G) [70,75], endothelial cells (Figure 1.14H) [186], neuronal cells (Figure 1.14I) [108,272,273], cardiac muscle cells

(Figure 1.14J) [276], and chondrocytes (Figure 1.14K) [140]. Although aforementioned *in vitro* results are promising, *in vivo* evaluation of the PolyHIPEs remains limited to the chick chorioallantoic membrane (CAM) assay which is a rapid and inexpensive *in vivo* platform to investigate initial tissue response to biomaterials and angiogenic agents [201,277]. We previously reported testing of *in vivo* biocompatibility and angiogenic activity of the PolyHIPEs in an ex-ovo CAM assay (Figure 1.14L-O) [13,75].

Bringing medical devices to market in many countries is challenging due to the strict regulations on the commercialisation process [278]. For commercialisation and clinical use of PolyHIPE matrices, there are still many issues that need to be investigated, such as; the long-term behaviour of PolyHIPEs *in vivo* and their clinical validation, the evaluation of the integration of them with host tissue, how their mechanical properties change over time, sterilisation routes, and shelf life of these matrices [279].

One of the most important changes in the Medical Device Regulations (MDR) that will come into force on May 2020 is that the human origin cells and tissues or their derivatives (in the same way as those of animal origin) will be considered as a high-risk medical device (Class III) [280]. Due to these regulatory restrictions, human or animal-sourced medical devices and implants will likely have more restrictive approval processes and a more challenging pathway for clinical approval [281–283]. Thus, synthetically sourced PolyHIPE matrices, in particular, are promising alternative substrates to be used for the fabrication of medical devices.

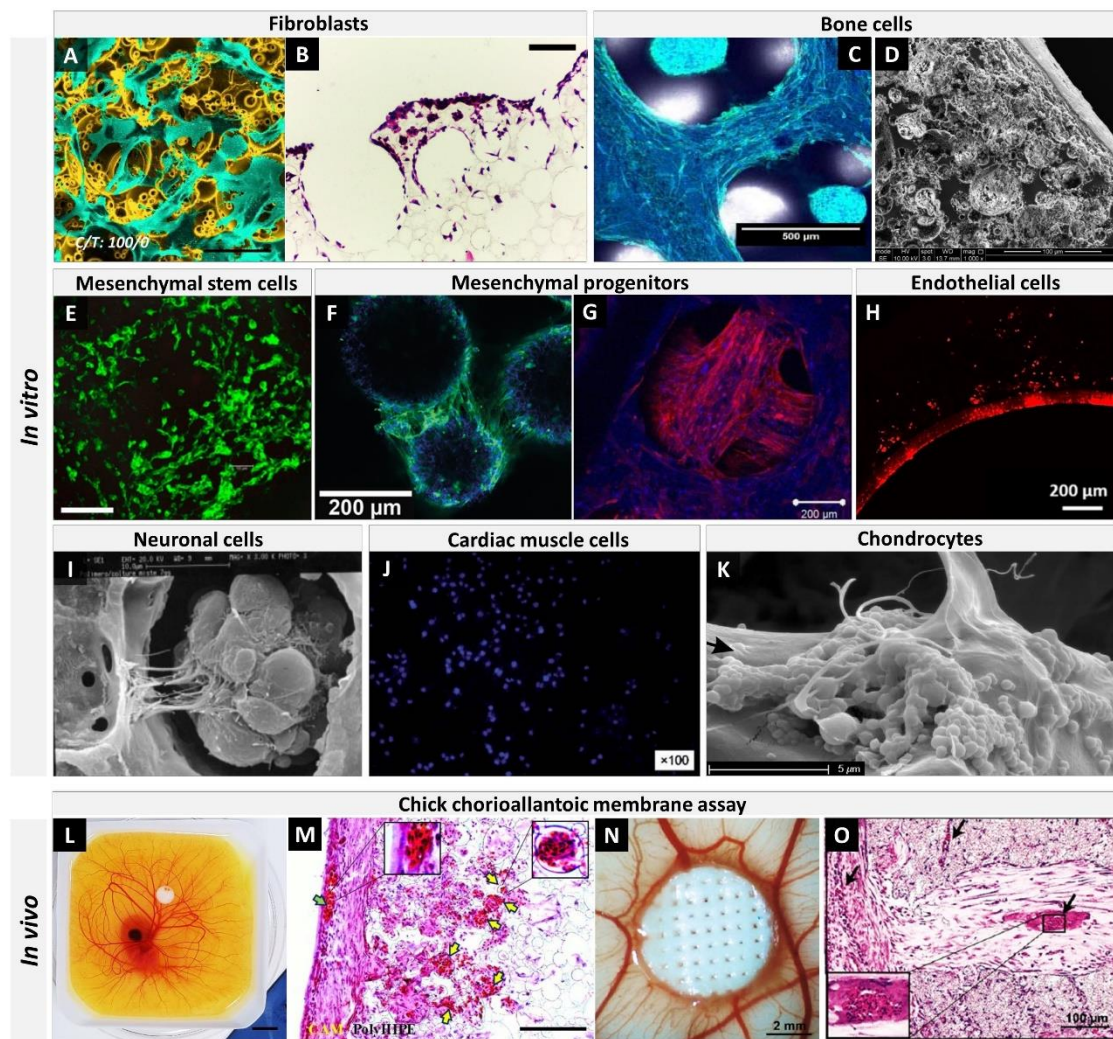


**Figure 1.14:** (A) False coloured scanning electron microscopy (SEM) image of human dermal fibroblasts on PCL PolyHIPE [42] (scale bar: 250  $\mu\text{m}$ ), (B) H&E image of L929 fibroblasts on thiolene PolyHIPE [107] (scale bar: 200  $\mu\text{m}$ ), (C) confocal microscopy image of MG63 bone cells on EHA:IBOA PolyHIPE (DAPI and Phalloidin-FITC) [133] (scale bar: 500  $\mu\text{m}$ ), (D) SEM image of murine long-bone osteocytes (MLO-A5s) on PCL PolyHIPE [13] (scale bar: 100  $\mu\text{m}$ ), (E) confocal microscopy image of mouse bone mesenchymal stem cells (mBMSCs) on PCL PolyHIPE (Calcein-AM stained)[146] (scale bar: 200  $\mu\text{m}$ ), (F) confocal microscopy image of human embryonic stem cell-derived mesenchymal progenitor cells (hES-MPs) on EHA:IBOA PolyHIPE (DAPI and Phalloidin-FITC) [97] (scale bar: 200  $\mu\text{m}$ ), (G) confocal microscopy image of hES-MPs on EHA PolyHIPE (DAPI and Phalloidin-TRITC) [70] (scale bar: 200  $\mu\text{m}$ ), (H) fluorescent microscopy image of human aortic endothelial cells (HAECs) on PCL PolyHIPE (Phalloidin-TRITC) [186] (scale bar: 200  $\mu\text{m}$ ), (I) SEM image of mix nerve cells (extracted from mice retina) on dextran PolyHIPE [108] (scale bar: 10  $\mu\text{m}$ ), (J) fluorescent microscopy image of cardiac muscle cells (H9c2s) on polyacrylamide PolyHIPE (DAPI) [276], (K) SEM image of human articular chondrocytes on polyester PolyHIPE [140] (scale bar: 5  $\mu\text{m}$ ), (L) PCL PolyHIPE on chick

chorioallantoic membrane (CAM) [13] (scale bar: 10 mm), (M) H&E image of PCL PolyHIPE on CAM at day 14 (green arrow indicates the blood vessel on the CAM itself; yellow arrows indicate the blood vessels in PCL PolyHIPE [13] (scale bar: 100  $\mu\text{m}$ ), (N) in vitro bone ECM decorated 3D printed PCL PolyHIPE on CAM [75] (scale bar: 2 mm), (O) H&E image of in vitro bone ECM decorated 3D printed PCL PolyHIPE on CAM at day 14 (black arrows indicate the blood vessels) [75] (scale bar: 100  $\mu\text{m}$ ). Images were reproduced with permission from the indicated references. Images A, C, D, F, G, H, K were adapted from [42], [133], [13], [97], [70], [186], [140], respectively, L and M were adapted from [13], N and O were adapted from [75], under The Creative Commons License. The image B was adapted with permission from [107], Copyright 2015 Royal Society of Chemistry. Image E was adapted with permission from [146], Copyright 2017 American Chemical Society. The image I was adapted with permission from [108], Copyright 2005 John Wiley and Sons. Image J was adapted with permission from [276], Copyright 2015 Royal Society of Chemistry.

### **1.2.7. Conclusion and prospective outlook**

Emulsion templating is a favourable scaffold fabrication technique with various advantages, such as enabling high porosity, providing high interconnectivity, having high tunability of the architecture, mechanical properties and functionality, being suitable to be fabricated in various forms using a wide range of materials. Important to note is that emulsion templating can be used as a reliable fabrication method, but the production is dependent on a large number of process variables, and the fabrication setup is extremely sensitive to changes in the composition and condition of the process. Thus, to be able to have control over the morphology and the mechanical properties of the scaffolds, it is important to know the effect of individual parameters on the PolyHIPE properties. We devised this review as a guide text for the use of emulsion templating as a TE scaffold fabrication route by summarising the key points that should be considered during the PolyHIPE fabrication process.

The main challenge of emulsion templating is to remove the toxic organic solvents used in emulsion composition and other impurities such as unreacted monomers and

residual surfactant. Thus, especially solvent-free and surfactant-free HIPE compositions are considered as promising and cost-effective as they eliminate the solvent and impurity removal steps.

For improved scaffold-biological tissue interaction, more studies focusing on the development of o/w PolyHIPEs with enhanced mechanical properties and development functionalised w/o PolyHIPEs is needed. We are confident that emulsion templating will become an increasingly popular scaffold manufacturing technique in the next decade by considering the increasing number of publications on emulsions templating and TE. Also, future studies that concentrate on the investigation of long term behaviour of PolyHIPE matrices *in vivo* would aid to establish a greater degree of understanding on the potential of emulsion templated matrices to be used in the clinic.

### 1.3. Research Aim and Objective

The main aim of the work presented in this thesis is to develop emulsion templated substrates that can be used for tissue engineering applications and to investigate their potential to be used as scaffolds in the clinics.

To achieve the main goal, the following aims and objectives were targeted in each chapter;

1. Chapter 1 is a review article that investigates emulsion templating as solely a scaffold fabrication technique and summarises the basics of the techniques while highlighting the related literature. Although photocurable polycaprolactone (PCL) was used as a polymer in this thesis, the review summarises an overall roadmap that can be applied to any polymer to fabricate emulsion templated scaffolds.
2. The aim of Chapter 2 is the development of emulsion templated matrices made of solely photocurable PCL as a monomer by achieving the following tasks;
  - a. Investigating the effect of diluting solvent on characteristics of HIPEs and PolyHIPEs and having control on morphological and mechanical properties of these matrices by changing the diluting solvent volume and composition.
  - b. Performing an initial cytotoxicity test on PCL PolyHIPEs with fibroblasts.
3. The aim of Chapter 3 is investigating the suitability of emulsion templated PCL matrices to be used as a guided bone regeneration membrane by achieving the following tasks;

- a. Investigating the effect of moulding material on the surface morphology of emulsion templated matrices.
  - b. Development of an open porous membrane made of photocurable PCL PolyHIPE.
  - c. Development of bilayer membrane made of PCL PolyHIPE and electrospun PCL.
  - d. Improving the cell-material interaction via air-plasma treatment.
  - e. Investigating the infiltration potential of bone cells within PCL PolyHIPE.
  - f. Investigating the suitability of morphology of PCL PolyHIPE for the growth of blood vessels through the pores.
4. The aim of Chapter 4 is increasing the osteogenic and angiogenic performance of multiscale porous scaffolds by *in vitro* generated extracellular matrix decoration by achieving the following tasks;
- a. Development of the printing of photocurable PCL-based emulsions with high viscosity.
  - b. Fabrication of multiscale porous polymeric scaffolds by combining emulsion templating and 3D printing.
  - c. The population of polymeric scaffolds with bone cells to generate bone extracellular matrix.
  - d. Investigating the decellularisation approaches to remove DNA while keeping the extracellular matrix.
  - e. Investigating the cell attachment, proliferation and extracellular matrix deposition of embryonic mesenchymal stem cell progenitors *in vitro* on PCL only and biohybrid scaffolds.

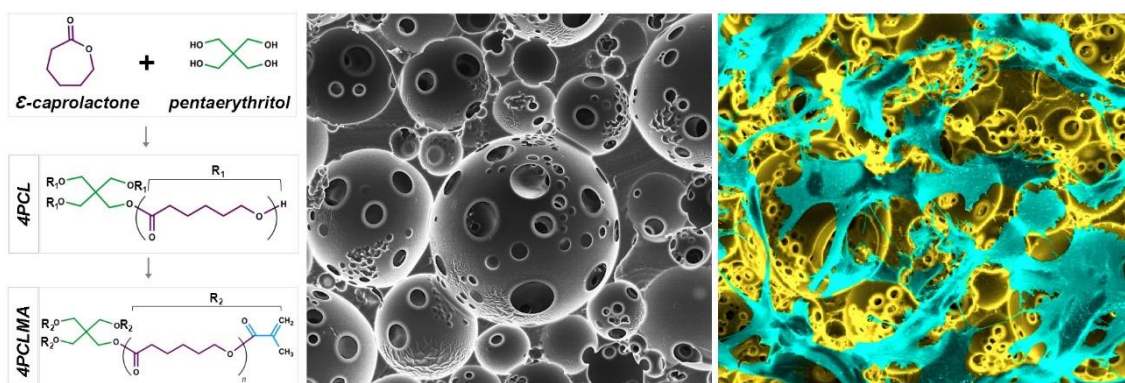
- f. Investigating the angiogenic performance of PCL only and biohybrid scaffolds *in vivo* using CAM assay.
5. In Chapter 5, the overall conclusion and future work of this study are discussed.
6. The aim of Chapter 6 is to describe the development of artistic visual materials with various techniques; such as false SEM colouring and scientific and medical illustration.



# CHAPTER 2

---

## Emulsion templated scaffolds manufactured from photocurable polycaprolactone



### **Abstract**

Emulsion templating is an emerging route for the production of highly porous scaffolds (PolyHIPEs) with interconnected porosity. Polycaprolactone (PCL) is one of the most extensively used synthetic, bioresorbable polymer for scaffold materials for both hard and soft tissues. PolyHIPEs have previously been shown to be challenging to formulate from PCL due to the high viscosity of the polymer, which limits the efficient mixing of the two phases of the emulsion. Herein, we present the development of PolyHIPEs made of photocurable 4-arm polycaprolactone methacrylate (4PCLMA) by optimising the diluting solvent composition of the oil phase. The relationship between oil phase viscosity and solvent combinations, the balance between solvent and oil phase density were investigated. Tuning the balance of these parameters was found to be critical to obtain stable HIPEs.

Stable 4PCLMA HIPEs and 4PCLMA PolyHIPEs with open pores were successfully produced via using chloroform as a diluent, and via using chloroform/toluene blends as a diluent, we were able to tune the pore size. 4PCLMA PolyHIPE scaffolds were shown to be capable of supporting cell attachment, growth, and migration.

**Keywords:** *polycaprolactone; emulsion; tissue engineering*

## 2.1. Introduction

Tissue Engineering (TE) aims to devise solutions for the healing of critical defects, i.e., defects which cannot heal naturally, within the host tissue. In a typical TE approach, biodegradable scaffolds are used to fill the defect site to provide temporary mechanical support and to serve as a three-dimensional substrate for cell attachment and proliferation. These TE scaffolds need to have a highly interconnected porous architecture to enable cell infiltration, nutrient flow and integration of the material within the host tissue [7,284,285].

Both natural and synthetic polymers can be used to produce biodegradable TE scaffolds. Natural polymers closely mimic the native extracellular matrix structure and composition, but they exhibit a number of disadvantages compared to synthetic polymers; (i) they present the risk of pathogen transmission, (ii) they can present a high degree of batch-to-batch variability, and (iii) they potentially contain protein impurities which may lead immune reaction [286]. Some advantages of synthetic polymers over naturally sourced ones are that their production is relatively inexpensive, and they can be tuned to create polymers with a range of mechanical and chemical properties [287,288].

Polycaprolactone (PCL) is one of the most extensively used synthetic and bioresorbable polymers and has been used for FDA approved drug delivery devices and sutures [289]. This makes PCL an attractive and promising biomaterial for use in other clinically relevant biomedical applications. PCL scaffolds can be used for both hard and soft tissues [17,290,291], such as bone [10], cartilage [292], vascular grafts [293], skin [294,295] and nerve [290]. Various manufacturing techniques such as gas foaming [10,11], porogen leaching [10,12] and additive manufacturing [17] have been used to introduce porosity into PCL-based scaffolds. Nevertheless, these processes have limitations, gas foaming and porogen leaching results inadequate pore interconnectivity [296], while current additive manufacturing techniques lack the resolution to build scaffolds on length scales relevant to influence cell behaviour (1-50  $\mu\text{m}$ ).

Emulsion templating is an alternative and attractive route to introduce a highly interconnected porosity into scaffolds materials [297]. The process involves mixing two immiscible liquids where one liquid (internal droplet phase) is dispersed within a continuous connected phase (the polymer) in the presence of a surfactant which stabilizes the emulsion [298]. When the volume of the dispersed droplet phase ( $\varphi$ ) is greater than 74.05%, which is the maximum packaging density of uniform spherical droplets, the emulsion is classified as a High Internal Phase Emulsion (HIPE) [299]. When the continuous phase is solidified by bulk polymerisation, that structure is defined as Polymerised HIPE (PolyHIPE).

The porosity and interconnectivity of PolyHIPEs can be tuned by the emulsion conditions or components used. Temperature, stirring speed, surfactant type/quantity, and internal phase volume are the parameters shown to affect the

morphology [35,38,69,70,97,99]. Since the specific pore size range required for cell ingrowth is cell and tissue-dependent [300], the properties of PolyHIPEs can, therefore, be tailored towards specific cell types and applications [65,131].

PolyHIPE foams made of biodegradable materials such as polypropylene fumarate (dimethacrylate) [36,38], thiol-enes [135], and ethylene glycol dimethacrylate [210] have been reported. However, fabrication of HIPE foams made of PCL is challenging because of the high viscosity of the polymer, which constrains the mixing of two phases during emulsion formation [35,115–117].

The earliest reported PolyHIPE made from PCL was created by copolymerisation of PCL diacrylate with substantial amounts of non-degradable monomers [35]. In particular, up to 40 wt. % PCL diacrylate was incorporated into the PolyHIPE composition, but the emulsion did not form beyond this mixing ratio due to the high viscosity of the oil phase. This was confirmed by Lumelsky et al. who developed vinyl terminated PCL-based PolyHIPE and highlighted that the high viscosity of PCL limited the incorporation of PCL to above 50 wt. % [117].

The viscosity of the oil phase can be reduced via increasing the temperature of the system or diluting the oil phase with a solvent. Diluting the polymer with solvents (defined as diluents or porogenic solvents) is an attractive method to control the viscosity of the oil phase compared to simply increasing the temperature, as raising the temperature can lead to emulsion separation due to the increased mobility of the water droplets [69,99].

Busby et al. used toluene as a diluent to produce a PCL diacrylate-based PolyHIPE, but the monoliths did not show an open cellular PolyHIPE structure [35]. Also, David et al.

produced polyurethane PolyHIPE foams via step-growth polymerisation of diisocyanate and PCL triol and used tetrahydrofuran to reduce to the high viscosity of the oil phase [106]. Changotade et al. used toluene as a diluent to create PCL polyurethane PolyHIPEs [105]. Johnson et al. used 1,2-dichloroethane as a porogenic solvent to reduce the viscosity of the oil phase, which was a blend of the photocurable monomers containing thiol and PCL triacrylate, and they were able to incorporate up to 76% PCL-TA into the PolyHIPE structure [107].

Recently, the development of non-reactive PCL-based PolyHIPEs has been reported. This requires dissolving high molecular weight PCL beads in various solvents such as dichloromethane [146,153,184], toluene [138], tetrahydrofuran/methanol [185], to produce stable PolyHIPEs from these emulsions via solvent evaporation.

All these studies concluded that either to reduce the viscosity of functionalised PCL or to dissolve the high molecular weight PCL, a diluting solvent needs to be used for PolyHIPE production. Although the effect of solvent on the PolyHIPE morphology has been investigated [36,301], these studies have been limited to single-solvents and only show the effect of solvent type or volume on the PolyHIPE morphology and emulsion stability. The effect of solvent blends, and in particular the interplay between the different solvent densities and their effect on emulsion stability and morphology are yet to be clearly established.

In this study, we investigated the most suitable solvent composition to dilute 4-arm PCL methacrylate (4PCLMA) to produce a PolyHIPE scaffold. Chloroform and toluene were tested systematically as diluent solvents. The effects of solvent volume, solvent density and oil phase viscosity on the stability of HIPEs and the morphology of PolyHIPEs were investigated. Stable 4PCLMA HIPEs and open porous 4PCLMA

PolyHIPEs were successfully developed using chloroform as a diluent, and we were able to tune the pore size via using chloroform/toluene blends as a diluent. To be able to control the scaffold morphology using different solvent blends allows us to tailor scaffolds for specific tissue engineering applications. Cell viability of human dermal fibroblasts (HDFs) on the 4PCLMA PolyHIPE scaffolds was investigated, and they were compared to a commercial PolyHIPE-based scaffold, Alvetex®.

## **2.2. Experimental**

### **2.2.1. Materials**

Pentaerythritol (98%),  $\epsilon$ -caprolactone, tin(II) 2-ethylhexanoate (stannous octoate (SnOct<sub>2</sub>)), triethylamine (TEA), methacrylic anhydride (MAAn), hydrochloric acid (HCl), photoinitiator (PI) (2,4,6-Trimethylbenzoyl Phosphine Oxide/2-Hydroxy-2-Methylpropiophenone blend), Dulbecco's Modified Eagle Media (DMEM), fungizone, fetal calf serum (FCS), penicillin/streptomycin (PS), L-glutamine, trypsin, paraformaldehyde, resazurin sodium salt, glutaraldehyde, ethanol, hexamethyldisilazane (HMDS), hematoxylin solution, eosin y solution, were all purchased from Sigma Aldrich. Dichloromethane (DCM), industrial methylated spirit (IMS), xylene and methanol were purchased from Fisher Scientific. DPX mounting medium for microscopy was obtained from Merck. The surfactant Hypermer B246-SO-M was received as a sample from Croda. Tissue freezing medium was purchased from Leica Biosystems. Alvetex® polystyrene scaffolds were obtained from Reinnervate. All materials were used without further purification.

## 2.2.2. Synthesis of 4PCLMA

Throughout the manuscript, 4PCL and 4PCLMA were used to define 4-arm non-methacrylated PCL and 4-arm methacrylated PCL, respectively.

Synthesis of 4PCLMA has been performed in two steps: (i) 4PCL synthesis via ring-opening polymerisation, (ii) methacrylate functionalisation of hydroxyl end groups of 4PCL.

### 2.2.2.1. Synthesis of 4PCL

Under nitrogen flow, pentaerythritol (12.00 g, 0.088 mol) and  $\epsilon$ -caprolactone (80.49 g, 0.705 mol) were added into a three-neck round-bottomed flask, and the system was heated to 160°C using an oil bath while being mixed at 200 rpm using a magnetic stirrer. When the pentaerythritol was completely dissolved, 50  $\mu$ l of tin(II) 2-ethylhexanoate (1.25 g/ml, 0.08 wt. % of the monomer) was added from the middle neck of the round flask, and the system was left overnight to react to form 4PCL. Finally, the system was removed from the oil bath and left to cool down in the ambient atmosphere.

### 2.2.2.2. Methacrylate functionalisation of 4PCL

4PCL was dissolved in 300 mL of DCM, and then TEA (52.65 g, 0.52 mol) was added. Reagents were stirred, and a further 200 mL of DCM was added to ensure everything was dissolved. The flask was placed in an ice bath. MAAn (80.22 g, 0.52 mol) was dissolved in 100 mL DCM and transferred into a dropping funnel (~1 drop per second). When the MAAn was completely dispensed, the ice bath was removed, and the system was maintained at room temperature (RT) overnight while continuously stirring (375 rpm). To remove the TEA, MAAn, and salts, the 4PCLMA pre-polymer was washed with

HCl solution (1 M, 1000 mL) prepared from concentrated HCl (37%, 12 M) and deionised water (dH<sub>2</sub>O). Subsequently, the mixture was washed twice with dH<sub>2</sub>O to remove any salt. Using a rotary evaporator, almost all solvent was removed. The 4PCLMA solution was transferred into a bottle filled with methanol and placed in a -80°C freezer until the precipitate formed at the bottom (overnight). The supernatant methanol was removed, and fresh methanol was added. These steps were repeated at least three times. Any remaining solvent was removed using a rotary evaporator, and then 4PCLMA was stored in a cold durable glass in the freezer (-20°C).

### **2.2.2.3. Characterisation of 4PCLMA**

#### **2.2.2.3.1. *Proton nuclear magnetic resonance***

To confirm the structure of 4PCLMA, proton (<sup>1</sup>H) NMR spectroscopy analysis was performed on an AVANCE III spectrometer at 400 MHz. The spectra were recorded using an 8.2 kHz acquisition window, with 64k data points in 16 transients with a 60 s recycle delay (to ensure full relaxation). Deuterated chloroform was used as a diluent (CDCl<sub>3</sub>). Spectra were analyzed using MestReNova software. Chemical shifts were referenced relative to CDCl<sub>3</sub> at 7.27 ppm.

#### **2.2.2.3.2. *Gel permeation chromatography***

Molecular weight and molecular weight distributions of 4PCLMA were determined using a Viscotek GPCmax VE200 gel permeation chromatography (GPC) system with a differential refractive index detector (Waters 410). Tetrahydrofuran was used as the eluting solvent at a flow rate of 1 mL/minute at 40 °C, and polystyrene standards were used as the calibration sample.

### **2.2.2.3.3. Gel fraction analysis**

Gel fraction analysis was conducted to measure the extent of crosslinking. 4PCLMA and 6% (w/w) PI were mixed in a glass vessel, and the mixture was injected into circular moulds with a diameter of 3.7 mm and the height of 1.5 mm, and photocured for 3 minutes on both sides. Initial weights of each sample ( $W_0$ ) were recorded. Then, samples were immersed in 15 mL of DCM to solubilize the uncross-linked 4PCLMA for 24 hours, and the specimens were left to dry for 6 hours in the fume cupboard and then vacuum-dried overnight at ambient temperature. The dry weights of the extracted samples ( $W_i$ ) were recorded. The same protocol was applied to the control samples apart from the DCM washing. The gel fractions were calculated using Equation 1 [302];

$$Gel\ fraction\ (\%) = \frac{W_i}{W_0} \times 100 \quad (1)$$

## **2.2.3. Preparation and characterisation of 4PCLMA PolyHIPEs**

### **2.2.3.1. Preparation of 4PCLMA HIPEs**

The term ‘oil phase’ is used to describe the combination of all the water-immiscible/low immiscible parts of the emulsion, this includes; the polymer, surfactant, photoinitiator, and solvent(s) used as a diluting agent (if applicable). Unless otherwise stated, the amount of 4PCLMA (0.40 g, 1.13 g/mL), surfactant (0.04 g, 0.94 g/mL), photoinitiator (0.06 g, 1.12 g/mL) and water (2 mL, internal phase is 82 vol. %) were kept constant in one batch of emulsion. 4PCLMA and the surfactant were added into a glass vial ( $\varnothing=25$  mm) and heated to 40 °C to dissolve the surfactant, then left to cool down. Single solvent/solvent blends (Table 2.1 and 2.2) and PI were added in the 4PCLMA-surfactant mixture, respectively. All were mixed at 375 rpm using a

magnetic stirrer (8×20 mm) for 1 minute at RT. Once the homogeneous mixture was created, water was added dropwise in 2 minutes, and the emulsion was mixed for further 2 minutes.

The term 'stable emulsion' is used to indicate that there is no observable separation of phase or coalescence of droplets in the HIPE before polymerisation.

### *2.2.3.2. Nomenclature of the 4PCLMA PolyHIPEs*

The PolyHIPE samples prepared to investigate the effect of the single solvent in this study are referred to using a code of the form XY where X is the type of the solvent used to dilute oil phase ((T) toluene, (C) chloroform and (CT)), Y indicates the volume of solvent (in mL) used in one batch of PolyHIPE (per 0.40 g polymer; this was kept constant throughout the study). For example, C0.40 is the PolyHIPE sample prepared by using 0.40 mL of chloroform as a diluting solvent of the oil phase. NS defines the group which is prepared without any diluting solvent.

The PolyHIPE samples were prepared to investigate the effect of changing the solvent ratio in a solvent blend are referred to using a code of the form C/T: K/L where K indicated chloroform percentage in a solvent blend and L indicated the toluene percentage in a solvent blend. For example, C/T:20/80 means 20 wt. % of the total solvent is chloroform, 80 wt. % is toluene.

### *2.2.3.3. Viscosity measurements of the oil phases of the 4PCLMA HIPEs*

AR2000 (TA Instruments, Ettenleur, The Netherlands) was used to characterise the viscosity of the oil phase of HIPEs. 40mm 2° steel cone plates were used with the gap of 55 micrometres at 25 °C. 0.6 mL of sample was injected, and a continuous ramp step

was applied with a shear between 0.01 to 100 s<sup>-1</sup> for 1 minute using linear mode and 50 points per decade.

#### 2.2.3.4. *Polymerisation of 4PCLMA HIPE*

For scanning electron microscopy (SEM) of the samples, 4PCLMA PolyHIPE was pipetted into silicon moulds. For cell culture, 4PCLMA PolyHIPE was loaded into a 2 mL syringe. All HIPE compositions were UV cured immediately (within 10 seconds) once prepared to capture the microstructure before breakdown. Both groups were cured for 3 minutes on both sides using the OmniCure Series 1000 curing system (100 W, Lumen Dynamics, Canada). The reported light density of the UV lamp is 18 W/cm<sup>2</sup> with a spectral output from 250-600 nm [303]. The resulting parts were recovered either from the silicon mould or syringe and soaked in methanol for removal of non-cured material for 2 hours. Following this, the samples were gradually transferred to increasing concentrations of water (50%, 100%) and then left in 100% water for a day. As it is reported that PCL PolyHIPE tends to collapse during drying [107], the samples were taken out and left in a -80°C freezer for an hour, then transferred into the vacuum oven and left for a day to preserve the porous structure of 4PCLMA PolyHIPE.

#### 2.2.3.5. *Determination of the densities and the porosities*

The densities of PolyHIPEs were calculated by measuring the mass and volume values of the cylindrical samples (diameter: 3.7 mm, height: 1.5 mm, n=3). The density of bulk 4PCLMA (n=3) was measured by gas pycnometer (Micromeritics AccuPyc II 1340, USA). The porosities of the 4PCLMA PolyHIPEs were calculated using Equation 2 [61,62].

$$\% \text{ Porosity} = \left(1 - \frac{\rho_{\text{PolyHIPE}}}{\rho_{\text{wall}}}\right) \times 100 \quad (2)$$

Where  $\rho_{\text{PolyHIPE}}$  is the PolyHIPE density and  $\rho_{\text{wall}}$  is the density of PolyHIPE wall. For the density of the wall, the measured density of the bulk polymer was used.

The expected density of 4PCLMA PolyHIPE was calculated using Equation 3;

$$\rho_{\text{expected}} = \rho_{\text{polymer}} \times (1 - \theta) \times (\text{gel fraction}) \quad (3)$$

Where  $\rho_{\text{polymer}}$  is the density of the bulk polymer,  $\theta$  is internal phase volume fraction (0.82), and the gel fraction was calculated as explained in Section 2.2.2.3.3.

#### 2.2.3.6. *Investigating the stability of 4PCLMA HIPEs*

The long-term stabilities of HIPE groups of C/T:60/40, C/T:80/20 and C/T:100/0 were tested. Emulsions were prepared using the standard protocol described in Section 2.2.3.1. The emulsions were transferred into small diameter glass vials ( $\varnothing=16$  mm) to observe any separation. The samples were covered with aluminium foil and left for five days at RT in a place, free from vibration, with a closed lid. On day 5, the emulsions were polymerised, as described in Section 2.2.3.4, in the bottle to preserve the structure. The pore sizes and amount of emulsion separation were investigated using SEM.

#### 2.2.3.7. *Morphological characterisation of 4PCLMA PolyHIPEs*

To observe the microarchitecture of 4PCLMA PolyHIPE, scaffolds were cut vertically using a razor blade and sections mounted on carbon pad adhered aluminium stubs. Samples were gold sputter-coated in 15 kV for 2.5 minutes to increase conductivity.

FEI Inspect F SEM (Philips/FEI XL-20 SEM, Cambridge, UK) was used with 10 kV power.

To calculate the average pore size and pore size distribution of the scaffolds, the following image processing steps were applied (detailed in Figure 2.7). SEM images were imported into Adobe Photoshop CS6. Fifty voids were selected randomly, and the pores were framed with a solid colour in the new layer using the ellipse tool. The areas of each pore were measured using Image J, and the diameters were calculated in Microsoft Office Excel 2016. Since the void diameters are assumed to have been exactly bisected, a statistical correction factor ( $2/\sqrt{3}$ ) was applied to adjust for the underestimation of diameter because of uneven sectioning and finally pore size histograms were created [66].

#### 2.2.3.8. *Mechanical characterisation of PCLMA PolyHIPes*

Dog-bone-shaped tensile test samples (overall length (LO); 32.5 mm, thickness (T); 2 mm, gage length (G); 7.6 mm, width of the narrow section (W); 3.2 mm, the radius of the fillet (R); 12.7, the distance between grips; 22.5 mm, width overall (WO); 8mm) were fabricated using silicon moulds based on a modified version of ASTM D638-14 (standard test method for tensile properties of plastics), Type V specimens [304]. 0.5 mL 4PCLMA PolyHIPE was pipetted into the moulds and cured for 3 minutes on each side. They were washed with methanol overnight and gradually transferred into phosphate-buffered saline (PBS) (50%, 100%) and tested as wet as it represents the cell culture conditions better. Samples were tested using Zwick Roell Z 0.5 mechanical testing machine equipped with 500 N load cell. Grip distance and extension rate was set to 10 mm and 0.02 mm/s, respectively. Both the force and elongation data were recorded. The modulus was determined using the linear-elastic region of each

sample's stress-strain curve. The ultimate tensile strength (UTS) was calculated that of the maximum force applied divided by to the cross-sectional area of the sample. Ultimate elongation is the elongation at the failure point.

### 2.2.3.9. Biological assessment of 4PCLMA PolyHIPEs

#### 2.2.3.9.1. 4PCLMA PolyHIPE scaffold fabrication and treatment for cell culture

The 4PCLMA PolyHIPE which was cured in the syringe was cut into 1 mm slices using a scalpel blade to make thin discs. Air plasma treatment was applied to enhance cell attachment on PolyHIPEs. As demonstrated in our previous work, the plasma coating improves cell attachment on these typically hydrophobic surfaces [70]. Briefly, the lid of a six-well plate was covered with aluminium foil, and the foil was pierced using a scalpel to enable diffusion of the air. Scaffolds were placed on the foil, and they were placed in the plasma machine (Figure 2.1). Air plasma (Diener Electronic, Ebhausen, Germany) was applied to PolyHIPE scaffolds with a power of 50 W and a pressure of 0.8 mbar for 60 seconds. PolyHIPEs were flipped over, and the same procedure was repeated for the other surface.

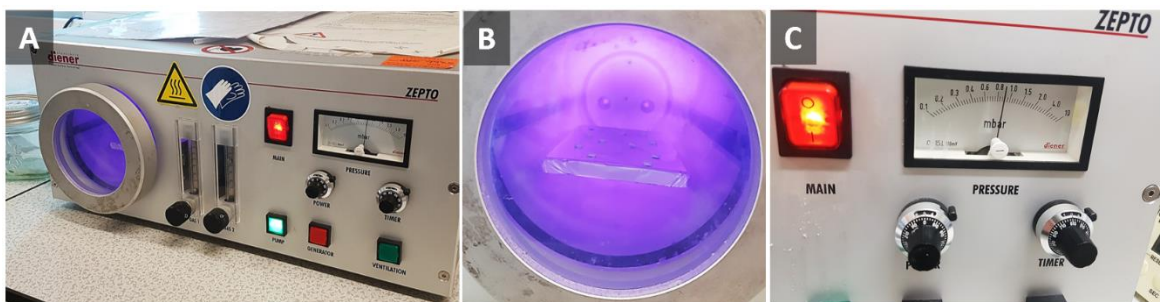


**Figure 2.1:** (A) Air plasma machine used in this study, (B) PolyHIPEs during air plasma treatment, (C) parameters used for air plasma treatment.

Alvetex® scaffolds were used as a control. 13 mm diameter Alvetex® scaffolds were cut by using a sterile punch (6 mm) to obtain the same diameter as our scaffolds.

4PCLMA PolyHIPE scaffolds were washed with 100% methanol for 24 hours with four changes to remove any remaining contaminants of surfactant, solvent or uncured material. For disinfection, 4PCLMA PolyHIPE scaffolds and Alvetex® were left in 70% ethanol for 2 hours and then transferred into PBS in sterile conditions, 4 PBS washes were applied in 24 hours. DMEM supplemented with 10% FCS, 1% L-glutamine, 1% PS and 0.25% fungizone was used as a cell culture medium. Scaffolds were then placed into 24 well-plate, and they were conditioned with culture media for an hour in the incubator.

#### **2.2.3.9.2. Isolation of human dermal fibroblasts and general cell culture**

Primary HDFs were isolated from donated skin of a patient. Skin samples were taken from a donor undergoing abdominoplasty with informed consent (Ethical approval for the tissue acquisition was granted by the local ethical approval committee of the NHS Trust, Sheffield, UK, ethics reference: 15/YH/0177).

Briefly, the skin was cut into 0.5 cm<sup>2</sup> pieces by using a sterile scalpel and left in Difco trypsin (0.1% (w/v)) (including D-glucose (0.1% (w/v) in PBS) overnight at 4 °C and washed with PBS. The epidermis was removed from dermis mechanically. Following mincing the dermal layer, they were transferred into 0.5% (w/v) collagenase A solution and incubated overnight at 37 °C for dissociating the tissue. The cell suspension was centrifuged at 2000 rpm for 10 minutes to obtain a cell pellet. Finally, HDFs were suspended in the media, expanded and frozen down for further use.

For cell culture experiments of this study, HDFs were used between passage 7-8. Cells were defrosted into T75 flask and cultured until 90% confluence. Then, cells were trypsinised, counted and centrifuged. The cell pellet was re-suspended in fresh media (25000 cells/20 µm). The media in 24 well plate was aspirated, and 20 µm of cell

suspension was placed over the surface of each scaffold homogenously and left for 2 hours in the incubator (37.5°C, 5% CO<sub>2</sub>) for cell attachment. To prevent drying of cells and to keep them inside of the well humid during this time, 4 mL medium was injected into the reservoirs between wells. After 2 hours, scaffolds were transferred into a fresh well plate, 2 mL of media was supplied into each well and incubated. For all cell culture experiments, the medium was changed in every 2-3 days.

#### **2.2.3.9.3. Assessment of cell viability on 4PCLMA PolyHIPE scaffolds**

Resazurin reduction (RR) assay was applied to measure the cellular metabolic activity and estimate the cell viability on scaffolds. Resazurin solution (non-fluorescent, blue) is reduced by the cells and forms resorufin (fluorescent, pink) which is detectable by a fluorescence plate reader. 1 mM resazurin stock solution in dH<sub>2</sub>O was diluted to 100 µM in culture media to make the resazurin working solution. 1 mL of RR solution was added into each well, and the scaffolds were transferred into a fresh well plate using sterile forceps. The well plates were protected from light and incubated for 4 hours at 37°C. From each scaffold, triplicate samples of 200 µl of the reduced solution were added to a 96 well plate. It was measured three times using a spectrofluorometer (FLX800, BIO-TEK Instruments, Inc.) at an excitation wavelength of 540 nm and an emission wavelength of 630 nm. Scaffolds were washed twice with PBS before adding fresh media. RR assay was performed at three time points (day 1, day 4, and day 7) with fresh scaffold/cell constructs for each.

#### **2.2.3.9.4. Assessment of cell penetration on 4PCLMA PolyHIPE scaffolds**

After 7 days culture of HDFs on 4PCLMA PolyHIPEs, scaffolds were washed three times with PBS, and they were fixed in 3.7% paraformaldehyde for 1 hour at RT before washing three more times with PBS. Excess fluid was removed by placing the scaffolds

on filter paper for 5 minutes before being soaked in 2 mL of freezing media in a 5 mL container. The container was kept in a vacuum oven for 2 minutes in freezing media to be penetrated into all the pores. Scaffolds were transferred into cryomolds filled with freezing media and cryomolds were immersed in liquid nitrogen for solidification. Blocks were removed from the moulds, and they were mounted into pins. 7 µm sections were sliced on glass slides using the cryostat (Leica CM1860 UV, Milton Keynes, UK). Slides were soaked in dH<sub>2</sub>O for 1 minute, and stained with hematoxylin solution for 1.5 minutes and washed with dH<sub>2</sub>O water for 4 minutes. The slides were then stained in eosin for 5 minutes. After washing with dH<sub>2</sub>O water, slides were dehydrated in 70% and 100 % IMS and dunked into xylene to remove excess dye. The slides were then mounted with DPX and viewed using a light microscope (Motic BA210, China).

#### **2.2.3.9.5. Preparation of the biological samples for SEM**

On day 4, scaffolds were washed three times with PBS after removing culture media. They were fixed in 2.5% glutaraldehyde (in PBS) at RT for 1 hour to preserve cell structure. They were rinsed with PBS for 15 minutes (3 times) and soaked in dH<sub>2</sub>O water for 5 minutes. Following this, samples were subjected to serial ethanol washes to be dehydrated (35%, 60%, 80%, 90%, and 100% for 15 minutes for each concentration). Finally, samples were treated with drying agent HMDS/ethanol (1:1) for 1 hour and 100% HMDS for 5 minutes before air drying. Samples were gold coated and visualised using methods described in Section 2.2.3.7. The false colouring of SEM images was performed manually using Adobe Photoshop CS6.

#### **2.2.4. Statistical analysis**

Statistical analyses were performed by using GraphPad Prism 6 using one-way and two-way analysis of variance (ANOVA) for mechanical testing and cellular metabolic activity assays, respectively, and plotted as mean $\pm$ SD. A difference was deemed statistically significant if the p-value was less than 0.05 and the statistical differences are denoted in the figures. The total number of replicates (n) is stated in the figure legends.

### **2.3. Results and Discussion**

#### **2.3.1. Synthesis and characterisation of the photocurable 4PCLMA**

4PCL was synthesised by ring-opening polymerisation of  $\epsilon$ -caprolactone in the presence of pentaerythritol and Sn(Oct)<sub>2</sub> as an initiator and a catalyst, respectively. Subsequently, it was methacrylate functionalised with MAAn to add photocurable end groups, as detailed in Figure 2.2A. The 4PCL synthesis and methacrylation were confirmed by <sup>1</sup>H-NMR spectroscopy.

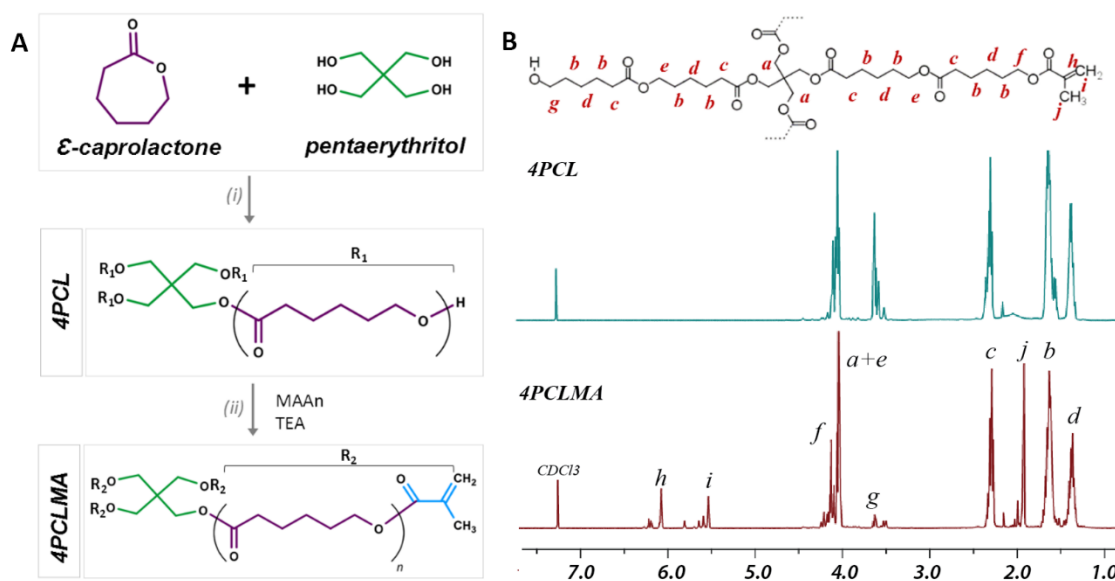


**Figure 2.2:** A. (i) Synthesis of 4PCL from the monomers via ring-opening polymerisation, (ii) methacrylate functionalisation of the hydroxyl end groups (4PCLMA), B. Chemical structure diagram and proton NMR spectrum of 4PCL and 4PCLMA and the relative assignments. Hydrogen environments in the polymer are labelled a-j.

The  $^1\text{H-NMR}$  analysis confirms the chemical composition of caprolactone in both 4PCL and 4PCLMA with the peaks at 1.6, 2.3, 1.4 and 4.1 ppm. 4PCL has methylene groups adjacent to hydroxyl end groups shown with a peak at 3.6 ppm. The methacrylation process reduces the number of these groups as they are converted into methacrylate groups; which are indicated at peaks 1.9, 5.5 and 6.1 ppm. These peaks only appear in the 4PCLMA and verify the methacrylation reaction (Figure 2.2B). This  $^1\text{H-NMR}$  data correlates well with the PCL methacrylate synthesised by Messori et al. [305]. The molecular weight of the 4PCLMA was determined by GPC analysis.  $M_w$  and  $M_n$  values are 3531 g/mol and 2648 g/mol, respectively, which gives a dispersity index of 1.33.

Photocurable PCL is not a commercially available product, and it has to be synthesised in house, so there are a limited number of studies using photocurable PCL as a PolyHIPE-based scaffold material [107]. There are other reported PCL-based PolyHIPEs, but in those studies, the PCL-based PolyHIPEs were produced via thermal

curing [35,116] or solvent evaporation [146,180], which involved a long duration (6-48 h) step for curing. In those processes, a stable emulsion is required to maintain its morphology during the polymerisation period. In our approach, the PolyHIPE was cured via photochemical crosslinking, which can be carried out in a matter of seconds to minutes, depending on the intensity of the light source and the size of the object. Via photocuring, the HIPE is almost instantaneously converted into a PolyHIPE which locks the emulsion microstructure [107,306]. 4PCLMA was chosen due to its relatively high number of functional groups, increasing the monomer functionality causes an increase in the polymerisation rate and the crosslinking density [107,307]. This is confirmed in this study; the gel fraction of the 4PCLMA was measured to be high ( $92.1\pm 3.9\%$ ), which indicates a high cross-linking density.

The cure depth in our experiments was maximum 4.5 mm, and throughout our experiments, we did not observe any cure-depth dependent difference in microstructure of 4PCLMA PolyHIPEs. This indicates that the 4PCLMA PolyHIPE was cured throughout by the high power UV-lamp. This is in line with the observations made by Kimmins et al. [308] who were able to photo-cure a 35 mm thick monolith of highly crosslinked glycidyl methacrylate-based PolyHIPE.

### **2.3.2. Diluent solvent type and amount affect the 4PCLMA PolyHIPE morphology**

#### **2.3.2.1. Incorporation of chloroform as a diluent creates porous structures**

In the first attempt of synthesis of 4PCLMA PolyHIPE, no solvent was used. This resulted in droplets of PCL floating around the water phase, Figure 2.3A. We attributed

this to the 4PCLMA oil phase being too viscous to create an emulsion when no solvent is used.

The individual contributions of the oil phase components to its viscosity were investigated. The addition of the surfactant to 4PCLMA slightly increased the viscosity of the mixtures, and the addition of PI contributed to the reduction in the overall viscosity, Figure 2.3B. But viscosity of the oil phase remained too high to form an emulsion.

Although the high viscosity of the continuous phase increases the kinetic stability, the viscosity needs to be low enough to enable efficient mixing [36,101]. When the viscosity of the polymer is too high to create a HIPE, it can be reduced by diluting the polymer with solvents [36,107]. In this study, we chose chloroform and toluene as diluent solvents to be tested because they have very low miscibility in water, and they are reported as good solvents for PCL in the literature [309].

The oil phase prepared with the lowest volume of chloroform, C0.25 (for the nomenclature see Section 2.2.3.2.) was the most viscous diluted oil phase in our study (Figure 2.3C). This oil phase did not form a stable emulsion above 77 vol. % of internal (aqueous) phase and inverted into a water-in-oil-in-water (w/o/w) emulsion. It may be due to the high viscosity of the oil phase and the high viscosity of the emulsion. The viscosity of the oil phase limits the maximum internal phase volume that can be incorporated [310,311]. As for the viscosity of the emulsion depends on various factors, including the volume fraction of the dispersed phase and the viscosity of the continuous phase [65,95]. The viscosity of the emulsion increases with an increasing amount of internal (aqueous) phase [66,93,95], and this may limit the incorporation of water into the emulsion, and the water addition results in emulsion break down.

Interestingly, the breakdown occurs at an internal phase volume close to the close packing limit of uniform, non-deformed spherical particles [312]. Beyond this limit, the internal droplets are compressed into polyhedral cells separated by thin films [310] and form a HIPE.

No visual separation was observed in group C0.40 either during mixing or when mixing stopped, and this group resulted in open porosity which is characterised by windows, the smaller voids on pores connecting adjacent pores to each other, as described by Christenson et al. [36].

The higher volume of chloroform emulsions (C0.55 and C0.70) started to break down in minutes. The emulsion likely separates out by gravity-induced coalescence, where the oil phase film around the water droplets ruptures, and the water droplets merge. The velocity of the single droplet during this process can be estimated with Stoke's equation (Equation 4) where,  $v$  is the velocity of the droplet,  $D$  is the droplet diameter under gravitational force,  $\Delta\rho$  is the density difference between water and oil phase,  $n$  is the viscosity of the oil phase and  $g$  is the gravitational force [172];

$$v = D^2 \Delta\rho g / 18n \quad (4)$$

Adding chloroform as a diluting solvent for the oil phase has a dual effect on the emulsion; it increases the density difference between the water and oil phases (Table 2.1) and reduces the viscosity of the oil phase. Both of these effects will speed up the droplet travel, according to Stoke's law.

**Table 2.1:** Composition details of 4PCLMA PolyHIPE groups which were prepared by using no solvent or single solvent of chloroform or toluene.

Sample ID	V <sub>solvent</sub> (ml)	ρ <sub>oil phase</sub> (g/ml)	Separation during mixing	Separation right after mixing	Porous structure	D (μm)
NS	0.00	1.11	-	-	N	-
C0.25	0.25	1.19	Y	N	Y	6±3
C0.40	0.40	1.22	N	N	Y	69±31
C0.55	0.55	1.25	N	Y	Y	139±84
C0.70	0.70	1.27	N	Y	Y	427±182
T0.25	0.25	1.06	N	N	N	-
T0.40	0.40	1.04	N	N	N	-
T0.55	0.55	1.02	N	N	N	-
T0.70	0.70	1.01	N	N	Y	24±7

*N: no separation, Y: separation was observed*

SEM analysis was used to characterise microstructures of the PolyHIPEs, and the morphology of each composition is shown in Figure 2.3D. The average pore size in group C0.25 was 6±3μm. Then, a further increase in the amount of chloroform (from C0.40 to C0.70) resulted in an increase in pore size of the monoliths from 69±31 μm to 427±182 μm (pore size distributions are provided in Figure 2.8).

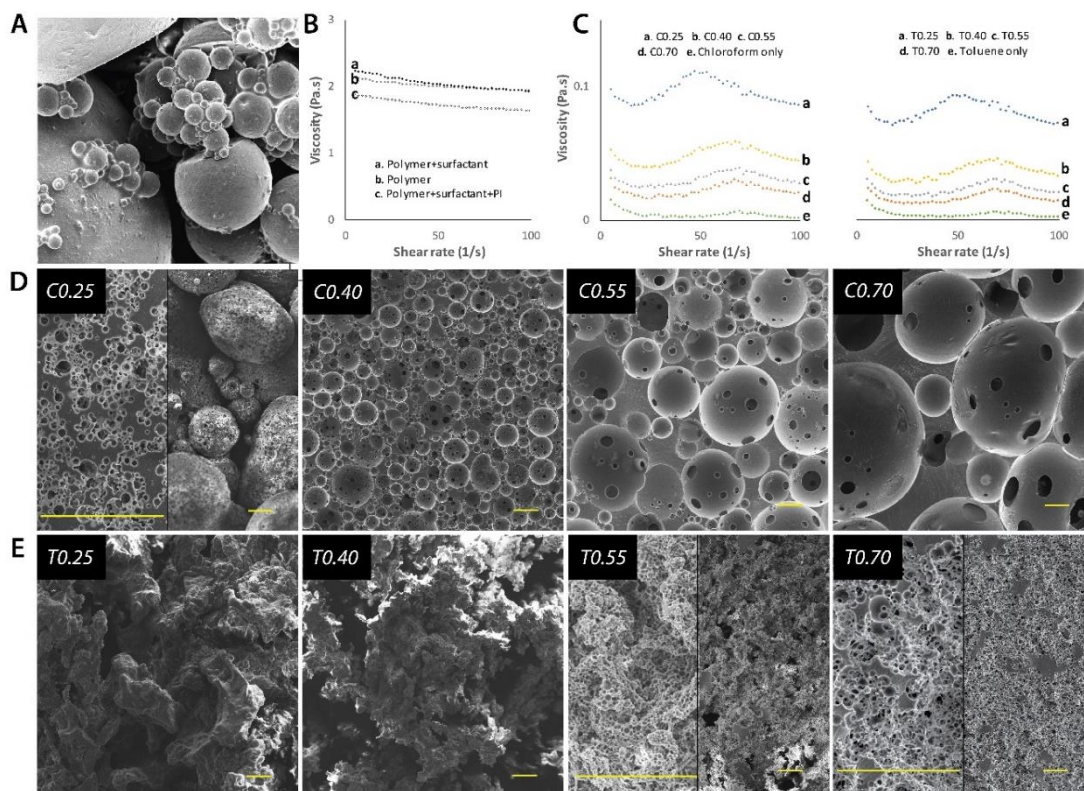


**Figure 2.3:** SEM micrograph of A. NS, B. 4PCLMA PolyHIPE composition prepared using chloroform as a diluting solvent, C. SEM images of each 4PCLMA PolyHIPE composition prepared using toluene as a diluting solvent (scale bar: 100 $\mu$ m). B. The viscosity of the oil phase components without any solvent ( $n=4$ ).

In summary, while the viscosity of C0.25 was not low enough to hold the whole volume of the internal phase, all other three groups (C0.40, C0.55, and C0.70) formed an emulsion and resulted in open porous cellular morphology. However, C0.40 was the only group to form a stable emulsion for the single chloroform volumes tested. When using a solvent to dilute the pre-polymer, there is a narrow range over which a stable emulsion can be formed. The viscosity should be low enough to enable mixing of the two phases, but high enough to form a stable emulsion [36,107].

### 2.3.2.2. Incorporation of toluene as a diluent increases stability of the 4PCLMA HIPEs

When toluene was used as a diluent, the viscosity of the oil phase was lower than when chloroform was used, despite both solvents having a similar viscosity (0.56 mPaS and 0.60 mPaS at 20°C for chloroform and toluene, respectively). The viscosity of the oil phases prepared with either solvent showed a similar pattern as the solvent volume was increased, Figure 2.3C. The difference in 4PCLMA solvation by either chloroform or toluene could be the main contributing factor affecting the small difference in the oil phase viscosity. Similarly, Zverev et al. also reported that polymer viscosity is different in good and poor solvents. Polymers have a higher viscosity in good solvents due to higher the mean square end-to-end distance of the macromolecules compared to poor solvents [313].

The solvation of a polymer in a solvent is dictated by the free energy of mixing (Equation 5); where  $\Delta G_m$  is the Gibbs free energy change on mixing,  $\Delta H_m$  is the enthalpy change on mixing,  $T$  is the absolute temperature, and  $\Delta S_m$  is the entropy change on mixing.

$$\Delta G_m = \Delta H_m - T\Delta S_m \quad (5)$$

$\Delta H_m$  of mixing can be expressed with Equation 6 [314];

$$\Delta H_m = V_{mix} \left[ \left( \frac{\Delta E_1^V}{V_1} \right)^{1/2} - \left( \frac{\Delta E_2^V}{V_2} \right)^{1/2} \right]^2 \Phi_1 \Phi_2 \quad (6)$$

Where  $V_{mix}$  is the volume of the mixture,  $\Delta E^V$  is the energy of vaporisation,  $V$  is the molar volume of each species in the mixing,  $\phi$  is the volume fraction. Equation 6 can be rewritten as [314]:

$$\frac{\Delta H_m}{V} = (\delta_1 - \delta_2)^2 \Phi_1 \Phi_2 \quad (7)$$

Where  $V$  is the molar volume of solvent,  $\delta$  is the solubility parameter of the solvent (1) and the polymer (2), respectively. For better polymer-solvent miscibility or dissolution  $\Delta H_m$  must be smaller than the entropic term ( $-T\Delta S_m$ ) in Equation 5. Therefore, a smaller difference between solubility parameters  $(\delta_1 - \delta_2)^2$  improves the solubility of the polymer in a solvent (Equation 7) [309,314].

The solubility parameters of PCL, chloroform, and toluene are 10.00, 9.21 and 8.91  $(\text{cal}/\text{cm}^3)^{1/2}$ , respectively [309]. This indicates that chloroform is a better solvent than toluene for PCL, which is also confirmed by Bordes et al. [309].

The viscosity of the oil phase is also an important parameter that determines the success of the emulsification process, for example, T0.25 (for the nomenclature, see the Section 2.2.3.2.) makes a successful emulsion while C0.25 does not since the oil phase of T0.25 exhibits a lower viscosity compared to oil phase of C0.25. Interestingly, apart from T0.70, no interconnected pores were observed in 4PCLMA PolyHIPE scaffolds with toluene as porogenic solvent. Although group T0.70 has an interconnected porous structure, its cellular morphology is more disordered than 4PCLMA PolyHIPEs with chloroform as a porogenic solvent. Although the detectable average pore sizes of T0.70 and C0.70 were measured as  $24 \pm 7 \mu\text{m}$  and  $427 \pm 182 \mu\text{m}$ , respectively, it is hard to determine the individual pores and the windows of group T0.70. The structure appears to exhibit very small pores interconnected by large windows; both these features have been associated with a small interfacial tension between the water and organic phase as reported [35,66]. This may explain the disordered morphology observed in T0.70. The question remains, as to why a porous

structure was not observed in the other emulsion templated polymers with toluene as porogenic solvent.

To investigate the potential effect of the surfactant, the emulsions were prepared with toluene as a porogenic solvent and without surfactant. Interestingly, despite the low interconnectivity, all samples exhibited porous morphologies (Figure 2.10). Adding the surfactant has a strong influence on the microstructure of the produced PolyHIPE.

The surfactant used in this study is an oil-soluble, polymeric emulsifier made of A-B-A block copolymer (polyhydroxystearic acid-polyethylene glycol-polyhydroxystearic acid) (Hypermer 256) with a Hydrophile-Lipophile Balance (HLB) of 4.6. The assembly of the block copolymer is strongly affected by the solvents they are in contact with [315,316]. Although 10% Hypermer 246 was found to be a suitable surfactant system for chloroform diluted oil phases to obtain typical open cellular PolyHIPE morphology [49], further investigation is needed to find a better surfactant for materials with toluene as porogenic solvent. In this study, we aimed to use chloroform as a dominant solvent, and toluene is used to tune the pore size, interconnectivity, and stability of the 4PCLMA PolyHIPEs.

Emulsions with toluene as a porogenic solvent did not exhibit any observable separation after addition of water and turned to white, which is a general behaviour of the emulsion formation as the droplets of water scatter the light, suggesting that more stable emulsions were formed with toluene compared to chloroform as the diluting solvent. This can be attributed to the following: (i) the larger polarity difference between toluene and water compared to chloroform and water [317] which results in the formation of more stable HIPEs [318,319], (ii) the droplet diameter is much smaller with toluene (e.g. T0.70  $24\pm 7$   $\mu\text{m}$  compared to C0.70  $427\pm 182$   $\mu\text{m}$ ) which

reduces the speed of gravity-driven coalescence (Equation 4), (iii) the speed of gravity-driven coalescence is reduced by matching the density difference between the oil phase (Table 2.1) and the water phase, and (iv) the lower interfacial tension of the toluene diluted oil phases and water compared to the chloroform diluted systems. It is because, the interfacial energy is directly correlated to the interfacial tension (Equation 8), and low interfacial energy increases emulsion stability [320], [321].

$$E = \Delta A \times \delta \quad (8)$$

Where E is energy,  $\Delta A$  is an increase in the area,  $\delta$  is the interfacial tension.

#### **2.3.2.3. 4PCLMA PolyHIPE morphology can be tuned by solvent blend as a diluent**

To show the translational morphological changes from C0.40 (C/T:100/0) to T0.40 (C/T:0/100), 4PCLMA PolyHIPEs whose oil phases were diluted with a solvent blend of chloroform and toluene were investigated (Figure 2.4). The viscosity of the oil phase gradually reduced from C/T:100/0 to C/T:0/100, Figure 2.11A. As expected, no visual separation or emulsion instability was observed in all these solvent blend groups until the moment of solidification because both C0.40 and T0.40 were stable emulsions and their blends expected to be stable.

Although any apparent porous PolyHIPE structure was not observed in either C/T:40/60 or C/T:20/80, closed pores showed up in the group C/T:40/60. Open porous, cellular morphology was observed in only three groups whose chloroform ratio in diluting solvent composition was 60% or more. The average pore diameters were  $15 \pm 4 \mu\text{m}$ ,  $20 \pm 7 \mu\text{m}$ ,  $69 \pm 31 \mu\text{m}$  for C/T:60/40, C/T:80/20, C/T:100/0, respectively (pore size distributions are provided in Figure 2.9).

Decreasing the ratio of C/T reduces the pore sizes, but it increases the degree of interconnectivity which is important for the transport of nutrients, removal of waste products and migration of cells [99]. The degree of interconnectivity is calculated as the ratio of the average window diameter ( $d$ ) to an average pore diameter ( $D$ ) [69]. For C/T:60/40, C/T:80/20, and C/T:100/0, window diameters were measured as  $3.7\pm 1.7 \mu\text{m}$ ,  $3.6\pm 1.7 \mu\text{m}$ , and  $10.5\pm 4.8 \mu\text{m}$ , respectively, and the degrees of interconnectivities ( $d/D$ ) were calculated as 0.24, 0.18, and 0.15, respectively. Higher interconnectivity is related to lower interfacial tension, as previously discussed. When interfacial tension is lower, the walls between the pores become thinner and shrink comparably more, which results in an increase in window size [46,66,301].

To conclude, as chloroform was found to be a better diluting solvent to form PolyHIPE structure, it was determined that it needs to be used as a dominant solvent for the solvent volumes tested. By the addition of a comparably smaller volume of toluene into a solvent composition, cellular morphology; pore size and interconnectivity can be controlled. Since HIPEs of C/T:60/40, C/T:80/20, and C/T:100/0 are stable, and their monoliths have open cellular pore morphologies, these three groups were selected for further investigation.

#### **2.3.2.4. Determination of the densities and the porosities**

The density of 4PCLMA was measured as  $1.13 \text{ g cm}^{-3}$ . Densities and porosities of C/T:60/40, C/T:80/20 and C/T:100/0 were calculated as  $0.35 \text{ g cm}^{-3}$ ,  $0.34 \text{ g cm}^{-3}$  and  $0.31 \text{ g cm}^{-3}$ , and 69%, 70% and 73% respectively. There is no statistical difference found in the porosity of these groups. Interestingly, the internal phase volume was 82 vol. % (which would yield an expected density of  $0.19 \text{ g cm}^{-3}$ ), and although the internal phase volume is responsible for the porosity of the PolyHIPE, the measured

porosity was lower. This could be due to either shrinkage after crosslinking and drying [59] or a collapse in the PolyHIPE morphology [62]. In this study, a typical 15-20 % shrinkage in each dimension of 4PCLMA PolyHIPE samples was observed after crosslinking and drying, and SEM analysis of the samples did not indicate any significant microstructural collapse occurring in tested groups of the 4PCLMA PolyHIPEs. The HIPE still produces an interconnected foam, despite having a lower porosity as typically observed in PolyHIPEs. This is in line with the study by Menner et al., who produced open cellular monoliths with a porosity of 70% [53].

#### **2.3.2.5. 4PCLMA HIPEs prepared using solvent blends are stable enough for photo-polymerisation**

After 5 days, there were very thin dense layers (less than 1 mm, ~10% (v/v) of the emulsion) at the bottom of the bottles of groups C/T:60/40, C/T:80/20 and C/T:100/0. Due to the slow coalescence of the droplets (the effect can be seen only in days) and the higher density of the oil phase compared to the water, the oil phase tends to accumulate at the bottom of the bottle. Due to both solvent and water evaporation, the bottles had condensation droplets on the wall, as shown in Figure 2.11B.

Over 5 days the average pore sizes of the samples increased to  $43 \pm 15 \mu\text{m}$ ,  $51 \pm 20 \mu\text{m}$  and  $87 \pm 32 \mu\text{m}$  for C/T:60/40, C/T:80/20 and C/T:100/0 (SEM images and pore size distributions are provided in Figure 2.11C and Figure 2.12). Although the stability of the emulsions still needs to be improved for long-term storage, once created, emulsions are typically polymerised within a few minutes to hours so that slow coalescence is unlikely to pose a problem.

**Table 2.2:** Details of compositions of 4PCL PolyHIPE prepared by using solvent blends of chloroform and toluene.

Sample ID	V <sub>individual solvent</sub> (ml)	$\rho_{oil}$ phase (g/ml)	Separation during	Separation right after	Porous structure	D <sup>a</sup> ( $\mu$ m)	d <sup>b</sup> ( $\mu$ m)	d / D <sup>c</sup>	D <sup>d</sup> ( $\mu$ m)
<b>0:10</b>	C:0.0								
<b>(C:T)</b>	T:0.4	1.04	N	N	N	-	-	-	-
<b>2:8</b>	C:0.8								
<b>(C:T)</b>	T:3.2	1.06	N	N	N	-	-	-	-
<b>4:6</b>	C:1.6								
<b>(C:T)</b>	T:2.4	1.09	N	N	N	-	-	-	-
<b>6:4</b>	C:2.4								
<b>(C:T)</b>	T:1.6	1.13	N	N	Y	15 $\pm$ 4	3.7 $\pm$ 1.7	0.24	43 $\pm$ 15
<b>8:2</b>	C:3.2								
<b>(C:T)</b>	T:0.8	1.17	N	N	Y	20 $\pm$ 7	3.6 $\pm$ 1.7	0.18	51 $\pm$ 20
<b>10:0</b>	C:0.4								
<b>(C:T)</b>	T:0.0	1.22	N	N	Y	69 $\pm$ 31	10.5 $\pm$ 4.8	0.15	87 $\pm$ 32

<sup>a</sup> An average void diameter (cured right after preparation), <sup>b</sup> An average interconnecting window diameter, <sup>c</sup> The degree of interconnectivity, <sup>d</sup> An average void diameter (cured 5 days later for stability test), N: no separation, Y: separation was observed

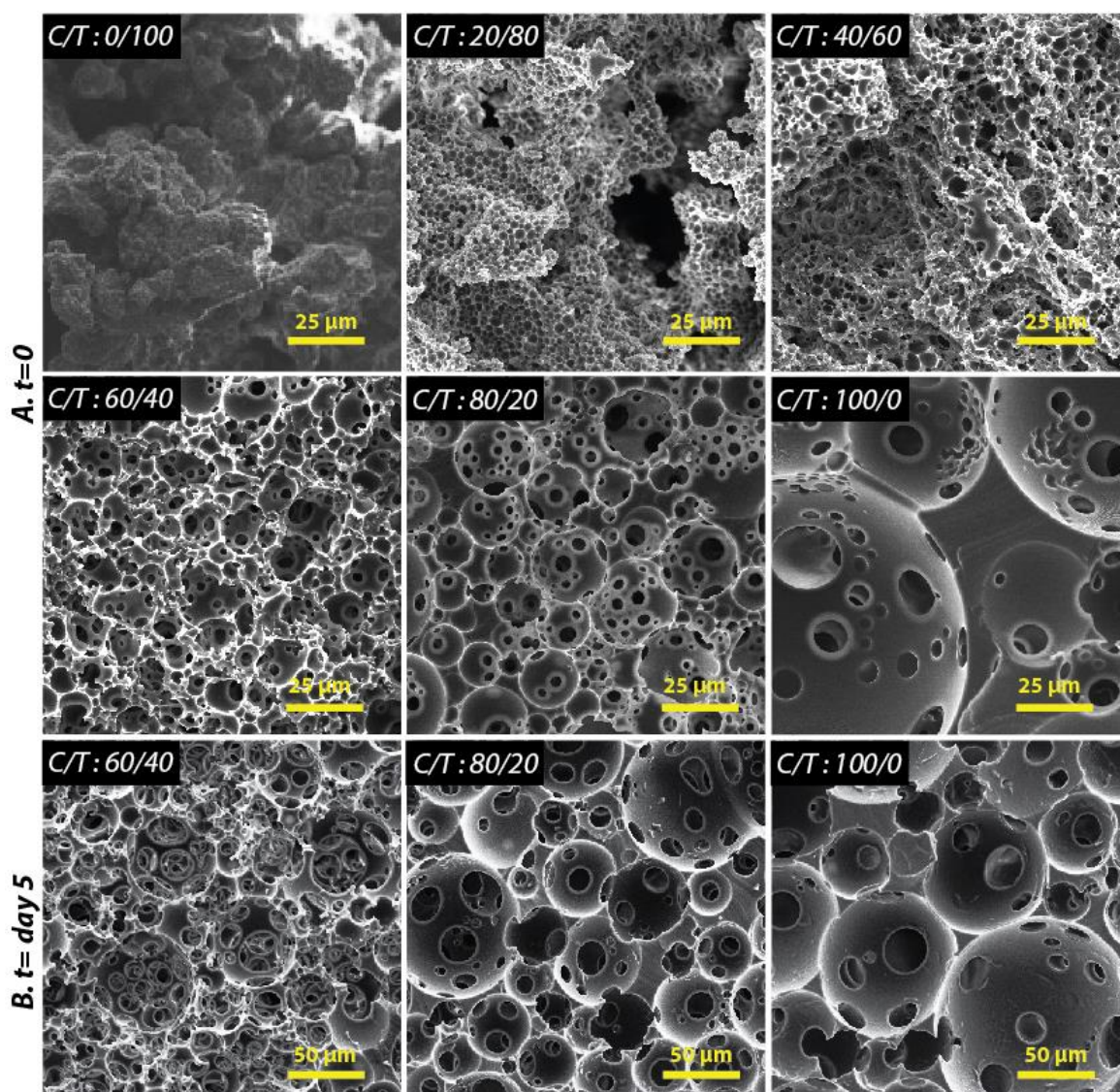


**Figure 2.4:** A. SEM images of C/T:60/40, C/T:80/20 and C/T:100/0; polymerised A. Right after preparation of HIPE, B. 5 days after preparation (scale bars: 100µm).

### 2.3.3. Morphology of 4PCLMA PolyHIPE affects the mechanical properties

Changing between the solvent blend ratios (C/T:60/40, C/T:80/20 and C/T:100/0) affects the mechanical properties of the material and the PolyHIPE morphology. The lowest elastic modulus was observed in group C/T: 60/40 (Figure 2.5A). This is likely due to two structural features of this group; (i) the highest interconnectivity and (ii) the smallest pore size. Interconnectivity results in a large open area on the surface of

the pores leading to lower structural integrity due to the interconnected windows [66], and Young's modulus increases with the increasing pore size as previously reported by Krajnc et al. and Kovačič et al. [87,88]. Gibson et al. also reported that at constant volumetric porosity, larger pore size results in thicker struts between pores which increase the modulus of the scaffolds [89]. The lowest UTS was observed in group C/T: 60/40, However, either UTS or ultimate elongation did not show a direct relationship between pore size. The greatest elongation, up to 98%, was recorded in the scaffolds with medium pore size Figure 2.5C. The elongation values of other groups were around 66% and 84% for scaffolds with smallest and largest pore sizes, respectively.

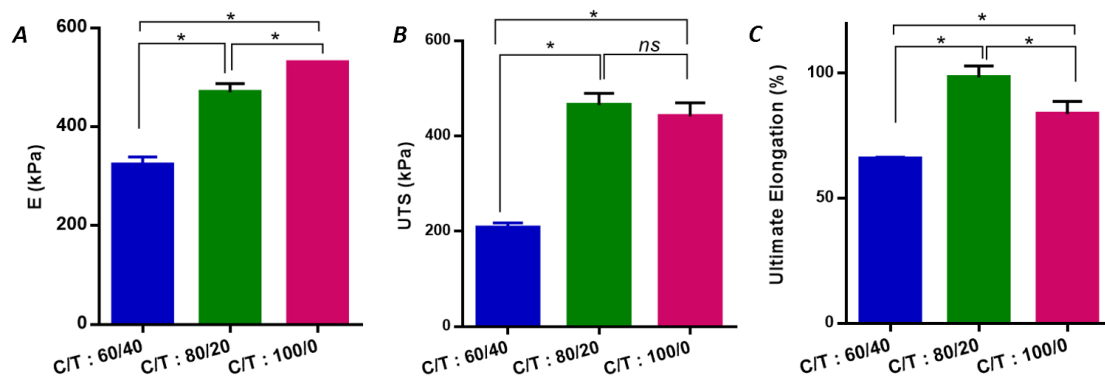


**Figure 2.5:** Mechanical properties of C/T:60/40, C/T:80/20 and C/T:100/0 A.Elastic modulus, B. Ultimate tensile strength, C. Percentage elongation at failure (\*:  $p < 0.05$ , ns: no significant difference,  $n=3$ ).

The mechanical test data of the 4PCLMA PolyHIPE scaffolds indicates that the materials are likely to be suitable for use in soft TE, as the elastic modulus of soft tissues is lower than 1 MPa [99,322,323].

### **2.3.4. 4PCLMA PolyHIPEs can support the attachment, growth, and infiltration of HDFs**

There was a significant increase in the cellular metabolic activity of HDFs from day 1 to day 7 on both 4PCLMA PolyHIPE scaffolds and Alvetex®, Figure 2.6A. At day 1 and day 4, there was no significant difference between any groups. At day 7, while there were no significant differences between 4PCLMA PolyHIPE groups, the cellular metabolic activity of HDFs on Alvetex® scaffolds was significantly higher than C/T:60/40 and C/T:100/0. The thinner structure and higher porosity make Alvetex® (200 µm thick, 90% porous) a more optimised scaffold for studying cell ingrowth than the 4PCLMA PolyHIPE scaffold (1 mm thick, internal phase 82 vol. %). Interesting to note is that there was no significant difference between C/T:80/20 and Alvetex® at day 7. HDFs attached and spread on the surface of all 4PCLMA PolyHIPE scaffolds at day 4 before the culture reached confluence on the surface. Additionally, the cells grew into the pores of the scaffold and exhibited a flat morphology, especially in the scaffolds with larger pore size, see Figure 2.6B. False-coloured SEM images are presented to distinguish the presumed cellular material from the scaffold; the original SEM images are provided in 2.12.

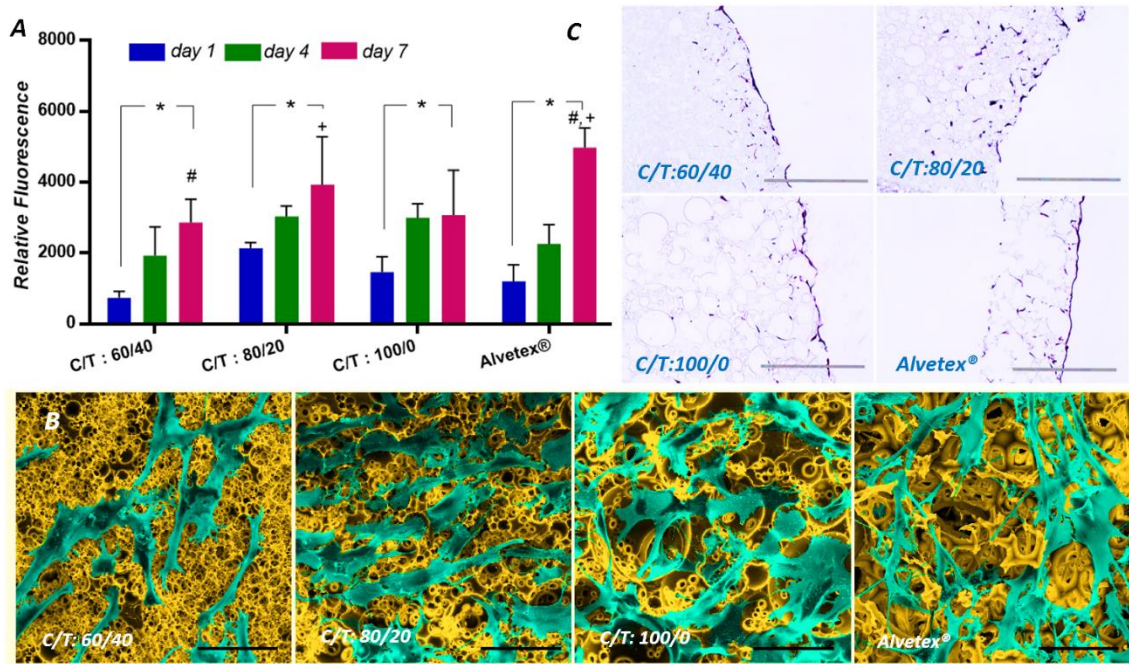


**Figure 2.6:** A. Biological assessment of 4PCLMA PolyHIPE scaffolds. A. Resazurin reduction assay results which show the cellular metabolic activity of HDSs for 7 days on PolyHIPE scaffolds (ANOVA, multiple comparisons, ns,  $0.05 > p$ , \*, +, #,  $p \leq 0.05$ ,  $n=3$ ), B. SEM images of 4-day cultured HDFs on C/T:60/40, C/T:80/20, C/T:100/0 and Alvetex®, respectively (top view). SEM images were false-coloured for clear visibility of the cells on the scaffold surface. (yellow: scaffold, turquoise: cells (Scale bars: 50 $\mu$ m) C. H&E stain of a section of 4PCLMA PolyHIPE groups after 7 days of cell culture (scale bar: 250 $\mu$ m).

The potential of the scaffolds to support cell ingrowth was investigated with histological staining. Cells penetrated up to 250  $\mu$ m over 7 days of culture into the highly interconnected 4PCLMA PolyHIPEs, Figure 2.6C. However, they appeared to be more evenly distributed through the scaffolds with smaller pore sizes compared to those with larger pores. The group (C/T: 100/0) with largest pore sizes ( $69 \pm 31 \mu$ m) showed the lowest penetration in comparison with the other two groups (C/T:80/20 and C/T:60/40 with  $15 \pm 4 \mu$ m and  $20 \pm 7 \mu$ m pore sizes, respectively). This is likely to be because of its smaller degree of interconnectivity in comparison with the other two scaffolds.

Johnson et al. investigated the cellular metabolic activity (day 3 and day 7) and migration (day 7) of L929 fibroblasts on fully degradable, 90-95% porous, three PCL-based thiolene scaffolds and Alvetex® with pore sizes 62, 68, 82 and 40  $\mu\text{m}$ , respectively [107]. They observed a reduction in cellular metabolic activity from day 3 to day 7 on the Alvetex® scaffolds. This is likely due to higher seeding density (500.000 cells per scaffold,  $\emptyset = 20 \text{ mm}$ ) than used in our study (25.000 cells per scaffold,  $\emptyset = 6 \text{ mm}$ ). In contrast, the cell viability of fibroblasts increased from day 3 to day 7 in PCL-based thiolene PolyHIPEs. Although cells accumulated on the surface due to high seeding density, as shown in the H&E sections, they also penetrated through the structure. Additionally, Akay et al. manufactured styrene-based PolyHIPEs with average pore sizes of 40  $\mu\text{m}$ , 60  $\mu\text{m}$ , and 100  $\mu\text{m}$  by changing the emulsification temperature [131]. They cultured rat osteoblast on PolyHIPE scaffolds for 35 days. While there was a significant increase from day 1 to day 35 in cellular metabolic activity on each PolyHIPE scaffold, there was no significant difference between scaffolds of different pore sizes at day 35. Interestingly, while the cell penetration depth was over 300  $\mu\text{m}$  in 40  $\mu\text{m}$  porous scaffolds in 7 days, it was  $\sim 250 \mu\text{m}$  and  $\sim 50 \mu\text{m}$  for scaffolds with 60  $\mu\text{m}$  and 100  $\mu\text{m}$  pore sizes, respectively, which is a similar trend observed as in our study.

Overall the cell culture and ingrowth on 4PCLMA scaffolds is comparable by the other PolyHIPE scaffolds highlighted in the literature, and in particular, the commercially available Alvetex® scaffold.

## **2.4. Conclusions**

In this study, we developed PolyHIPE scaffolds made of photocurable 4PCLMA. Solvent dilution was used to reduce the viscosity of the oil phase and enable mixing of two phases of the emulsion. Chloroform and toluene were used as diluents. We revealed that solvent composition and volume have a high impact on both emulsion stability and PolyHIPE morphology due to the joint contribution of the density and the viscosity of the oil phase. Overall, chloroform was found to be a better porogenic solvent to dilute the oil phase for creating porous scaffolds. On the other hand, when toluene was used to dilute the oil phase, HIPEs were found more stable due to less difference between the densities of the oil and water phases. Both open porous and comparably stable HIPEs were successfully created when solvent blends of chloroform and toluene were used to dilute the oil phase. The pore and interconnect sizes of the 4PCLMA PolyHIPEs were shown to be tunable by adjusting the chloroform and toluene ratios in the solvent blend. These changes in morphology affect mechanical properties, demonstrating that conditions could be adjusted to create a scaffold of the required mechanical properties. 4PCLMA PolyHIPE scaffolds supported cell attachment, growth and penetration in comparable rate to commercial scaffolds when HDFs were cultured on them indicating that this material is suitable as a material for building TE scaffolds.

## **2.5. Supporting information**

For measurements of the pores, the following protocol was applied. SEM images were imported into Adobe Photoshop CS6. A random rectangular area was selected. By using the ellipse tool, pores in that area were framed in a new layer and saved as 8-bit tiff document. The original images were imported into Image J to set the scale (global

calibration). Then, the processed images were imported into Image J and by using the following process>binary>make binary steps, each file was converted into a binary image. Using analyze>set measurements, the desired parameter was selected (area). Finally, using the analyze tab, analyze particles command was chosen, and the individual area of each pore was measured and provided pop up in a separate window. This data was transferred to excel to calculate pore diameters (roundness of pores was assumed to be 1) with the correction factor.

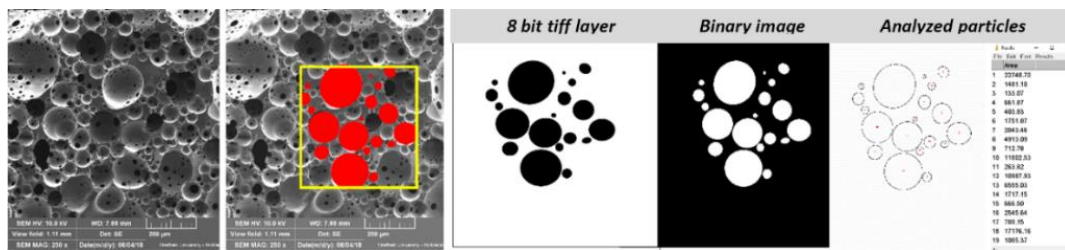


**Figure 2.7:** The processing steps of pore size calculation, from left to right: the SEM image was imported into Adobe Photoshop CS6, using the ellipse tool pores are framed in a new layer, the image is saved as a black and white 8-bit tiff file, the file is converted into a binary image, the area of each pore was calculated.

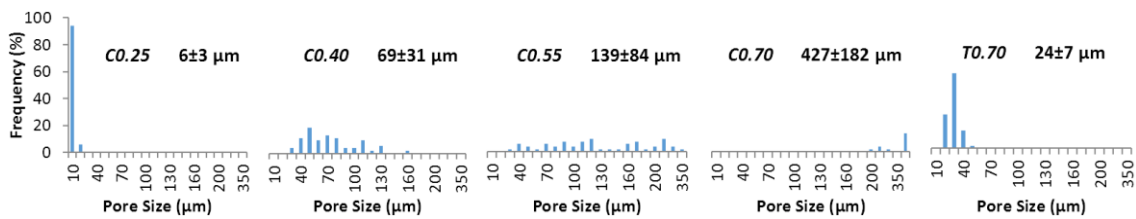


**Figure 2.8:** Average pore sizes and pore size distributions of 4PCLMA PolyHIPEs prepared by using single solvents of either chloroform or toluene.

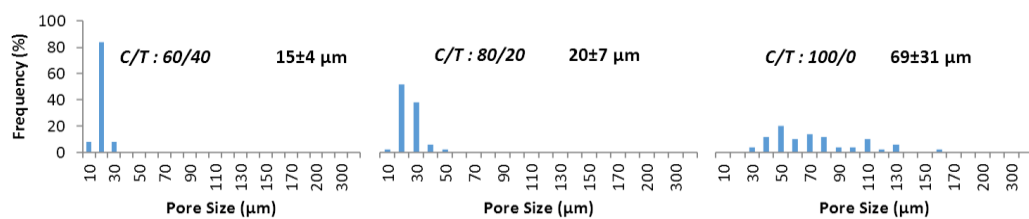


**Figure 2.9:** Average pore sizes and pore size distributions of 4PCLMA PolyHIPEs prepared by using solvent blends of chloroform and toluene.

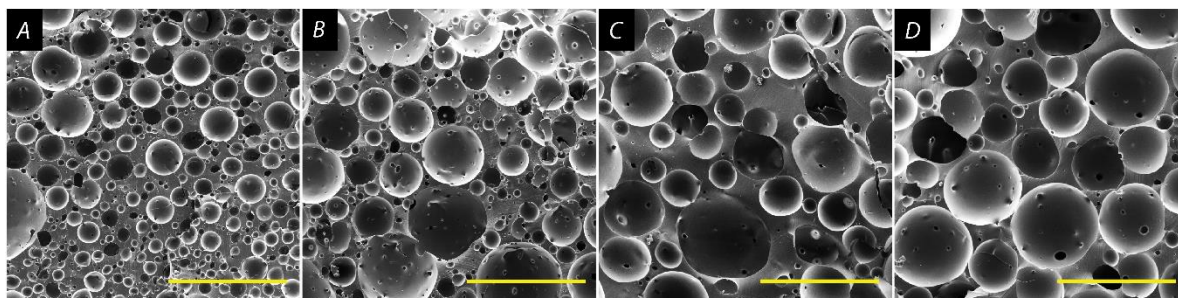


**Figure 2.10:** 4PCLMA PolyHIPE compositions whose oil phases were diluted with (A. 0.25 mL, B. 0.40 mL, C. 0.55 mL, and D. 0.70 mL) toluene prepared without surfactant (scale bar: 500 μm).

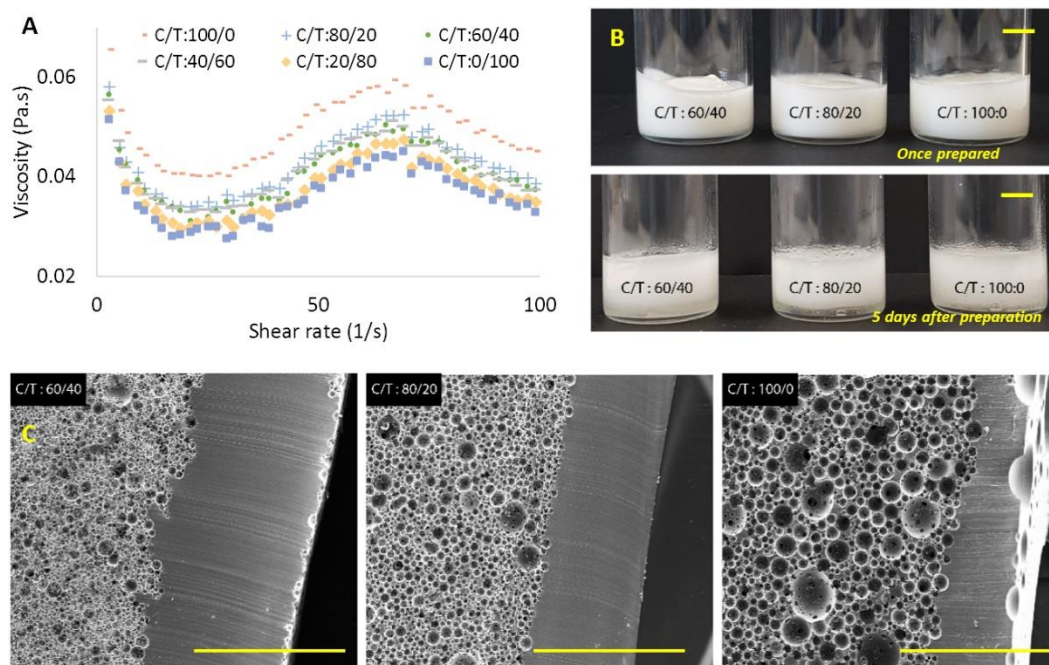


**Figure 2.11:** A. Viscosity changes with changing solvent ratios of chloroform and toluene in the solvent blend ( $n=4$ ), B. Macro images of emulsions once prepared and 5 days after preparation

(scale bar: 5mm), C. SEM image of the bottom of the cured emulsion 5 days later, which shows separation at the bottom of the bottle (scale bar: 1mm).

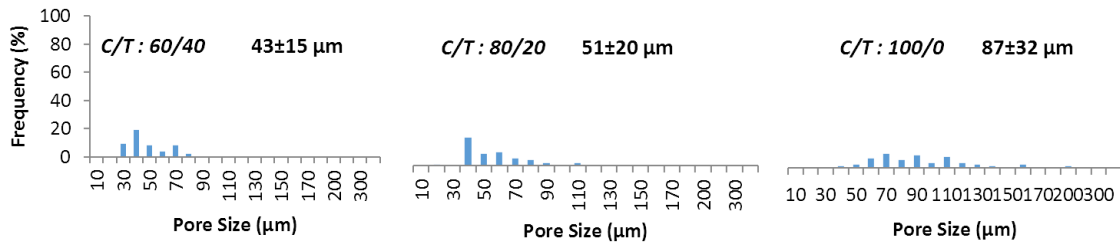


**Figure 2.12:** Average pore sizes and pore size distributions of HIPE compositions which were prepared by using solvent blends of chloroform and toluene (samples were cross-linked 5 days later for stability tests).

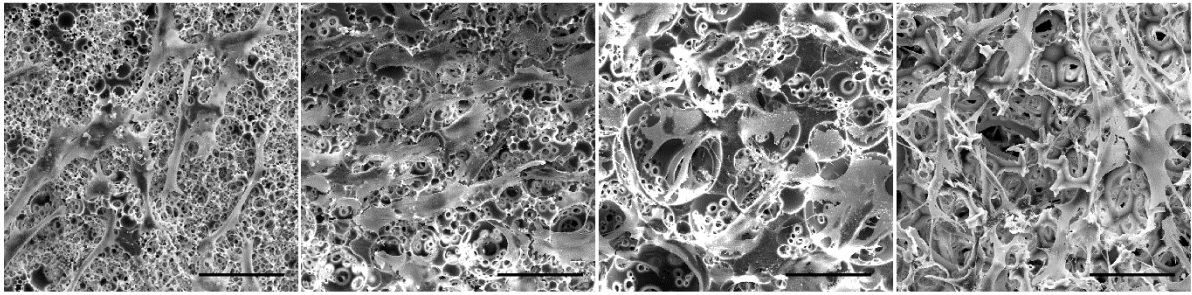
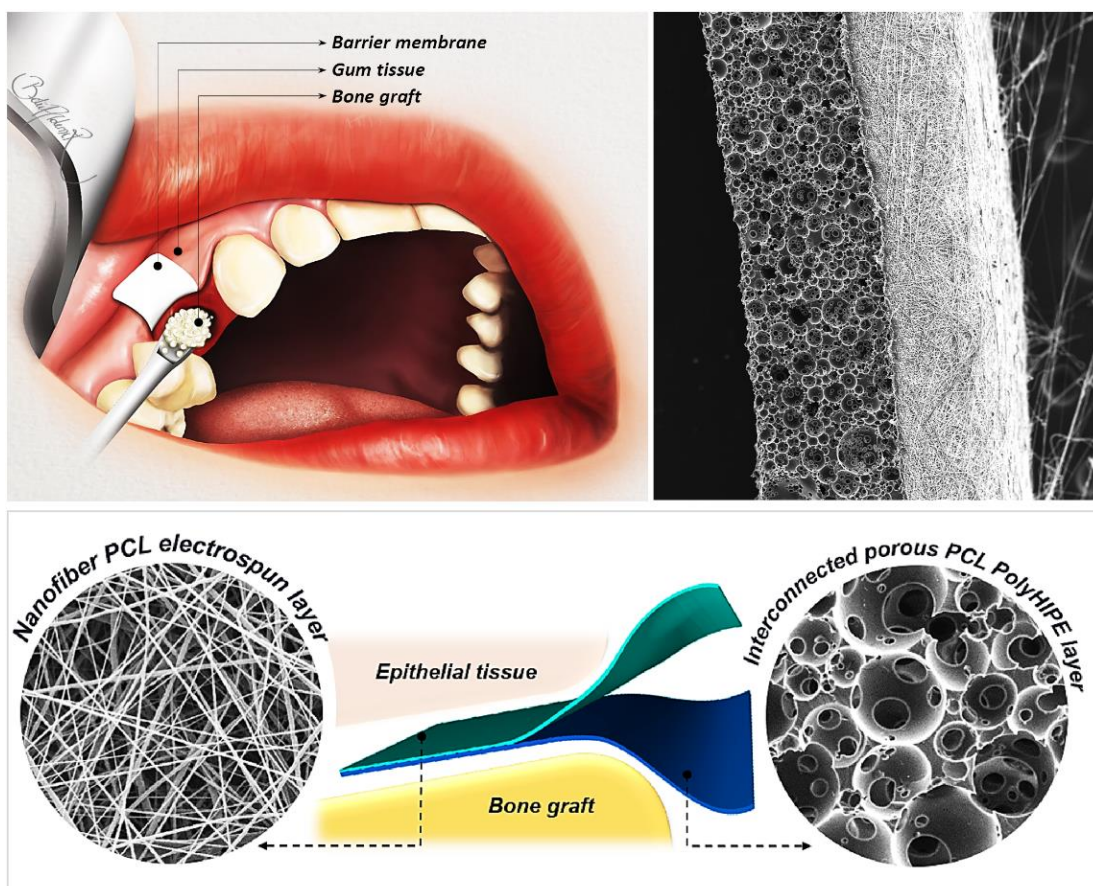


**Figure 2.13:** Original SEM images of 4-day cultured fibroblasts on C/T:60/40, C/T:80/20, C/T:100/0 and Alvetex®, respectively (scale bar: 250μm).

# CHAPTER 3

---

## A novel bilayer polycaprolactone membrane for guided bone regeneration: combining electrospinning and emulsion templating



### *Abstract*

Guided bone regeneration is a common dental implant treatment where a barrier membrane (BM) is used between epithelial tissue and bone or bone graft to prevent the invasion of the fast-proliferating epithelial cells into the defect site to be able to

preserve a space for infiltration of slower-growing bone cells into the periodontal defect site. In this study, a bilayer polycaprolactone (PCL) BM was developed by combining electrospinning and emulsion templating techniques. First, a 250 µm thick polymerised high internal phase emulsion (PolyHIPE) was manufactured and treated with air plasma, which was shown to enhance the cellular infiltration. Then, four solvent compositions were investigated to find the best composition for electrospinning nanofibrous PCL barrier layer on PCL PolyHIPE. The biocompatibility and the barrier properties of the electrospun layer were demonstrated over four weeks *in vitro* by histological staining. Following *in vitro* assessment of cell viability and cell migration, cell infiltration and the potential of PCL PolyHIPE for supporting blood vessel ingrowth were further investigated using an *ex-ovo* chick chorioallantoic membrane assay. Our results demonstrated that the nanofibrous PCL electrospun layer was capable of limiting cell infiltration for at least four weeks, while PCL PolyHIPE supported cell infiltration, calcium and mineral deposition, and blood vessel ingrowth.

**Keywords:** *guided tissue regeneration, guided bone regeneration, barrier membrane, PolyHIPE, electrospinning, polymer, polycaprolactone, CAM assay, GTR, GBR*

### **3.1. Introduction**

In the US, almost 50% of the adult population experiencing a type of periodontitis which may eventually cause tooth extraction if it is not treated. It is estimated that more than 200 million of the US population will suffer from partial tooth loss by 2027. Losing a tooth may have an adverse effect on the psychology and social life of the

patient [258] in addition to its economic burdens. In 2010, it was estimated that the global cost of dental diseases to be USD 442 billion [324].

Periodontal regenerative procedures require the use of guided tissue regeneration/guided bone regeneration membranes (GTR/GBR) in various conditions such as socket preservation, grafting, maxillary sinus elevation and the treatment of the chronic periodontitis [325]. The main principle of the GTR/GBR procedure is to place a barrier membrane (BM) between epithelial tissue and bone or bone graft to prevent migration of the fast-proliferating epithelial cells into the defect site to be able to preserve a space for infiltration of bone cells into periodontal defect site [326,327].

The earliest developed membranes were made of non-resorbable materials such as cellulose filters, polytetrafluoroethylene (e-PTFE), and titanium meshes but the necessity of a second surgery for removal led to the development of resorbable membranes [328]. The most common natural membranes are made of porcine, bovine, or human collagen. Despite their high biocompatibility, the main disadvantages of collagen membranes are their potential for antigenicity, poor mechanical properties, and rapid degradation [329,330]. Alternatively, synthetic polymers such as Polyglycolic acid (PGA) and Polylactic acid (PLA) have been commonly investigated for the fabrication of BMs. Although they are biodegradable and non-cytotoxic, their rapid degradation can generate an acid environment around the implant, which may cause adverse inflammatory tissue reactions [331,332].

Polycaprolactone (PCL) is another bioresorbable synthetic polymer, which degrades more slowly and consequently does not produce an overly acidic environment in the degradation process [331]. FDA approved biomedical devices made of PCL are already on the market, which makes PCL a promising material for other biomedical

applications. Additionally, due to its ease of fabrication in different forms, PCL is used as a scaffold material for both hard and soft tissue engineering [289]. It has previously been reported for various biomedical applications including drug delivery applications [333,334], periodontal regeneration [335,336], vascular grafts [337], bone tissue engineering applications [338,339], and wound healing [340,341]. One of the main drawbacks of PCL, as with many other synthetic polymers is that it is hydrophobic, which limits the polymer-cell interaction [342,343]. Plasma treatment is one of the most common and effective ways to promote hydrophilicity of the polymer surfaces by adding polar groups to the surface of the material without altering the bulk properties [228–232].

A BM is expected to be in contact with both hard and soft tissues, and it has different functions on each side. While being cell occlusive on the side in contact with soft tissue, it should encourage bone regeneration on the other side. There are many methods used in barrier membrane fabrication; such as solvent casting [344,345], electrospinning [336,346–349], phase inversion, freeze-drying [350,351], and 3D printing [352,353].

Electrospinning is a versatile technique for fabricating fibres with varying diameters from a few nanometres to several micrometres from a wide variety of materials [354]. PCL is also one of the widely-used polymers that have been electrospun for its use in numerous applications [355]. Several solvents and solvent blends have been reported to be used to dissolve PCL for preparing the electrospinning solution [356]. Although several parameters have been associated with the size of fibres [357], the composition and the ratio of solvents have been demonstrated to have a significant effect on fibre diameters [358]. As electrospun nanofibers are shown to prevent cell infiltration

without limiting the diffusion of oxygen and nutrients, electrospinning is a promising method to manufacture a physical barrier.

Emulsion templating is another scaffold manufacturing technique where polymer solution and water are mixed in the presence of surfactants to form an emulsion. When the water droplets are encapsulated in a polymer solution, it is called water in oil (w/o) emulsion. If the internal phase volume (water content) is increased over 74% (v/v), the emulsion is called a high internal phase emulsion (HIPE) [39,91,359,360]. After solidification of the polymer phase (continuous phase) by thermal curing or photocuring or solvent evaporation, the structure is locked, and water droplets are removed. The resulting porous structure is defined as polymerised HIPE (PolyHIPE). PolyHIPEs are favourable as a tissue engineering scaffolds because of their highly interconnected porous structures which have been previously demonstrated as promoting cell migration and tissue ingrowth [9,36,42,107,131,162].

Manufacturing of scaffolds made of photocurable PCL by using emulsion templating technique is challenging because of the high viscosity of the polymer, which constrains the mixing of two phases during emulsion formation. We have recently developed and reported a production route of PolyHIPEs made of photocurable PCL and showed the biocompatibility of the material by using human dermal fibroblasts [42]. However, this developed composition has not been used for any specific application yet, and the use of emulsion templated PolyHIPEs in GBR/GTR barrier membrane applications has not previously been reported.

In this study, we combined two methods; emulsion templating and electrospinning to manufacture a bilayer, bioresorbable BM made of PCL. Emulsion templating is selected for manufacturing of the layer, which will be in contact with bone/bone graft. 250  $\mu\text{m}$

thick PCL PolyHIPE layer was manufactured and treated with air plasma to enhance the cellular infiltration. Following the *in vitro* evaluation of the biological performance, the suitability of PCL PolyHIPE morphology for blood vessel infiltration through the pores was further investigated using an ex-ovo chick chorioallantoic membrane (CAM) assay. Electrospinning was selected to manufacture the nanofibrous barrier layer. Four different solvent compositions were tested in terms of their abilities to enable nanofiber production. The biocompatibility and the barrier properties of the electrospun layer were tested over four weeks *in vitro* by histological staining.

## **3.2. Experimental**

### **3.2.1. Materials**

Pentaerythritol (98%),  $\epsilon$ -caprolactone, tin (II) 2-ethylhexanoate, triethylamine (TEA), methacrylic anhydride (MAAn), photoinitiator (PI) (2,4,6-Trimethylbenzoyl Phosphine Oxide/2-Hydroxy-2-Methylpropiophenone blend), fungizone, fetal calf serum (FCS), penicillin/streptomycin (PS), L-glutamine, trypsin, 37% formaldehyde (FA) solution, resazurin sodium salt, glutaraldehyde, ethanol, hexamethyldisilazane (HMDS), perchloric acid, picric acid, hematoxylin solution, eosin Y solution, porcine gelatine, beta-glycerolphosphate ( $\beta$ GP), ascorbic acid 2-phosphate (AA2P), PCL ( $M_n$ : 80.000 g/mol), Triton X-100, Alizarin red S, Polydimethylsiloxane (PDMS, silicone), and Dulbecco's Modified Eagle's Medium (DMEM) were purchased from Sigma Aldrich (Poole, UK). Direct Red 80 (Sirius Red) was purchased from Fluka (Buchs, Switzerland). Acetone, dimethylformamide (DMF), chloroform, and industrial methylated spirit (IMS), dichloromethane (DCM), and methanol were purchased from Fisher Scientific (Pittsburgh, PA, USA). The surfactant Hypermer B246-SO-M was

received as a sample from Croda (Goole, UK). Conditioning Minimum Essential Alpha Medium ( $\alpha$ -MEM) was purchased from Lonza (Slough, UK). 4',6-diamidino-2-phenylindole (DAPI) solution and phalloidin Tetramethylrhodamine (TRITC) were purchased from ThermoFisher Scientific (San Jose, CA, USA). Optimum cutting temperature tissue freezing medium (OCT-TFM) was purchased from Leica Biosystems (Newcastle, UK). Collagenase A was purchased from Roche (Indianapolis, IN, USA).

### **3.2.2. Manufacturing of the PCL PolyHIPE, PCL electrospun, and bilayer membrane**

#### **3.2.2.1. Synthesis of PCL methacrylate**

The PCL used in this study is 4-arm PCL methacrylate (4PCLMA), and the detailed synthesis of 4PCLMA (Figure 3.1A) is described elsewhere [42]. Throughout the paper, the term 'PCL PolyHIPE' will be used to describe 4PCLMA PolyHIPE unless otherwise stated.

Briefly, pentaerythritol and  $\epsilon$ -caprolactone were mixed in a round flask at 160°C while stirring continuously at 200 rpm. When pentaerythritol was dissolved, tin (II) 2-ethylhexanoate was added, and the system was removed from the oil bath to cool down. PCL was dissolved in DCM, and then TEA was added. The flask was placed in an ice bath. MAAn was dissolved in DCM and transferred into a dropping funnel. When the addition of MAAn was completed, the ice bath was removed, and the system was kept at the room temperature (RT) overnight with stirring at 375 rpm. To remove the TEA, MAA and salts formed, the methacrylated PCL was washed with HCl solution, and then with pure deionised water. Almost all solvent was evaporated using a rotary

evaporator. Three methanol washes were applied, and any remaining solvent was removed by using the rotary evaporator. 4PCLMA was stored in an appropriate vessel in the freezer (-20°C) for further use.

### **3.2.2.2. Preparation PCL HIPEs**

4PCLMA (0.4 g) and the surfactant Hypermer (10% w/w of polymer) were added into a glass vial and heated to 40°C to dissolve surfactant which is crucial for emulsion stability. Solvent blend (150% w/w of polymer, 80% chloroform, 20% toluene (w/w)) and PI (10% w/w of polymer) were added in a 4PCLMA-surfactant mixture, respectively and mixed at 375 rpm using a magnetic stirrer for 1 minute at RT. Once the homogeneous mixture formed, 2.5 mL of water (internal phase volume 85% v/v) was added dropwise in 2 minutes, and the emulsion was mixed further 2 minutes more, as illustrated in Figure 3.1B.

### **3.2.2.3. Optimisation of manufacturing of PCL PolyHIPEs**

The emulsion templating technique was selected due to its ability to manufacture scaffolds with interconnected architecture. However, during the polymerisation, the material in contact with emulsion has been reported to have a significant effect on PolyHIPE morphology [45].

To find the best manufacturing method in terms of creating interconnected scaffolds, we briefly polymerised PCL HIPEs in PDMS moulds, with the upper surface in contact with air, glass, and PDMS, and we investigated the morphology of the surface and transverse sections with SEM.

### **3.2.2.4. Manufacturing of PCL PolyHIPE layer**

PCL HIPEs were manufactured by either polymerisation in silicone moulding and sectioning of 250 µm samples using a vibratome (Bio-Rad Polaron Division) or syringe

moulding and sectioning of 1 mm samples using a scalpel. For the fabrication of a bilayer BM, 250  $\mu\text{m}$  sections of PCL PolyHIPE were used. 1 mm thick PCL PolyHIPE samples were used alone for MLO-A5 cell culture, measurements of their metabolic activity, Alizarin Red and Sirius Red staining, histological evaluation of infiltration of MLO-A5s and CAM experiments.

Briefly, PCL HIPE was pipetted into either silicon templates or 2.5 mL syringes (diameter of 6 mm) and cured 3 minutes to both sides using the OmniCure Series 1000 curing system (Lumen Dynamics, Canada) (Figure 3.1C). The resulting parts were recovered, soaked in 100% methanol for 24 hours with four changes to remove any remaining contaminants of surfactant, solvent or uncured material. Then the samples were left in methanol (50% (v/v) in water) for 24 hours and water for a further 24 hours. Finally, the samples were taken out from the water and left in the freezer ( $-80^{\circ}\text{C}$ ) for an hour then transferred into a vacuum oven and left for a day to preserve the porous structure of PCL PolyHIPE without any collapse.



### **3.2.2.5. Assessment of solvent compositions in terms of their ability to form the nanofibrous structure**

PCL (10% (w/w)) pellets were dissolved in acetone (100%), acetone:chloroform (30:70 w/w), DCM:methanol (90:10 w/w), and chloroform:DMF (70:30 w/w). The mixtures were magnetically stirred overnight.

Fabrication of PCL electrospun fibres using chloroform:DMF (70:30) [361,362], acetone [363–365], acetone:chloroform (30:70) [293] has previously been reported in the literature. The use of DCM:methanol (90:10) for the fabrication of PCL electrospun meshes had previously been investigated by our group [366]. Accordingly, in this study, these four previously reported solvent compositions were selected to be compared in terms of their ability to form the nanofibrous structure.

Solutions (~5 mL) were loaded into 5 mL syringes fitted with 0.6 mm inner diameter (ID) blunt syringe tips. The syringe was then placed in a syringe pump (Genie™Plus, KentScientific, Connecticut, USA). Aluminium foil was used as the collector and placed at a distance of 17 cm from the needle tips. The pump was set to 40 µl/minutes, and 17 kV voltage was applied both to the collector and the tips. Solutions of PCL prepared with various solvent blends were then electrospun at RT for 40 minutes.

Single-layer of electrospun PCL (without PolyHIPE layer) manufactured using each polymer solutions were morphologically investigated, as explained in Section 3.2.3.1. In the rest of the text, the following nomenclatures are used for electrospinning groups. Acetone (100) defines acetone (100%). Acetone:chloroform (30:70) refers to acetone:chloroform (30:70 w/w). DCM:methanol (90:10) denotes DCM:methanol (90:10 w/w), and chloroform:DMF (70:30) refers to chloroform:DMF (70:30 w/w).

### **3.2.2.6. Manufacturing of bilayer PCL BM**

The aluminium foil collector was sprayed with methanol, and 250 µm thick sections of PCL PolyHIPE layer were placed onto it. This step was performed immediately before electrospinning of the PCL barrier layer. Chloroform:DMF (70:30) solvent blend was used for the production of PCL electrospun barrier layer, as explained in Section 3.2.2.5. 10% PCL solution was loaded into 5 mL syringes fitted with 0.6 mm ID blunt syringe tip. PCL was then electrospun onto PCL PolyHIPE layers with a rate of 40 µl/minutes and a voltage of 17 kV for 40 minutes (Figure 3.1E, F).

### **3.2.3. Morphological, mechanical and surface characterisation**

#### **3.2.3.1. Morphological characterisation**

Micro-architectures of PCL PolyHIPE, PCL electrospun, and bilayer BM were examined using a scanning electron microscope (SEM). All samples were gold-coated with a voltage of 15 kV for 2.5 minutes using a gold sputter coater (Edwards sputter coater S150B, Crawley, UK) to increase conductivity. SEM (Philips/FEI XL-20 SEM; Cambridge, UK) was used with 10 kV power.

SEM images of the PCL fibres and PCL PolyHIPE were analysed for the determination of the fibre diameters, pore size distributions, and window size using ImageJ software (Bethesda, MD, USA). Total of 54 different fibre diameters and 54 pore sizes were measured for each group of PCL electrospun layers, 100 pores and 150 windows were measured for PCL PolyHIPE. All measurements were taken from three different areas of three different samples.

### **3.2.3.2. Mechanical characterisation**

The bilayer BM was mechanically tested under dry and wet conditions using a mechanical testing unit (BOSE Electroforce Test Instruments, Minnesota, USA) equipped with a 22.5 N load cell. Briefly, mechanical testing samples were cut into 10 mm x 3 mm pieces and clamped to the device with two tensile grips, and the tensile tests were performed on each sample at a rate of 0.1 mm/s until the samples failed. Elastic modulus (E), ultimate tensile strength (UTS) and elongation (%) values were calculated from stress ( $\sigma$ ) and strain ( $\epsilon$ ) curves of each sample. The elastic modulus was determined as the slope of the initial linear section of the curve. UTS was obtained from the curve as the maximum stress that the samples could withstand. Ultimate elongation was measured as the percentage elongation of the samples at the break.

### **3.2.3.3. Contact angle measurements**

Contact angle measurements were conducted to evaluate the effect of air plasma treatment on the hydrophilicity of PCL PolyHIPE. In brief, a 5  $\mu$ l water droplet was dropped onto the surface of the either non-treated or plasma-treated PCL PolyHIPE, and the water contact angles were determined via drop shaper analyser (Krüss DSA100, Germany) under ambient laboratory conditions.

## **3.2.4. Biological assessment**

### **3.2.4.1. Cell culture of HDFs**

HDFs were isolated from skin grafts taken from patients using a well-established protocol [367]. Briefly, the dermis was minced into 10 mm<sup>2</sup> pieces, and the pieces were incubated overnight at 37°C in 0.5% (w/v) collagenase A solution. The cell suspension was then centrifuged at 1000 rpm for 5 minutes and resuspended and cultured in DMEM containing 10% (v/v) FBS, 100 IU mL<sup>-1</sup> penicillin, 100 mg mL<sup>-1</sup> streptomycin,

2mM L-glutamine and 0.625  $\mu\text{g mL}^{-1}$  amphotericin B. HDFs were used between passage 4-8. The investigations were carried out following the rules of the Declaration of Helsinki of 1975. Ethical approval for the tissue acquisition was granted by the National Research Ethics Service (NRES) Committee Yorkshire & The Humber-Sheffield (REC ref: 15/YH/0177, REC opinion date: 03/06/2015).

#### **3.2.4.2. HDF cell seeding onto the PCL electrospun layer**

Bilayer BMs were used as test samples to measure the metabolic activity and for histological assessment of HDFs. BMs were cut into 10 mm circles using a biopsy punch (Stiefel, Slough, UK) and 70% ethanol solution was used as an antiseptic agent for 45 minutes prior to cell seeding.  $2 \times 10^4$  HDFs were trypsinised, centrifuged, and resuspended in 100  $\mu\text{l}$  of DMEM growth medium and pipetted on PCL electrospun (barrier) side of the bilayer BM. Before submerging the BMs into HDFs culture medium, they were incubated at 37°C for 2 hours to allow HDFs to attach. BMs were kept in culture for 4 weeks by changing the culture medium every 2 days.

#### **3.2.4.3. Cell culture of murine long bone osteocytes (MLO-A5)**

MLO-A5, murine osteoblast cell line (kindly donated by Dr Lynda Bonewald) was used to evaluate the potential of PCL PolyHIPE as GBR membrane as it was previously used for evaluation of bone tissue engineering applications [162]. The T75 flasks were coated with 0.1% gelatin solution for 2 hours at 37°C and washed gently with PBS prior to cell culture. Cells were expanded on gelatine-coated T75 flasks in basal media containing  $\alpha$ -MEM supplemented with 10% fetal bovine serum, 2mM L-glutamine and 100 mg/mL penicillin/streptomycin. MLO-A5s cultured until 90% confluence and media was changed in every 2-3 days. Cells were used between passages 35-36.

#### **3.2.4.4. MLO-A5 cell seeding onto the PCL PolyHIPE layer**

To be able to test the full infiltration capacity of MLO-A5s through PCL PolyHIPE, monolayer, 1 mm PCL PolyHIPE samples (without electrospun layer) were used for biological assessment of PCL PolyHIPE.

Prior to cell seeding, PCL PolyHIPEs were left in 70% ethanol for 2 hours and then transferred into PBS in sterile conditions, four washes were applied in 24 hours to replace the ethanol with PBS. Finally, they were conditioned with basal media for an hour in the incubator in 24 well plates to remove the PBS completely and not to dilute the media used during the cell seeding stage with PBS. MLO-A5s were trypsinised, counted, and centrifuged. The cell pellet was re-suspended in fresh basal media ( $2.5 \times 10^4$  cells in 20  $\mu$ L). The cell suspension was placed over the surface of each PCL PolyHIPE homogenously. Before PolyHIPE layers were moved to the fresh wells, and 2 mL basal media was supplied into the wells, they were left for 2 hours in the incubator (37.5°C, 5% CO<sub>2</sub>) for cell attachment. 2 mL of media was supplied. A day after, basal media was replaced with supplemented media consisting of basal media supplemented with 5 mM  $\beta$ GP and 50  $\mu$ g/mL AA2P. Media was changed every 2–3 days.

#### **3.2.4.5. Assessment of metabolic activity**

AlamarBlue® assay was performed in order to track the metabolic activities of HDFs on the PCL electrospun and MLO-A5s on PCL PolyHIPE. 0.1 mM AlamarBlue® working solution was prepared by 10 $\times$  dilution of the 1 mM AlamarBlue® stock solution with growth medium. At days 1, 7, 14, 21, and 28 growth media were removed, and the samples were washed with PBS. 1 mL of AlamarBlue® working solution was added to each well and incubated at 37°C for 4 hours. After an incubation period, 200  $\mu$ l of the

solution was transferred into 96-well plate, and the fluorescence readings were done at an excitation wavelength of 540 nm and an emission wavelength of 635 nm. Fresh samples were used for the measurements at each time point.

#### **3.2.4.6. Assessment of calcium deposition**

Alizarin red powder was dissolved in deionised water at 1 w/v% in a water bath and filtered to remove particles to make Alizarin red solution (ARS). PCL PolyHIPE's were submerged in 1 mL of ARS solution and incubated for 1 hour. ARS solution was removed, and the samples were washed every five minutes with deionised water and gentle orbital shaking until the water remains clear. They were submerged with 1 mL of 5% perchloric acid to destain and left for further 30 minutes with gentle orbital shaking. 150  $\mu$ L of the destain solution in triplicates were transferred into a clear 96 well plate and read at an absorbance of 405 nm.

#### **3.2.4.7. Assessment of collagen deposition**

Sirius red (direct 80) powder was dissolved in saturated picric acid (1 w/v%) to form Sirius red solution (SRS) and filtered to ensure no particles remain. PCL PolyHIPE's were submerged with 1 mL of SRS solution and left for 1 hour. SRS solution was removed, and the samples were washed every five minutes with deionised water and gentle orbital shaking until the water remains clear. They were submerged with 1 mL of 0.2 M sodium hydroxide (NaOH):methanol (1:1) to destain and left for 30 minutes with gentle orbital shaking. 150  $\mu$ L of the destain solution in triplicates were transferred into a clear 96 well plate and read at an absorbance of 405 nm.

#### **3.2.4.8. Haematoxylin & Eosin (H&E) and Alizarin red staining**

Bilayer BM and PCL PolyHIPE cultured with HDFs and MLO-A5s, respectively for 1-week and 4-week and PCL PolyHIPE on CAM were stained with H&E using a standard

protocol [368]. Briefly, samples were washed with PBS before (once) and after (three times) fixing them in 3.7% FA for 30 minutes at RT. Meanwhile, cryomoulds were filled with OCT-TFM. Samples were embedded into it, and the rest of the volume was then filled with OCT-TFM to the top. Cryomoulds were placed into liquid nitrogen and incubated for 5-7 minutes until solidified. Frozen blocks were fixed on mounting platforms, and placed into a cryostat (Leica CM1860 UV, Milton Keynes, UK) before sections were sliced at 5-10  $\mu\text{m}$  and immediately mounted onto the surface of Thermo SuperFrost® Plus slides. For H&E staining, slides were stained with hematoxylin for 90 seconds and eosin for 5 minutes. For calcium staining, slides were stained with 2% (w/v, in water) ARS for 5 minutes. Excess dye is shaken off, and the slides were rinsed, dehydrated, cleared and mounted the slide using the permanent mounting medium.

#### **3.2.4.9. Preparation of biological samples for SEM**

On day 28, the PCL PolyHIPE discs seeded with MLO-A5s were washed 3 times with PBS and fixed with 2.5% glutaraldehyde at RT for 1 hour and rinsed with PBS. Then the discs were soaked in deionised water for 5 minutes prior to dehydration of the samples with serial ethanol washes. Finally, HMDS is used as the chemical drying agent, and the discs were soaked in HMDS:ethanol (1:1) solution for 1 hour and transferred into 100% HMDS for 5 minutes. The samples were then air-dried overnight in a fume hood and gold-coated at a current of 15 mA for 2.5 minutes with a gold sputter (Edwards sputter coater S150B, Crawley, England) prior to imaging under SEM (Philips/FEI XL-20 SEM; Cambridge, UK).

#### **3.2.4.10. Fluorescent staining**

At days 7 and 28, PCL PolyHIPE discs were fixed with 3.7% FA for 30 minutes and washed gently with PBS prior to submerging into 0.1% (v/v) Triton X 100 (in PBS)

solution for 20 minutes. After serial PBS washes, phalloidin-TRITC (1:500 diluted in PBS from stock solution) solution was added onto samples to visualize F-actin filaments of the cells and incubated for 30 minutes at RT in the dark. Discs were washed three times with PBS. To stain the cell nuclei, DAPI solution (1:1000 diluted in PBS) was added onto the PolyHIPE discs and incubated for 10-15 minutes at RT in the dark; samples were then washed three times with PBS and imaged under a fluorescent microscope (Olympus IX3, Tokyo, Japan).

#### **3.2.4.11. Ex-ovo CAM assay**

An ex-ovo CAM assay was used to evaluate the potential of PCL PolyHIPE layer for the suitability of blood vessel ingrowth, as described previously [201,277]. Briefly, fertilised chicken eggs (*Gallus Domesticus*) were purchased from Henry Stewart & Co. MedEggs (Norwich, UK) and cleaned with 20% IMS solution. Eggs were incubated at 37.5°C for 3 days in an egg incubator (RCOM King SURO, P&T Poultry, Powys, Wales). At the end of day 3, the embryos were transferred gently into sterile Petri dishes and incubated at 38°C in a humidified cell culture incubator (Binder, Tuttlingen, Germany). On day 7, PCL PolyHIPE discs were implanted to CAM, and the chicks were incubated for further 7 days. On day 14, the chicks were euthanised, and the CAMs with the PolyHIPE discs integrated to them were removed and fixed in 3.7% FA solution. Sections of the CAMs were taken and stained with H&E as described in Section 3.2.4.8.

#### **3.2.5. Statistical analysis**

Statistical analysis was carried out using one-way and two-way analysis of variance (ANOVA) using statistical analysis software (GraphPad Prism, California, USA). Where relevant, n values are given in figure captions. Error bars indicate standard deviations in the graphs unless otherwise stated.

### **3.3. Results and Discussion**

#### **3.3.1. Manufacturing and characterisation of the PCL PolyHIPE layer**

The surface of PCL PolyHIPEs polymerised in contact with air, glass, or PDMS showed different morphologies (Figure 3.2A-C). When the surface was not covered by any substrate, and UV was directly applied on PCL HIPEs, the surface was porous, but it did not have open interconnected cellular morphology (Figure 3.2A). When the surface of the HIPE was in contact with glass, the surface showed microscale roughness, rather than pores (Figure 3.2B). In terms of interconnectivity, the best surface morphology was obtained when the PDMS sheet was used as a cover. PCL PolyHIPE surfaces created this way had a mixture of open and closed porous morphology (Figure 3.2C).

The significant influence of the mould material on PolyHIPE has been reported previously [45]. This study correlated the surface interconnectivity with the following potential scenarios on the PolyHIPE-mould interface; (i) PolyHIPE can potentially bind to mould surface leading to difficulties in demoulding, (ii) the mould can leach materials leading to contamination of the PolyHIPE surface, and (iii) partial phase separation of the emulsion which leads to closed-pore PolyHIPE surfaces.

Figure 3.2D shows the transverse section of PCL PolyHIPE. It has a homogenous, open cellular architecture with interconnected porosity. Pore interconnects are pathways for cells, waste and nutrients, the interconnectivity of the scaffold is a crucial feature for cell invasion, tissue integration and vascularisation [369–372]. To be able to benefit from the interconnected inner morphology of the scaffolds, the PCL PolyHIPE layer was decided to be created by sectioning bulk pieces into slices as described in Section 3.2.2.3.

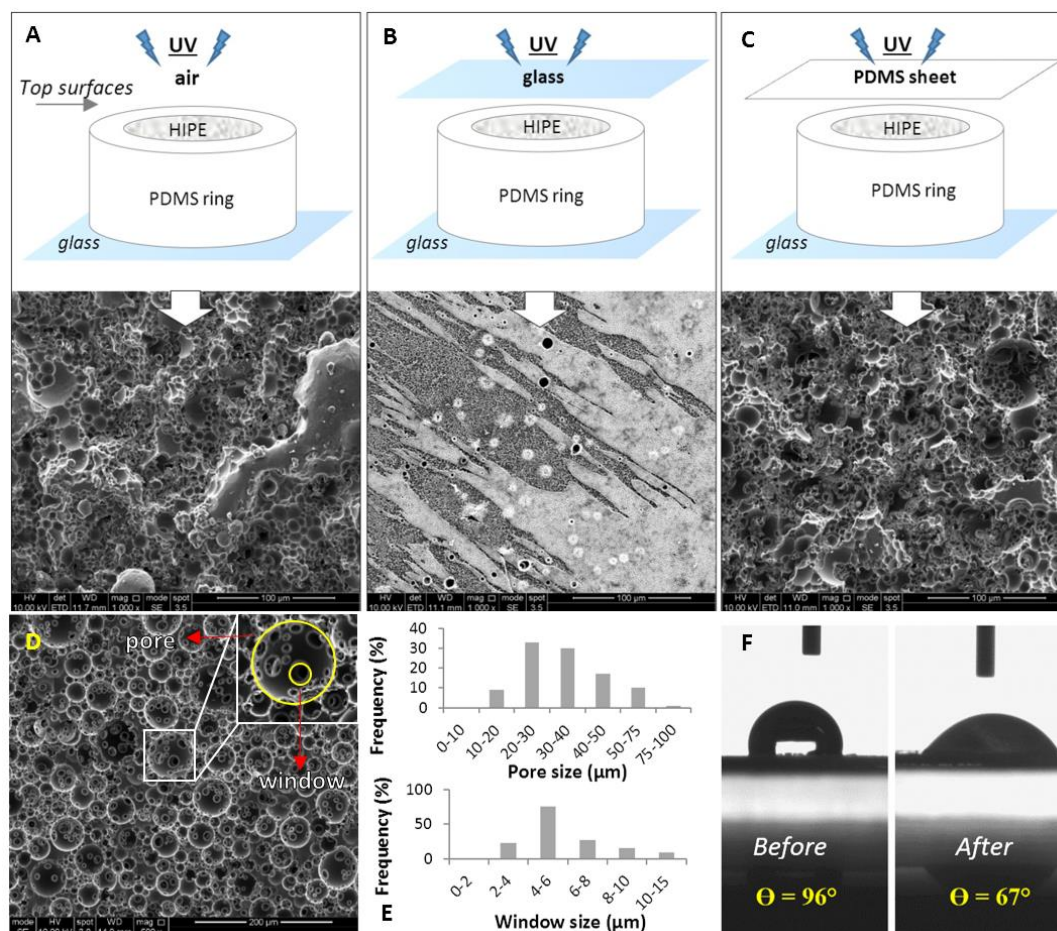


**Figure 3.2:** SEM images of the top surfaces PCL PolyHIPEs cured in contact with; (A) air, (B) glass, and (C) PDMS sheet. (D) SEM image of the transverse section of PCL PolyHIPEs. (E) Pore size and window size distributions of the inner section. (F) Contact angle measurements of a water droplet on PCL PolyHIPE before and after air plasma treatment ( $n=3$ ).

The pore sizes of the PCL PolyHIPE layer were distributed between 10-78  $\mu\text{m}$ ; the average pore size (D) was found  $34 \pm 13 \mu\text{m}$ , 90% of the pores have the pore sizes between 20-75  $\mu\text{m}$  range (Figure 3.2E). The window sizes were distributed between 2-13  $\mu\text{m}$  range, and the average window size (d) was measured as  $6 \pm 2 \mu\text{m}$  (Figure 3.2E), which gives the degree of connectivity ( $d/D$ ) as 0.18. In our previous study, when the same solvent composition was used to dilute PCL (80:20 chloroform:toluene (w/w)) the average pore size and the window size was found  $20 \pm 7 \mu\text{m}$  and  $4 \pm 2$ , respectively [42]. The difference between the pore and window size found in the

previous study and the current work can be explained with the two main compositional changes; (i) increasing the internal phase volume from 82% to 85%, and (ii) increasing the total solvent volume from 0.40 mL to 0.46 mL. A higher internal phase volume is expected to reduce the average pore size while increasing the average window diameter as water droplets will need to be more tightly packed. On the other side, the increasing solvent amount is expected to show a dramatic increase in the average pore diameter [373]. The overall effect of these two compositional changes resulted in approximately 50% increase in average pore size and window diameter.

The main drawback of PCL to be used as tissue engineering scaffold material is its hydrophobicity, which limits cell attachment to the material surface. To overcome this, oxidising the surface by plasma treatment is one of the most popular methods for enhancing cell attachment [70,361,374–377]. In this study, our finding also proved that air plasma treatment changes the surfaces from hydrophobic to hydrophilic and this change encourages the cell attachment and cellular infiltration on PCL PolyHIPE layer which will be further discussed following sections. Contact angles of the water droplets on non-treated (P-) and air plasma treated (P+) PCL PolyHIPEs were measured as  $67\pm 4^\circ$  and  $96\pm 4^\circ$ , respectively (Figure 3.2F).

### **3.3.2. Assessment of the metabolic activity of MLO-A5s on PCL PolyHIPE and the cellular infiltration through PCL PolyHIPE layer**

At all-time points, the metabolic activity of MLO-A5s cultured on P+ PCL PolyHIPEs was slightly higher than MLO-A5s cultured on P- PCL PolyHIPEs, but there was no statistical difference observed between these two groups (Figure 3.3A). Metabolic

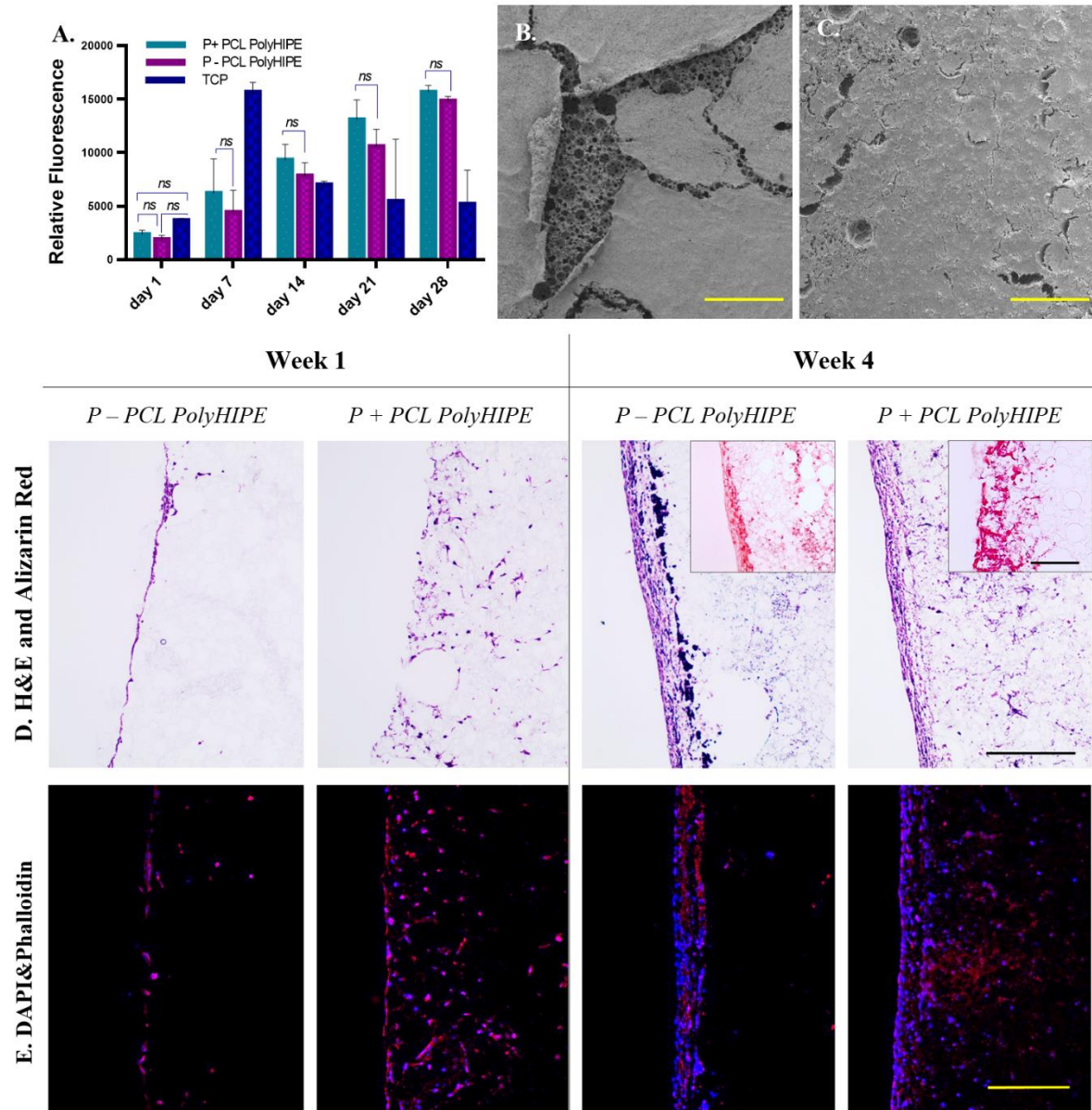
activities of MLO-A5s on both P+ and P- PCL PolyHIPEs increase from day 1 to day 28 gradually, but the dramatic decrease was observed in the metabolic activity of the MLO-A5s on tissue culture plate (TCP) after day 7.

Figure 3.3B and Figure 3.3C clearly show the positive impact of air plasma treatment of PCL PolyHIPE on the attachment of MLO-A5s to the surface at day 28. While the layer of MLO-A5s is peeled off from the surface of P- PCL PolyHIPE, cells on P+ PCL PolyHIPE are still integrated with the PolyHIPE layer. The preparation steps of the biological samples for SEM includes multiple washing steps and drying (Section 3.2.2.4.). The loosely attached cell layer detached from P- PCL PolyHIPE at the end of all these steps, probably due to limited cell penetration into the pores.

Although air plasma treatment seems as it has not had a significant effect on the metabolic activity of MLO-A5s, H&E and fluorescent images support the finding from SEM images, and they show that air plasma treatment has a huge impact on cell infiltration (Figure 3.3D, E). At week 1, while MLO-A5s only accumulated on the surface of the P- PCL PolyHIPE with nearly no infiltration, they were observed as migrating through the pores the P+ PCL PolyHIPE.

Even during the seeding of the MLO-A5s on the PCL PolyHIPE layer, the positive effect of plasma treatment was observed. Once the cell suspension was placed on the top of the PCL PolyHIPE, it immediately absorbed by P+ PolyHIPE but stayed as a droplet on the P- layer. This indicates that even from the cell-seeding stage onwards, plasma treatment encourages cells to migrate into the pores of the PCL PolyHIPE layer. Although MLO-A5s tend to densely accumulate on the top of both PCL PolyHIPEs at week 4, cell migration up to 400  $\mu\text{m}$  was observed on P+ PolyHIPEs. This positive influence of air plasma treatment on polymer scaffold has also been demonstrated *in*

*in vivo*. Valence et al. had reported improvement of cell attachment and infiltration within a vascular graft upon plasma treatment when materials were implanted subcutaneously [232].



**Figure 3.3:** (A) Metabolic activity of MLO-A5s cultured on P-, P+ PCL PolyHIPEs, and TCP for 4 weeks. SEM images of the top surfaces of (B) P+ and (C) P- PCL PolyHIPEs cultured MLO-A5s on for 4 weeks (Scale bar represents 500  $\mu$ m). (D) H&E and Alizarin Red, and (E) Fluorescent

*staining of MLO-A5s cultured on P+ and P- PCL PolyHIPEs for 1 week and 4 weeks (Scale bar represents 250  $\mu$ m, blue: DAPI, red: Phalloidin TRITC).*

Interestingly, on H&E slides, very small-sized haematoxylin-stained particles (different than haematoxylin stained cells) were observed only at week 4 at both P+ and P- PCL PolyHIPEs (Figure 3.3D). Fluorescent staining shows that they are not cells. It has been previously reported that haematoxylin selectively stains calcium-containing particles [378]. Alizarin red staining images show densely accumulated calcium on the top of P- PCL PolyHIPE and comparably less dense stains in deeper pores, while there is dense calcium deposition on P+ PCL PolyHIPE up to 400  $\mu$ m deep (Figure 3.3D).

### **3.3.3. Assessment of the extracellular matrix (ECM) deposition of MLO-A5s on PCL PolyHIPE layer**

As MLO-A5s cultured in supplemented media, they were expected to deposit calcified ECM [162,379,380]. Prideaux et al. previously reported that supplementation of MLO-A5 cell cultures with AA2P and  $\beta$ GP showed a significant increase in ECM mineralisation compared to the non-supplemented group [381].

Calcium and collagen deposition on P+ PCL PolyHIPE gradually increased from day 7 to day 28 (All subsequent studies were conducted on P+ PCL PolyHIPE only). ECM deposition, mineral nodules, and collagen fibres of MLO-A5s cultured on PCL PolyHIPE layer for 4 weeks are shown in Figure 3.4B. An SEM image of the cross-section of the PCL PolyHIPE shows the pores densely filled with cells and extracellular material (Figure 3.4C). Additionally, sub-micrometric crystalline debris was observed in regions beyond the maximum cell ingrowth (Figure 3.4D, E), these indicate the

existence of calcium deposits deep within the PolyHIPE layer, as also observed in on H&E and Alizarin red images.

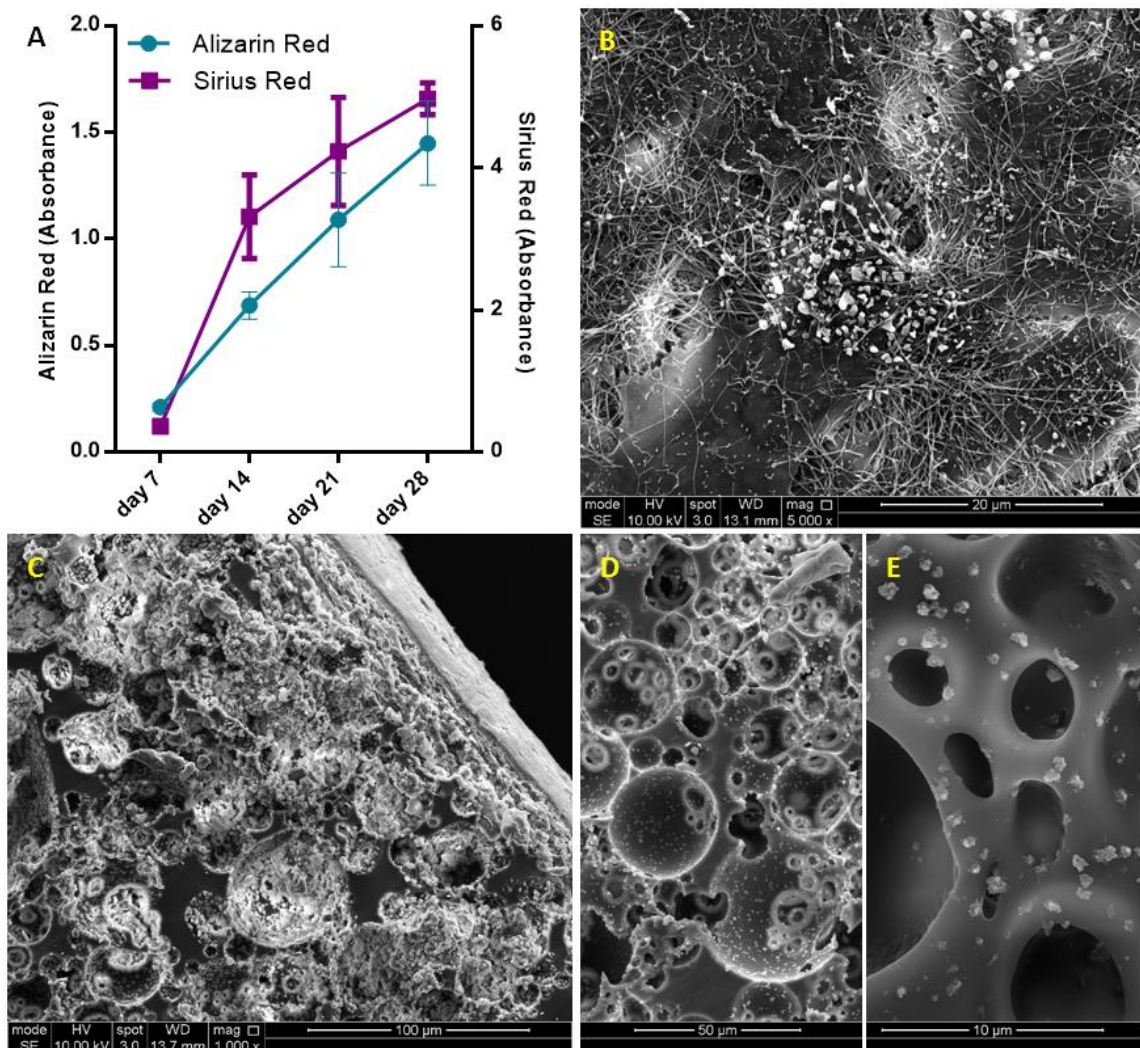


**Figure 3.4:** (A) Assessment of calcium and collagen deposition of MLO-A5s after 7, 14, 21 and 28-day culture on PCL PolyHIPE by using Alizarin Red and Sirius Red, respectively. (B) Scanning electron microscopy images of the surface, and (C, D, E) the cross-section of PCL PolyHIPE cultured with MLO-A5s for 28 days in supplemented media.

These calcium deposits look similar to surfaces of PolyHIPE layer incubated in simulated body fluid, which is commonly used to test the ability of the formation of bone-like apatite or mineral deposition on scaffolds [382–384]. The source and mechanism of the formation of the deposited calcium-containing crystals will be investigated in future studies.

### **3.3.4. Assessment of the performance of PCL PolyHIPE for supporting blood vessel ingrowth using ex-ovo CAM assay**

The CAM assay is a well-established method for the assessment of angiogenesis and initial response to biomaterials [201,277,385]. In an ex-ovo CAM assay, the embryos are transferred into petri dish on day 3 (Figure 3.5A) and incubated until day 7 (Figure 3.5B) which is the day of material implantation. At day 14, the following features can be assessed macroscopically (Figure 3.5C) and histologically (Figure 3.5D): (i) biocompatibility, (ii) cellular infiltration capacity and (iii) the performance of the PCL PolyHIPE layer for supporting vascularisation.

Our laboratory has reported the average survival rate for the ex-ovo CAM assay as 68% for intermediate and 83% for experienced users [277]. The survival rate of the chicks was approximately 75% and 73% for non-implanted, and PCL PolyHIPE implanted groups, respectively, in line with previous investigations. Thus, the PCL PolyHIPE showed good biocompatibility, and the implantation of the material did not affect the survival rate of the chicks.

The integration of the CAM tissue into PCL PolyHIPE was examined. Extensive cell infiltration was observed from the CAM tissue to PCL PolyHIPE, showing complete integration of the material with the membrane. During the isolation of the PCL PolyHIPE from the CAM, it was not possible to separate it from the CAM, which is also an indication of strong integration. This is in line with studies reported by other groups on the good-integration of PCL porous scaffolds with CAM [386–388]. The infiltration capacity of the cells into PCL PolyHIPE was better in the ex-ovo CAM assay (Figure 3.5D) when compared with the *in vitro* histology data (Figure 3.3D). This is potentially

due to the continuous contact of the PCL PolyHIPE with a dense and dynamic cell population in the CAM.

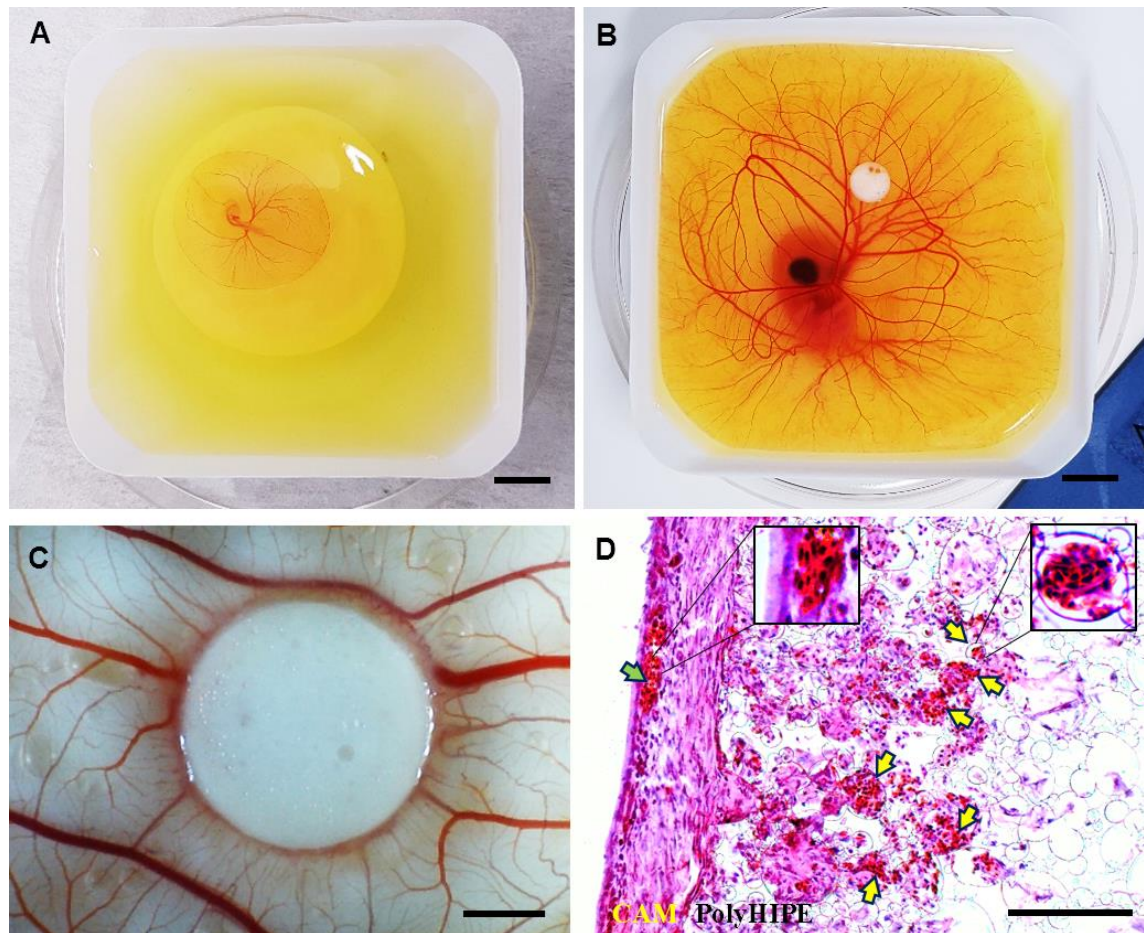


**Figure 3.5:** Chick embryos in a petri dish on (A) embryonic development day 3 and (B) embryonic development day 7 (Scale bar represents 10 mm). (C) PCL PolyHIPE on CAM at day 14 (Scale bar represents 2 mm). (D) H&E images of PCL PolyHIPE on CAM at day 14 (Green arrow indicates the blood vessel on CAM itself; yellow arrows indicate the blood vessels in PCL PolyHIPE. Scale bar represents 100  $\mu\text{m}$ ).

Assessment of the PolyHIPE material on the CAM demonstrated that the structure and the pore size of the PolyHIPE were suitable for supporting blood vessel ingrowth through the PolyHIPE. H&E staining shows that alongside the high level of integration of the host CAM tissue with the PolyHIPE layer, many blood vessels were found

growing into the pores of PCL PolyHIPE and through the interconnections (Figure 3.5D) in only 7 days.

Current understanding of vascularisation of porous scaffolds indicates that the pore size should be at least 250  $\mu\text{m}$  for vascularisation to occur [389,390], but some studies suggest smaller pore sizes can also allow for the ingrowth of blood vessels. Madden et al. have shown that 30-40  $\mu\text{m}$  pore size with 15  $\mu\text{m}$  interconnects are suitable for vascularisation in rats [391]. Similarly, Baker et al. reported that particulate-leached PCL scaffolds with 5-200  $\mu\text{m}$  pore range allowed extensive vascularisation in the scaffold when implanted subcutaneously into rats [392]. Klenke et al. observed vascularisation in ceramic particles with macropores ranged from 40 to 280  $\mu\text{m}$  [393]. Finally, our group has demonstrated the vascularisation of polylactic acid electrospun scaffolds with a mean pore size of 4.25  $\mu\text{m}$  in the CAM assay [394].

By using the CAM assay, we have shown the performance of the developed BM for supporting tissue integration and vascularisation. Both are critical factors in avoiding delay in osteogenesis and tissue regeneration and overcoming the rejection of an implant [395,396].

### **3.3.5. Assessment of solvent compositions in terms of their ability to form the nanofibrous structure**

The mean diameters of the PCL fibres where polymer solutions were prepared with different solvents were  $0.35 \pm 0.10 \mu\text{m}$ ,  $0.74 \pm 0.32 \mu\text{m}$ ,  $1.69 \pm 0.75 \mu\text{m}$ , and  $0.47 \pm 0.22 \mu\text{m}$ , and the average pore sizes were  $6.28 \pm 2.30 \mu\text{m}$ ,  $8.34 \pm 4.96 \mu\text{m}$ ,  $9.84 \pm 5.25 \mu\text{m}$ , and  $3.57 \pm 2.08 \mu\text{m}$  for acetone (100), acetone:chloroform (30:70), DCM:methanol (90:10), and chloroform:DMF (70:30) groups, respectively (Figure 3.6).

Except for the acetone (100) group, a decrease in the pore sizes was observed when the diameter of the PCL fibres gets smaller. Although the acetone (100) led to the formation of the smallest diameter PCL fibres, the smallest pore size was calculated for the electrospun layer prepared with chloroform:DMF (70:30).

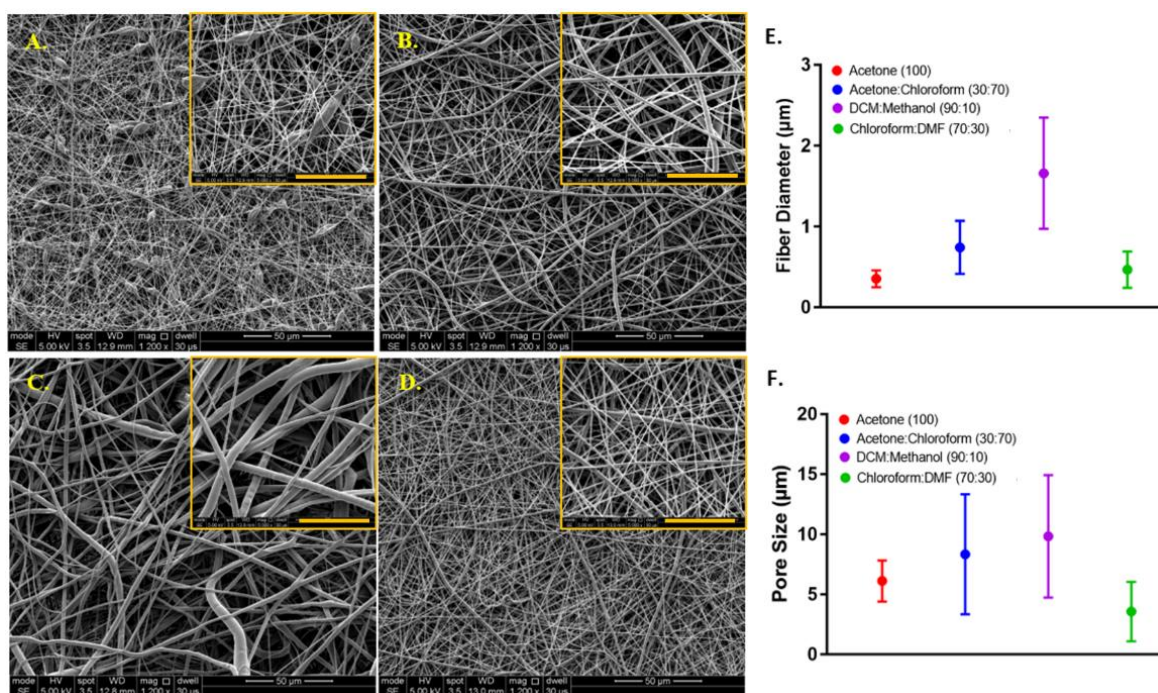


**Figure 3.6:** Morphological characterisation of the electrospun PCL fibres, where polymer solutions were prepared with different solvents. SEM image of PCL electrospun prepared by dissolving PCL in (A) acetone (100), (B) acetone:chloroform (30:70), (C) DCM:methanol (90:10), (D) chloroform:DMF (70:30). The graphs show (E) the fibre diameter and (F) the pore size distributions, respectively. Yellow scale bars represent 20 μm.

When acetone was used as the sole solvent, it was difficult to electrospin the solution, and bead formation occurred. The undesirable bead formation during electrospinning is likely to increase pore size between the fibres [397]. One of the main reason for the formation of thinner fibres and beads has been reported as the lower viscosity of the electrospinning solution [398]. It has previously been shown that among the five solvents used in this study, acetone has the lowest viscosity [399]. Zverev et al.

reported that the viscosity of the polymer solution changes with the solubility, and low viscosity is linked with poor solubility when other parameters kept constant [400].

The electrospinnability of the PCL solutions from high to low was: chloroform:DMF (70:30) > acetone:chloroform (30:70) > acetone (100) > DCM:methanol (90:10). The quality of the PCL electrospinning was assessed based on smooth fibre formation, bead or particle formation and continuous electrospinning of the solution, which depend on parameters such as solubility, viscosity, dielectric constant, and conductivity [401].

The solubility of the polymer in a solvent has a major effect on electrospinning nanofibres. DCM, methanol, chloroform, DMF and acetone (as single solvents or solvent blends) are common solvents for dissolving PCL and widely used for the production of PCL fibres with electrospinning [356,402]. Among these solvents, PCL has a higher solubility in chloroform and DCM, whereas the solubility of PCL is poor in DMF, acetone, and methanol [309].

When acetone was used as the single solvent to dissolve PCL, the solution resulted in poor electrospinnability and the formation of undesired beads during the electrospinning process. Using the acetone:chloroform (30:70) solvent blend significantly increased the electrospinnability of PCL, which can be explained by the addition of chloroform to the solvent mixture, in which PCL has higher solubility [403]. The ability to electrospin PCL dissolved in DCM:methanol (90:10) was very poor, and we did not manage to obtain nanofibers when this solvent used for electrospinning. This can be explained by the low dielectric constant and conductivity of the main solvent, DCM, in the solvent blend [404]. The best solvent blend for electrospinning PCL nanofibers was chloroform:DMF (70:30) solvent composition used. Although DMF is not classified as a good solvent for PCL, it has a high dielectric constant and, it is a

polyelectrolyte [405]. Due et al. previously reported that the addition of DMF to the solvent blend improves the electrospinnability of PCL and leads to smaller diameter fibre formation. [406]. Kanani et al. had shown that when DMF was added to methylene chloride, and the solvent mixture used for electrospinning PCL, the spinning process was improved, and uniform nanofibers were obtained [358]. Hsu et al. demonstrated a reduction in the diameter of electrospun PCL fibres with the addition of DMF to chloroform [407]. Bolgen et al. observed a dramatic decrease in diameter (from 1300 nm to 300 nm) when DMF was included in the solvent mixture up to 40% [408].

In this study, the chloroform:DMF (70:30) solvent blend was selected for the manufacturing of nanofibrous barrier layer due to multiple factors including the improved electrospinnability, the decreased fibre diameter, and the smaller pore size.

### **3.3.6. Manufacturing and characterisation of the PCL bilayer barrier membrane**

Following the optimisations of manufacturing of PCL electrospun and PCL PolyHIPE layers, two layers were combined to fabricate the bilayer BM (Figure 3.7A-D). The complete integration of both layers can be seen from SEM images. This is more likely due to the fact that both polymers are PCL, and the solvent composition used for electrospinning PCL can partially dissolve the surface of the PCL PolyHIPE layer. No delamination of the two layers was observed, and the BM preserved its integrity during the experiments.

Figure 3.7E-J shows the handling ability of the PCL bilayer BM. The resulting BM was very flexible and allowed manual handling, including bending and twisting without

losing its structural integrity. Figure 3.7I shows the space making ability of the BM, which is defined as the ability to maintain a space for cells without any collapse.

For this study, the thicknesses of the PCL electrospun and PCL PolyHIPE layers were determined as 200  $\mu\text{m}$  and 250  $\mu\text{m}$ , respectively. The thicknesses of the PCL electrospun and PCL PolyHIPE layers can be controlled easily by changing the electrospinning time and slicing thickness, respectively. To show the controllability of the thickness of the PCL electrospun layer, Figure 3.7B shows a bilayer membrane with a low thickness where PCL was electrospun on PolyHIPE for 20 minutes instead of 40 minutes. Thicker membranes are assumed to have better barrier performances in addition to higher mechanical strength [409] and a longer degradation time and which results in the GTR membrane being present during a longer time period [410]. The question of the optimum barrier membrane thickness can be answered to some extent, experimentally *in vitro*, but ideally, it needs to be investigated *in vivo* in future studies. Here, the tunability of the thickness of individual layers is an advantage in our manufacturing method as we can provide BMs of varying thicknesses for comparative evaluation of performance and rate of breakdown *in vivo*.

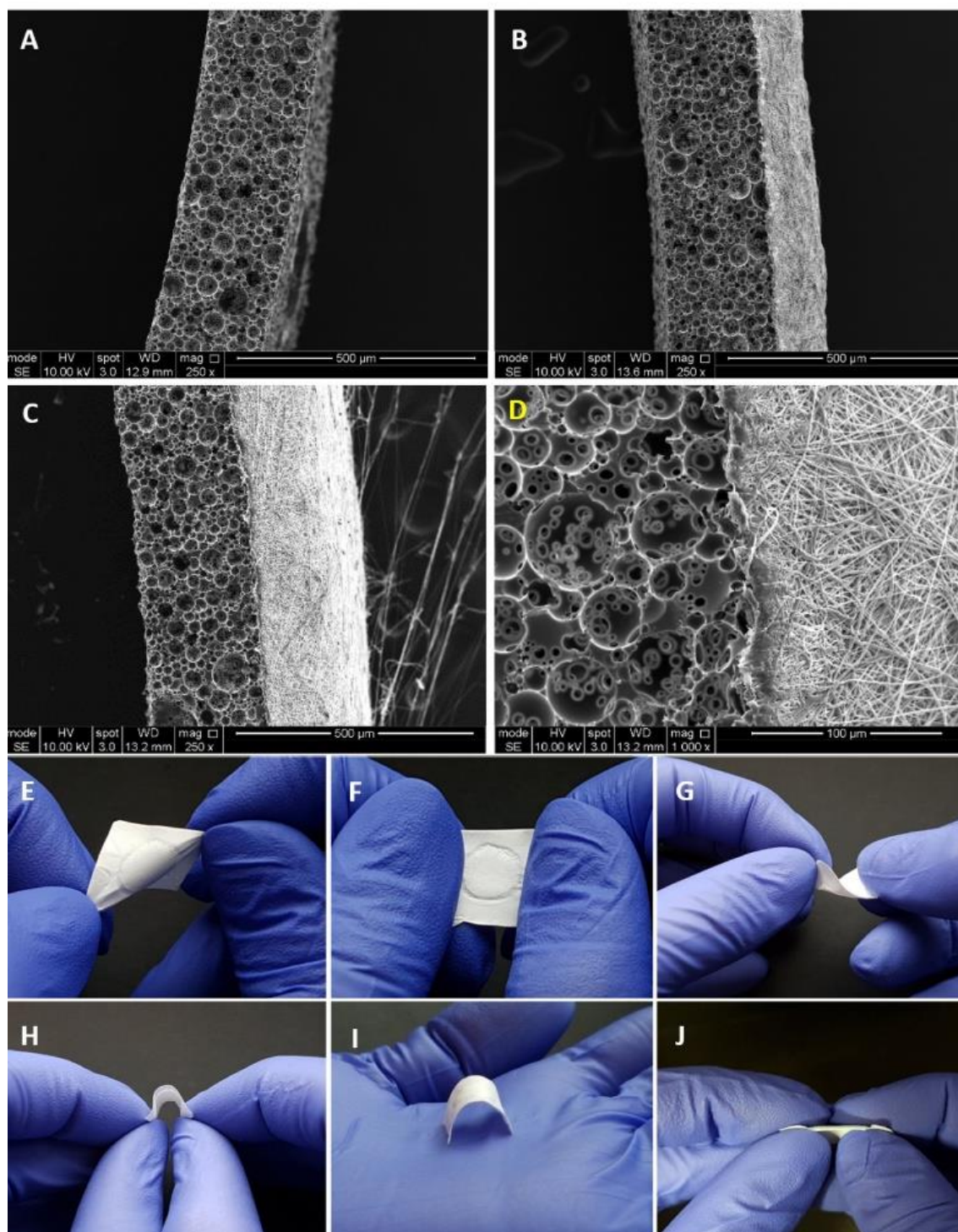


**Figure 3.7:** SEM images of (A) 250 μm sectioned PCL PolyHIPE layer, (B) 20 minutes PCL electrospun on PCL PolyHIPE, (C) 40 minutes PCL electrospun on PCL PolyHIPE, (D) Higher magnification SEM image showing the border of two layers. Macro images of the bilayer PCL BM to show the suitability of the design for (E-F) stretching in different axes, (G-H) bending, (I) space making, and (J) side view of the BM to show the integration of the two layers.

Tensile tests of the BMs were conducted on both dry and wet conditions. Biomedical implants are usually in contact with body fluids, which significantly influences their performance in comparison with their dry state. The mechanical behaviour of an implant under wet conditions is important for better representing the *in vivo* conditions [411].

Both the E and UTS values of dry BMs were significantly higher compared with the wet BM samples. But there was not any statistically significant difference between the elongation of the BMs in dry and wet state (Figure 3.8).

The UTS of the BM s were measured as  $137.3 \pm 6.7$  KPa and  $75.0 \pm 4.2$  KPa for dry and wet samples, respectively. The elastic modulus and elongation of dry and wet BMs are  $452.1 \pm 24.5$  KPa and  $304.2 \pm 12.9$  KPa; and  $79.3 \pm 3.5\%$  and  $83.2 \pm 2.1\%$ , respectively.

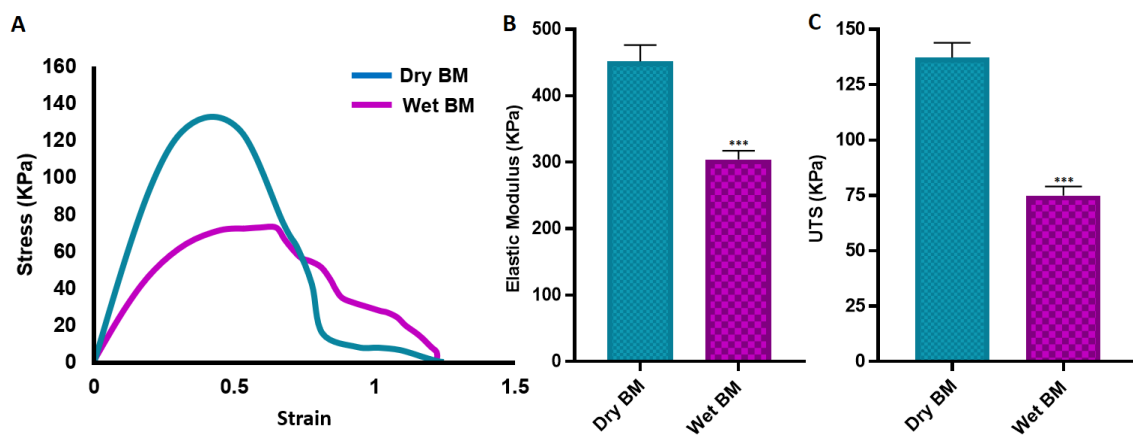


**Figure 3.8:** Mechanical properties of the BM under dry and wet conditions. (A) Representative stress-strain curves, (B) Elastic modulus, (C) UTS of the BMs under dry and wet conditions (\*\* $p \leq 0.001$ , ns  $p \geq 0.05$ ,  $n = 3$ ).

The mechanical properties of the developed membrane show similarities with other developed membranes in literature. Lee et al. reported tensile strength of commercial collagen membrane (Ossix plus) around 110 KPa and 20 KPa for the dry and wet state, respectively [409]. Poly(lactic-co-glycolic acid) (PLGA) membrane fabricated with

freezing and lyophilisation has been reported to have similar UTS with our BM where the elongation of the PLGA membrane was approximately eight times lower [412]. Similarly, the tensile strength of the freeze gelled chitosan membrane has been demonstrated approximately four times and ten times lower, respectively under dry and wet conditions when compared with the developed BM in this study [351]. Electrospun chitosan membrane with random fibre orientation has been shown to have slightly higher UTS in wet state, but at the same time, it was approximately ten times less elastic than our BM, and the elongation was almost six times lower [413]. Another study has revealed that the polysaccharide/bioactive glass membrane produced using the layer by layer deposition technique has very similar mechanical properties in terms of UTS and E values with our BM [414].

### **3.3.7. Assessment of the metabolic activity of HDFs on PCL electrospun layer and the ability of the PCL electrospun layer to act as a cell barrier**

The metabolic activities of HDFs growing on the PCL electrospun layer gradually increased from day 1 to 28 (Figure 3.9) showing the biocompatibility of the bilayer PCL membrane. Although the metabolic activities of the HDFs growing on TCP were higher at each time point, they started to drop after day 14. This decrease is more likely to be due to the limited to two dimensional surface of the TCP, which restricts the capacity of cells to expand [415].

Histological analysis of the PCL electrospun layer showed that HDFs were not able to penetrate due to the small pore sizes of nanofibrous random PCL fibres. Instead, they were observed as growing on the surface of the electrospun barrier layer and not

migrating towards the PolyHIPE layer (Figure 3.9) confirming the ability of cell-occlusiveness of the electrospun PCL layer. Randomly orientated nanofibrous scaffolds have been demonstrated as a physical barrier to cell penetration while allowing the diffusion of nutrients. Previous work from our laboratory has shown that keratinocytes and fibroblasts were successfully segregated when separated by a nanofibrous Poly(3-hydroxybutyrate-co-3-hydroxyvalerate) (PHBV) layer [348]. Similarly, Vaquette et al. showed that fibroblasts seeded on a random fibre mat did not penetrate the scaffold and colonised on the surface and formed a 30  $\mu\text{m}$  thick cell sheet [416].

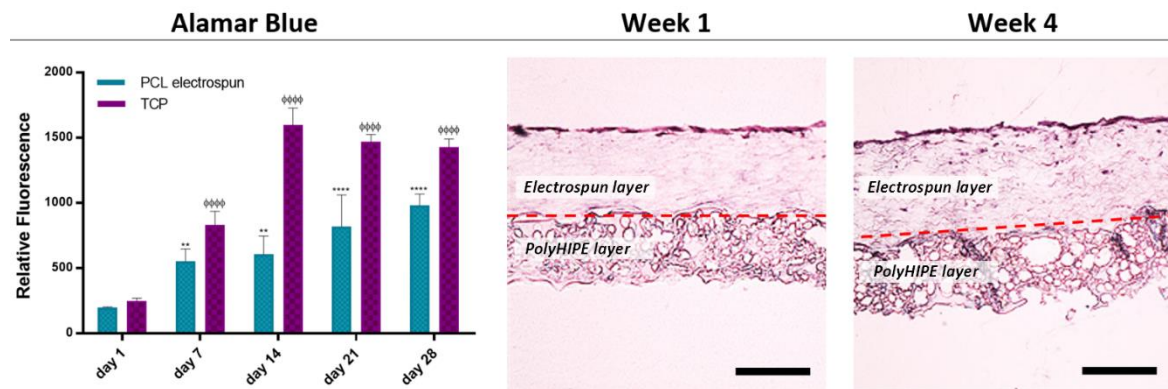


**Figure 3.9:** Evaluation of the biocompatibility and the barrier properties of the bilayer BM. The metabolic activity of the HDFs growing on PCL electrospun layer from day 1 to day 28 is given in the graph (\*\*\*) and  $\Phi\Phi\Phi p \leq 0.001$ , \*\* and  $\Phi\Phi p \leq 0.01$ , \* and  $\Phi p \leq 0.05$ ,  $n = 3$ ). Histological images demonstrate the barrier properties of the PCL electrospun layer over 4 weeks. Dotted line indicates the boundary of the two layers (Scale bar represents 200  $\mu\text{m}$ ).

As the crucial time for epithelial invasion has been reported as the first 14 days of implantation, then the barrier function limiting the epithelial invasion up to 14 days is considered sufficient for GBR applications [417,418].

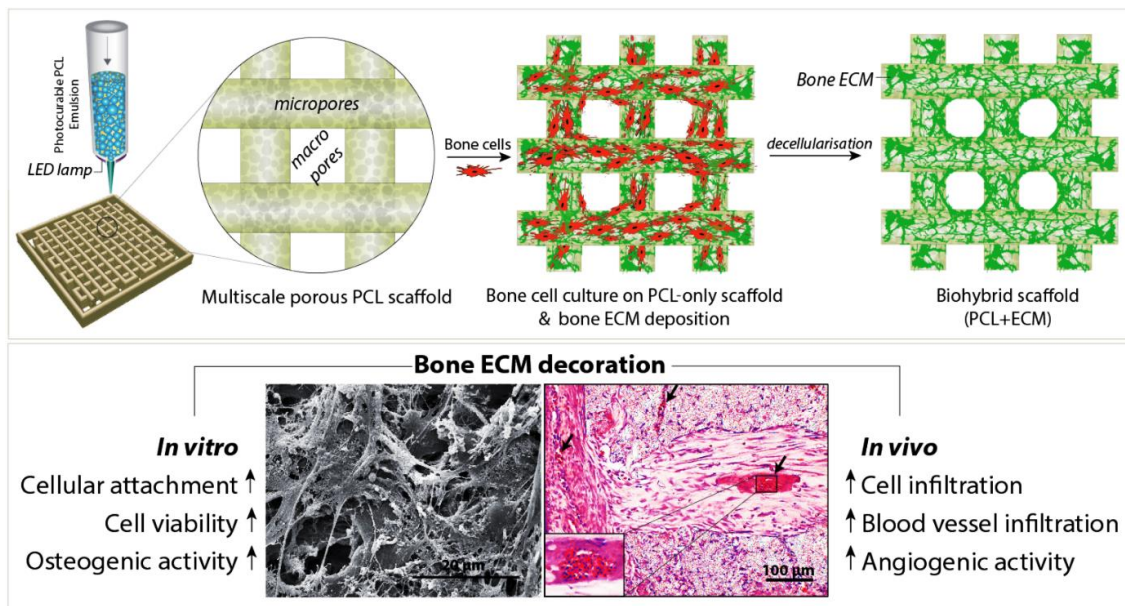
### 3.4. Conclusions

In the present study, a bilayer BM made of a biodegradable synthetic polymer, PCL was successfully fabricated by combining electrospinning and with emulsion templating. The resulting BM showed no delamination, and its structure was qualitatively resilient to torsion and stretching, and it was straightforward to handle. The electrospun layer of the BM has been confirmed for its barrier features for the prevention of soft tissue invasion whereas the interconnected PCL PolyHIPE layer has shown potential for use as the bone promoting layer providing the key requirements such as cell compatibility, supporting cellular infiltration, and promoting collagen and mineral deposition. Furthermore, the pore structure of the PCL PolyHIPE layer has been found to be suitable for blood vessel ingrowth. In conclusion, by combining two methods of fabricating, an FDA approved polymer, PCL, a bilayer BM that is a good candidate for a diverse range of GTR applications can be fabricated. Further exploration of the *in vivo* performance of the developed BM will be interesting in future studies.



# CHAPTER 4

## Boosting the osteogenic and angiogenic performance of multiscale porous polycaprolactone scaffolds by *in vitro* generated extracellular matrix decoration



### Abstract

Tissue engineering (TE)-based bone grafts are favourable alternatives to autografts and allografts. Both biochemical properties and the architectural features of TE scaffolds are crucial in their design process. Synthetic polymers are attractive biomaterials to be used in the manufacturing of TE scaffolds, due to various advantages; such as being relatively inexpensive, enabling precise reproducibility, possessing tunable mechanical/chemical properties, and ease of processing. However, such scaffolds need modifications to improve their limited interaction with biological

tissues. Structurally, multiscale porosity is advantageous over single scale porosity, therefore, in this study, we have considered two key points in the design of a bone repair material; (i) manufacture of multiscale porous scaffolds made of photocurable polycaprolactone (PCL) by a combination of emulsion templating and 3D printing, and (ii) decoration of these scaffolds with *in vitro* generated bone-like extracellular matrix (ECM) to create biohybrid scaffolds that have improved biological performance compared to PCL-only scaffolds. Multiscale porous scaffolds were fabricated, bone cells were cultured on them, and then they were decellularised. The biological performance of these constructs was tested *in vitro* and *in vivo*. Mesenchymal progenitors were seeded on PCL-only, and biohybrid scaffolds. Cells not only showed improved attachment on biohybrid scaffolds but also exhibited a significantly higher rate of cell growth and osteogenic activity. The chick chorioallantoic membrane (CAM) assay was used to explore the angiogenic potential of the biohybrid scaffolds. CAM assay indicated that the presence of the *in vitro* generated ECM on polymeric scaffolds resulted in higher angiogenic potential and a high degree of tissue infiltration. This study demonstrated that multiscale porous biohybrid scaffolds present a promising approach to improve bioactivity, encourage precursors to differentiate into mature bone, and to induce angiogenesis.

**Keywords:** *tissue engineering, emulsion templating, 3D printing, decellularisation, angiogenesis, PolyHIPE, biohybrid*

## **4.1. Introduction**

Bone grafting is the second most frequent tissue transplantation technique worldwide after blood transfusion [262]. Autogenous bone grafts are considered to be the gold

standard as they have osteogenic, osteoinductive and osteoconductive properties [419–421]. However, autologous bone is mostly harvested from the iliac crest (hip) with limited availability and carries the risk of donor site morbidity [422]. An acellular alternative to the autograft is an allograft, which is more abundantly available without size limitations [423]. However, allografts need to be processed and cleaned after isolation to prevent an immune response and disease transmission [424,425]. These treatments considerably affect the physical and biological properties of the bone, and the process results in grafts with comparably poor regenerative potential and/or weak mechanical properties depending on the treatment (demineralisation, deproteination, irradiation) [419,424]. The regulations of the European Union for medical devices, known as the Medical Device Directive (MDD) [426] were replaced with a new set of Medical Device Regulations (MDR) [280] in 2017, and the new MDR will come into force on May 2020. With the new MDR, human origin cells and tissues or derivatives will also be considered as a high-risk medical device (Class III) in addition to those of animal origin (Rule 18). Due to these regulatory restrictions, allografts including demineralised and deproteinised bone matrices (DMB and DPB) will likely have more restrictive approval processes and a more challenging pathway for clinical approval [281–283].

Alternatively, scaffold-based tissue engineering (TE) has gained great attention over the last years. Scaffolds are biodegradable porous matrices, made from natural or synthetic materials, which aim to mimic both the biochemical and structural features of native tissues for the regeneration of the defect site [28,427,428].

To date, several techniques including; electrospinning [429,430], particle leaching [431,432], freeze-drying [433,434], and additive manufacturing [18,435] have been

widely used for fabrication of bone TE scaffolds. Recently, emulsion templating has gained particular attention as a scaffold fabrication technique due to its ability to introduce up to 99% porosity with high interconnectivity into TE scaffolds. Emulsion templating is based on creating a stable emulsion by mixing two immiscible liquids and then polymerising the continuous phase. Emulsion droplets act as a pore template during polymerisation, and they are removed afterwards. When the internal phase volume (total droplet volume) of the emulsion is greater than 74%, it is defined as High Internal Phase Emulsion (HIPE). Typically, the average pore range of polymerised HIPEs (PolyHIPEs) varies from microns to 10s of microns [45]. As multiple length scale porosity is advantageous for bone regeneration when compared to single scale porosity [436], combining emulsion templating with additive manufacturing enables the fabrication of hierarchically porous scaffolds [70,76,146,162].

PolyHIPEs are most commonly created using water-in-oil (w/o) emulsions where a synthetic hydrophobic polymer is used as the continuous phase. Synthetic polymers have various advantages over ceramics and natural polymers such as; having tailorable physical, chemical, and mechanical properties, precise reproducibility, controllable biodegradability, and processability [219,437,438]. However, they have the disadvantage of having comparably limited interaction with biological tissues [439,440]. One approach to overcome this limitation is the decoration of polymeric scaffolds with ceramic particles [441] or exogenous extracellular matrix (ECM) components [442] such as peptides [443,444], proteins and growth factors [445,446]. Nevertheless, the incorporation of a limited number of exogenous ECM elements is not entirely sufficient to mimic the unique complexity of the natural ECM [447], which is a rich source of bioactive molecules [448,449]. For this reason, TE adopts cell-based approaches in which live cells are implanted with the biomaterial. However, the use of

live cells is clinically risky, expensive, and time-consuming [450]. Therefore, there has been an increasing interest in using cell-derived ECM to increase the biological performance of the scaffolds while avoiding the implantation of live cells [419,449,451–455].

Recently, we reported the development of polycaprolactone (PCL)-based PolyHIPes and demonstrated their initial cell-compatibility [42] and their potential use in guided bone regeneration [13]. However, due to the hydrophobic nature of the PCL, cell infiltration was limited unless the PCL-based scaffolds were treated with air-plasma [13]. Although there is an increasing demand for the use of emulsion templated scaffolds for various TE applications [46,186] due to their ability to create structures with favourable morphological properties, there are only a limited number of studies establishing methods to improve the cell-material interactions of PolyHIPE scaffolds, and these are limited to the incorporation of a single biologically active agent [136,223] or hydroxyapatite (HA) [131,134].

Herein, we aimed to consider both the structural and biochemical requirements for the development of scaffolds for bone regeneration and suggest an alternative approach to improve the biological performance of w/o PolyHIPes. Firstly, we manufactured multiscale porous polymeric scaffolds by combining emulsion templating and 3D printing techniques, taking advantage of the photo-cure ability of the synthesised PCL (Figure 4.1). Subsequently, we populated them with bone cells to decorate these scaffolds with an *in vitro* cell-derived ECM. Finally, we decellularised these constructs to obtain biohybrid scaffolds made of PCL and bone-like matrix. The biohybrid scaffolds were then evaluated for their ability to support cell attachment, cell viability, and osteogenic differentiation using human embryonic stem cell-derived

mesenchymal progenitor cells (hES-MPs). The angiogenic potential of the biohybrid multiscale porous scaffolds was assessed using a well-established *in vivo* assay, *ex-ovo* chick chorioallantoic membrane assay (CAM).

## 4.2. Experimental

### 4.2.1. Materials

Pentaerythritol (98%),  $\epsilon$ -caprolactone, tin (II) 2-ethylhexanoate, triethylamine (TEA), methacrylic anhydride (MAAn), photoinitiator (2,4,6-Trimethylbenzoyl Phosphine Oxide/2-Hydroxy-2-Methylpropiophenone blend), fungizone, fetal calf serum (FCS), penicillin/streptomycin (PS), L-glutamine, trypsin, 37% formaldehyde (FA) solution, resazurin sodium salt, glutaraldehyde, ethanol, hydrochloric acid (HCl), sodium hydroxide (NaOH), hexamethyldisilazane (HMDS), perchloric acid, picric acid, hematoxylin solution, eosin Y solution, porcine gelatine, beta-glycerolphosphate ( $\beta$ GP), ascorbic acid 2-phosphate (AA2P), dexamethasone, Triton X-100 (Triton), deoxyribonuclease (DNase), and Alizarin red S were purchased from Sigma Aldrich (Poole, UK). Direct Red 80 (Sirius Red) was purchased from Fluka (Buchs, Switzerland). Chloroform, industrial methylated spirit (IMS), dichloromethane (DCM), and methanol (MeOH) were purchased from Fisher Scientific (Pittsburgh, PA, USA). The surfactant Hypermer B246-SO-M was received as a sample from Croda (Goole, UK). Minimum Essential Alpha Medium ( $\alpha$ -MEM) was purchased from Lonza (Slough, UK). Quant-iT™ PicoGreen® dsDNA Assay (PG) Kit and human fibroblastic growth factor (hFGF) were obtained from Life Technologies (Frederick, Maryland, USA). Optimum cutting temperature tissue freezing medium (OCT-TFM) was purchased from Leica Biosystems (Newcastle, UK).

## 4.2.2. Manufacturing and characterisation of the multiscale porous PCL scaffolds

Multiscale porous photocurable PCL-based scaffolds were created in three main steps: (i) synthesis of 4-arm hydroxyl-terminated polycaprolactone (4PCL) and methacrylate functionalisation of 4PCL (4PCLMA) to make the polymer photocurable, (ii) preparation of the emulsions made of 4PCLMA, and (iii) simultaneous 3D printing and cross-linking of 4PCLMA-based emulsions.

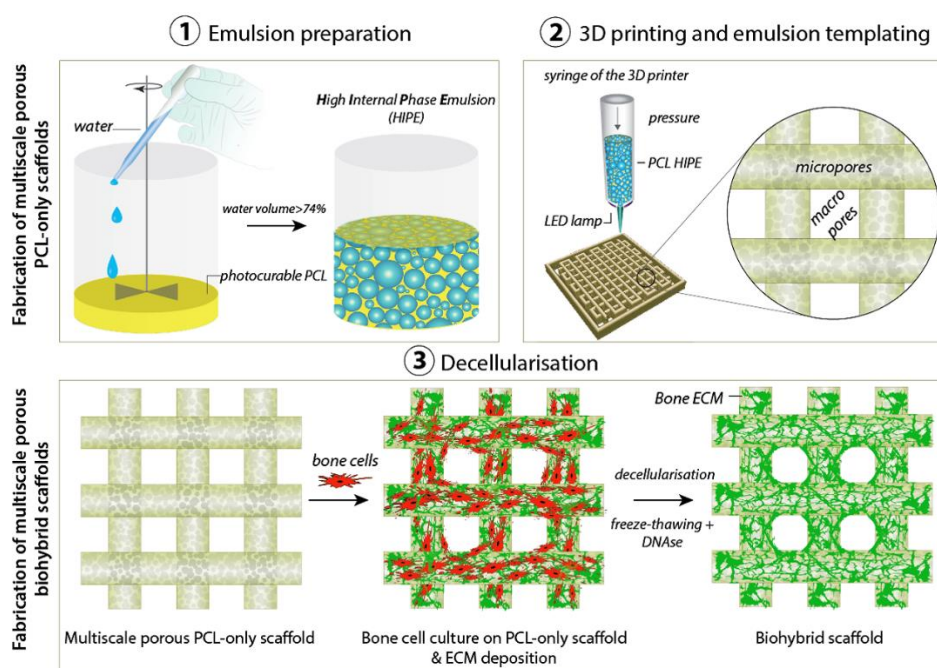


**Figure 4.1:** Manufacturing routes of the multiscale porous photocurable polycaprolactone (PCL) scaffolds (step 1, 2) and multiscale porous biohybrid scaffolds (step 1-3). (1) Preparation of the emulsion made of photocurable PCL and water, (2) the transfer of the PCL-based high internal phase emulsion (HIPE) into the syringe, pressure-assisted 3D printing and simultaneous cross-linking, and (3) the culture of bone cells on PCL-only scaffold to be decellularised and generation of the biohybrid scaffolds.

### 4.2.2.1. Synthesis and methacrylation of 4PCL

The detailed synthesis of the polymer, 4PCLMA has been described elsewhere [42]. Briefly, under nitrogen flow, pentaerythritol (0.088 mol) and  $\epsilon$ -caprolactone

(0.705 mol) were added into a three-neck round-bottomed flask, and the system was heated to 160 °C using an oil bath while being mixed at 200 rpm. When the pentaerythritol was completely dissolved, the catalyst, tin(II) 2-ethylhexanoate was added, and the system was left overnight to form 4PCL before being removed from the oil bath and left to cool down in the ambient atmosphere.

4PCL was dissolved in 300 mL of DCM, and then TEA (0.705 mol) was added. Reagents were stirred, and a further 200 mL of DCM was added to ensure everything was dissolved. The flask was placed in an ice bath. MAA<sub>n</sub> (0.705 mol) was dissolved in 100 mL DCM and transferred into a dropping funnel (~1 drop per second). When the MAA<sub>n</sub> was completely dispensed, the ice bath was removed, and the system was maintained at room temperature (RT) for 68 hours while being mixed. It was then washed with HCl solution, and then with deionised water (dH<sub>2</sub>O) to remove TEA, MAA, and salts formed. Almost all solvent was evaporated using a rotary evaporator. Three methanol washes were applied, and any remaining solvent was removed using a rotary evaporator. 4PCLMA was stored in the freezer (-20 °C) for further use.

#### **4.2.2.2. Characterisation of 4PCL and 4PCLMA**

To confirm the structure of 4PCL and 4PCLMA, and also to measure the degree of methacrylation, proton (<sup>1</sup>H) nuclear magnetic resonance (NMR) spectroscopy analysis was performed on an AVANCE III spectrometer at 400 MHz. The spectra were recorded using an 8.2 kHz acquisition window, with 64 k data points in 16 transients with a 60 s recycle delay (to ensure full relaxation). Deuterated chloroform was used as a diluent (CDCl<sub>3</sub>). Spectra were analysed using MestReNova software. Chemical shifts were referenced relative to CDCl<sub>3</sub> at 7.26 ppm.

The weight average molecular weight ( $M_w$ ) and number average molecular weight ( $M_n$ ) distributions of 4PCLMA were determined using a Viscotek GPCmax VE200 gel permeation chromatography (GPC) system with a differential refractive index detector (Waters 410). Tetrahydrofuran was used as the eluting solvent at a flow rate of 1 mL/minute at 40 °C, and polystyrene standards were used as the calibration sample.

#### **4.2.2.3. Preparation of 4PCLMA-based HIPEs**

Throughout this study, the only polymer used was 4PCLMA, and it has been entitled as PCL in the rest of the text except Section 4.3.1 unless otherwise stated. PCL (0.2 g) and 10% (w/w) surfactant were added into a glass vial ( $\varnothing=25$  mm) and heated to 40 °C to dissolve surfactant and left for cooling. Chloroform/toluene solvent blend (40/60 (w/w), 0.3 g) was added to the PCL-surfactant mixture and mixed at 375 rpm using a magnetic stirrer (8x20 mm) for 1 minute at RT. Once the homogeneous mixture was created, 2 mL water was added dropwise for PCL HIPEs ( 89% internal phase volume), and the emulsion was mixed for a further 5 minutes at 375 rpm and 5 minutes at 1000 rpm.

#### **4.2.2.4. Viscosity measurements**

AR2000 (TA Instruments, Ettenleur, The Netherlands) was used to characterise the viscosity of the PCL HIPEs. 40 mm 2° steel cone plates were used with a gap of 55  $\mu$ m at 25 °C. 0.6 mL of sample was injected, and a continuous ramp step was applied with a shear between 0.01 and 10  $s^{-1}$  for 1 minute using linear mode and 50 points per decade.

#### **4.2.2.5. 3D printing and polymerisation of PCL-based HIPEs**

A 10x10x1.4 mm tetragonal prism was designed using Solidworks (2012) and saved as a standard tessellation language (.stl) file format. This file was imported into

Repetier host to convert .stl format to .gcode format, which is a layer by layer design of the scaffold to make it recognisable by the printer (Figure 4.2). During the conversion, the following parameters were set: layer height; 100  $\mu\text{m}$ , infill; 36% rectilinear, and speed; 13 mm/s (Table 4.1).

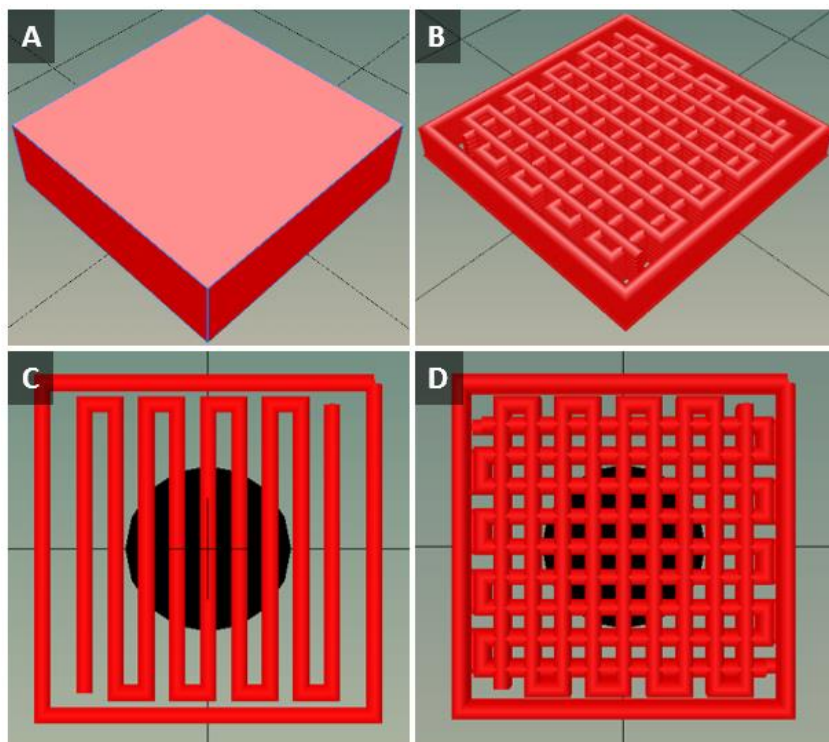


**Figure 4.2:** Isometric view of (A) the 3D design of the tetragonal prism (10x10x1.4 mm, .stl) and (B) the layer-by-layer design of the scaffold. (C) Top view of a single layer and (D) complete model of the layer-by-layer design.

The Gcode file was imported into Bioprint software, and the PCL-based HIPE was loaded into a syringe with a 30G precision tip needle. The syringe was connected to the compressor line and placed into a three-axis dispensing control system at RT. The pressure was set to 20 psi; however, slightly adjusted throughout the process for the best results. Multiscale porous PCL scaffolds were prepared by simultaneous printing and crosslinking of the PCL-based HIPE with the help of the integrated LED lamp (400-410 nm) of the printer (Biobots, Philadelphia, PA, USA).

**Table 4.1:** Design and processing parameters of the scaffolds.

<b>Dimensions of the model</b>	10x10x1.4 mm
<b>Layer height</b>	100 $\mu\text{m}$
<b>Infill</b>	36% rectilinear
<b>Speed</b>	13 mm/s
<b>Pressure</b>	20 psi
<b>Needle size</b>	Inner diameter; 150 $\mu\text{m}$ (30 G) Outer diameter; 310 $\mu\text{m}$

#### 4.2.2.6. Morphological investigation of the multiscale porous PCL scaffolds

Scanning electron microscopy (SEM) was used to investigate the microarchitecture of the scaffolds. Samples were gold sputter-coated in 15 kV for 2.5 minutes to increase conductivity. A FEI Inspect F SEM (Philips/FEI XL-20 SEM, Cambridge, UK) was used with 10 kV power. 20 pores, 20 struts, and 50 micropores were selected randomly, and measurements were taken. A statistical correction factor ( $2/\sqrt{3}$ ) was applied to micropore measurements to adjust the underestimation of diameter because of uneven sectioning [66]. The degree of interconnectivity was calculated by dividing the average window size by the average pore size ( $d/D$ ) [42,69], and the degree of openness was calculated by dividing open surface area to total surface area [50,70]. The window diameters of 50 micropores (426 windows in total) were measured.

### **4.2.3. Manufacturing of the biohybrid scaffolds via *in vitro* generated ECM matrix deposition on multiscale porous PCL scaffolds**

Biohybrid scaffolds, made of PCL and bone ECM, were manufactured in three main steps; (i) manufacturing of the multiscale porous PCL scaffolds as described in Section 4.2.2, (ii) cellularisation, and (iii) decellularisation of these scaffolds.

#### **4.2.3.1. Cellularisation of the multiscale porous PCL scaffolds with bone cells**

Multiscale porous PCL scaffolds were washed with 100% ethanol four times (24 hours each) to remove any remaining contaminants of surfactant, solvent or uncured material. Then, they were left in 70% ethanol for 2 hours and then transferred into PBS in sterile conditions, four PBS washes were applied in 24 hours.  $\alpha$ -MEM supplemented with 10% FCS, 2 mM L-glutamine and 100 mg/mL PS was used as a basal cell culture media (BM). Scaffolds were conditioned with BM for two hours in the incubator. Murine Osteoblast/Osteocyte-like cells (MLO-A5s) were defrosted into gelatine-coated T75 flasks and cultured until 90% confluence. MLO-A5s were expanded, trypsinised, counted and centrifuged. The cell pellet was re-suspended in fresh BM media (25000 cells / 20  $\mu$ m). The media in the well plate was aspirated, and 20  $\mu$ m of cell suspension was placed on the whole surface of each scaffold homogeneously and left for 2 hours in an incubator (37 °C, 5% CO<sub>2</sub>) for cell attachment. During this time, to prevent cells from drying out and keep the inside of the well humid, 4 mL BM media was injected into the spaces between the wells. After 2 hours, 2 mL of BM media was supplied into each well and incubated overnight. On the following day, scaffolds were transferred into a fresh well plate and incubated with supplemented media (SM) consisting of BM with 50  $\mu$ g/mL AA2P and 5 mM  $\beta$ GP for 28 days. Cell culture media was changed every 2-3 days.

#### **4.2.3.2. Decellularisation of the multiscale porous PCL scaffolds populated with bone cells**

Three different decellularisation methods were used for devitalisation of multiscale porous PCL scaffolds cultured with MLO-A5s; freezing and thawing (ft), Triton and ammonia (ta), and DNase. Four different combinations of these protocols were tested; (i) ft only, (ii) ft+ta, (iii) ft+DNase, (iv) ft+ta+DNase, and they were compared in terms of their efficiency of DNA removal. Before applying each decellularisation protocol, culture media was removed, and scaffolds were washed twice with PBS. Each method is described in the following section. At the end of the application of a decellularisation method, scaffolds were washed with warm (37 °C) PBS three times to remove the cellular component. Combined protocols were applied by following the individual protocols in order.

The method of ft is categorised as mechanical decellularisation, and it is applied by alternating the temperature between freezing temperatures and biological temperatures. The ft technique leads to lysis of cells by the help of intracellular ice crystals. Although this technique maintains ECM properties, its usage as a single-step method has been found to be inefficient based on DNA removal [456]. Herein, we applied consecutive three freeze-thaw cycles. For one freeze-thaw cycle, scaffolds were left in -80 °C for 15 minutes and transferred into a 37 °C water bath for 30 minutes.

Triton is a non-ionic detergent and used as a chemical decellularisation agent, it disrupts lipid-lipid and lipid-protein interactions, and it is less damaging to ECM structure in comparison with ionic detergents such as sodium dodecyl sulphate. Triton is commonly used with ammonium hydroxide (triton + ammonium hydroxide: ta),

which is an acid, and it also solubilises the cell membrane and nuclear components [457]. Scaffolds were incubated in a 1 mL mixture of Triton (0.5%) and ammonium hydroxide (20 mM in PBS) for 10 minutes at 37 °C and the solution was removed afterwards.

DNase is as an enzymatic decellularisation agent, used for breaking down of DNA fragments and removal of the nucleotides lysis of the cell membrane with another complementary method. There are no reported adverse effects of DNase on ECM [458–460]. Scaffolds were incubated in 1 mL DNase solution (0.2 mg/mL) in an incubator for an hour.

#### **4.2.4. Cellularisation of the biohybrid scaffolds with mesenchymal progenitors**

Multiscale porous PCL-only scaffolds and biohybrid scaffolds were seeded with hES-MPs (Cellartis, Sweden) for testing their biological performance. HES-MPs were defrosted into gelatine-coated T75 flasks and cultured until 90% confluence with BM. During the expansion of cells, BM was supplemented with hFGF at 4 ng/mL to stop differentiation of cells to other cell types. After the expansion of cells, they were trypsinised, counted, and centrifuged. The cell pellet was re-suspended in fresh media (25000 cells / 20 µm). The media in the 24 well plate was aspirated, and 20 µm of cell suspension was placed on the whole surface of each scaffold homogenously and left for 2 hours in an incubator (37 °C, 5% CO<sub>2</sub>) for cell attachment. During this time, to prevent cells from drying out and keep the inside of the well humid, 4 mL BM media was injected into the spaces between the wells. After 2 hours, 2 mL of BM media was supplied into each well and incubated overnight. On the following day, scaffolds were

transferred into the fresh well plate and incubated with osteogenic media (OM) consisting of SM with 100 nM dexamethasone for 28 days. Cell culture media was changed every 2-3 days.

#### **4.2.5. Biological characterisation of PCL-only and biohybrid scaffolds**

##### **4.2.5.1. Cell viability assay**

Resazurin reduction (RR) assay was applied to measure the cellular metabolic activity and estimate the cell viability on scaffolds. Resazurin solution (non-fluorescent, blue) is reduced by the cells and forms resorufin (fluorescent, pink) which is detectable by a fluorescence plate reader. 1mM Resazurin stock solution (in dH<sub>2</sub>O) was diluted to 100 µM in culture media to make the resazurin working solution. 1 mL of resazurin working solution was added into each well, and the scaffolds were transferred into a fresh well plate using sterile forceps. The well plates were protected from light and incubated for 4 hours at 37 °C. From each scaffold, triplicate samples of 200 µL of the reduced solution were added to a 96 well plate. This was measured three times using a spectrofluorometer (FLX800, BIO-TEK Instruments, Inc.) at an excitation wavelength of 540 nm and an emission wavelength of 630 nm. RR assay was performed at days 1, 7, 14, 21, and 28 of culture for both MLO-A5s and hES-MPs using a fresh scaffold for each time points.

##### **4.2.5.2. Measuring DNA content**

To find the cell seeding efficiencies of MLO-A5s and hES-MPs and to measure the remaining DNA content following the decellularisation of the scaffolds, a Quant-iT™ PicoGreen® dsDNA Assay Kit was used. Scaffolds were washed with PBS three times, and 500 µL cell digestion buffer was added and incubated for 30 minutes. The three freeze-thaw cycles were applied, and scaffolds were vortexed for 15 seconds. Scaffolds

were removed, and the remaining buffer was mixed homogenously. The sample and the Picogreen working solution were transferred into 96 well-plate (1:1) as triplicates. The plate was covered with aluminium foil and incubated at RT for 10 minutes with gentle shaking. The resulting solution was read by using spectrofluorometer at an excitation wavelength of 485 nm and an emission wavelength of 528 nm.

#### **4.2.5.3. Measuring ECM deposition**

Alizarin red (AR) and Sirius red (SR) staining was conducted to measure calcium and collagen deposition, respectively. Culture media was removed, and scaffolds were washed with PBS. Scaffolds were transferred into 1 mL 3.7% FA and left for 2 hours at RT. FA was removed, and scaffolds were washed twice with dH<sub>2</sub>O. AR powder was dissolved in dH<sub>2</sub>O at 1% (w/v) in a water bath and filtered to remove particles to make alizarin red solution (ARS). SR powder was dissolved in saturated picric acid (1% (w/v)) to form Sirius red solution (SRS) and filtered to ensure no particles remained. Scaffolds were submerged in 1 mL of SRS or ARS and left for 1 hour. The solution was removed, and scaffolds were washed every five minutes with dH<sub>2</sub>O while being mixed until the water remains clear. Scaffolds were submerged with a known volume of 5% perchloric acid or 0.2 M NaOH:MeOH (1:1) to destain the AR and SR, respectively, for 1 hour with gentle orbital shaking. 150 µL of the destain solution in triplicates were transferred into a clear 96 well plate and read at an absorbance of 405 nm.

#### **4.2.5.4. SEM of Biological Samples**

Scaffolds were washed three times with PBS after removing culture media and fixed in 2.5% (in PBS) glutaraldehyde at RT for 1 hour to preserve cell structure. They were rinsed with PBS for 15 minutes (3 times) and soaked in dH<sub>2</sub>O for 5 minutes. Following this, samples were subjected to serial ethanol washes to be dehydrated (35%, 60%,

80%, 90%, and 100% for 15 minutes for each concentration). Finally, samples were treated with drying agent HMDS/ethanol (1:1) for 1 hour and 100% HMDS for 5 minutes before air drying. Samples were gold coated and visualised using methods described in Section 4.2.2.6.

#### **4.2.5.5. Energy Dispersive X-ray analysis (EDX)**

Biological samples were prepared in the same way as described in Section 4.2.5.4. and carbon-coated. SEM microscopy (FEI Inspect F50 (Philips/FEI XL-20 SEM, Cambridge, UK)) with an energy dispersive analyser was used with 10 kV power for scanning and EDX elemental mapping.

#### **4.2.5.6. *Ex ovo* CAM assay**

Fertilised eggs (Henry Steward Co. Ltd, UK) were cracked, and embryos were transferred into weighing boats inserted inside the Petri dishes at embryonic development day (EDD) 3. The *ex-ovo* chick embryos were cultured in an incubator at 38 °C from EDD 3 to EDD 8 without any further modification. At EDD 8, PCL-only scaffolds (negative control), hybrid scaffolds, and scaffolds cultured with MLO-A5s (4 weeks) (positive control) were cut by using a sterile punch ( $\varnothing=6\text{mm}$ ) and placed on CAM and incubated. At EDD 14, digital images were taken, and embryos were sacrificed by cutting their arteries. Scaffolds were isolated with 1 cm CAM margin for histological assessment.

#### **4.2.5.7. Morphometric quantification of the angiogenesis**

At EDD 14, the macro-images of the scaffolds on CAM were taken with a digital microscope (Figure 4.3A). Four digital images from each group were quantified using a modified version of a well-established method [201,461,462]. A 10 mmx10 mm region was cropped in each image. To improve the discernability of the blood vessels,

the following parameters were set to all images in Adobe Photoshop CS6 ; brightness and contrast; -50/10, unsharp; 50/10/0, smart sharpen; 100/5 with gaussian blur and reduced noise; 5/0/0/50 (Figure 4.3B). A new layer was created in Photoshop, and all discernable vessels were drawn digitally using a Wacom Intuos Pro Medium Tablet with 2 pixels size-hard round brush (Figure 4.3C).

The layer created for the drawing of blood vessels was exported from Photoshop and imported into Image J (Figure 4.3D). The image was converted to binary, inverted and saved (Figure 4.3E). The number of blood vessels was calculated by counting the total count of the vessels touching the border of the scaffolds. The total vessel length and the total number of junctions were quantified using Angiotool (National Cancer Institute, MD, USA) (Figure 4.3F).

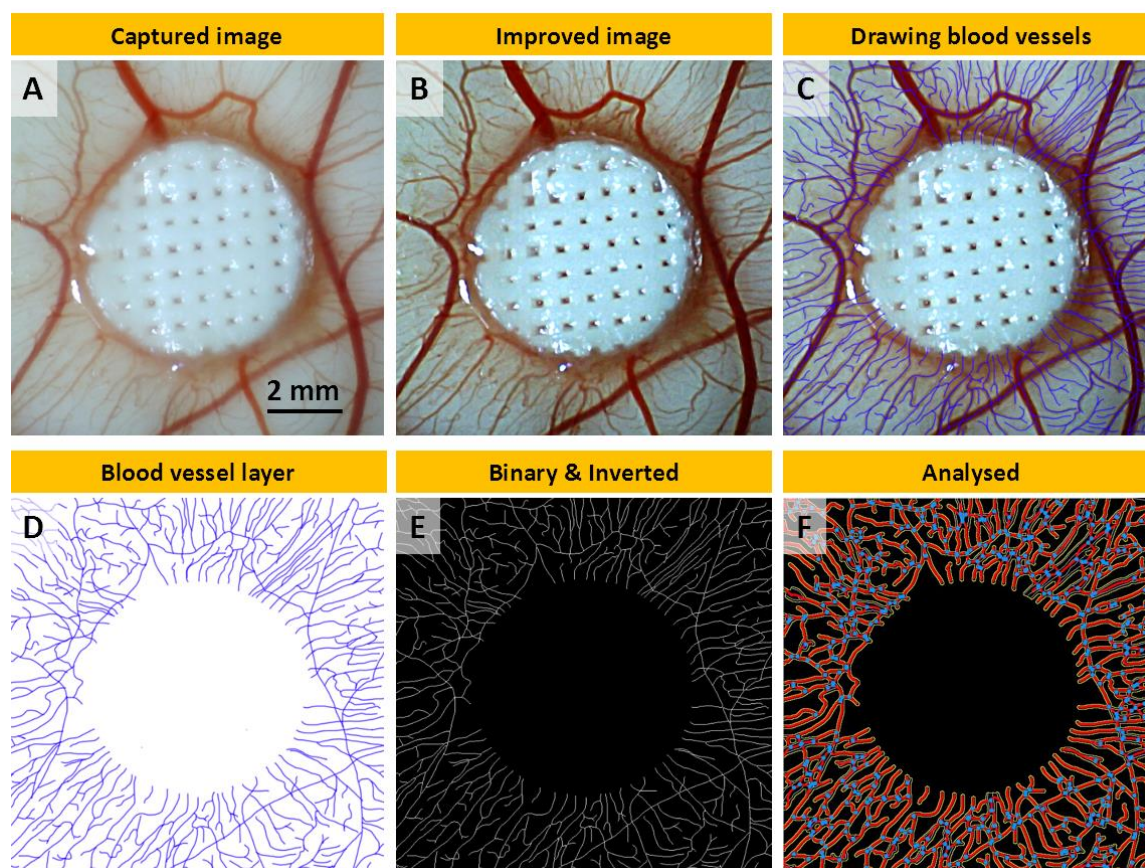


**Figure 4.3:** Steps of the morphometric quantification of angiogenesis; (A) macro-image as captured, (B) improved image using Photoshop, (C) drawn discernable blood vessels, (D) exported blood vessel layer from Photoshop, (E) binary and inverted image in Image J, (F) analysed image using Angiotool.

#### 4.2.5.8. Haematoxylin&Eosin staining

Haematoxylin&Eosin (H&E) staining on PolyHIPE scaffolds has been described in detail elsewhere [42]. Briefly, scaffolds isolated from CAM were washed with PBS and fixed in 3.7% FA. Scaffolds were transferred into cryomolds filled with freezing media and frozen. Sections with 5-8  $\mu\text{m}$  thickness were sliced on glass slides using the cryostat (Leica CM1860 UV, Milton Keynes, UK). Slides were stained with hematoxylin and eosin for 1.5 minutes and 5 minutes, respectively. After washing with  $\text{dH}_2\text{O}$ , slides were dehydrated in IMS and dunked into xylene. The slides were then mounted with DPX, and the images were captured using a light microscope (Motic BA210, China).

#### **4.2.6. Statistical analysis**

Statistical analysis was carried out using GraphPad Prism. Comparisons of more than two groups were performed with one-way ANOVA to find the statistical significance. Where relevant, n values are given in figure captions. Error bars indicate standard deviations in the graphs unless otherwise stated.

### **4.3. Results and Discussion**

#### **4.3.1. Synthesis and characterisation of the photocurable PCL**

The chemical structure and  $^1\text{H}$  NMR spectra of 4PCL and 4PCLMA are given in Figure 4.4A-4.4C, 4.4E. The peaks of the hydroxyl ends (-OH) are framed with the dark grey box and labelled with “a”. These peaks represent the ends which were not methacrylated. The peaks of the methacrylate group are framed with yellow boxes and labelled with “b, c and d”. From these results, it is clear that all the hydroxyl ends that showed up in 4PCL, have been converted to methacrylate ends following the methacrylation reaction. This suggests that the 4PCLMA used in this study is 100% methacrylated. It was reported that the higher degree of methacrylation crosslinks the photocurable monomers to a higher degree, and this results in a mechanically stronger material [463–465]. GPC results showed that the  $M_w$  and  $M_n$  values were 2069 g/mol and 1771 g/mol, respectively and the dispersity index was calculated as 1.17 ( $M_w/M_n$ ).

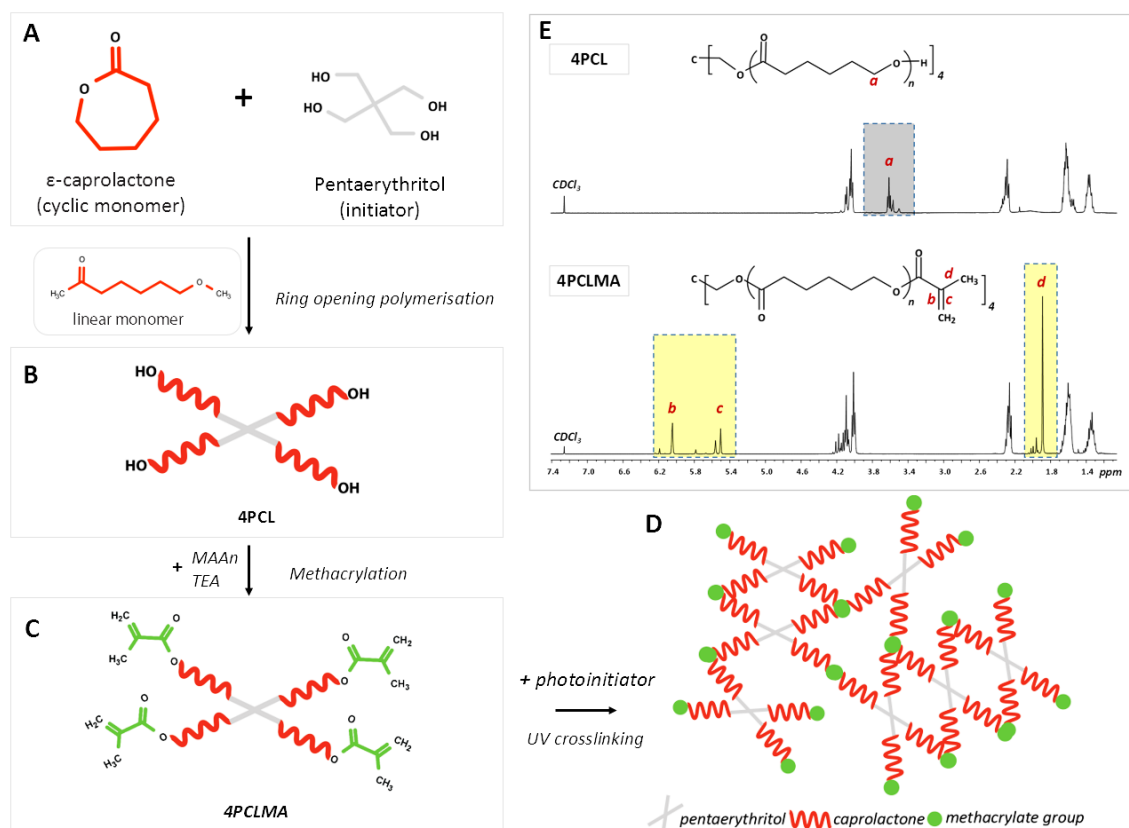


**Figure 4.4:** The synthesis scheme of 4-arm photocurable polycaprolactone: (A-B) monomer and initiator were used for the synthesis of hydroxyl-terminated 4-arm polycaprolactone (4PCL). (B-C). 4PCL was methacrylated. (D) Schematic demonstration of the photocured (UV-crosslinked) network showing a building block made of 4PCLMA. (E)  $^1\text{H}$  NMR spectrum of 4PCL, 4PCLMA and relative assignments. Dark grey region: peaks of the hydroxyl group, light yellow regions: peaks of the methacrylate group, which only showed up after methacrylation reaction while they are absent in 4PCL.

PCL is a synthetic polymer that has drawn considerable attention for use in the fabrication of TE scaffolds due to having various advantages such as being cell-compatible, bioresorbable and having an ease of processability [466]. Also, PCL has been approved by the Food and Drug Administration (FDA) for its use in several medical products, such as; drug delivery devices and sutures [289]. However, there are a limited number of studies that use photocurable PCL in biomedical applications [42,107,467,468]. Photocurable polymers need to have photoreactive groups such as acrylates or methacrylates to be able to be crosslinked via UV and to create a polymer

network in the presence of photoinitiator (Figure 4.4D) [467]. However, as commercial PCL does not contain these photoreactive groups, photocurable PCL needs to be synthesised *in house*. Photocurable polymers can be polymerised within seconds, they have higher solvent resistance over the non-crosslinked polymers, and they do not need the high temperatures, which are required for thermally initiated polymerisation [469]. Due to being processable at mild operational conditions, photocurable polymers are considered to be good candidates for use in 3D printing applications [470,471].

#### **4.3.2. Fabrication of multiscale porous PCL scaffolds by a combination of emulsion templating and 3D printing**

There are two main issues that should be considered in the design of emulsion inks for the 3D printing process; (i) emulsions need to have a viscosity high enough to hold the printed shape until gelation (crosslinking), (ii) emulsion templated scaffolds need to have a pore size distribution that does not limit cell infiltration. It is essential to highlight the fact that in w/o emulsions, emulsion viscosity is inversely proportional with the size distribution of the water droplets [78]. Thus, the viscosity of the emulsion should be high enough for successful printing of the emulsion inks and low enough to enable the manufacturing of the scaffolds with a pore size ranges that allow cell infiltration.

Both viscosity and pore size can be tuned by controlling the internal phase volume, type/amount of surfactant used, process temperature, and mixing conditions [78–81]. Sears et al. reported 3D printing of acrylate-based emulsion inks, prepared by mixing up to 2500 rpm. In their study, the rheology of the inks was optimised for high accuracy

printing of the emulsion to fabricate lattice design scaffolds for bone TE, but the micropore size was not reported [76]. Yang et al. reported the use of mechanical shaking for the emulsification process and demonstrated the successful fabrication of 3D printed emulsion templated scaffolds with an average micropore size of 20  $\mu\text{m}$  [146].

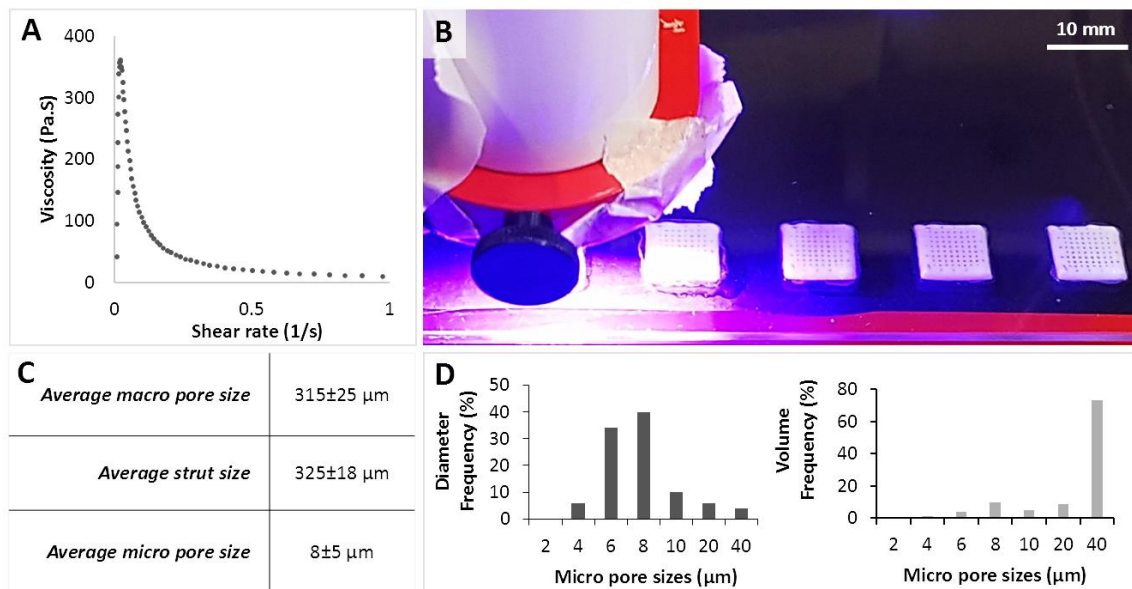


**Figure 4.5:** (A) Viscosity of the polycaprolactone (PCL)-based high internal phase emulsion (HIPE) prepared to be used in the printing process. (B) 3D printing and simultaneous cross-linking of PCL HIPE. (C) Morphological characterisation ( $n_{\text{macropore}}=20$ ,  $n_{\text{strut}}=20$  and  $n_{\text{micropore}}=50$ ) and (D) micropore size distribution of the scaffolds in terms of the diameter frequency and the volume frequency.

As relative viscosity increases with the increasing volume fraction of the dispersed phase [93,472], we maximised the inner phase volume. The maximum water volume achieved was 89% where a further increase in the water volume beyond that resulted in phase separation of the emulsion at the reported process conditions. PCL-based HIPE showed shear-thinning behaviour, which enables their extrusion through the nozzle with applied pressure [473] (Figure 4.5A). Throughout the printing process, no phase separation was observed in PCL-based HIPEs. Similarly, we have previously shown the stability of the photocurable PCL-based HIPEs over 5 days [42].

Pore size is one of the critical features that affect the biological performance of bone TE scaffolds in terms of cell attachment, infiltration [284,474], bone formation [86,475,476], differentiation [474,477], osseointegration [393,478] and vascularisation [86,393]. Recently multiscale porous scaffolds, developed to mimic the hierarchical structure of natural bone, have attracted great attention [479–482], and multiscale porosity has been found to be more favourable for bone regeneration compared to single scale pore designs [86,436]. While macropores encourage vascularisation and osteointegration [481], incorporation of microporosity into scaffolds has been reported to provide grooves and roughness on the surface topology of the scaffolds, which facilitate cell adhesion [86,483]. These also provide a larger surface area, thereby higher protein absorption [484,485]. The reported optimal micro- and macro- pore size ranges for bone TE scaffolds in the literature are conflicting, as the compositions of the scaffolds, pore shapes, mechanical properties, cell types used in the experiments, test conditions, and duration of the experiments vary [7,86]. However, in general, scaffolds with macropores sized over 300  $\mu\text{m}$  and micropores sized less than 10-50  $\mu\text{m}$  have been recommended and used by many researchers for bone regeneration studies [86,481,482].

In this study, the multiscale porous PCL-only scaffolds were easily fabricated by 3D printing and the simultaneous cross-linking of PCL HIPEs (Figure 4.5B). No post-process was required to polymerise the PCL scaffolds. The average sizes of the macropores, struts, and micropores were measured as  $315\pm 25$   $\mu\text{m}$ ,  $325\pm 18$   $\mu\text{m}$ , and  $8\pm 5$   $\mu\text{m}$  (Figure 4.5C, 4.5D), respectively. Micropores of the scaffolds exhibited open-cell morphology which is characterised by the presence of windows on the walls of the pores. Average window diameter was measured as 1.6  $\mu\text{m}$ , both the degree of

openness and the degree of interconnectivity of the PolyHIPEs were measured as 0.2, which is in line with the reported values in the literature [42,70].

The microporous architecture of the scaffolds was found to be different at the surface of the struts compared to within the core of the scaffolds (Figure 4.6C, 4.6D). This is because the surface of the PolyHIPE is known to be affected by the contact materials such as the mould or air, and monoliths result in different morphologies at the surface and the cross-section [13]. However, as the pores on the surface still exhibited an open porosity, we believe this morphological difference did not pose a limitation to our system. A similar structural difference also can be seen in the study reported by Binks et al. for 3D printed non-photocurable PCL PolyHIPE scaffolds [146].

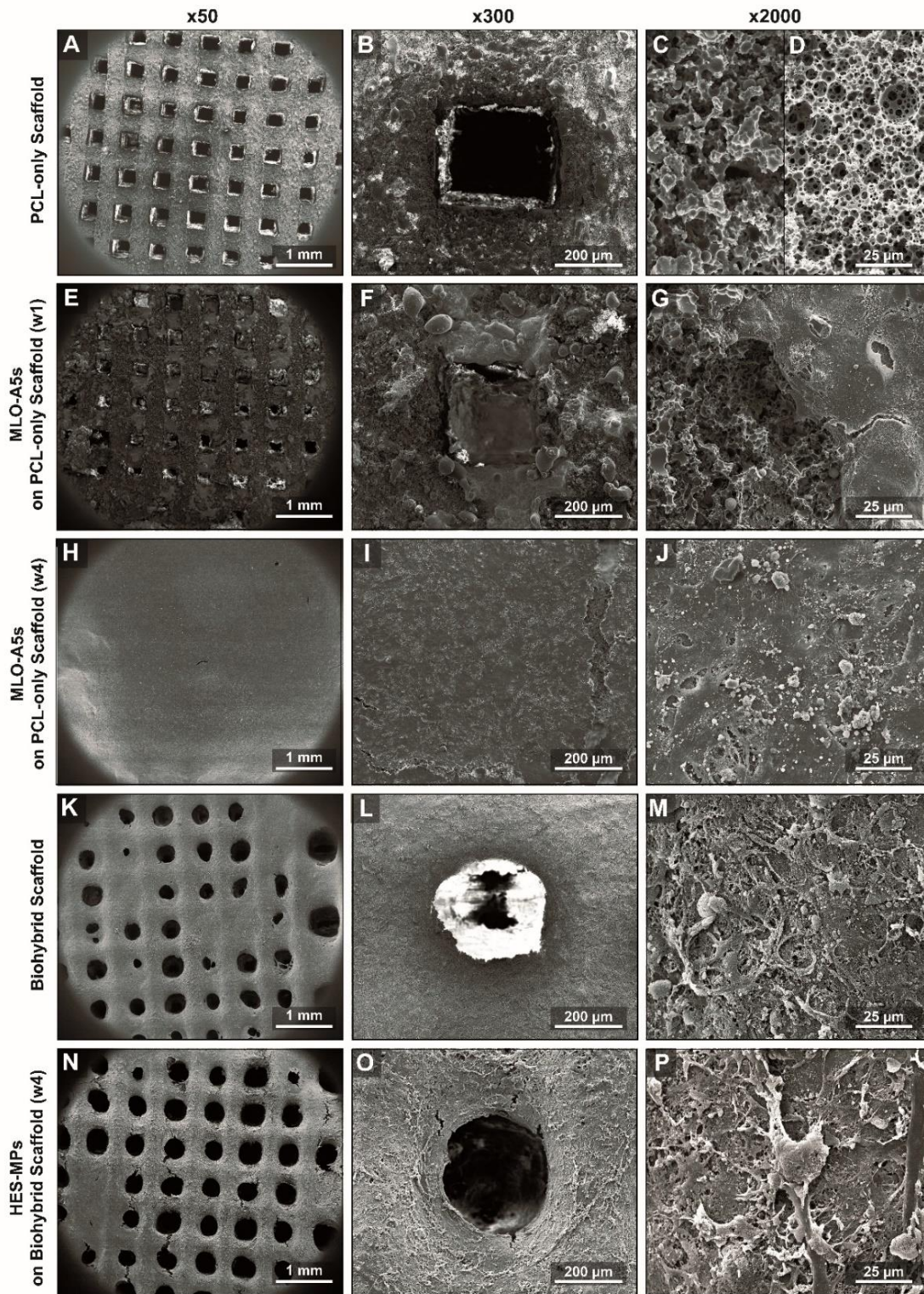


**Figure 4.6:** SEM micrographs (A-D) multiscale porous PCL-only scaffolds immediately after manufacture, (E-G) after 1-week of MLO-A5 culture, (H-J) after 4-weeks of MLO-A5 culture, (K-M) after the decellularisation process (biohybrid scaffold), (N-P) after 4-weeks of the culture of hES-MPs on the biohybrid scaffolds. First column macro view of the scaffold, the second column

*shows the single pore, and the third column shows the microsurface of the scaffold at different stages of the experiment. All the images were captured from the top view.*

### **4.3.3. Generation of the biohybrid scaffolds and evaluation of their biological activity**

#### *4.3.3.1. Bone ECM deposition on the multiscale porous PCL scaffolds*

MLO-A5 cells are late-stage osteoblasts (pre-osteocytes) which have been shown to mineralise in 3 days in supplemented media and to rapidly-produce bone-like matrix. We use this mouse cell line in the proof-of-concept of this study as they have been previously reported to produce mineral (in culture), which has similar characteristics to that of native bone as measured by Fourier transformed infrared spectroscopy [486].

Despite the long incubation time for cell seeding (2 hours) and conditioning of the scaffolds with media, the seeding efficiency of MLO-A5s was found to be less than 15% using a DNA quantification assay (Figure 4.7A). This is likely because; (i) the macroporosity of the scaffolds caused the cell suspension to drain from the scaffolds to the tissue culture plate (TCP) and (ii) the hydrophobicity of PCL limiting the cell-surface interactions and inhibiting cell attachment. Recently we have shown that air plasma treatment can increase cell attachment, viability, and infiltration on hydrophobic PolyHIPE scaffolds [42,70]. However, in this study, air plasma treatment was not used to be able to show the single impact of ECM deposition on the biological activity of the scaffolds.

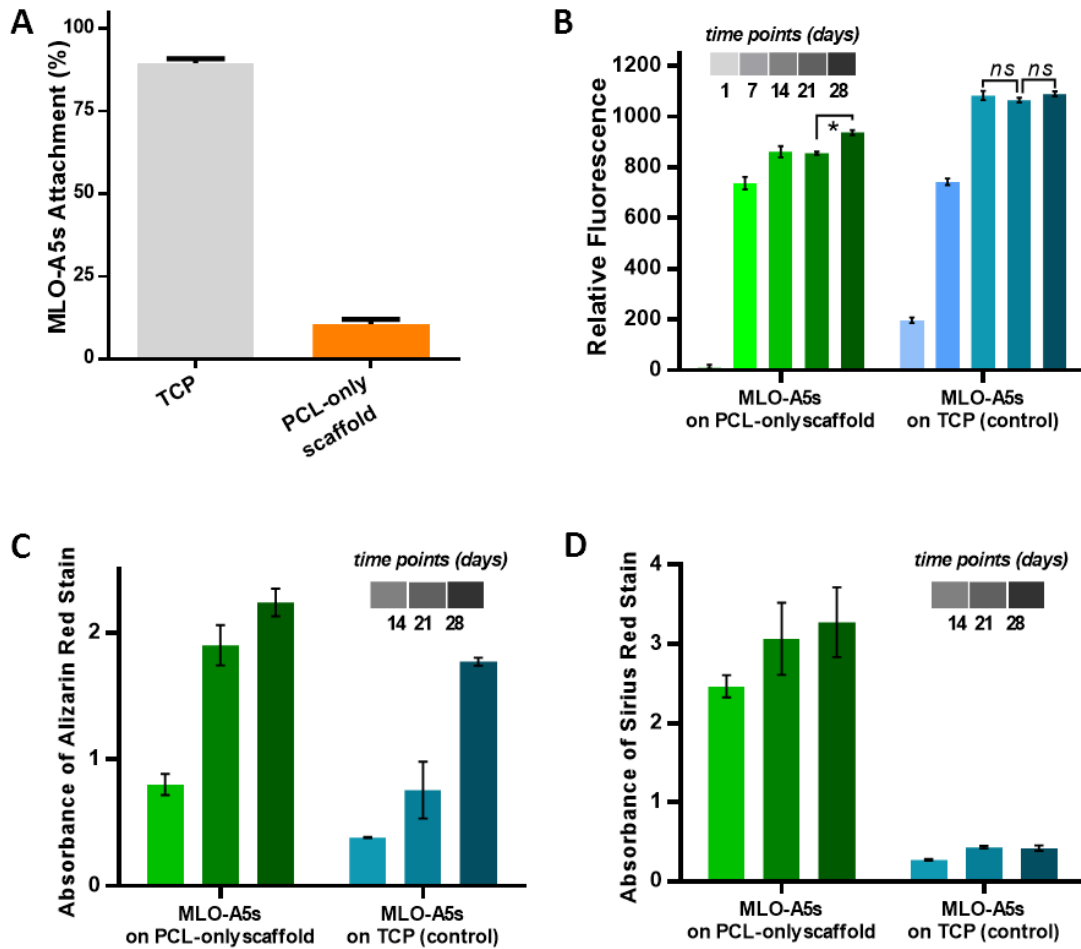


**Figure 4.7:** (A) Cell seeding efficiency of MLO-A5s on multiscale porous PCL-only scaffolds ( $n=5$ ). (B) Metabolic activity ( $n=5$ ), (C) mineral, and (D) collagen deposition of MLO-A5s on multiscale porous PCL-only scaffolds and TCP as control over 28 days ( $n=3$ , \*:  $p<0.05$ ,  $p>0.5$ ; ns: not significant).

Although the culture began with low cell numbers on multiscale porous PCL scaffolds at day 1, the cell viability of MLO-A5s dramatically increased from day 1 to day 7 and continued to increase until day 28 (Figure 4.7B). Cell viability of MLO-A5s cultured on TCP increased steadily from day 1 to day 14 and then remained stable, likely due to reaching confluence in the limited 2D growth area that TCP provided.

Mineral and collagen deposition of MLO-A5s cultured on multiscale porous PCL-only scaffolds showed a dramatic increase from day 14 to day 28 (Figure 4.7C, 4.7D). There

was a progressive population of bone cells on the struts and the pores of the scaffold (Figure 4.6A-4.6J). At week 4, complete coverage of the surface with cells and deposited ECM material (Figure 4.6H) containing mineralised nodules (Figure 4.6I) was observed.

#### **4.3.3.2. Decellularisation of the multiscale porous PCL scaffolds populated with bone cells**

The fundamental aim of the decellularisation process is to remove the genetic material, which may trigger an immune response [487] while preserving ECM components [458]. There are various decellularisation methods described in the literature [458]. Depending on the target tissue, cell line and the scaffold design, various combinations of these methods have been performed to disintegrate the cell membrane and to remove the cellular material [488]. While multiple methods are combined, and longer washing steps are applied for decellularisation of the whole organs or tissues [458,489], less harsh methods are used for decellularisation of the *in vitro* generated ECM on scaffolds [419,451–455].

Herein, we compared the efficiency of ft, ft+ta, ft+DNase, and ft+ta+DNase treatments in terms of DNA removal, and the remaining DNA amounts were measured as 26%, 14%, 5%, and 4% of the total amount of initial DNA, respectively. There was no significant difference found in the remaining DNA contents of the groups decellularised via ft+DNase and ft+ta+DNase. Thus, Ft+DNase treatment was chosen as the decellularisation method for this study due to its ability to remove DNA up to 95%.

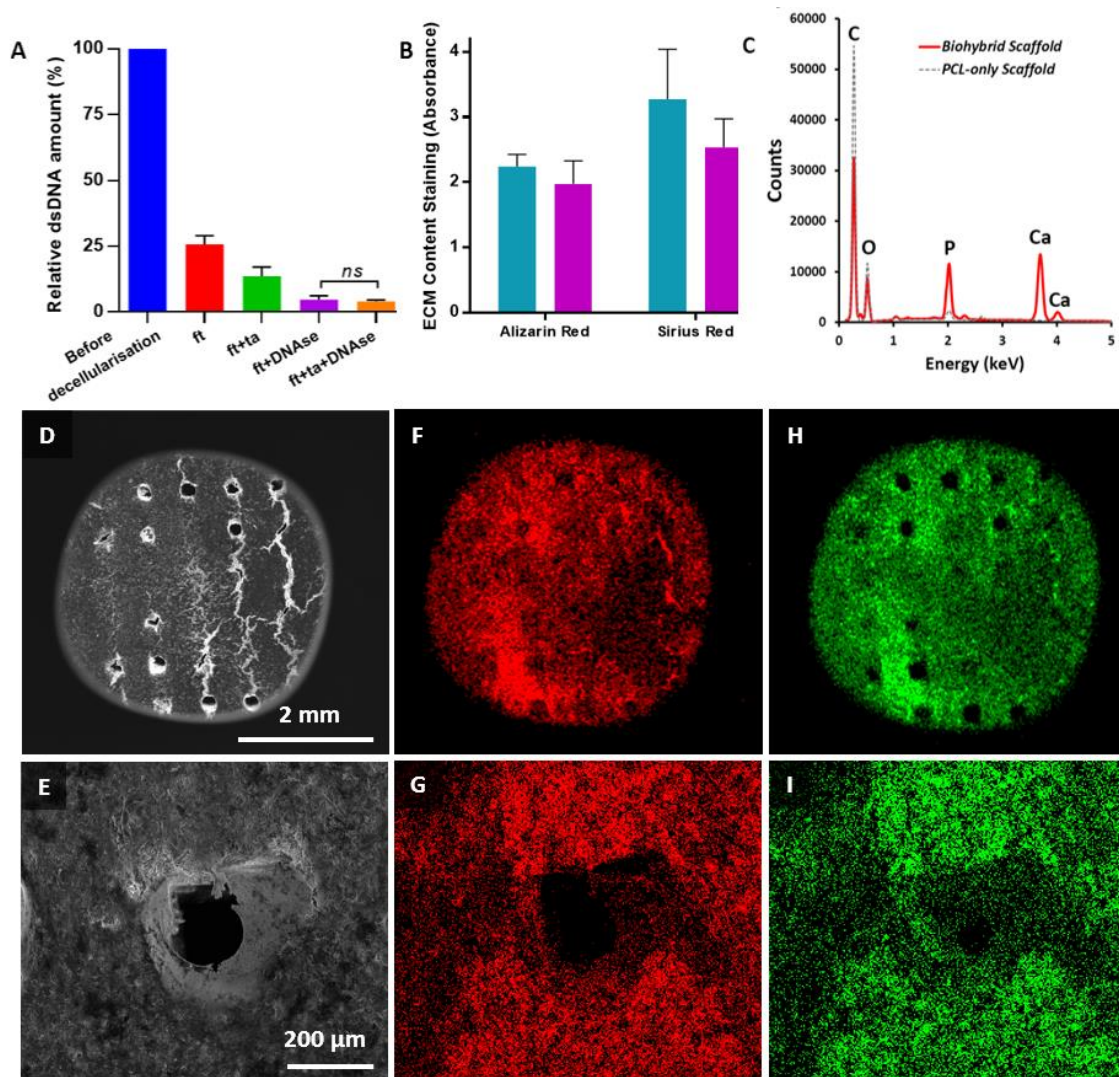


**Figure 4.8:** (A) Comparison of the various decellularisation techniques in terms of remaining DNA content ( $n=3$ ), (B) Calcium and collagen content of the scaffolds cultured with MLOs for 4 weeks (blue) and scaffolds that are decellularised (purple) ( $n=3$ ,  $p>0.05$ ; ns: not significant), (C) EDX spectrum of the decellularised scaffold showing the peaks of carbon (C), phosphorus (P), calcium (Ca), and oxygen (O), (D, E) SEM images of the decellularised scaffolds in lower and higher magnifications, respectively (top-view). (F-I) EDX elemental mapping of Ca (red) and P (green).

Following the decellularisation, 88% and 77% of the deposited calcium and collagen amounts were found to be preserved on biohybrid scaffolds. The Ft+DNase method was successful in the removal of 95% of the total DNA while preserving most of the collagen and mineral deposited onto the scaffolds. Although the macropores were

covered with MLO-A5s after 4 weeks of culture, the multiple washing steps of the decellularisation process seemed to disrupt the ECM layer covering the macropores and resulted in a mostly open porous structure (Figures 4.6K-4.6M). EDX analysis of the biohybrid scaffolds also showed that the remaining elemental composition consisted of mostly calcium (Ca) and phosphorus (P); the main inorganic constituents of native bone tissue (Figure 4.8). Some trace elements, such as; sodium (Na), magnesium (Mg), silicon (Si), and sulphur (S) were also found within the deposited ECM. The small peak that corresponds to the presence of P detected on the PCL-only scaffolds is likely to come from the photoinitiator that joined the structure of the polymer during free-radical polymerisation.

#### **4.3.3.3. Evaluation of the biological activity of the biohybrid scaffolds using hES-MPs**

HES-MPs are able to differentiate into osteogenic, chondrogenic and adipogenic cell lines. The gene expression profile of hES-MPs is similar to human mesenchymal stem cells (MSCs), but they have a higher proliferation rate [490,491]. In this study, they were used as a representative of osteoprogenitor cells to understand the initial steps that may occur when human osteoprogenitors encounter biohybrid scaffolds *in vivo*.

Seeding efficiencies of hES-MPs were found to be 11% and 34% on PCL-only and biohybrid scaffolds, respectively. ECM deposition onto the polymeric scaffold increased the initial cell attachment up to 3-fold compared to PCL-only scaffold. Cell adhesion is a process that is modulated by surface receptors; integrins which can recognise ECM proteins [492]. Similarly, the presence of ECM proteins on the surfaces has been reported to have a positive impact on cell attachment and growth [451,493,494]. Also, the remaining ECM deposited on the surfaces has been reported

to increase the roughness of the surfaces of the substrates, and this is likely to enhance the initial cell attachment [495].

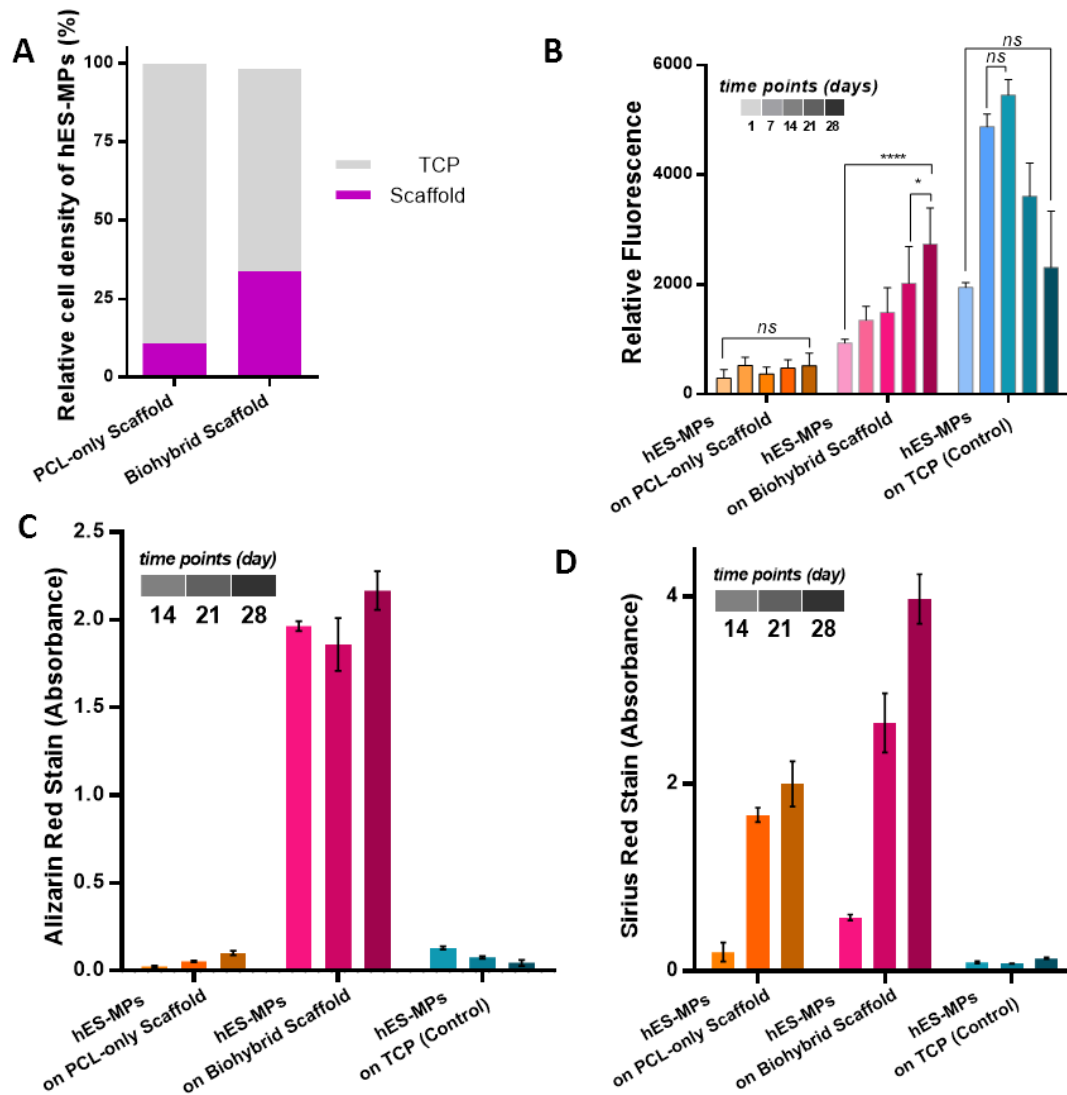


**Figure 4.9:** (A) Seeding efficiencies of human embryonic stem cell-derived mesenchymal progenitor cells (hES-MPs) on polycaprolactone (PCL) -only and biohybrid scaffolds ( $n=6$ ), (B) the metabolic activity ( $n=6$ ), (C) mineral ( $n=3$ ), and (D) collagen deposition of hES-MPs on PCL-only, biohybrid scaffolds, and on tissue culture plate (TCP) as a control in 28 days culture ( $n=3$ ) (\*:  $p<0.05$ , \*\*\*\*:  $p<0.001$ , ns: not significant).

While hES-MPs cultured on PCL-only scaffolds barely survived over 28 days, the cell viability of hES-MPs cultured on biohybrid scaffolds showed a significant increase

from day 14 to day 28. The viability of hES-MPs growing on TCP increased until day 14, and cells started to detach from the surface of the TCP after that point.

Various properties, such as biochemical composition [429,496,497], morphology [498], and mechanical properties [499] of the substrates have been shown to affect the osteogenic activities of stem-cells. Similarly, in our system, the amounts of newly formed ECM; collagen and mineral by hES-MPs on biohybrid scaffolds was dramatically higher compared with ECM deposition on PCL-only scaffolds. Although hES-MPs cultured on both PCL-only and the biohybrid scaffolds were supplemented with OM, hES-MPs on PCL-only scaffolds was not able to deposit a significant amount of calcium. Similar to our findings, Datta et al., previously showed that *in vitro* cell-generated ECM decoration on titanium implants stimulates the differentiation of rat marrow stromal cells even in the absence of osteogenic supplements, although this effect is shown to increase with the supplementation of osteogenic factors [451]. Baroncelli et al. have shown more than a 20-fold increase in the calcium deposition of MSCs on ECM decorated substrates compared to plain ones [495]. Tour et al. also reported that decoration of HA scaffolds with *in vitro* generated ECM obtained from both rat osteoblasts and rat fibroblasts enhanced the osteogenic activity and reduced the inflammatory response *in vivo* [455].

#### **4.3.3.4. Evaluation of the angiogenic activity of the biohybrid scaffolds using CAM assay**

CAM assay is a rapid (two-weeks) and a cost-effective bioassay which has been widely accepted as an *in vivo* platform to investigate initial tissue response to biomaterials and angiogenic factors [201,277,500]. In practice, it is comparatively easier than other *in vivo* assays, most of which require several surgical procedures. The CAM assay

allows direct visualisation of newly formed blood vessels in the area of implantation throughout the duration of the experiment when performed *ex-ovo* (shell-less) [501].

Angiogenesis and host tissue integration are crucial for osseointegration of bone grafts after implantation [502–504]. Herein, we used *ex-ovo* CAM assays to evaluate: (i) initial *in vivo* response, (ii) angiogenic response, and (iii) the degree of cell and tissue integration with scaffolds.

Angiogenic effects of various cell types, including adipose-derived MSCs [462,505], human dermal microvascular endothelial cells [506], and fibroblasts [505,506] on CAM have previously been reported. However, it has not been studied whether the cells cause the angiogenic effect or the ECM they deposit during the implantation period. In our CAM assay experiments, PCL scaffolds populated with MLO-A5 were used as positive control and PCL-only scaffolds were used as a negative control as these should not possess any angiogenic properties.

The *ex-ovo* CAM assay demonstrated that ECM deposition and presence of MLO-A5s did not show a negative impact on embryo survival rate, which was above 70%. Scaffolds with either ECM or live MLO-A5s significantly increased the number of blood vessels, total vessel length and the total number of junctions in comparison to the PCL-only group. Scaffolds cultured with MLO-A5s showed a better performance in terms of all the three measurements mentioned above; however, only the number of blood vessels was significantly different from other groups.

At EDD 14, while isolating scaffolds, it was not possible to peel the CAM layer from the scaffold, and there was a complete integration of CAM with scaffolds in all three groups (Figure 4.10G-4.10O). However, while there was limited cell infiltration from CAM to the PCL-only scaffold, the ECM containing group showed higher infiltration through

both macro- and micro- pores whereas the highest infiltration was observed in the cell containing group. Additionally, blood vessels growing in the macropores were clearly detectable in the ECM and cell loaded groups.

Pham et al. have also previously shown that *in vitro* generated ECM increased the vascularisation of the constructs implanted intramuscularly in a rat animal model [419]. They hypothesised that it is potentially because of the contribution of the angiogenic factors that are released into the *in vitro* deposited ECM. Although future investigations are necessary to validate the composition of the ECM present here in terms of growth factors, angiogenic factors and cytokines; our conclusions are in line with their hypothesis. Additionally, we also consider the contribution of the trace elements whose presence were verified using EDX analysis. Zhang et al. reported that Mg, Ca, and Si-containing ceramic scaffolds improved vascularisation and bone regeneration *in vivo* [507]. Similarly, Mg is reported to be a vital trace element in bone, and its role in bone regeneration and vascularisation has been investigated by many other researchers [508–510].

Accordingly, the findings from the quantification of both macro and histology images support the notion that ECM deposition increased the angiogenic activity and tissue infiltration of the PCL scaffolds. Although this response was slightly higher when the cells were maintained alive in the scaffolds, this needs to be weighed against the difficulties and limitations of implanting live cells in a clinical situation.

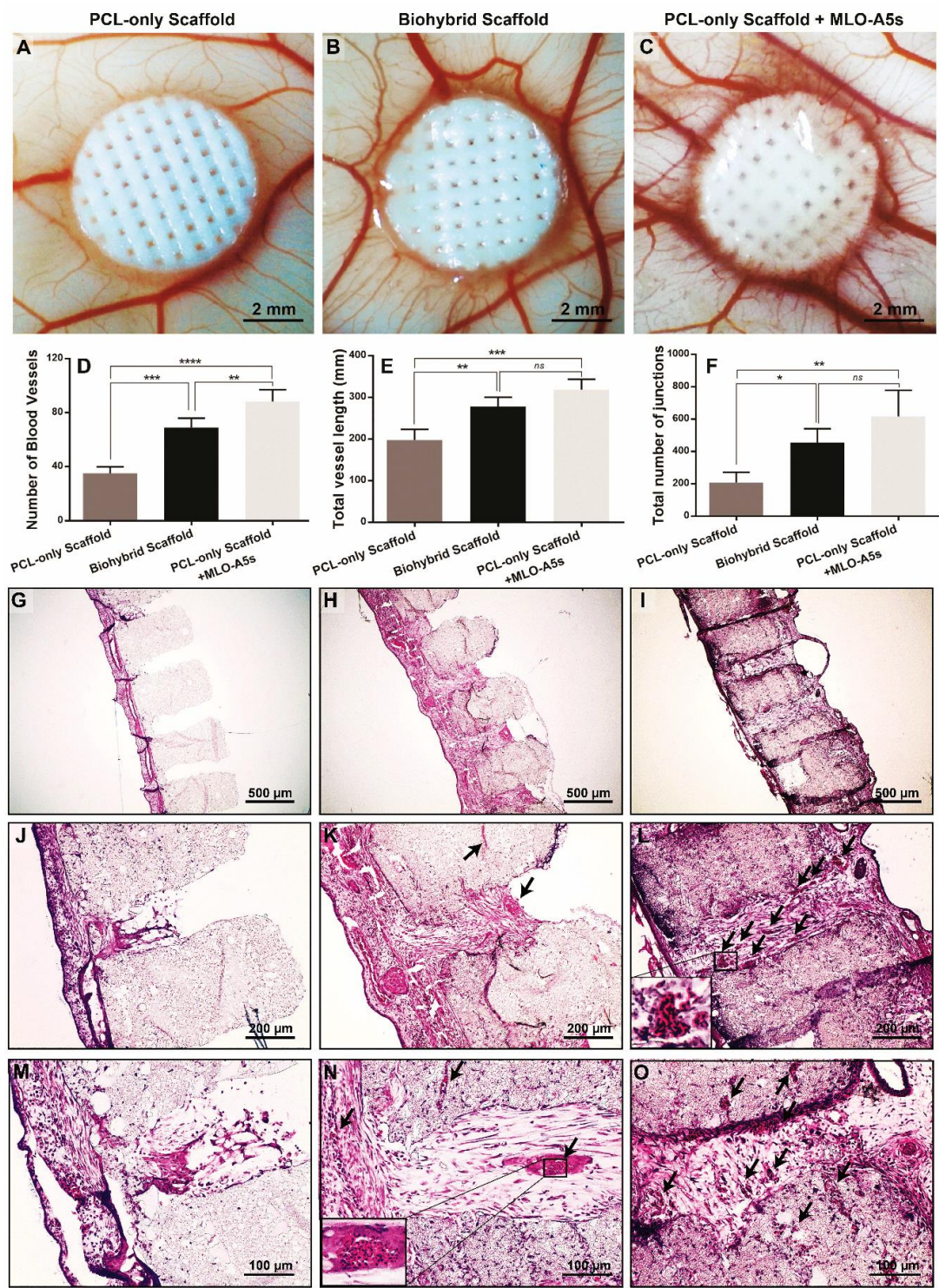


**Figure 4.10:** Evaluation of the angiogenic potential of polycaprolactone (PCL)-only, PCL-only populated with murine long bone osteocyte cells (MLO-A5s), and biohybrid scaffolds using chick chorioallantoic membrane (CAM) assay; (A-C) Macro images were taken on embryonic development day 14, (D-F) quantification of the number of blood vessels, total vessel length and the total number of junctions. (n=4, \*: p<0.05, \*\*: p<0.01, \*\*\*: p<0.005, \*\*\*\*: p<0.001, ns: not

significant), (G-O) histological evaluation of the scaffolds isolated from CAM (Black arrows indicate the blood vessels).

#### **4.4. Conclusions**

In this study, we developed biomimetic and biohybrid scaffolds for bone TE. Hierarchically porous PCL-based scaffolds were successfully fabricated by combining emulsion templating and 3D printing techniques. Following the culture of bone cells on these scaffolds for bone ECM deposition, the decellularisation procedure successfully removed the 95% of the DNA, while preserving most of the collagen and mineral on the scaffolds. By testing the scaffolds for their ability to support osteoprogenitors, it was revealed that bone-derived ECM improved cell attachment, proliferation and ECM deposition ability of hES-MPs. Bone-derived ECM also significantly improved the angiogenic activity in *ex-ovo* CAM assay where the blood vessels were found to be growing through the macropores of the scaffolds on CAM. The results suggested that biohybrid scaffolds made of PCL PolyHIPE, and cell generated ECM exhibit both osteogenic and angiogenic properties.

To conclude, the ECM decorated multiscale porous scaffolds developed in this study appear to have great potential to be used as a bone graft substitute. While we used a mouse cell line in this proof-of-concept study, this technique could be easily adapted for use with donated human MSC-derived ECM to create a product to replace cadaveric donor bone graft or patient-specific MSCs to replace autologous bone graft. Additionally, it will be interesting to evaluate the developed biohybrid scaffolds for their use as an *in vitro* tissue model mimicking the native bone niche.



# CHAPTER 5

---

## Overall conclusion and future work

The main focus of the research in this thesis was to develop tetramethacrylate functionalised polycaprolactone (4PCLMA)-based emulsion templated matrices for tissue engineering applications.

In the first chapter, it was emphasised that emulsion templating is a complex fabrication process that is sensitive to changes in various parameters. This study enables the precise engineering of the emulsion templated matrices by optimisation of each parameter that has an impact on the characteristics of HIPEs and PolyHIPEs. To date, the individual effects of most of the parameters on the final PolyHIPE structure have been reported. Although it was not in the scope of this thesis, future studies exploring the dependence of the final morphology on individual parameters via mathematical models would be interesting to implement. In this way, it would be possible to formulate the compositions virtually for any specific applications. Also, it may be possible to conduct multiscale computational modelling of these structures to predict their physical properties.

In the second chapter, the development of PolyHIPEs made of 4PCLMA was reported. The findings from this study contributed to our understanding of the effect of the diluting solvent on the morphological and mechanical properties of PolyHIPE. Chloroform, toluene and their blends were used as diluting solvents. Stable HIPEs were successfully created, and the tunability of PolyHIPEs by solvent volume and

compositions was shown. Results suggested that the density and polarity of the solvent, the solubility of the solvent in the internal phase, and solubility of the polymer in the diluting solvent are some of the parameters that should be considered during the solvent selection process. I demonstrated that emulsions, where toluene alone was used as a diluting solvent (in the tested volumes) did not show typical open-porous PolyHIPE. However, as shown in the supporting data, when the surfactant was excluded from the composition, PolyHIPEs diluted with toluene showed a porous structure. These findings suggest that the interactions between the surfactant and the diluting solvent also should be investigated while formulating the emulsion composition, as previously suggested by Moglia et al. [38].

In the third chapter, we have shown the potential use of PCL PolyHIPE membranes for dental applications. For this, we needed to create a membrane with a thickness of hundreds of micrometres. Investigations on the effect of moulding material on the surface morphology of PolyHIPEs has shown that moulded emulsions have shown partially or fully closed morphology on the surface. Thus we have fabricated cylindrical structures and sectioned them using a vibratome and managed to obtain a fully open-porous structure all over the membrane. However, further research is needed to explore the ways of obtaining open porous morphology on moulded PolyHIPE scaffolds.

All scaffolds fabricated for the *in vitro* cell culture tests and *ex-ovo* CAM assays were disinfected using ethanol, and throughout the experiments, I didn't observe any sign of infection. However, for clinical purposes, it is critical to investigate a convenient sterilisation route for PCL PolyHIPEs. I have previously autoclaved PCL PolyHIPE discs (data not shown) just to see if there will be any difference in their properties, colour

and integrity. There were not any observable changes between samples that were autoclaved vs non- autoclaved. However, research is needed to better understand the effect of sterilisation route on the chemical and mechanical features of PCL PolyHIPES.

In the last section, I successfully fabricated photocurable 4PCLMA-based multiscale porous scaffolds by combining emulsion templating and additive manufacturing. I have shown that the decoration of these scaffolds with cell generated bone extracellular matrix (ECM) enhanced osteogenic and angiogenic performance of those scaffolds. As proof of concept, murine bone cells were used to populate the scaffolds for ECM production. However, the use of mesenchymal stem cells would be more relevant to show the clinical potential of those biohybrid scaffolds. Results showed that the presence of ECM within the polymeric structure significantly increased the biological performance of the scaffolds. Although calcium and collagen deposition was quantified and elemental analysis and mapping were conducted, further research is required to demonstrate that angiogenic and osteogenic biomolecules exist in the compositions of the bone ECM. Also, fabricated biohybrid scaffolds are structurally and biologically close representatives of natural bone niches. Thus, it would be interesting to use the biohybrid scaffolds as an *in vitro* test platforms.

PCL is one of the widely used synthetic polymers for the fabrication of scaffolds of soft and hard tissue engineering. It is biodegradable and processable to various shapes. However, its long degradation time, 2-4 years, is seen as the biggest disadvantage of the use of PCL to be used as a biomaterial in scaffolds structure. Most studies use linear, high molecular weight (60.000-90.000 g/mol) PCL as it is commercially available. However, studies have shown that networks created by crosslinking of functionalised PCL that is synthesised *in house* have a significantly higher degradation rate [511,512].

The number of arms (branch) and the degree of functionalisation (methacrylation/acrylation) are some of the parameters that have an impact on the mechanical properties and the degradation rate of PCL. Thus, further investigations are needed to establish this relationship. Also, it would be interesting to explore the dependence of degradation rate on the morphological properties of PolyHIPEs such as pore size, window size, and degree of interconnectivity. As these parameters change the surface area, a significant difference is expected in their degradation profiles.

*In vitro* cell culture data indicates that PCL PolyHIPE scaffolds are promising candidates to be used as tissue engineering scaffolds. However, future studies on *ex vivo* organ model and *in vivo* animal models are essential to test these matrices in physiologically relevant conditions. Long-term *in vivo* tests are also needed to show host tissue integration and the *in vivo* degradation profile of these matrices.

Finally, emulsion templating is a highly tunable and favourable fabrication technique that enables the production of precisely engineered tissue engineering scaffolds. 4PCLMA is also a highly tunable biomaterial. We have shown that 4PCLMA-based emulsion templated matrices are promising substrates to be used in various tissue engineering applications. However, as both, the technique and the biomaterial are quite novel, and there are still endless areas that can be explored to establish a greater degree of understanding in this field.

# CHAPTER 6

---

## **pArt of science**

*“Draw what can’t be seen ....  
and tell thousands about it without saying a word.”*

*- Frank Netter, MD/ 1906-1991, ABD*

### **6.1. Introduction**

As researchers, when we explore something, we are passionate about sharing it in a way that would be received more easily. We write articles; we do presentations. And visual materials: photography, microscopy images, basic sketches, detailed illustrations, 3D models, are often the best narrators of our research. Visual communication tools are powerful ways to grab the attention of the audience and enhance the memorability of the subject [513]. Similarly, throughout my research, I needed visual materials to tell my story. I have gained experience in different techniques, such as; medical and scientific illustration and false coloring of scanning electron microscopy (SEM) images, which are summarised in this chapter.

### **6.2. Medical and Scientific Illustration**

Medical and scientific illustrations are effective ways of conveying certain information to an observer by visual communication. Illustrations are generally used for articles, journal and book covers, atlases, education of the patients or advertisement purposes.

Even a single frame may illustrate anatomy, a medical problem, a proposed solution/design, and the treatment all at the same time. Although photography also can be used with similar purposes, illustration enables simplifying and modifying the frame. For example; Figure 6.1A, 6.1C shows the complex anatomy of the ulnar side wrist by an intraoperative photograph. However, a simple illustration can be used to show the only necessary details (Figure 6.1B, 6.1D).

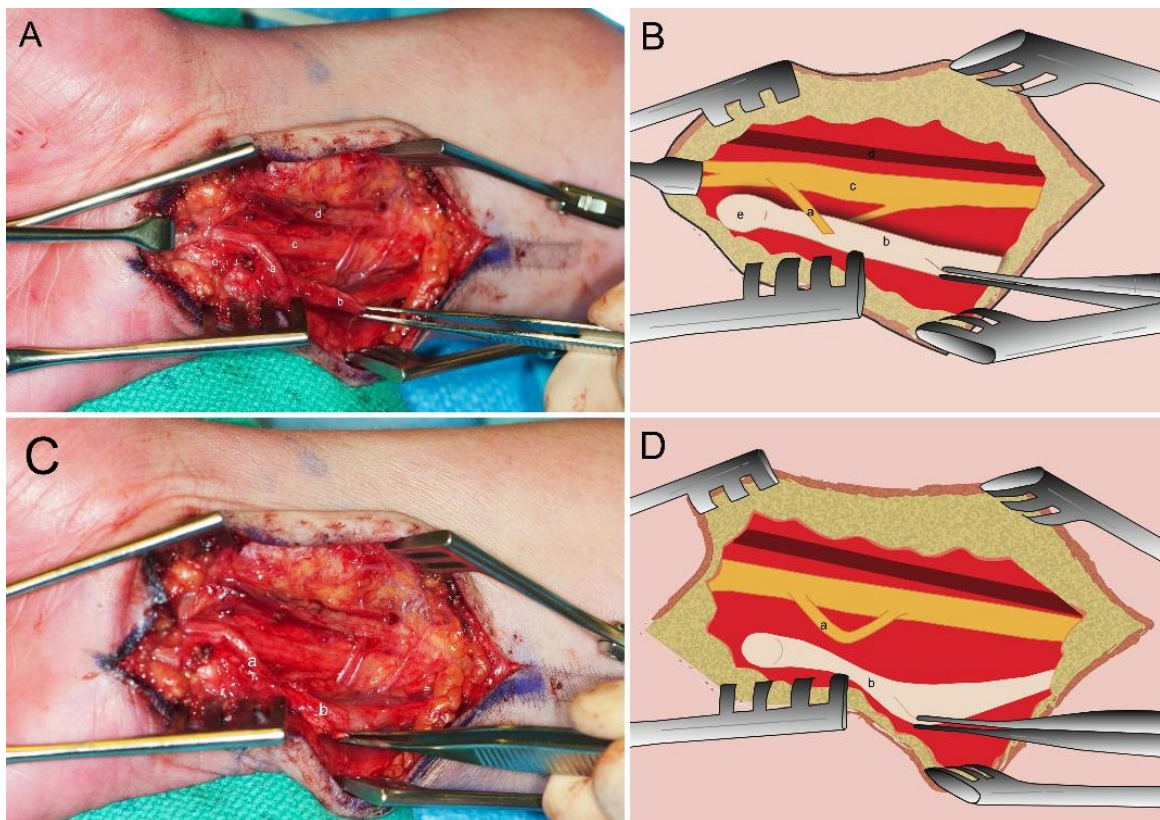


**Figure 6.1:** Power of an illustration to simplify the scene. Intraoperative photograph (A) and illustration (B) of the entrapped ulnar nerve by flexor carpi ulnaris tendon. Intraoperative photograph (C) and illustration (D) of the release of nerve loop from flexor carpi ulnaris tendon. a. the ulnar nerve, b. flexor carpi ulnaris tendon, c. main trunk, d. ulnar artery, e. pisiform bone. Image reprinted from [514] with the kind permission of the Journal of Neurosurgery Publishing Group.

Various basic scientific illustrations were presented in the previous chapters of this thesis to explain a specific application or procedure. I have also created medical illustrations with greater details for publications (Figure 6.2, Figure 6.3).

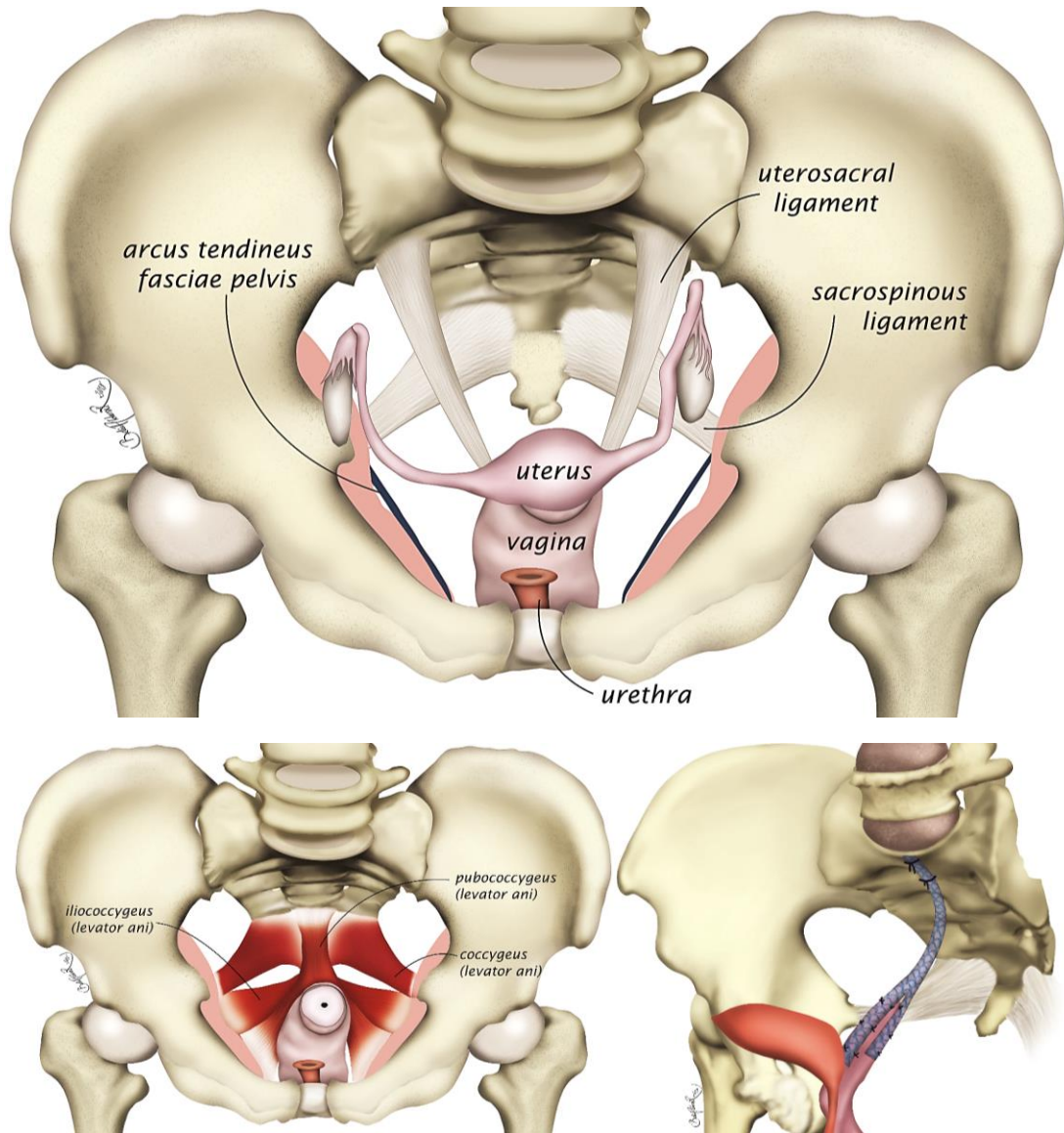


**Figure 6.2:** The medical illustration showing the anatomical features of pelvic floor created for the study published in *Nature Reviews Urology* [15].

The creation process of detailed medical illustrations is more time consuming when compared with the basic vector-based illustrations. The process starts with the preliminary investigation on the subject and searches for reference images, 3D models,

or videos. If the drawing is about the operation, then attending a real operation helps to understand the procedure and the anatomy better. Following the creation of the first sketch, the illustration is coloured and detailed. Finally, it is finalised with the labelling (if needed) and the signature of the artist. Nowadays, there are as many digital techniques that enable real-time manipulation with endless tools. I use Adobe Photoshop and Wacom Medium Pro drawing tablet to create my illustrations.

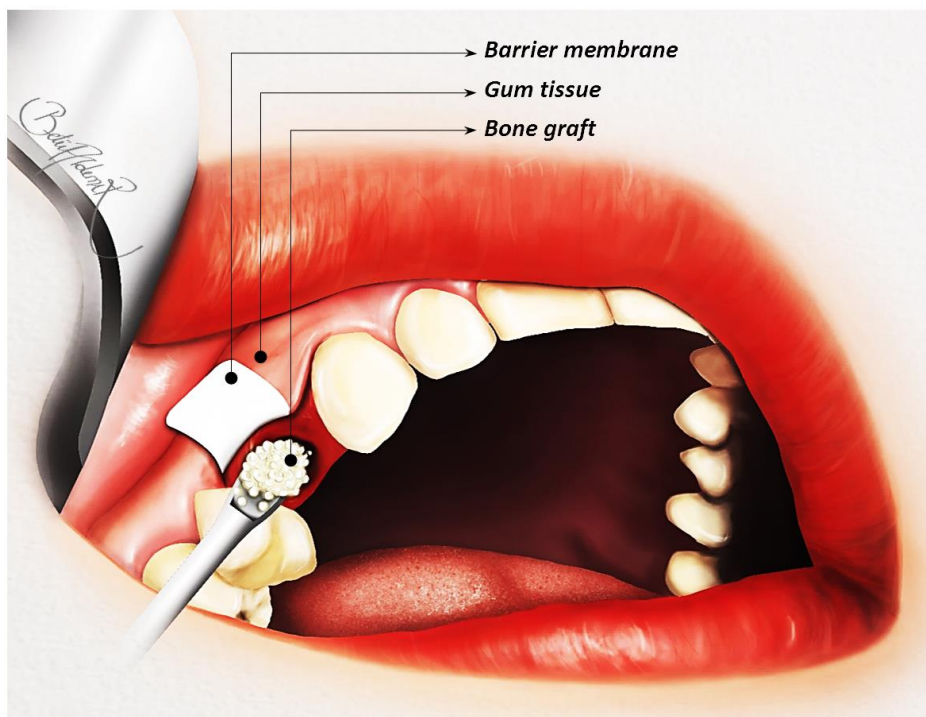


**Figure 6.3:** Graphical abstract figure drawn for the research presented in Chapter 3, published on *Materials* [13].

### 6.3. False Coloured SEM Images

SEM is one of the most informative imaging techniques in the field of biomaterials and tissue engineering to monitor morphology of the biomaterials, scaffolds, and cells. However, SEM images are usually monochrome. Although SEM images have strong contrast which creates a perception of high depth, and it has great image resolution,

complex structures composed of multiple components can be hard to interpret at a greyscale. In addition, from the aesthetical point of view, colour helps the human brain to identify different components [515]. Thus, for better interpretation, black and white images are colourised using computer technologies. Although fully automated systems that enable pseudo/ false colourisation of the SEM images is highly desirable, currently there is not any fully accurate system for this application. Semi-automated systems where colour assignments are required to be performed by the user have been reported [516,517]. Although they exhibited highly promising results, they still have an inaccuracy in the detection of the edges (Figure 6.4).

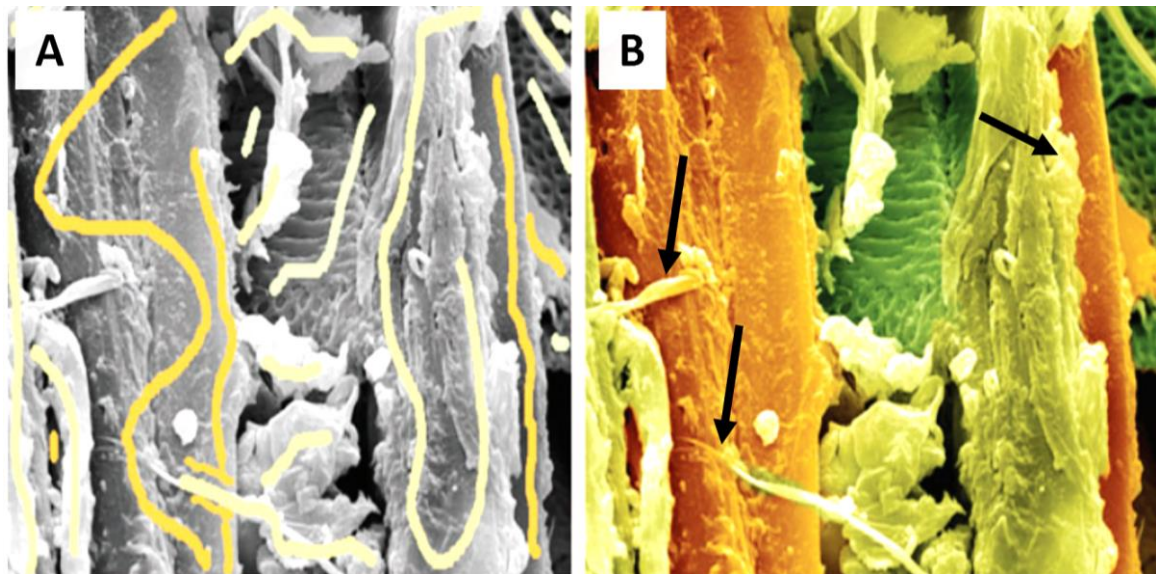


**Figure 6.4:** *Semi-automated false SEM colouring. Cellulose-fibre-epoxy composite SEM sample images. (A) Image after marking with colours on monochrome SEM image and (B) after false colourisation. Black arrows show the inaccuracy in the detection of the edges. Images are adapted from [517] with the kind permission of John Wiley and Sons.*

Alternatively, whole colourisation process can be performed manually. Although this technique is time-consuming, it enables the multitone colouring of the images and this results in more artistic images. Figure 6.5 and Figure 6.6 are the SEM images in which I performed manual false-colouring. Comparison of original and processed images strongly emphasises the power of the colour on SEM images.

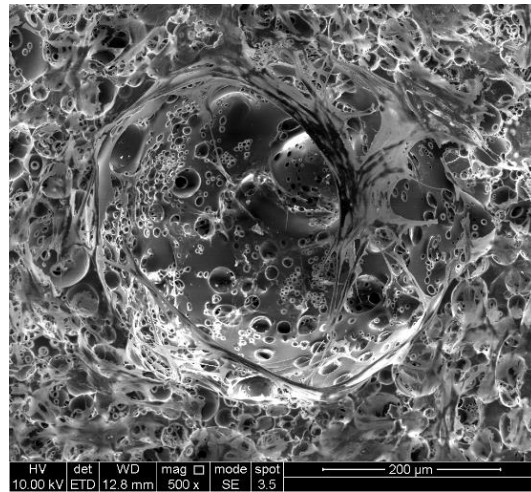


**Figure 6.5:** Recreation. (Top) Original scanning electron microscopy image and (Bottom) False scanning electron microscopy image of 4 days culture of human dermal fibroblasts on polycaprolactone PolyHIPE scaffold. Winners of Department of Materials Science and Engineering 2019 Image Competition, in the category of Biomaterials, and The University of Sheffield, Faculty of Engineering Photography Competition, category of The Future of Engineering.

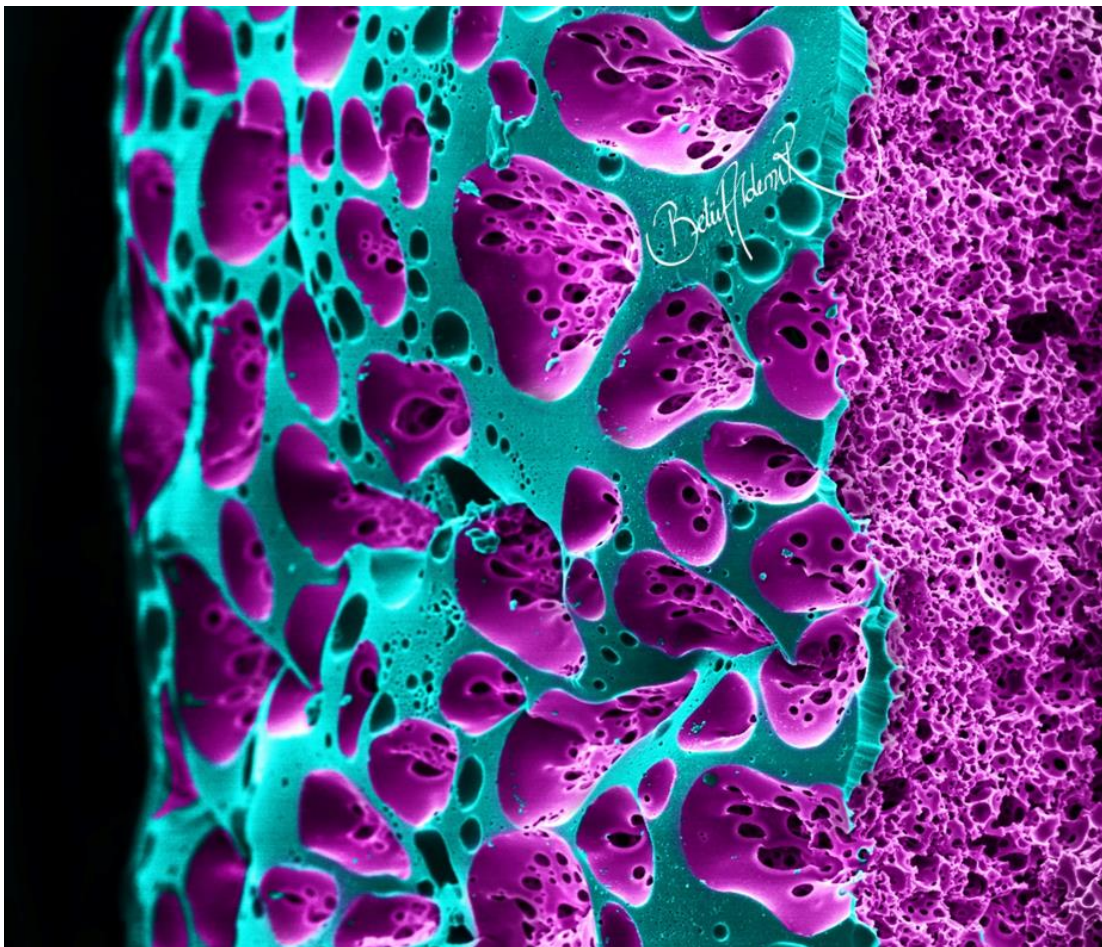
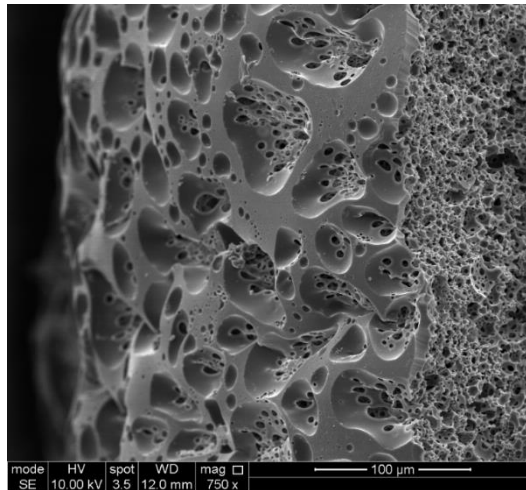


**Figure 6.6:** Dali's Crumpet. (Top) Original scanning electron microscopy image and (Bottom) False scanning electron image the cross-section of polycaprolactone PolyHIPE scaffold which has different morphologies inside and outside. Although this heterogeneity can be a problem to be solved for scaffold engineering, this false coloured scanning electron microscope image reminds Dali's "Persistence of Memory" and crumpets.

## 6.4. Conclusion

There is no doubt we all prefer a presentation with eye-catching and informative images than a presentation full of lines of words. Visual materials have a great role in the cognitive process of our psychologies. In addition to their ability to catch the attention of the audience, they have a role in better understanding and memorability of the subjects.

As researchers, we also benefit from the visual tools in our communication with the science community and also with non-specific audiences. To me, art is an intellectual process like science, and science is a creative process like art. Both require commitment, imagination, critical thinking, design, and technical skills. And both are needed equally. One of the best representations of this approach is the lovely motto of Massachusetts Institute of Technology (MIT): “Mens et Manus”: “Mind and Hand” in Latin and complementary to this message is the depiction of a craftsman at the anvil and the scholar with a book on the MIT seal.

---

---

*“It should be remembered that nothing in Nature stands alone; but that every art and science has a relation to some other art or science, and that it requires a knowledge of these others, as far as this connection takes place, to enable us to become perfect in that which engages our particular attention.”*

*-John Hunter, MD  
1728-1793, UK*

---

---

## REFERENCES

- [1] R. Langer, J.P. Vacanti, Tissue engineering, *Science* (80-. ). 260 (1993) 920–926. doi:10.1126/science.8493529.
- [2] K. Dzobo, N.E. Thomford, D.A. Senthebane, H. Shipanga, A. Rowe, C. Dandara, M. Pillay, K.S.C.M. Motaung, Advances in regenerative medicine and tissue engineering: Innovation and transformation of medicine, *Stem Cells Int.* 2018 (2018). doi:10.1155/2018/2495848.
- [3] F.J. O'Brien, Biomaterials & scaffolds for tissue engineering, *Mater. Today.* 14 (2011) 88–95. doi:10.1016/S1369-7021(11)70058-X.
- [4] L. Robert, R. Langer, J.P. Vacanti, A. Atala, *Principles of Tissue Engineering*, Elsevier, 2014. doi:10.1016/C2011-0-07193-4.
- [5] Y. Luo, G. Engelmayr, D.T. Auguste, L. da Silva Ferreira, J.M. Karp, R. Saigal, R. Langer, 3D Scaffolds, in: *Princ. Tissue Eng. Fourth Ed.*, 2013. doi:10.1016/B978-0-12-398358-9.00024-0.
- [6] M.P. Nikolova, M.S. Chavali, Recent advances in biomaterials for 3D scaffolds: A review, *Bioact. Mater.* (2019). doi:10.1016/j.bioactmat.2019.10.005.
- [7] S. Bose, M. Roy, A. Bandyopadhyay, Recent advances in bone tissue engineering scaffolds, *Trends Biotechnol.* 30 (2012) 546–554. doi:10.1016/j.tibtech.2012.07.005.
- [8] D.F. Williams, On the mechanisms of biocompatibility, *Biomaterials.* 29 (2008) 2941–2953. doi:10.1016/j.biomaterials.2008.04.023.
- [9] S.J. Hollister, Porous scaffold design for tissue engineering, *Nat. Mater.* 4 (2005) 518–524. doi:10.1038/nmat1421.
- [10] T.Y. Bak, M.S. Kook, S.C. Jung, B.H. Kim, Biological effect of gas plasma treatment on CO<sub>2</sub> gas foaming/salt leaching fabricated porous polycaprolactone scaffolds in bone tissue engineering, *J. Nanomater.* 2014 (2014) 1–6. doi:10.1155/2014/657542.
- [11] A. Salerno, M. Oliviero, E. Di Maio, S. Iannace, P.A. Netti, Design of porous polymeric scaffolds by gas foaming of heterogeneous blends, *J. Mater. Sci. Mater. Med.* 20 (2009) 2043–2051. doi:10.1007/s10856-009-3767-4.

- [12] J. Reignier, M.A. Huneault, Preparation of interconnected poly( $\epsilon$ -lunate-caprolactone) porous scaffolds by a combination of polymer and salt particulate leaching, *Polymer (Guildf)*. 47 (2006) 4703–4717. doi:10.1016/j.polymer.2006.04.029.
- [13] B. Aldemir Dikici, S. Dikici, G.C. Reilly, S. MacNeil, F. Claeysens, A Novel Bilayer Polycaprolactone Membrane for Guided Bone Regeneration: Combining Electrospinning and Emulsion Templating, *Materials (Basel)*. 12 (2019) 2643. doi:10.3390/ma12162643.
- [14] S. Dikici, F. Claeysens, S. MacNeil, Pre-Seeding of Simple Electrospun Scaffolds with a Combination of Endothelial Cells and Fibroblasts Strongly Promotes Angiogenesis, *Tissue Eng. Regen. Med.* 17 (2020) 445–458. doi:10.1007/s13770-020-00263-7.
- [15] N. Mangir, B. Aldemir Dikici, C.R. Chapple, S. MacNeil, Landmarks in vaginal mesh development: polypropylene mesh for treatment of SUI and POP, *Nat. Rev. Urol.* 16 (2019) 675–689. doi:10.1038/s41585-019-0230-2.
- [16] S. Dikici, F. Claeysens, S. MacNeil, Bioengineering Vascular Networks to Study Angiogenesis and Vascularization of Physiologically Relevant Tissue Models in Vitro, *ACS Biomater. Sci. Eng.* 6 (2020) 3513–3528. doi:10.1021/acsbmaterials.0c00191.
- [17] L. Elomaa, S. Teixeira, R. Hakala, H. Korhonen, D.W. Grijpma, J. V. Seppälä, Preparation of poly( $\epsilon$ -caprolactone)-based tissue engineering scaffolds by stereolithography, *Acta Biomater.* 7 (2011) 3850–3856. doi:10.1016/j.actbio.2011.06.039.
- [18] B. Aldemir Dikici, S. Dikici, O. Karaman, H. Oflaz, The effect of zinc oxide doping on mechanical and biological properties of 3D printed calcium sulfate based scaffolds, *Biocybern. Biomed. Eng.* 37 (2017) 733–741. doi:10.1016/j.bbe.2017.08.007.
- [19] A. Richez, H. Deleuze, P. Vedrenne, R. Collier, Preparation of ultra-low-density microcellular materials, *J. Appl. Polym. Sci.* 96 (2005) 2053–2063. doi:10.1002/app.21668.
- [20] W. Guenther, Process for the production of porous plastics and products comprising polymerizing a monomer in a water-in-oil emulsion, 1959. <https://patents.google.com/patent/US3256219A/en#patentCitations>.
- [21] J.C. Fletcher, H.E. Marsh Jr., US Patent 4039489 - Oil and fat absorbing polymers, 1977. <http://www.google.com/patents/US4039489>.
- [22] W. Guenther, Method of producing porous polymerizates from water-in-oil emulsions,

1971. <https://patents.google.com/patent/US3734867A/en>.

- [23] Y. Zhang, Y. Shen, Y. Chen, Y. Yan, J. Pan, Q. Xiong, W. Shi, L. Yu, Hierarchically carbonaceous catalyst with Brønsted-Lewis acid sites prepared through Pickering HIPEs templating for biomass energy conversion, *Chem. Eng. J.* 294 (2016) 222–235. doi:10.1016/j.cej.2016.02.092.
- [24] J. Yang, G. Yang, H. Liu, L. Bai, Q. Zhang, Novel porous monolithic column using poly(high internal phase emulsion) methacrylate as materials for immunoglobulin separation performance on HPLC, *Chinese J. Chem.* 28 (2010) 229–234. doi:10.1002/cjoc.201090058.
- [25] P.W. Small, D.C. Sherrington, Design and application of a new rigid support for high efficiency continuous-flow peptide synthesis, *J. Chem. Soc. Chem. Commun.* (1989) 1589–1591. doi:10.1039/C39890001589.
- [26] I.J. Brown, S. Sotiropoulos, Electrodeposition of Ni from a high internal phase emulsion (HIPE) template, *Electrochim. Acta.* 46 (2001) 2711–2720. doi:10.1016/S0013-4686(01)00481-9.
- [27] K.J. Lissant, The geometry of high-internal-phase-ratio emulsions, *J. Colloid Interface Sci.* 22 (1966) 462–468. doi:10.1016/0021-9797(66)90091-9.
- [28] C.A. Vacanti, The history of tissue engineering, *J. Cell. Mol. Med.* 10 (2006) 569–576. doi:10.1111/j.1582-4934.2006.tb00421.x.
- [29] U. Meyer, The history of tissue engineering and regenerative medicine in perspective, in: *Fundam. Tissue Eng. Regen. Med.*, 2009: pp. 5–12. doi:10.1007/978-3-540-77755-7\_1.
- [30] D. Barby, Z. Haq, Low Density Porous Cross-Linked Polymeric Materials and Their Preparation and Use As Carriers for Included Liquids, US4522953A, 1985. <https://patents.google.com/patent/US4522953/en>.
- [31] D.W. Lee, J.M. Piret, D. Gregory, D.J. Haddow, D.G. Kilburn, Polystyrene Macroporous Bead Support for Mammalian Cell Culture, *Ann. N. Y. Acad. Sci.* 665 (1992) 137–145. doi:10.1111/j.1749-6632.1992.tb42581.x.
- [32] D.W. Lee, D. Gregory, J.M. Piret, D.G. Kilburn, D.J. Haddow, High Density BHK Culture Using Porous Microcarriers, in: *Anim. Cell Technol.*, Elsevier, 1992: pp. 480–487. <https://linkinghub.elsevier.com/retrieve/pii/B9780750604215501094>.

- [33] N. Kitagawa, Hydrophilic polymeric material and method of preparation, US6218440B1, 2001. <https://patents.google.com/patent/US6218440B1/en>.
- [34] K.L. Thunhorst, M.D. Gehlsen, R.E. Wright, E.W. Nelson, S.D. Koecher, D. Gold, Foams made by photopolymerization of emulsions, 2003. <https://patents.google.com/patent/WO2001021693A1/en?q=Thunhorst+01%2F21693>.
- [35] W. Busby, N.R. Cameron, C.A.B. Jahoda, Emulsion-Derived Foams (PolyHIPEs) Containing Poly( $\epsilon$ -caprolactone) as Matrixes for Tissue Engineering, *Biomacromolecules*. 2 (2001) 154–164. doi:10.1021/bm0000889.
- [36] E.M. Christenson, W. Soofi, J.L. Holm, N.R. Cameron, A.G. Mikos, Biodegradable fumarate-based polyHIPEs as tissue engineering scaffolds, *Biomacromolecules*. 8 (2007) 3806–3814. doi:10.1021/bm7007235.
- [37] S. Padbury, Reprocell, (2010). <https://news.reprocell.com/reinnervate-launches-alvetex-a-breakthrough-product-for-enabling-routine-3d-cell-culture> (accessed December 5, 2019).
- [38] R.S. Moglia, J.L. Holm, N.A. Sears, C.J. Wilson, D.M. Harrison, E. Cosgriff-Hernandez, Injectable polyHIPEs as high-porosity bone grafts, *Biomacromolecules*. 12 (2011) 3621–3628. doi:10.1021/bm2008839.
- [39] D.W. Johnson, C. Sherborne, M.P. Didsbury, C. Pateman, N.R. Cameron, F. Claeysens, Macrostructuring of emulsion-templated porous polymers by 3D laser patterning, *Adv. Mater.* 25 (2013) 3178–3181. doi:10.1002/adma.201300552.
- [40] M. Sušec, S.C. Ligon, J. Stampfl, R. Liska, P. Krajnc, Hierarchically porous materials from layer-by-layer photopolymerization of high internal phase emulsions, *Macromol. Rapid Commun.* 34 (2013) 938–943. doi:10.1002/marc.201300016.
- [41] Y. Hu, X. Gu, Y. Yang, J. Huang, M. Hu, W. Chen, Z. Tong, C. Wang, Facile fabrication of poly(l -Lactic Acid)-Grafted hydroxyapatite/poly(lactic- co -glycolic Acid) scaffolds by pickering high internal phase emulsion templates, *ACS Appl. Mater. Interfaces*. 6 (2014) 17166–17175. doi:10.1021/am504877h.
- [42] B. Aldemir Dikici, C. Sherborne, G.C. Reilly, F. Claeysens, Emulsion templated scaffolds manufactured from photocurable polycaprolactone, *Polymer (Guildf)*. 175 (2019) 243–254. doi:10.1016/j.polymer.2019.05.023.

- [43] G. Schrimpf, P. Friedl, Growth of human vascular endothelial cells on various types of microcarriers, *Cytotechnology*. 13 (1993) 203–211. doi:10.1007/BF00749816.
- [44] G. Akay, S. Downes, V.J. Price, Microcellular polymer as cell growth media and novel polymers, EP1183328B1, 2000. <https://patents.google.com/patent/EP1183328B1/en>.
- [45] N.R. Cameron, High internal phase emulsion templating as a route to well-defined porous polymers, *Polymer (Guildf)*. 46 (2005) 1439–1449. doi:10.1016/j.polymer.2004.11.097.
- [46] M.S. Silverstein, PolyHIPEs: Recent advances in emulsion-templated porous polymers, *Prog. Polym. Sci.* 39 (2014) 199–234. doi:10.1016/j.progpolymsci.2013.07.003.
- [47] M.S. Silverstein, Emulsion-templated porous polymers: A retrospective perspective, *Polymer (Guildf)*. 55 (2014) 304–320. doi:10.1016/j.polymer.2013.08.068.
- [48] T. Zhang, R.A. Sanguramath, S. Israel, M.S. Silverstein, Emulsion Templating: Porous Polymers and beyond, *Macromolecules*. 52 (2019) 5445–5479. doi:10.1021/acs.macromol.8b02576.
- [49] M.S. Silverstein, N.R. Cameron, PolyHIPEs - Porous Polymers from High Internal Phase Emulsions, in: *Encycl. Polym. Sci. Technol.*, 2010. doi:10.1002/0471440264.pst571.
- [50] I. Pulko, P. Krajnc, High internal phase emulsion templating - A path to hierarchically porous functional polymers, *Macromol. Rapid Commun.* 33 (2012) 1731–1746. doi:10.1002/marc.201200393.
- [51] T.C. Hales, A proof of the Kepler conjecture, *Ann. Math.* 162 (2005) 1065–1185. doi:10.4007/annals.2005.162.1065.
- [52] S.U. Pickering, CXCVI. - Emulsions, *J. Chem. Soc. Trans.* 91 (1907) 2001–2021. doi:10.1039/CT9079102001.
- [53] A. Menner, R. Powell, A. Bismarck, Open porous polymer foams via inverse emulsion polymerization: Should the definition of high internal phase (ratio) emulsions be extended?, *Macromolecules*. 39 (2006) 2034–2035. doi:10.1021/ma052705x.
- [54] S.S. Manley, N. Graeber, Z. Grof, A. Menner, G.F. Hewitt, F. Stepanek, A. Bismarck, New insights into the relationship between internal phase level of emulsion templates and gas-liquid permeability of interconnected macroporous polymers, *Soft Matter*. 5 (2009)

- 4780–4787. doi:10.1039/b900426b.
- [55] V.H. Bartl, W. Von Bonin, Über die Polymerisation in umgekehrter Emulsion, *Die Makromol. Chemie.* 57 (1962) 74–95. doi:10.1002/macp.1962.020570105.
- [56] V.H. Bartl, W. von Bonin, Über die polymerisation in umgekehrter emulsion. II, *Die Makromol. Chemie.* 66 (1963) 151–156. doi:10.1002/macp.1963.020660115.
- [57] J.L. Robinson, R.S. Moglia, M.C. Stuebben, M.A.P. Mcenery, E. Cosgriff-Hernandez, Achieving interconnected pore architecture in injectable PolyHIPEs for bone tissue engineering, *Tissue Eng. - Part A.* 20 (2014) 1103–1112. doi:10.1089/ten.tea.2013.0319.
- [58] N.R. Cameron, D.C. Sherrington, L. Albiston, D.P. Gregory, Study of the formation of the open-cellular morphology of poly(styrene/divinylbenzene) polyHIPE materials by cryo-SEM, *Colloid Polym. Sci.* (1996). doi:10.1007/BF00655236.
- [59] J.H. Chen, T.T.M. Le, K.C. Hsu, Application of polyHIPE membrane with tricaprilmethylammonium chloride for Cr(VI) ion separation: Parameters and mechanism of transport relating to the pore structure, *Membranes (Basel).* (2018). doi:10.3390/membranes8010011.
- [60] G.F. Guimarães, E. Marcelino, I. Cesarino, F.B. Vicente, C.R. Grandini, R.P. Simões, Minimization of polymerization shrinkage effects on composite resins by the control of irradiance during the photoactivation process, *J. Appl. Oral Sci.* (2018). doi:10.1590/1678-7757-2017-0528.
- [61] I. Barbara, M.A. Dourges, H. Deleuze, Preparation of porous polyurethanes by emulsion-templated step growth polymerization, *Polymer (Guildf).* (2017). doi:10.1016/j.polymer.2017.11.018.
- [62] M. Ovadia, M.S. Silverstein, High porosity, responsive hydrogel copolymers from emulsion templating, *Polym. Int.* (2016). doi:10.1002/pi.5052.
- [63] S.J. Pierre, J.C. Thies, A. Dureault, N.R. Cameron, J.C.M. Van Hest, N. Carette, T. Michon, R. Weberskirch, Covalent enzyme immobilization onto photopolymerized highly porous monoliths, *Adv. Mater.* 18 (2006) 1822–1826. doi:10.1002/adma.200600293.
- [64] M. Sušec, R. Liska, G. Russmüller, J. Kotek, P. Krajnc, Microcellular open porous monoliths for cell growth by thiol-ene polymerization of low-toxicity monomers in high internal phase emulsions, *Macromol. Biosci.* (2015). doi:10.1002/mabi.201400219.

- [65] A. Barbetta, M. Dentini, E.M. Zannoni, M.E. De Stefano, Tailoring the porosity and morphology of gelatin-methacrylate polyHIPE scaffolds for tissue engineering applications, *Langmuir*. 21 (2005) 12333–12341. doi:10.1021/la0520233.
- [66] A. Barbetta, N.R. Cameron, Morphology and surface area of emulsion-derived (PolyHIPE) solid foams prepared with oil-phase soluble porogenic solvents: Span 80 as surfactant, *Macromolecules*. 37 (2004) 3188–3201. doi:10.1021/ma0359436.
- [67] A. Kataruka, S.B. Hutchens, PDMS polymerized high internal phase emulsions (polyHIPEs) with closed-cell, aqueous-filled microcavities, *Soft Matter*. (2019). doi:10.1039/c9sm01732a.
- [68] M. Costantini, C. Colosi, J. Guzowski, A. Barbetta, J. Jaroszewicz, W. Świążkowski, M. Dentini, P. Garstecki, Highly ordered and tunable polyHIPEs by using microfluidics, *J. Mater. Chem. B*. (2014). doi:10.1039/c3tb21227k.
- [69] R.J. Carnachan, M. Bokhari, S.A. Przyborski, N.R. Cameron, Tailoring the morphology of emulsion-templated porous polymers, *Soft Matter*. 2 (2006) 608. doi:10.1039/b603211g.
- [70] R. Owen, C. Sherborne, G.C. Reilly, F. Claeysens, T. Paterson, N.H. Green, G.C. Reilly, F. Claeysens, Emulsion templated scaffolds with tunable mechanical properties for bone tissue engineering, *J. Mech. Behav. Biomed. Mater.* 54 (2016) 159–172. doi:10.1016/j.jmbbm.2015.09.019.
- [71] M.S. Silverstein, N.R. Cameron, M. Hillmyer, *Porous Polymers*, 2011. doi:10.1002/9780470929445.
- [72] O.G. Kravchenko, G. Gedler, S.G. Kravchenko, D.L. Feke, I. Manas-Zloczower, Modeling compressive behavior of open-cell polymerized high internal phase emulsions: Effects of density and morphology, *Soft Matter*. 14 (2018) 1637–1646. doi:10.1039/c7sm02043k.
- [73] I. Pulko, J. Wall, P. Krajnc, N.R. Cameron, Ultra-high surface area functional porous polymers by emulsion templating and hypercrosslinking: Efficient nucleophilic catalyst supports, *Chem. - A Eur. J.* 16 (2010) 2350–2354. doi:10.1002/chem.200903043.
- [74] S. Mezhoud, M. Paljevac, A. Koler, B. Le Droumaguet, D. Grande, P. Krajnc, Novel hypercrosslinking approach toward high surface area functional 2-hydroxyethyl methacrylate-based polyHIPEs, *React. Funct. Polym.* 132 (2018) 51–59.

- doi:10.1016/j.reactfunctpolym.2018.09.009.
- [75] B. Aldemir Dikici, G.C. Reilly, F. Claeysens, Boosting the osteogenic and angiogenic performance of multiscale porous polycaprolactone scaffolds by in vitro generated extracellular matrix decoration, *ACS Appl. Mater. Interfaces*. 12 (2020) 12510–12524. doi:10.1021/acsami.9b23100.
- [76] N.A. Sears, P.S. Dhavalikar, E.M. Cosgriff-Hernandez, Emulsion Inks for 3D Printing of High Porosity Materials, *Macromol. Rapid Commun.* 37 (2016) 1369–1374. doi:10.1002/marc.201600236.
- [77] S. Bhagavathi Kandy, G.P. Simon, W. Cheng, J. Zank, K. Joshi, D. Gala, A.R. Bhattacharyya, Effect of Incorporation of Multiwalled Carbon Nanotubes on the Microstructure and Flow Behavior of Highly Concentrated Emulsions, *ACS Omega*. (2018). doi:10.1021/acsomega.8b00579.
- [78] A.N. Iliya Anisa, A.H. Nour, Affect of viscosity and droplet diameter on water-in-oil (w/o) emulsions: An experimental study, *World Acad. Sci. Eng. Technol.* 62 (2010) 691–694.
- [79] R.E. Ford, C.G.L. Furmidge, Physico-chemical studies on agricultural sprays VIII.—Viscosity and spray drop size of water-in-oil emulsions, *J. Sci. Food Agric.* 18 (1967) 419–428. doi:10.1002/jsfa.2740180910.
- [80] C.F. Welch, G.D. Rose, D. Malotky, S.T. Eckersley, Rheology of High Internal Phase Emulsions, 22 (2006) 1544–1550. doi:10.1021/la052207h.
- [81] A.K. Das, D. Mukesh, V. Swayambunathan, D.D. Kotkar, P.K. Ghosh, Concentrated Emulsions. 3. Studies on the Influence of Continuous-Phase Viscosity, Volume Fraction, Droplet Size, and Temperature on Emulsion Viscosity, *Langmuir*. 8 (1992) 2427–2436. doi:10.1021/la00046a015.
- [82] A. Sun, S. Gunasekaran, Yield stress in foods: Measurements and applications, *Int. J. Food Prop.* (2009). doi:10.1080/10942910802308502.
- [83] Malvern Instruments, Understanding yield stress measurements, *Annu. Trans. Nord. Rheol. Soc.* (2012).
- [84] Malvern Instruments, *A Basic Introduction to Rheology*, 2016.
- [85] R. Owen, C. Sherborne, G.C. Reilly, F. Claeysens, Data for the analysis of PolyHIPE scaffolds with tunable mechanical properties for bone tissue engineering, *Data Br.* 5

- (2015) 616–620. doi:10.1016/j.dib.2015.09.051.
- [86] V. Karageorgiou, D. Kaplan, Porosity of 3D biomaterial scaffolds and osteogenesis, *Biomaterials*. 26 (2005) 5474–5491. doi:10.1016/j.biomaterials.2005.02.002.
- [87] S. Huš, P. Krajnc, PolyHIPEs from Methyl methacrylate: Hierarchically structured microcellular polymers with exceptional mechanical properties, *Polymer (Guildf)*. 55 (2014) 4420–4424. doi:10.1016/j.polymer.2014.07.007.
- [88] S. Kovačič, E. Žagar, C. Slugovc, Strength versus toughness of emulsion templated Poly(Dicyclopentadiene) foams, *Polymer (Guildf)*. 169 (2019) 58–65. doi:10.1016/j.polymer.2019.02.045.
- [89] S. Lin-Gibson, J.A. Cooper, F.A. Landis, M.T. Cicerone, Systematic investigation of porogen size and content on scaffold morphometric parameters and properties, *Biomacromolecules*. (2007). doi:10.1021/bm061139q.
- [90] B.H.L. Oh, A. Bismarck, M.B. Chan-Park, Injectable, interconnected, high-porosity macroporous biocompatible gelatin scaffolds made by surfactant-free emulsion templating, *Macromol. Rapid Commun.* 36 (2015) 364–372. doi:10.1002/marc.201400524.
- [91] N.R. Cameron, D.C. Sherrington, High Internal Phase Emulsions (HIPEs) - Structure, Properties and Use in Polymer Preparation, in: *Adv. Polym. Sci.*, Springer Berlin Heidelberg, Berlin, Heidelberg, 1996: pp. 162–214. doi:10.1007/3-540-60484-7\_4.
- [92] R. Pal, E. Rhodes, A novel viscosity correlation for non-newtonian concentrated emulsions, *J. Colloid Interface Sci.* (1985). doi:10.1016/0021-9797(85)90181-X.
- [93] M.A. Farah, R.C. Oliveira, J.N. Caldas, K. Rajagopal, Viscosity of water-in-oil emulsions: Variation with temperature and water volume fraction, *J. Pet. Sci. Eng.* 48 (2005) 169–184. doi:10.1016/j.petrol.2005.06.014.
- [94] C. Zhou, M. Qiao, X. Zhang, Y. Zhu, S. Zhang, J. Chen, Production of High Internal Phase Emulsion with a Miniature Twin Screw Extruder, *ACS Omega*. (2019). doi:10.1021/acsomega.9b01156.
- [95] H.A. Barnes, Rheology of emulsions - a review, *Colloids Surfaces A Physicochem. Eng. Asp.* (1994). doi:10.1016/0927-7757(93)02719-U.
- [96] X. Fan, S. Zhang, Y. Zhu, J. Chen, Macroporous polymers prepared via frozen UV

- polymerization of the emulsion-templates stabilized by a low amount of surfactant, *RSC Adv.* (2018). doi:10.1039/c8ra01000e.
- [97] T.E. Paterson, G. Gigliobianco, C. Sherborne, N.H. Green, J.M. Dugan, S. MacNeil, G.C. Reilly, F. Claeysens, Porous microspheres support mesenchymal progenitor cell ingrowth and stimulate angiogenesis, *APL Bioeng.* 2 (2018) 026103. doi:10.1063/1.5008556.
- [98] Y. Wang, X. Wan, J. He, U. Azhar, H. Chen, J. Zhao, A. min Pang, B. Geng, A one-step fabrication and modification of HIPE-templated fluoro-porous polymer using PEG-b-PHFBMA macrosurfactant, *J. Mater. Sci.* (2020). doi:10.1007/s10853-019-04296-9.
- [99] S. Caldwell, D.W. Johnson, M.P. Didsbury, B.A. Murray, J.J. Wu, S.A. Przyborski, N.R. Cameron, Degradable emulsion-templated scaffolds for tissue engineering from thiol-ene photopolymerisation, *Soft Matter.* 8 (2012) 10344–10351. doi:10.1039/c2sm26250a.
- [100] S. Huš, M. Kolar, P. Krajnc, Tailoring morphological features of cross-linked emulsion-templated poly(glycidyl methacrylate), *Des. Monomers Polym.* (2015). doi:10.1080/15685551.2015.1070503.
- [101] U. Kuhlmann, *Encyclopedia of Food Sciences and Nutrition*, *J. Mol. Biol.* 301 (2000) 1163–1178. doi:10.1017/CBO9781107415324.004.
- [102] W. Busby, N.R. Cameron, C.A.B. Jahoda, Tissue engineering matrixes by emulsion templating, *Polym. Int.* 51 (2002) 871–881. doi:10.1002/pi.934.
- [103] M.S. Silverstein, H. Tai, A. Sergienko, Y. Lumelsky, S. Pavlovsky, PolyHIPE: IPNs, hybrids, nanoscale porosity, silica monoliths and ICP-based sensors, *Polymer (Guildf).* 46 (2005) 6682–6694. doi:10.1016/j.polymer.2005.05.022.
- [104] W. Busby, N.R. Cameron, C.A.B. Jahoda, Emulsion-Derived Foams (PolyHIPes) Containing Poly( $\epsilon$ -caprolactone) as Matrixes for Tissue Engineering, *Biomacromolecules.* 2 (2001) 154–164. doi:10.1021/bm0000889.
- [105] S. Changotade, G. Radu Bostan, A. Consalus, F. Poirier, J. Peltzer, J.J. Lataillade, D. Lutomski, G. Rohman, Preliminary in Vitro Assessment of Stem Cell Compatibility with Cross-Linked Poly( $\epsilon$ -caprolactone urethane) Scaffolds Designed through High Internal Phase Emulsions, *Stem Cells Int.* (2015). doi:10.1155/2015/283796.
- [106] D. David, M.S. Silverstein, Porous polyurethanes synthesized within high internal phase

- emulsions, *J. Polym. Sci. Part A Polym. Chem.* (2009). doi:10.1002/pola.23624.
- [107] D.W. Johnson, C.R. Langford, M.P. Didsbury, B. Lipp, S.A. Przyborski, N.R. Cameron, Fully biodegradable and biocompatible emulsion templated polymer scaffolds by thiol-acrylate polymerization of polycaprolactone macromonomers, *Polym. Chem.* 6 (2015) 7256–7263. doi:10.1039/c5py00721f.
- [108] A. Barbetta, M. Dentini, M.S. De Vecchis, P. Filippini, G. Formisano, S. Caiazza, Scaffolds based on biopolymeric foams, *Adv. Funct. Mater.* 15 (2005) 118–124. doi:10.1002/adfm.200400072.
- [109] P. Krajnc, D. Štefanec, I. Pulko, Acrylic acid “reversed” PolyHIPEs, *Macromol. Rapid Commun.* 26 (2005) 1289–1293. doi:10.1002/marc.200500353.
- [110] R. Pons, C. Solans, M.J. Stebé, P. Erra, J.C. Ravey, Stability and rheological properties of gel emulsions, in: *Trends Colloid Interface Sci.* VI, 2007: pp. 110–113. doi:10.1007/bfb0116290.
- [111] H. Kunieda, N. Yano, C. Solans, The stability of gel-emulsions in a water/nonionic surfactant/oil system, *Colloids and Surfaces.* 36 (1989) 313–322. doi:10.1016/0166-6622(89)80246-X.
- [112] V. Rajagopalan, C. Solans, H. Kunieda, ESR study on the stability of W/O gel-emulsions, *Colloid Polym. Sci.* 272 (1994) 1166–1173. doi:10.1007/BF00652387.
- [113] K.C. Powell, R. Damitz, A. Chauhan, Relating emulsion stability to interfacial properties for pharmaceutical emulsions stabilized by Pluronic F68 surfactant, *Int. J. Pharm.* 521 (2017) 8–18. doi:10.1016/j.ijpharm.2017.01.058.
- [114] F.O. Opawale, D.J. Burgess, Influence of interfacial properties of lipophilic surfactants on water- in-oil emulsion stability, *J. Colloid Interface Sci.* 197 (1998) 142–150. doi:10.1006/jcis.1997.5222.
- [115] Y. Lumelsky, J. Zoldan, S. Levenberg, M.S. Silverstein, R. V December, Porous Polycaprolactone - Polystyrene Semi-interpenetrating Polymer Networks Synthesized within High Internal Phase Emulsions, *Macromolecules.* 41 (2008) 1469–1474. doi:10.1021/ma7027177.
- [116] Y. Lumelsky, M.S. Silverstein, Biodegradable porous polymers through emulsion templating, *Macromolecules.* 42 (2009) 1627–1633. doi:10.1021/ma802461m.

- [117] Y. Lumelsky, I. Lalush-Michael, S. Levenberg, M.S. Silverstein, A degradable, porous, emulsion-templated polyacrylate, *J. Polym. Sci. Part A Polym. Chem.* 47 (2009) 7043–7053. doi:10.1002/pola.23744.
- [118] P. Kent, B.R. Saunders, The role of added electrolyte in the stabilization of inverse emulsions, *J. Colloid Interface Sci.* 242 (2001) 437–442. doi:10.1006/jcis.2001.7792.
- [119] M.W. Hayman, K.H. Smith, N.R. Cameron, S.A. Przyborski, Growth of human stem cell-derived neurons on solid three-dimensional polymers, *J. Biochem. Biophys. Methods.* 62 (2005) 231–240. doi:10.1016/j.jbbm.2004.12.001.
- [120] M.W. Hayman, K.H. Smith, N.R. Cameron, S.A. Przyborski, Enhanced neurite outgrowth by human neurons grown on solid three-dimensional scaffolds, *Biochem. Biophys. Res. Commun.* 314 (2004) 483–488. doi:10.1016/j.bbrc.2003.12.135.
- [121] W.D. Bancroft, The Theory of Emulsification, V, *J. Phys. Chem.* 17 (1913) 501–519. doi:10.1021/j150141a002.
- [122] P. Finkle, H.D. Draper, J.H. Hildebrand, The theory of emulsification, *J. Am. Chem. Soc.* 45 (1923) 2780–2788. doi:10.1021/ja01665a002.
- [123] W.C. Griffin, Classification of surface-active agents by “HLB,” *J. Soc. Cosmet. Chem.* 1 (1946) 311–326. <http://ci.nii.ac.jp/naid/10004943329/>.
- [124] W.C. Griffin, Calculation of HLB Values of Non-Ionic Surfactants, *J. Soc. Cosmet. Chem.* 5 (1954) 249–256.
- [125] D. Myers, *Surfactant Science and Technology: Third Edition*, 2005. doi:10.1002/047174607X.
- [126] S. Zhang, J. Chen, Synthesis of open porous emulsion-templated monoliths using cetyltrimethylammonium bromide, *Polymer (Guildf).* 48 (2007) 3021–3025. doi:10.1016/j.polymer.2007.04.009.
- [127] T. Zhang, M.S. Silverstein, Microphase-Separated Macroporous Polymers from an Emulsion-Templated Reactive Triblock Copolymer, *Macromolecules.* 51 (2018) 3828–3835. doi:10.1021/acs.macromol.8b00213.
- [128] J. Surh, G.T. Vladislavljević, S. Mun, D.J. McClements, Preparation and characterization of water/oil and water/oil/water emulsions containing biopolymer-gelled water droplets, *J. Agric. Food Chem.* 55 (2007) 175–184. doi:10.1021/jf061637q.

- [129] R.S. Moglia, M. Whitely, P. Dhavalikar, J. Robinson, H. Pearce, M. Brooks, M. Stuebben, N. Corder, E. Cosgriff-Hernandez, Injectable polymerized high internal phase emulsions with rapid in situ curing, *Biomacromolecules*. 15 (2014) 2870–2878. doi:10.1021/bm500754r.
- [130] M.G.A. Kassem, A.M.M. Ahmed, H.H. Abdel-Rahman, A.H.E. Moustafa, Use of Span 80 and Tween 80 for blending gasoline and alcohol in spark ignition engines, *Energy Reports*. (2019). doi:10.1016/j.egyr.2019.01.009.
- [131] G. Akay, M.A. Birch, M.A. Bokhari, Microcellular polyHIPE polymer supports osteoblast growth and bone formation in vitro., *Biomaterials*. 25 (2004) 3991–4000. doi:10.1016/j.biomaterials.2003.10.086.
- [132] F. Audouin, A. Heise, Synthesis of polymer-silica hybrid polyHIPEs by double in situ polymerization of concentrated water in oil emulsion, *Polymer (Guildf)*. 55 (2014) 403–409. doi:10.1016/j.polymer.2013.09.002.
- [133] A. Malayeri, C. Sherborne, T. Paterson, S. Mittar, I.O. Asencio, P. V. Hatton, F. Claeysens, Osteosarcoma growth on trabecular bone mimicking structures manufactured via laser direct write, *Int. J. Bioprinting*. 2 (2016) 67–77. doi:10.18063/IJB.2016.02.005.
- [134] A. Wang, T. Paterson, R. Owen, C. Sherborne, J. Dugan, J. Li, F. Claeysens, Photocurable High Internal Phase Emulsions (HIPEs) Containing Hydroxyapatite for Additive Manufacture of Tissue Engineering Scaffolds with Multi-Scale Porosity, *Mater. Sci. Eng. C*. 67 (2016) 51–58. doi:10.1016/j.msec.2016.04.087.
- [135] E. Lovelady, S.D. Kimmins, J. Wu, N.R. Cameron, Preparation of emulsion-templated porous polymers using thiol-ene and thiol-yne chemistry, *Polym. Chem*. 2 (2011) 559–562. doi:10.1039/c0py00374c.
- [136] S.A. Richardson, T.M. Rawlings, J. Muter, M. Walker, J.J. Brosens, N.R. Cameron, A.M. Eissa, Covalent Attachment of Fibronectin onto Emulsion-Templated Porous Polymer Scaffolds Enhances Human Endometrial Stromal Cell Adhesion, Infiltration, and Function, *Macromol. Biosci*. 19 (2019) 1–10. doi:10.1002/mabi.201800351.
- [137] M. Thakare, B. Israel, S. Garner, H. Ahmed, D. Elder, A. Capomacchia, Nonionic surfactant structure on the drug release, formulation and physical properties of ethylcellulose microspheres, *Pharm. Dev. Technol.* (2017). doi:10.1080/10837450.2016.1221431.
- [138] A. Samanta, B. Nandan, R.K. Srivastava, Morphology of electrospun fibers derived from

- High Internal Phase Emulsions, *J. Colloid Interface Sci.* 471 (2016) 29–36. doi:10.1016/j.jcis.2016.03.012.
- [139] M.M. Amiji, *Polymeric gene delivery: Principles and applications*, 2004. doi:10.1201/9780203500477.
- [140] J. Naranda, M. Sušec, U. Maver, L. Gradišnik, M. Gorenjak, A. Vukasović, A. Ivković, M.S. Rupnik, M. Vogrin, P. Krajnc, Polyester type polyHIPE scaffolds with an interconnected porous structure for cartilage regeneration, *Sci. Rep.* 6 (2016). doi:10.1038/srep28695.
- [141] A.S. Prakash, Selecting surfactants for the maximum inhibition of the activity of the multi drug resistance efflux pump transporter, P-glycoprotein: Conceptual development, *J. Excipients Food Chem.* 1 (2010) 51–59.
- [142] E. Slinde, T. Flatmark, Effect of the hydrophile-lipophile balance of non-ionic detergents (Triton X-series) on the solubilization of biological membranes and their integral b-type cytochromes, *BBA - Biomembr.* (1976). doi:10.1016/0005-2736(76)90049-3.
- [143] S. Zhou, A. Bismarck, J.H.G. Steinke, Ion-responsive alginate based macroporous injectable hydrogel scaffolds prepared by emulsion templating, *J. Mater. Chem. B.* 1 (2013) 4736–4745. doi:10.1039/c3tb20888e.
- [144] A. Barbetta, E. Barigelli, M. Dentini, Porous alginate hydrogels: Synthetic methods for tailoring the porous texture, *Biomacromolecules.* 10 (2009) 2328–2337. doi:10.1021/bm900517q.
- [145] S. Zhou, A. Bismarck, J.H.G. Steinke, Thermoresponsive macroporous scaffolds prepared by emulsion templating, *Macromol. Rapid Commun.* 33 (2012) 1833–1839. doi:10.1002/marc.201200336.
- [146] T. Yang, Y. Hu, C. Wang, B.P. Binks, Fabrication of Hierarchical Macroporous Biocompatible Scaffolds by Combining Pickering High Internal Phase Emulsion Templates with Three-Dimensional Printing, *ACS Appl. Mater. Interfaces.* 9 (2017) 22950–22958. doi:10.1021/acsami.7b05012.
- [147] I. Gurevitch, M.S. Silverstein, Polymerized pickering HIPEs: Effects of synthesis parameters on porous structure, *J. Polym. Sci. Part A Polym. Chem.* 48 (2010) 1516–1525. doi:10.1002/pola.23911.
- [148] S. Zhou, A. Bismarck, J.H.G. Steinke, Interconnected macroporous glycidyl methacrylate-grafted dextran hydrogels synthesised from hydroxyapatite nanoparticle stabilised

high internal phase emulsion templates, *J. Mater. Chem.* 22 (2012) 18824–18829. doi:10.1039/c2jm33294a.

- [149] B.P. Binks, S.O. Lumsdon, Stability of oil-in-water emulsions stabilised by silica particles, *Phys. Chem. Chem. Phys.* 1 (1999) 3007–3016. doi:10.1039/a902209k.
- [150] J.H. Schulman, J. Leja, Control of contact angles at the oil-water-solid interfaces: Emulsions stabilized by solid particles (BaSO<sub>4</sub>), *Trans. Faraday Soc.* 50 (1954) 598–605. doi:10.1039/tf9545000598.
- [151] R. Pal, A simple model for the viscosity of pickering emulsions, *Fluids*. 3 (2018). doi:10.3390/fluids3010002.
- [152] Y. Hu, S. Zou, W. Chen, Z. Tong, C. Wang, Mineralization and drug release of hydroxyapatite/poly(l-lactic acid) nanocomposite scaffolds prepared by Pickering emulsion templating, *Colloids Surfaces B Biointerfaces*. 122 (2014) 559–565. doi:10.1016/j.colsurfb.2014.07.032.
- [153] Y. Hu, H. Gao, Z. Du, Y. Liu, Y. Yang, C. Wang, Pickering high internal phase emulsion-based hydroxyapatite-poly( $\epsilon$ -caprolactone) nanocomposite scaffolds, *J. Mater. Chem. B*. (2015). doi:10.1039/c5tb00093a.
- [154] Y. Hu, J. Wang, X. Li, X. Hu, W. Zhou, X. Dong, C. Wang, Z. Yang, B.P. Binks, Facile preparation of bioactive nanoparticle/poly( $\epsilon$ -caprolactone) hierarchical porous scaffolds via 3D printing of high internal phase Pickering emulsions, *J. Colloid Interface Sci.* 545 (2019) 104–115. doi:10.1016/j.jcis.2019.03.024.
- [155] F. Kavousi, N. Nikfarjam, Highly interconnected macroporous structures made from starch nanoparticle-stabilized medium internal phase emulsion polymerization for use in cell culture, *Polymer (Guildf)*. 180 (2019). doi:10.1016/j.polymer.2019.121744.
- [156] H. Tan, J. Wei, G. Sun, C. Mu, W. Lin, T. Ngai, Interconnected macroporous 3D scaffolds templated from gelatin nanoparticle-stabilized high internal phase emulsions for biomedical applications, *Soft Matter*. 13 (2017) 3871–3878. doi:10.1039/c7sm00706j.
- [157] Y. Tunc, N. Hasirci, K. Ulubayram, Synthesis of emulsion-templated acrylic-based porous polymers: From brittle to elastomeric, *Soft Mater.* 10 (2012) 449–461. doi:10.1080/1539445X.2010.532848.
- [158] F. Audouin, M. Fox, R. Larragy, P. Clarke, J. Huang, B. O'Connor, A. Heise, Polypeptide-grafted macroporous PolyHIPE by surface-initiated N-carboxyanhydride (NCA)

- polymerization as a platform for bioconjugation, *Macromolecules*. 45 (2012) 6127–6135. doi:10.1021/ma3010263.
- [159] M.A. Bokhari, G. Akay, S. Zhang, M.A. Birch, The enhancement of osteoblast growth and differentiation in vitro on a peptide hydrogel - PolyHIPE polymer hybrid material, *Biomaterials*. 26 (2005) 5198–5208. doi:10.1016/j.biomaterials.2005.01.040.
- [160] A.S. Hayward, A.M. Eissa, D.J. Maltman, N. Sano, S.A. Przyborski, N.R. Cameron, Galactose-functionalized polyHIPE scaffolds for use in routine three dimensional culture of mammalian hepatocytes, *Biomacromolecules*. 14 (2013) 4271–4277. doi:10.1021/bm401145x.
- [161] A. Eibel, D.E. Fast, G. Gescheidt, Choosing the ideal photoinitiator for free radical photopolymerizations: Predictions based on simulations using established data, *Polym. Chem*. 9 (2018) 5107–5115. doi:10.1039/c8py01195h.
- [162] C. Sherborne, R. Owen, G.C. Reilly, F. Claeysens, Light-based additive manufacturing of PolyHIPEs: Controlling the surface porosity for 3D cell culture applications, *Mater. Des*. 156 (2018) 494–503. doi:10.1016/j.matdes.2018.06.061.
- [163] H.H. Mishbak, G. Cooper, P.J. Bartolo, Development and characterization of a photocurable alginate bioink for three-dimensional bioprinting, *Int. J. Bioprinting*. 5 (2019). doi:10.18063/IJB.V5I2.189.
- [164] R. Harikrishna, A.W. Shaikh, S. Ponrathnam, C.R. Rajan, S. Bhongale, Photopolymerization of high internal phase emulsions based on 2-ethylhexyl (meth)acrylates and ethylene glycol dimethacrylate, *Des. Monomers Polym*. 17 (2014) 1–6. doi:10.1080/15685551.2013.771312.
- [165] P. Kardar, M. Ebrahimi, S. Bastani, Influence of temperature and light intensity on the photocuring process and kinetics parameters of a pigmented UV curable system, *J. Therm. Anal. Calorim*. (2014). doi:10.1007/s10973-014-3984-z.
- [166] F. Jiang, D. Drummer, Curing kinetic analysis of acrylate photopolymer for additive manufacturing by photo-DSC, *Polymers (Basel)*. (2020). doi:10.3390/POLYM12051080.
- [167] J.M. Morancho, X. Fernández-Francos, X. Ramis, J.M. Salla, A. Serra, Photocuring and thermal post-curing of a cycloaliphatic epoxide resin with a trithiol and a vinyl epoxy compound, *J. Therm. Anal. Calorim*. (2015). doi:10.1007/s10973-015-4535-y.

- [168] K. Kambly, Characterization of Curing Kinetics and Polymerization Shrinkage in Ceramic-Loaded Photocurable Resins For Large Area Maskless Photopolymerization (Lamp), Georgia Institute of Technology, 2009.
- [169] U. Sevšek, J. Brus, K. Jeřabek, P. Krajnc, Post polymerisation hypercrosslinking of styrene/divinylbenzene poly(HIPE)s: Creating micropores within macroporous polymer, *Polymer (Guildf)*. 55 (2014) 410–415. doi:10.1016/j.polymer.2013.09.026.
- [170] R.T. Woodward, A. Jobbe-Duval, S. Marchesini, D.B. Anthony, C. Petit, A. Bismarck, Hypercrosslinked polyHIPEs as precursors to designable, hierarchically porous carbon foams, *Polymer (Guildf)*. (2017). doi:10.1016/j.polymer.2017.03.042.
- [171] A.C. Nalawade, R. V. Ghorpade, S. Shadbar, M.S. Qureshi, N.N. Chavan, A.A. Khan, S. Ponrathnam, Inverse high internal phase emulsion polymerization (i-HIPE) of GMMA, HEMA and GDMA for the preparation of superporous hydrogels as a tissue engineering scaffold, *J. Mater. Chem. B*. 4 (2016) 450–460. doi:10.1039/c5tb01873k.
- [172] R. Murakami, H. Moriyama, T. Noguchi, M. Yamamoto, B.P. Binks, Effects of the density difference between water and oil on stabilization of powdered oil-in-water emulsions, *Langmuir*. 30 (2014) 496–500. doi:10.1021/la4042056.
- [173] M. Bokhari, R.J. Carnachan, S.A. Przyborski, N.R. Cameron, Emulsion-templated porous polymers as scaffolds for three dimensional cell culture: Effect of synthesis parameters on scaffold formation and homogeneity, *J. Mater. Chem.* 17 (2007) 4088–4094. doi:10.1039/b707499a.
- [174] B. Donald, H. Zia, Low density porous cross-linked polymeric materials and their preparation, 1982. [https://worldwide.espacenet.com/publicationDetails/biblio?CC=EP&NR=0060138A1&KC=A1&FT=D&ND=3&date=19820915&DB=&locale=en\\_EP](https://worldwide.espacenet.com/publicationDetails/biblio?CC=EP&NR=0060138A1&KC=A1&FT=D&ND=3&date=19820915&DB=&locale=en_EP).
- [175] K. Jones, B.R. Lothian, A. Martin, G. Taylor, Z. Haq, Porous polymers, (1986). <https://www.google.com/patents/US4612334>.
- [176] T. Zhang, G. Xu, O. Regev, F.D. Blum, Low-temperature polymerization of methyl methacrylate emulsion gels through surfactant catalysis, *J. Colloid Interface Sci.* 461 (2016) 128–135. doi:10.1016/j.jcis.2015.09.003.
- [177] G. Tanny, Y. Kenigsberg, E. Shchori, Microporous membrane laminate, 1986. <https://patents.google.com/patent/EP0216622A2/en?q=Eur.Patent+0216622+tann>

y.

- [178] A. Barbetta, M. Massimi, L.C. Devirgiliis, M. Dentini, Enzymatic cross-linking versus radical polymerization in the preparation of gelatin polyHIPEs and their performance as scaffolds in the culture of hepatocytes, *Biomacromolecules*. 7 (2006) 3059–3068. doi:10.1021/bm060533l.
- [179] E. Sharma, A. Samanta, J. Pal, S.S. Bahga, B. Nandan, R.K. Srivastava, High Internal Phase Emulsion Ring-Opening Polymerization of Pentadecanolide: Strategy to Obtain Porous Scaffolds in a Single Step, *Macromol. Chem. Phys.* 217 (2016) 1752–1758. doi:10.1002/macp.201600117.
- [180] M.G. Pérez-García, M.C. Gutiérrez, J.D. Mota-Morales, G. Luna-Bárceñas, F. Del Monte, Synthesis of Biodegradable Macroporous Poly(l -lactide)/Poly( $\epsilon$ -caprolactone) Blend Using Oil-in-Eutectic-Mixture High-Internal-Phase Emulsions as Template, *ACS Appl. Mater. Interfaces*. 8 (2016) 16939–16949. doi:10.1021/acsami.6b04830.
- [181] A. Yadav, J. Pal, B. Nandan, R.K. Srivastava, Macroporous scaffolds of cross-linked Poly( $\epsilon$ -caprolactone) via high internal phase emulsion templating, *Polymer (Guildf)*. 176 (2019) 66–73. doi:10.1016/j.polymer.2019.05.034.
- [182] P. Utroša, O.C. Onder, E. Žagar, S. Kovačič, D. Pahovnik, Shape Memory Behavior of Emulsion-Templated Poly( $\epsilon$ -Caprolactone) Synthesized by Organocatalyzed Ring-Opening Polymerization, *Macromolecules*. 52 (2019) 9291–9298. doi:10.1021/acs.macromol.9b01780.
- [183] S.A. García-Landeros, J.M. Cervantes-Díaz, A. Gutiérrez-Becerra, J.B. Pelayo-Vázquez, G. Landazuri-Gomez, J. Herrera-Ordóñez, J.F.A. Soltero-Martínez, J.D. Mota-Morales, M.G. Pérez-García, Oil-in-eutectic mixture HIPEs co-stabilized with surfactant and nanohydroxyapatite: Ring-opening polymerization for nanocomposite scaffold synthesis, *Chem. Commun.* 55 (2019) 12292–12295. doi:10.1039/c9cc06292k.
- [184] Y. Hu, W. Han, Y. Chen, R. Zou, Y. Ouyang, W. Zhou, Z. Yang, C. Wang, One-Pot Fabrication of Poly( $\epsilon$ -Caprolactone)-Incorporated Bovine Serum Albumin/Calcium Alginate/Hydroxyapatite Nanocomposite Scaffolds by High Internal Phase Emulsion Templates, *Macromol. Mater. Eng.* 302 (2017). doi:10.1002/mame.201600367.
- [185] O.C. Onder, E. Yilgor, I. Yilgor, Preparation of monolithic polycaprolactone foams with controlled morphology, *Polymer (Guildf)*. 136 (2018) 166–178. doi:10.1016/j.polymer.2017.12.054.

- [186] S. Dikici, B. Aldemir Dikici, S.I. Bhaloo, M. Balcells, E.R. Edelman, S. MacNeil, G.C. Reilly, C. Sherborne, F. Claeysens, Assessment of the Angiogenic Potential of 2-Deoxy-D-Ribose Using a Novel in vitro 3D Dynamic Model in Comparison With Established in vitro Assays, *Front. Bioeng. Biotechnol.* 7 (2020) 1–20. doi:10.3389/fbioe.2019.00451.
- [187] A. Lee, C.R. Langford, L.M. Rodriguez-Lorenzo, H. Thissen, N.R. Cameron, Bioceramic nanocomposite thiol-acrylate polyHIPE scaffolds for enhanced osteoblastic cell culture in 3D, *Biomater. Sci.* 5 (2017) 2035–2047. doi:10.1039/c7bm00292k.
- [188] R.S. Moglia, J.L. Robinson, A.D. Muschenborn, T.J. Touchet, D.J. Maitland, E. Cosgriff-Hernandez, Injectable polyMIPE scaffolds for soft tissue regeneration, *Polymer (Guildf)*. 55 (2014) 426–434. doi:10.1016/j.polymer.2013.09.009.
- [189] A.S. Hayward, N. Sano, S.A. Przyborski, N.R. Cameron, Acrylic-acid-functionalized polyhipe scaffolds for use in 3d cell culture, *Macromol. Rapid Commun.* 34 (2013) 1844–1849. doi:10.1002/marc.201300709.
- [190] J.L. Robinson, M.A.P. McEnery, H. Pearce, M.E. Whitely, D.J. Munoz-Pinto, M.S. Hahn, H. Li, N.A. Sears, E. Cosgriff-Hernandez, Osteoinductive PolyHIPE Foams as Injectable Bone Grafts, *Tissue Eng. - Part A*. 22 (2016) 403–414. doi:10.1089/ten.tea.2015.0370.
- [191] M.E. Whitely, J.L. Robinson, M.C. Stuebben, H.A. Pearce, M.A.P. McEnery, E. Cosgriff-Hernandez, Prevention of Oxygen Inhibition of PolyHIPE Radical Polymerization Using a Thiol-Based Cross-Linker, *ACS Biomater. Sci. Eng.* 3 (2017) 409–419. doi:10.1021/acsbiomaterials.6b00663.
- [192] R. Diez-Ahedo, X. Mendibil, M.C. Márquez-Posadas, I. Quintana, F. González, F.J. Rodríguez, L. Zilic, C. Sherborne, A. Glen, C.S. Taylor, F. Claeysens, J.W. Haycock, W. Schaafsma, E. González, B. Castro, S. Merino, UV-Casting on Methacrylated PCL for the Production of a Peripheral Nerve Implant Containing an Array of Porous Aligned Microchannels, *Polymers (Basel)*. 12 (2020) 971. doi:10.3390/polym12040971.
- [193] M. Paljevac, L. Gradišnik, S. Lipovšek, U. Maver, J. Kotek, P. Krajnc, Multiple-Level Porous Polymer Monoliths with Interconnected Cellular Topology Prepared by Combining Hard Sphere and Emulsion Templating for Use in Bone Tissue Engineering, *Macromol. Biosci.* 18 (2018). doi:10.1002/mabi.201700306.
- [194] R. Owen, C. Sherborne, R. Evans, G. C. Reilly, F. Claeysens, G.C. Reilly, F. Claeysens, Combined Porogen Leaching and Emulsion Templating of Bone Tissue Engineering Scaffolds, *Int. J. Bioprinting*. 6 (2020) in press. doi:10.18063/ijb.v6i2.265.

- [195] X. Pei, L. Ma, B. Zhang, J. Sun, Y. Sun, Y. Fan, Z. Gou, C. Zhou, X. Zhang, Creating hierarchical porosity hydroxyapatite scaffolds with osteoinduction by three-dimensional printing and microwave sintering, *Biofabrication*. 9 (2017). doi:10.1088/1758-5090/aa90ed.
- [196] S. Kawata, H.B. Sun, T. Tanaka, K. Takada, Finer features for functional microdevices, *Nature*. 412 (2001) 697–698. doi:10.1038/35089130.
- [197] X. Yang, M. Mohseni, O. Bas, C. Meinert, E. New, N.J. Castro, Type II photoinitiator and tuneable PEG-based materials library for visible light photolithography, *Tissue Eng. Part A*. (2020). doi:10.1089/ten.tea.2019.0282.
- [198] J.S. Temenoff, A.G. Mikos, Injectable biodegradable materials for orthopedic tissue engineering, *Biomaterials*. 21 (2000) 2405–2412. doi:10.1016/S0142-9612(00)00108-3.
- [199] C. Guyot, S. Lerouge, Can we achieve the perfect injectable scaffold for cell therapy?, *Futur. Sci. OA*. 4 (2018). doi:10.4155/fsoa-2017-0153.
- [200] B. Chang, N. Ahuja, C. Ma, X. Liu, Injectable scaffolds: Preparation and application in dental and craniofacial regeneration, *Mater. Sci. Eng. R Reports*. 111 (2017) 1–26. doi:10.1016/j.mser.2016.11.001.
- [201] S. Dikici, N. Mangır, F. Claeysens, M. Yar, S. MacNeil, Exploration of 2-deoxy-D-ribose and 17 $\beta$ -Estradiol as alternatives to exogenous VEGF to promote angiogenesis in tissue-engineered constructs, *Regen. Med*. 14 (2019) 179–197. doi:10.2217/rme-2018-0068.
- [202] Y. Zhou, J. Chyu, M. Zumwalt, Recent Progress of Fabrication of Cell Scaffold by Electrospinning Technique for Articular Cartilage Tissue Engineering, *Int. J. Biomater*. (2018). doi:10.1155/2018/1953636.
- [203] I. Jun, H.S. Han, J.R. Edwards, H. Jeon, Electrospun fibrous scaffolds for tissue engineering: Viewpoints on architecture and fabrication, *Int. J. Mol. Sci*. (2018). doi:10.3390/ijms19030745.
- [204] W.J. Li, R.S. Tuan, Fabrication and application of nanofibrous scaffolds in tissue engineering, *Curr. Protoc. Cell Biol*. (2009). doi:10.1002/0471143030.cb2502s42.
- [205] M. Vlachou, A. Siamidi, S. Kyriakou, Electrospinning and Drug Delivery, in: *Electrospinning Electrospaying - Tech. Appl.*, 2019. doi:10.5772/intechopen.86181.

- [206] A. Samanta, S. Takkar, R. Kulshreshtha, B. Nandan, R.K. Srivastava, Hydroxyapatite stabilized pickering emulsions of poly( $\epsilon$ -caprolactone) and their composite electrospun scaffolds, *Colloids Surfaces A Physicochem. Eng. Asp.* 533 (2017) 224–230. doi:10.1016/j.colsurfa.2017.09.001.
- [207] N. Mangir, A.J. Bullock, S. Roman, N. Osman, C. Chapple, S. MacNeil, Production of ascorbic acid releasing biomaterials for pelvic floor repair, *Acta Biomater.* 29 (2016) 188–197. doi:10.1016/j.actbio.2015.10.019.
- [208] J. Pal, M. Skrifvars, B. Nandan, R.K. Srivastava, Electrospun composite matrices from tenside-free poly( $\epsilon$ -caprolactone)-grafted acrylic acid/hydroxyapatite oil-in-water emulsions, *J. Mater. Sci.* 52 (2017) 2254–2262. doi:10.1007/s10853-016-0518-z.
- [209] A. Samanta, S. Takkar, R. Kulshreshtha, B. Nandan, R.K. Srivastava, Electrospun composite matrices of poly( $\epsilon$ -caprolactone)-montmorillonite made using tenside free Pickering emulsions, *Mater. Sci. Eng. C.* 69 (2016) 685–691. doi:10.1016/j.msec.2016.07.046.
- [210] R. Moglia, M. Whitely, M. Brooks, J. Robinson, M. Pishko, E. Cosgriff-Hernandez, Solvent-free fabrication of polyHIPE microspheres for controlled release of growth factors, *Macromol. Rapid Commun.* (2014). doi:10.1002/marc.201400145.
- [211] M. Whitely, G. Rodriguez-Rivera, C. Waldron, S. Mohiuddin, S. Cereceres, N. Sears, N. Ray, E. Cosgriff-Hernandez, Porous PolyHIPE microspheres for protein delivery from an injectable bone graft, *Acta Biomater.* 93 (2019) 169–179. doi:10.1016/j.actbio.2019.01.044.
- [212] M.T. Gokmen, F.E. Du Prez, Porous polymer particles - A comprehensive guide to synthesis, characterization, functionalization and applications, *Prog. Polym. Sci.* 37 (2012) 365–405. doi:10.1016/j.progpolymsci.2011.07.006.
- [213] A. Samanta, S. Takkar, R. Kulshreshtha, B. Nandan, R.K. Srivastava, Facile Fabrication of Composite Electrospun Nanofibrous Matrices of Poly( $\epsilon$ -caprolactone)-Silica Based Pickering Emulsion, *Langmuir.* 33 (2017) 8062–8069. doi:10.1021/acs.langmuir.7b02119.
- [214] S. He, M.D. Timmer, M.J. Yaszemski, A.W. Yasko, P.S. Engel, A.G. Mikos, Synthesis of biodegradable poly(propylene fumarate) networks with poly(propylene fumarate)-diacrylate macromers as crosslinking agents and characterization of their degradation products, *Polymer (Guildf).* 42 (2001) 1251–1260. doi:10.1016/S0032-

3861(00)00479-1.

- [215] L.J. Suggs, M.S. Shive, C.A. Garcia, J.M. Anderson, A.G. Mikos, In vitro cytotoxicity and in vivo biocompatibility of poly(propylene fumarate-co-ethylene glycol) hydrogels, *J. Biomed. Mater. Res.* 46 (1999) 22–32. doi:10.1002/(SICI)1097-4636(199907)46:1<22::AID-JBM3>3.0.CO;2-R.
- [216] K.W. Lee, S. Wang, L. Lu, E. Jabbari, B.L. Currier, M.J. Yaszemski, Fabrication and characterization of poly(propylene fumarate) scaffolds with controlled pore structures using 3-dimensional printing and injection molding, *Tissue Eng.* 12 (2006) 2801–2811. doi:10.1089/ten.2006.12.2801.
- [217] F.K. Kasper, K. Tanahashi, J.P. Fisher, A.G. Mikos, Synthesis of poly(propylene fumarate), *Nat. Protoc.* 4 (2009) 518–525. doi:10.1038/nprot.2009.24.
- [218] C. Hoyle, C.N. Bowman, Thiol–Ene Click Chemistry, *Angew. Chemie Int. Ed.* (2010).
- [219] H.Y. Cheung, K.T. Lau, T.P. Lu, D. Hui, A critical review on polymer-based bio-engineered materials for scaffold development, *Compos. Part B Eng.* 38 (2007) 291–300. doi:10.1016/j.compositesb.2006.06.014.
- [220] M.S. Shoichet, Polymer scaffolds for biomaterials applications, *Macromolecules.* 43 (2010) 581–591. doi:10.1021/ma901530r.
- [221] M. Hoque, T. Nuge, T. Yeow, N. Nordin, R. Prasad, Gelatin Based Scaffolds for Tissue Engineering—a Review, *Polym. Res. J.* 9 (2015) 15.
- [222] L. Yuan, X. Li, L. Ge, X. Jia, J. Lei, C. Mu, D. Li, Emulsion Template Method for the Fabrication of Gelatin-Based Scaffold with a Controllable Pore Structure, *ACS Appl. Mater. Interfaces.* 11 (2019) 269–277. doi:10.1021/acsami.8b17555.
- [223] J.L. Ratcliffe, M. Walker, A.M. Eissa, S. Du, S.A. Przyborski, A.L. Laslett, N.R. Cameron, Optimized peptide functionalization of thiol-acrylate emulsion-templated porous polymers leads to expansion of human pluripotent stem cells in 3D culture, *J. Polym. Sci. Part A Polym. Chem.* 57 (2019) 1974–1981. doi:10.1002/pola.29353.
- [224] N.R. Richbourg, N.A. Peppas, V.I. Sikavitsas, Tuning the biomimetic behavior of scaffolds for regenerative medicine through surface modifications, *J. Tissue Eng. Regen. Med.* 13 (2019) 1275–1293. doi:10.1002/term.2859.
- [225] L. Kircher, P. Theato, N.R. Cameron, Functionalization of Porous Polymers from High-

Internal-Phase Emulsions and Their Applications, in: *Funct. Polym. by Post-Polymerization Modif. Concepts, Guidel. Appl.*, 2013: pp. 333–352. doi:10.1002/9783527655427.ch13.

- [226] L. Kircher, P. Theato, N.R. Cameron, Reactive thiol-ene emulsion-templated porous polymers incorporating pentafluorophenyl acrylate, *Polymer (Guildf)*. 54 (2013) 1755–1761. doi:10.1016/j.polymer.2013.01.024.
- [227] C.R. Langford, D.W. Johnson, N.R. Cameron, Chemical functionalization of emulsion-templated porous polymers by thiol-ene “click” chemistry, *Polym. Chem.* 5 (2014) 6200–6206. doi:10.1039/c4py00713a.
- [228] V. Jokinen, P. Suvanto, S. Franssila, Oxygen and nitrogen plasma hydrophilization and hydrophobic recovery of polymers, *Biomicrofluidics*. 6 (2012). doi:10.1063/1.3673251.
- [229] S. Shafei, J. Foroughi, Z. Chen, C.S. Wong, M. Naebe, Short oxygen plasma treatment leading to long-term hydrophilicity of conductive PCL-PPy nanofiber scaffolds, *Polymers (Basel)*. (2017). doi:10.3390/polym9110614.
- [230] M. Abedalwafa, F. Wang, L. Wang, C. Li, Biodegradable poly-epsilon-caprolactone (PCL) for tissue engineering applications: A review, *Rev. Adv. Mater. Sci.* (2013).
- [231] A.A. Ivanova, D.S. Syromotina, S.N. Shkarina, R. Shkarin, A. Cecilia, V. Weinhardt, T. Baumbach, M.S. Saveleva, D.A. Gorin, T.E.L. Douglas, B. V. Parakhonskiy, A.G. Skirtach, P. Cools, N. De Geyter, R. Morent, C. Oehr, M.A. Surmeneva, R.A. Surmenev, Effect of low-temperature plasma treatment of electrospun polycaprolactone fibrous scaffolds on calcium carbonate mineralisation, *RSC Adv.* 8 (2018) 39106–39114. doi:10.1039/c8ra07386d.
- [232] S. De Valence, J.C. Tille, C. Chaabane, R. Gurny, M.L. Bochaton-Piallat, B.H. Walpoth, M. Möller, Plasma treatment for improving cell biocompatibility of a biodegradable polymer scaffold for vascular graft applications, *Eur. J. Pharm. Biopharm.* 85 (2013) 78–86. doi:10.1016/j.ejpb.2013.06.012.
- [233] P. Pakeyangkoon, R. Magaraphan, P. Malakul, M. Nithitanakul, Surface Modification of High Internal Phase Emulsion Foam as a Scaffold for Tissue Engineering Application via Atmospheric Pressure Plasma Treatment, *Adv. Sci. Technol.* 77 (2012) 172–177. doi:10.4028/www.scientific.net/ast.77.172.

- [234] A.M. Eissa, F.S.V. Barros, P. Vrljicak, J.J. Brosens, N.R. Cameron, Enhanced Differentiation Potential of Primary Human Endometrial Cells Cultured on 3D Scaffolds, *Biomacromolecules*. 19 (2018) 3343–3350. doi:10.1021/acs.biomac.8b00635.
- [235] P. Pakeyangkoon, R. Magaraphan, P. Malakul, M. Nithitanakul, Effect of soxhlet extraction and surfactant system on morphology and properties of Poly(DVB)PolyHIPE, in: *Macromol. Symp.*, 2008: pp. 149–156. doi:10.1002/masy.200850424.
- [236] S. Fleith, A. Ponche, R. Bareille, J. Amédée, M. Nardin, Effect of several sterilisation techniques on homogeneous self assembled monolayers, *Colloids Surfaces B Biointerfaces*. 44 (2005) 15–24. doi:10.1016/j.colsurfb.2005.05.009.
- [237] S. Yoganarasimha, W.R. Trahan, A.M. Best, G.L. Bowlin, T.O. Kitten, P.C. Moon, P.A. Madurantakam, Peracetic acid: A practical agent for sterilizing heat-labile polymeric tissue-engineering scaffolds, *Tissue Eng. - Part C Methods*. 20 (2014) 714–723. doi:10.1089/ten.tec.2013.0624.
- [238] K.D. Andrews, J.A. Hunt, R.A. Black, Effects of sterilisation method on surface topography and in-vitro cell behaviour of electrostatically spun scaffolds, *Biomaterials*. 28 (2007) 1014–1026. doi:10.1016/j.biomaterials.2006.10.014.
- [239] F. Poncin-Epaillard, G. Legeay, Surface engineering of biomaterials with plasma techniques, *J. Biomater. Sci. Polym. Ed.* 14 (2003) 1005–1028. doi:10.1163/156856203769231538.
- [240] M. Griffin, N. Naderi, D.M. Kalaskar, E. Malins, R. Becer, C.A. Thornton, I.S. Whitaker, A. Mosahebi, P.E.M. Butler, A.M. Seifalian, Evaluation of Sterilisation Techniques for Regenerative Medicine Scaffolds Fabricated with Polyurethane Nonbiodegradable and Bioabsorbable Nanocomposite Materials, *Int. J. Biomater.* 2018 (2018). doi:10.1155/2018/6565783.
- [241] S. Lerouge, A. Simmons, *Sterilisation of biomaterials and medical devices*, 2012. doi:10.1533/9780857096265.
- [242] Z. Dai, J. Ronholm, Y. Tian, B. Sethi, X. Cao, Sterilization techniques for biodegradable scaffolds in tissue engineering applications, *J. Tissue Eng.* 7 (2016). doi:10.1177/2041731416648810.
- [243] W.J. Rogers, Sterilisation techniques for polymers, in: *Sterilisation Biomater. Med. Devices*, 2012: pp. 151–211. doi:10.1016/B978-1-84569-932-1.50007-6.

- [244] Great Britain, Home Office, Great Britain, Parliament, House of Commons, Annual statistics of scientific procedures on living animals: Great Britain 2018, 2018. [https://assets.publishing.service.gov.uk/government/uploads/system/uploads/attachment\\_data/file/835935/annual-statistics-scientific-procedures-living-animals-2018.pdf](https://assets.publishing.service.gov.uk/government/uploads/system/uploads/attachment_data/file/835935/annual-statistics-scientific-procedures-living-animals-2018.pdf).
- [245] M. Peric, I. Dumic-Cule, D. Grcevic, M. Matijasic, D. Verbanac, R. Paul, L. Grgurevic, V. Trkulja, C.M. Bagi, S. Vukicevic, The rational use of animal models in the evaluation of novel bone regenerative therapies, *Bone*. 70 (2015) 73–86. doi:10.1016/j.bone.2014.07.010.
- [246] R. Owen, G.C. Reilly, In vitro models of bone remodelling and associated disorders, *Front. Bioeng. Biotechnol.* 6 (2018). doi:10.3389/fbioe.2018.00134.
- [247] A. Abbott, Biology's new dimension, *Nature*. 424 (2003) 870–872. doi:10.1038/424870a.
- [248] M. Bokhari, R.J. Carnachan, N.R. Cameron, S.A. Przyborski, Culture of HepG2 liver cells on three dimensional polystyrene scaffolds enhances cell structure and function during toxicological challenge, *J. Anat.* 211 (2007) 567–576. doi:10.1111/j.1469-7580.2007.00778.x.
- [249] P. Sun, S. Yang, X. Sun, Y. Wang, Y. Jia, P. Shang, H. Tian, G. Li, R. Li, X. Zhang, C. Nie, Preparation of polyHIPE scaffolds for 3D cell culture and the application in cytotoxicity evaluation of cigarette smoke, *Polymers (Basel)*. 11 (2019). doi:10.3390/polym11060959.
- [250] L. Costello, N. Fullard, M. Roger, S. Bradbury, T. Dicolandrea, R. Isfort, C. Bascom, S. Przyborski, Engineering a multilayered skin equivalent: The importance of endogenous extracellular matrix maturation to provide robustness and reproducibility, in: *Methods Mol. Biol.*, 2019: pp. 107–122. doi:10.1007/978-1-4939-9473-1\_9.
- [251] C.E. Severn, A.M. Eissa, C.R. Langford, A. Parker, M. Walker, J.G.G. Dobbe, G.J. Streekstra, N.R. Cameron, A.M. Toye, Ex vivo culture of adult CD34+ stem cells using functional highly porous polymer scaffolds to establish biomimicry of the bone marrow niche, *Biomaterials*. 225 (2019). doi:10.1016/j.biomaterials.2019.119533.
- [252] A.D. Bershadsky, N.Q. Balaban, B. Geiger, Adhesion-Dependent Cell Mechanosensitivity, *Annu. Rev. Cell Dev. Biol.* 19 (2003) 677–695. doi:10.1146/annurev.cellbio.19.111301.153011.

- [253] A.J. Engler, S. Sen, H.L. Sweeney, D.E. Discher, Matrix Elasticity Directs Stem Cell Lineage Specification, *Cell*. 126 (2006) 677–689. doi:10.1016/j.cell.2006.06.044.
- [254] M. Tzaphlidou, Bone architecture: Collagen structure and calcium/phosphorus maps, *J. Biol. Phys.* (2008). doi:10.1007/s10867-008-9115-y.
- [255] X. Lin, S. Patil, Y.-G. Gao, A. Qian, The Bone Extracellular Matrix in Bone Formation and Regeneration, *Front. Pharmacol.* 11 (2020). doi:10.3389/fphar.2020.00757.
- [256] D.W. Buck, G.A. Dumanian, Bone biology and physiology: Part I. the fundamentals, *Plast. Reconstr. Surg.* (2012). doi:10.1097/PRS.0b013e31824eca94.
- [257] C. Jerome, B. Hoch, Skeletal System, in: *Comp. Anat. Histol.*, 2012. doi:10.1016/B978-0-12-381361-9.00005-6.
- [258] J.R. Porter, T.T. Ruckh, K.C. Papat, Bone tissue engineering: A review in bone biomimetics and drug delivery strategies, *Biotechnol. Prog.* (2009). doi:10.1002/btpr.246.
- [259] R. Florencio-Silva, G.R.D.S. Sasso, E. Sasso-Cerri, M.J. Simões, P.S. Cerri, Biology of Bone Tissue: Structure, Function, and Factors That Influence Bone Cells, *Biomed Res. Int.* (2015). doi:10.1155/2015/421746.
- [260] B. Clarke, Normal bone anatomy and physiology., *Clin. J. Am. Soc. Nephrol.* (2008). doi:10.2215/CJN.04151206.
- [261] L. Roseti, V. Parisi, M. Petretta, C. Cavallo, G. Desando, I. Bartolotti, B. Grigolo, Scaffolds for Bone Tissue Engineering: State of the art and new perspectives, *Mater. Sci. Eng. C.* (2017). doi:10.1016/j.msec.2017.05.017.
- [262] V. Campana, G. Milano, E. Pagano, M. Barba, C. Cicione, G. Salonna, W. Lattanzi, G. Logroscino, Bone substitutes in orthopaedic surgery: from basic science to clinical practice, *J. Mater. Sci. Mater. Med.* 25 (2014) 2445–2461. doi:10.1007/s10856-014-5240-2.
- [263] A. Kolk, J. Handschel, W. Drescher, D. Rothamel, F. Kloss, M. Blessmann, M. Heiland, K.D. Wolff, R. Smeets, Current trends and future perspectives of bone substitute materials - From space holders to innovative biomaterials, *J. Cranio-Maxillofacial Surg.* (2012). doi:10.1016/j.jcms.2012.01.002.
- [264] A.R. Amini, C.T. Laurencin, S.P. Nukavarapu, Bone tissue engineering: Recent advances

and challenges, *Crit. Rev. Biomed. Eng.* (2012). doi:10.1615/CritRevBiomedEng.v40.i5.10.

- [265] D. Durdevic, T. Vlahovic, S. Pehar, D. Miklic, H. Oppermann, T. Bordukalo-Niksic, I. Gavrankapetanovic, M. Jamakosmanovic, M. Milosevic, S. Martinovic, T.K. Sampath, M. Peric, L. Grgurevic, S. Vukicevic, A novel autologous bone graft substitute comprised of rhBMP6 blood coagulum as carrier tested in a randomized and controlled Phase I trial in patients with distal radial fractures, *Bone*. (2020). doi:10.1016/j.bone.2020.115551.
- [266] B. Trajkovski, M. Jaunich, W.D. Müller, F. Beuer, G.G. Zafiropoulos, A. Houshmand, Hydrophilicity, viscoelastic, and physicochemical properties variations in dental bone grafting substitutes, *Materials (Basel)*. (2018). doi:10.3390/ma11020215.
- [267] T. Ghassemi, A. Shahroodi, M.H. Ebrahimzadeh, A. Mousavian, J. Movaffagh, A. Moradi, Current concepts in scaffolding for bone tissue engineering, *Arch. Bone Jt. Surg.* (2018). doi:10.22038/abjs.2018.26340.1713.
- [268] M. Whitely, S. Cereceres, P. Dhavalikar, K. Salhadar, T. Wilems, B. Smith, A. Mikos, E. Cosgriff-Hernandez, Improved in situ seeding of 3D printed scaffolds using cell-releasing hydrogels, *Biomaterials*. 185 (2018) 194–204. doi:10.1016/j.biomaterials.2018.09.027.
- [269] C.R. Langford, D.W. Johnson, N.R. Cameron, Preparation of hybrid thiol-acrylate emulsion-templated porous polymers by interfacial copolymerization of high internal phase emulsions, *Macromol. Rapid Commun.* 36 (2015) 834–839. doi:10.1002/marc.201400733.
- [270] R. De Santis, F. Sarracino, F. Mollica, P.A. Netti, L. Ambrosio, L. Nicolais, Continuous fibre reinforced polymers as connective tissue replacement, *Compos. Sci. Technol.* 64 (2004) 861–871. doi:10.1016/j.compscitech.2003.09.008.
- [271] R. Landers, A. Pfister, U. Hübner, H. John, R. Schmelzeisen, R. Mülhaupt, Fabrication of soft tissue engineering scaffolds by means of rapid prototyping techniques, *J. Mater. Sci.* 37 (2002) 3107–3116. doi:10.1023/A:1016189724389.
- [272] A.R. Murphy, I. Ghobrial, P. Jamshidi, A. Laslett, C.M. O'Brien, N.R. Cameron, Tailored emulsion-templated porous polymer scaffolds for iPSC-derived human neural precursor cell culture, *Polym. Chem.* 8 (2017) 6617–6627. doi:10.1039/c7py01375b.
- [273] A.R. Murphy, J.M. Haynes, A.L. Laslett, N.R. Cameron, C.M. O'Brien, Three-dimensional

- differentiation of human pluripotent stem cell-derived neural precursor cells using tailored porous polymer scaffolds, *Acta Biomater.* 101 (2020) 102–116. doi:10.1016/j.actbio.2019.10.017.
- [274] W. Luo, S. Zhang, P. Li, R. Xu, Y. Zhang, L. Liang, C.D. Wood, Q. Lu, B. Tan, Surfactant-free CO<sub>2</sub>-in-water emulsion-templated poly (vinyl alcohol) (PVA) hydrogels, *Polymer (Guildf)*. 61 (2015) 183–191. doi:10.1016/j.polymer.2015.02.002.
- [275] Y. Hu, S. Ma, Z. Yang, W. Zhou, Z. Du, J. Huang, H. Yi, C. Wang, Facile fabrication of poly(L-lactic acid) microsphere-incorporated calcium alginate/hydroxyapatite porous scaffolds based on Pickering emulsion templates, *Colloids Surfaces B Biointerfaces*. 140 (2016) 382–391. doi:10.1016/j.colsurfb.2016.01.005.
- [276] W. Luo, R. Xu, Y. Liu, I. Hussain, Q. Lu, B. Tan, Emulsion-templated poly(acrylamide)s by using polyvinyl alcohol (PVA) stabilized CO<sub>2</sub>-in-water emulsions and their applications in tissue engineering scaffolds, *RSC Adv.* 5 (2015) 92017–92024. doi:10.1039/c5ra14345d.
- [277] N. Mangir, S. Dikici, F. Claeysens, S. Macneil, Using ex Ovo Chick Chorioallantoic Membrane (CAM) Assay to Evaluate the Biocompatibility and Angiogenic Response to Biomaterials, *ACS Biomater. Sci. Eng.* 5 (2019) 3190–3200. doi:10.1021/acsbiomaterials.9b00172.
- [278] T.A. Bertram, E. Tentoff, P.C. Johnson, B. Tawil, M. Van Dyke, K.B. Hellman, Hurdles in tissue engineering/regenerative medicine product commercialization: A pilot survey of governmental funding agencies and the financial industry, *Tissue Eng. - Part A*. (2012). doi:10.1089/ten.tea.2012.0186.
- [279] A.C. Plagnol, E. Rowley, P. Martin, F. Livesey, Industry perceptions of barriers to commercialization of regenerative medicine products in the UK, *Regen. Med.* (2009). doi:10.2217/rme.09.21.
- [280] Medical Device Regulation (MDR), (2017). <https://eur-lex.europa.eu/legal-content/EN/TXT/PDF/?uri=CELEX:32017R0745> (accessed January 31, 2020).
- [281] H.J. Haugen, S.P. Lyngstadaas, F. Rossi, G. Perale, Bone grafts: which is the ideal biomaterial?, *J. Clin. Periodontol.* 46 (2019) 92–102. doi:10.1111/jcpe.13058.
- [282] T.G. Maak, J.D. Wylie, Medical device regulation: A comparison of the United States and the European union, *J. Am. Acad. Orthop. Surg.* 24 (2016) 537–543. doi:10.5435/JAAOS-

D-15-00403.

- [283] A. Hammerl, C.E. Diaz Cano, E.M. De-Juan-Pardo, M. van Griensven, P.S.P. Poh, A Growth Factor-Free Co-Culture System of Osteoblasts and Peripheral Blood Mononuclear Cells for the Evaluation of the Osteogenesis Potential of Melt-Electrowritten Polycaprolactone Scaffolds, *Int. J. Mol. Sci.* 20 (2019) 1–12. doi:10.3390/ijms20051068.
- [284] C.M. Murphy, M.G. Haugh, F.J. O'Brien, The effect of mean pore size on cell attachment, proliferation and migration in collagen-glycosaminoglycan scaffolds for bone tissue engineering, *Biomaterials.* 31 (2010) 461–466. doi:10.1016/j.biomaterials.2009.09.063.
- [285] D.W. Hutmacher, Scaffold design and fabrication technologies for engineering tissues - State of the art and future perspectives, *J. Biomater. Sci. Polym. Ed.* 12 (2001) 107–124. doi:10.1163/156856201744489.
- [286] S. Bhatia, Natural Polymers vs Synthetic Polymer, in: *Nat. Polym. Drug Deliv. Syst.*, 2016: pp. 95–118. doi:10.1007/978-3-319-41129-3\_3.
- [287] X. Liu, J.M. Holzwarth, P.X. Ma, Functionalized Synthetic Biodegradable Polymer Scaffolds for Tissue Engineering, *Macromol. Biosci.* 12 (2012) 911–919. doi:10.1002/mabi.201100466.
- [288] E.S. Place, J.H. George, C.K. Williams, M.M. Stevens, Synthetic polymer scaffolds for tissue engineering, *Chem. Soc. Rev.* 38 (2009) 1139–1151. doi:10.1039/b811392k.
- [289] M.A. Woodruff, D.W. Hutmacher, The return of a forgotten polymer - Polycaprolactone in the 21st century, *Prog. Polym. Sci.* 35 (2010) 1217–1256. doi:10.1016/j.progpolymsci.2010.04.002.
- [290] L. Ghasemi-Mobarakeh, M.P. Prabhakaran, M. Morshed, M.H. Nasr-Esfahani, S. Ramakrishna, Bio-functionalized PCL nanofibrous scaffolds for nerve tissue engineering, *Mater. Sci. Eng. C.* 30 (2010) 1129–1136. doi:10.1016/j.msec.2010.06.004.
- [291] A. Cipitria, A. Skelton, T.R. Dargaville, P.D. Dalton, D.W. Hutmacher, Design, fabrication and characterization of PCL electrospun scaffolds - A review, *J. Mater. Chem.* 21 (2011) 9419–9453. doi:10.1039/c0jm04502k.
- [292] J.A.M. Steele, S.D. McCullen, A. Callanan, H. Autefage, M.A. Accardi, D. Dini, M.M. Stevens, Combinatorial scaffold morphologies for zonal articular cartilage engineering, *Acta Biomater.* 10 (2014) 2065–2075. doi:10.1016/j.actbio.2013.12.030.

- [293] B. Nottelet, E. Pektok, D. Mandracchia, J.C. Tille, B. Walpoth, R. Gurny, M. Möller, Factorial design optimization and in vivo feasibility of poly( $\epsilon$ -caprolactone)-micro- and nanofiber-based small diameter vascular grafts, *J. Biomed. Mater. Res. - Part A*. 89 (2009) 865–875. doi:10.1002/jbm.a.32023.
- [294] K. Ghosal, A. Manakhov, L. Zajíčková, S. Thomas, Structural and Surface Compatibility Study of Modified Electrospun Poly( $\epsilon$ -caprolactone) (PCL) Composites for Skin Tissue Engineering, *AAPS PharmSciTech*. 18 (2017) 72–81. doi:10.1208/s12249-016-0500-8.
- [295] H. Bahrami, S.H. Keshel, A.J. Chari, E. Biazar, Human unrestricted somatic stem cells loaded in nanofibrous PCL scaffold and their healing effect on skin defects, *Artif. Cells, Nanomedicine Biotechnol.* 44 (2016) 1556–1560. doi:10.3109/21691401.2015.1062390.
- [296] B. Subia, J. Kundu, S. C., Biomaterial Scaffold Fabrication Techniques for Potential Tissue Engineering Applications, in: *Tissue Eng.*, 2010: pp. 141–158. doi:10.5772/8581.
- [297] B. Aldemir Dikici, F. Claeysens, Basic Principles of Emulsion Templating and Its Use as an Emerging Manufacturing Method of Tissue Engineering Scaffolds, *Front. Bioeng. Biotechnol.* 8 (2020). doi:10.3389/fbioe.2020.00875.
- [298] N.R. Cameron, P. Krajnc, M.S. Silverstein, Colloidal Templating, in: *Porous Polym.*, 2011. doi:10.1002/9780470929445.ch4.
- [299] X. Wu, S., Liu, X. Yeung, K. W. K. Liu, C., Yang, Biomimetic porous scaffolds for bone tissue engineering, *Mater. Sci. Eng. R*. 80 (2014) 1–36. doi:10.1016/j.mser.2014.04.001.
- [300] I. Bružauskaitė, D. Bironaitė, E. Bagdonas, E. Bernotienė, Scaffolds and cells for tissue regeneration: different scaffold pore sizes—different cell effects, *Cytotechnology*. (2016). doi:10.1007/s10616-015-9895-4.
- [301] N.R. Cameron, A. Barbetta, The influence of porogen type on the porosity, surface area and morphology of poly(divinylbenzene) polyHIPE foams, *J. Mater. Chem.* 10 (2000) 2466–2471. doi:10.1039/B003596N.
- [302] S. Wang, D.H. Kempen, N.K. Simha, J.L. Lewis, A.J. Windebank, M.J. Yaszemski, L. Lu, Photo-cross-linked hybrid polymer networks consisting of poly(propylene fumarate) and poly(caprolactone fumarate): Controlled physical properties and regulated bone and nerve cell responses, *Biomacromolecules*. (2008). doi:10.1021/bm7012313.
- [303] R. Woods, S. Feldbacher, D. Zidar, G. Langer, V. Satzinger, V. Schmidt, N. Pucher, R. Liska,

- W. Kern, 3D optical waveguides produced by two photon photopolymerisation of a flexible silanol terminated polysiloxane containing acrylate functional groups, *Opt. Mater. Express.* (2014). doi:10.1364/ome.4.000486.
- [304] ASTM D638 -14, Standard Test Method for Tensile Properties of Plastics, 2014. doi:10.1520/D0638-14.1.
- [305] M. Messori, M. Degli Esposti, K. Paderni, S. Pandini, S. Passera, T. Riccò, M. Toselli, Chemical and thermomechanical tailoring of the shape memory effect in poly( $\epsilon$ -caprolactone)-based systems, *J. Mater. Sci.* 48 (2013) 424–440. doi:10.1007/s10853-012-6757-8.
- [306] S.D. Kimmins, P. Wyman, N.R. Cameron, Photopolymerised methacrylate-based emulsion-templated porous polymers, *React. Funct. Polym.* 72 (2012) 947–954. doi:10.1016/j.reactfunctpolym.2012.06.015.
- [307] C. Decker, Photoinitiated crosslinking polymerisation, *Prog. Polym. Sci.* (1996). doi:10.1016/0079-6700(95)00027-5.
- [308] S.D. Kimmins, P. Wyman, N.R. Cameron, Photopolymerised Methacrylate-Based Emulsion-Templated Porous Polymers, *React. Funct. Polym.* 72 (2012) 947–954. doi:10.1016/j.reactfunctpolym.2012.06.015.
- [309] C. Bordes, V. Fréville, E. Ruffin, P. Marote, J.Y. Gauvrit, S. Briançon, P. Lantéri, Determination of poly( $\epsilon$ -caprolactone) solubility parameters: Application to solvent substitution in a microencapsulation process, *Int. J. Pharm.* 383 (2010) 236–243. doi:10.1016/j.ijpharm.2009.09.023.
- [310] H.H. Chen, E. Ruckenstein, Effect of the nature of the hydrophobic oil phase and surfactant in the formation of concentrated emulsions, *J. Colloid Interface Sci.* (1991). doi:10.1016/0021-9797(91)90117-Q.
- [311] W. Busby, N.R. Cameron, C.A.B. Jahoda, Emulsion-derived foams (PolyHIPEs) containing poly( $S\epsilon$ -caprolactone) as matrixes for tissue engineering, *Biomacromolecules.* 2 (2001) 154–164. doi:10.1021/bm0000889.
- [312] N.R. Cameron, D.C. Sherrington, High Internal Phase Emulsions (HIPEs) - Structure , Properties and Use in Polymer Preparation, in: *Adv. Polym. Sci.*, 1996: pp. 163–214. doi:10.1007/3-540-60484-7\_4.
- [313] M.P. Zverev, P.I. Zubov, A.N. Barash, L.P. Nikonorova, L. V. Ivanova, The properties of

- solutions of polymers in good and poor solvents and of articles prepared from these solutions, *Polym. Sci. U.S.S.R.* 16 (1974) 589–598. doi:10.1016/0032-3950(74)90370-0.
- [314] B.A. Miller-Chou, J.L. Koenig, A review of polymer dissolution, *Prog. Polym. Sci.* 28 (2003) 1223–1270. doi:10.1016/S0079-6700(03)00045-5.
- [315] M. Su, L. Wang, G. Zhang, Y. Huang, Z. Su, Effects of interfacial tension on formation of poly(ethylene oxide)-block-polystyrene micelles from emulsions, *RSC Adv.* (2015). doi:10.1039/c4ra14157a.
- [316] Y. Yu, A. Eisenberg, Control of morphology through polymer-solvent interactions in crew-cut aggregates of amphiphilic block copolymers, *J. Am. Chem. Soc.* (1997). doi:10.1021/ja9709740.
- [317] C. Reichardt, *Solvents and Solvent Effects in Organic Chemistry*, 2004. doi:10.1002/3527601791.
- [318] H.H. Chen, E. Ruckenstein, Correlation between the stability of concentrated emulsions and the interfacial free energy between the two phases, *J. Colloid Interface Sci.* 138 (1990) 473–479. doi:10.1016/0021-9797(90)90229-H.
- [319] A. Barbetta, N.R. Cameron, S.J. Cooper, High internal phase emulsions (HIPEs) containing divinylbenzene and 4-vinylbenzyl chloride and the morphology of the resulting PolyHIPE materials, *Chem. Commun.* (2000). doi:10.1039/a909060f.
- [320] K. Wanli, L. Yi, Q. Baoyan, L. Guangzhi, Y. Zhenyu, H. Jichun, Interactions between alkali/surfactant/polymer and their effects on emulsion stability, *Colloids Surfaces A Physicochem. Eng. Asp.* (2000). doi:10.1016/S0927-7757(00)00461-1.
- [321] A. Barbetta, N.R. Cameron, Morphology and surface area of emulsion-derived (PolyHIPE) solid foams prepared with oil-phase soluble porogenic solvents: Three-component surfactant system, *Macromolecules.* (2004). doi:10.1021/ma035944y.
- [322] R. Akhtar, M.J. Sherratt, J.K. Cruickshank, B. Derby, Characterizing the elastic properties of tissues, *Mater. Today.* 14 (2011) 96–105. doi:10.1016/S1369-7021(11)70059-1.
- [323] S.J. Hollister, R.D. Maddox, J.M. Taboas, Optimal design and fabrication of scaffolds to mimic tissue properties and satisfy biological constraints, *Biomaterials.* 23 (2002) 4095–4103. doi:10.1016/S0142-9612(02)00148-5.

- [324] Z. Sheikh, N. Hamdan, Y. Ikeda, M. Grynypas, B. Ganss, M. Glogauer, Natural graft tissues and synthetic biomaterials for periodontal and alveolar bone reconstructive applications: A review, *Biomater. Res.* (2017). doi:10.1186/s40824-017-0095-5.
- [325] C. Dimova, B. Evrosimovska, K. Zlatanovska, J. Zarkova, Alveolar augmentation using different bone substitutes, in: *Handb. Bioceram. Biocomposites*, 2016. doi:10.1007/978-3-319-12460-5\_51.
- [326] M.A. Saghiri, A. Asatourian, F. Garcia-Godoy, N. Sheibani, The role of angiogenesis in implant dentistry part II: The effect of bone-grafting and barrier membrane materials on angiogenesis, *Med. Oral Patol. Oral Cir. Bucal.* (2016). doi:10.4317/medoral.21200.
- [327] D. Buser, B. Hoffmann, J.P. Bernard, A. Lussi, D. Mettler, R.K. Schenk, Evaluation of filling materials in membrane-protected bone defects - A comparative histomorphometric study in the mandible of miniature pigs, *Clin. Oral Implants Res.* (1998). doi:10.1034/j.1600-0501.1998.090301.x.
- [328] M.J. Rowe, K. Kamocki, D. Pankajakshan, D. Li, A. Bruzzaniti, V. Thomas, S.B. Blanchard, M.C. Bottino, Dimensionally stable and bioactive membrane for guided bone regeneration: An in vitro study, *J. Biomed. Mater. Res. - Part B Appl. Biomater.* (2016). doi:10.1002/jbm.b.33430.
- [329] S.-W. Lee, S.-G. Kim, Membranes for the Guided Bone Regeneration, *Maxillofac. Plast. Reconstr. Surg.* 36 (2014) 239–246. doi:10.14402/jkamprs.2014.36.6.239.
- [330] M.C. Bottino, V. Thomas, G. Schmidt, Y.K. Vohra, T.M.G. Chu, M.J. Kowolik, G.M. Janowski, Recent advances in the development of GTR/GBR membranes for periodontal regeneration - A materials perspective, *Dent. Mater.* (2012). doi:10.1016/j.dental.2012.04.022.
- [331] J. Wang, L. Wang, Z. Zhou, H. Lai, P. Xu, L. Liao, J. Wei, Biodegradable polymer membranes applied in guided bone/tissue regeneration: A review, *Polymers (Basel)*. 8 (2016). doi:10.3390/polym8040115.
- [332] J. Liu, D.G. Kerns, Mechanisms of Guided Bone Regeneration: A Review, *Open Dent. J.* (2014). doi:10.2174/1874210601408010056.
- [333] G. Cheng, C. Yin, H. Tu, S. Jiang, Q. Wang, X. Zhou, X. Xing, C. Xie, X. Shi, Y. Du, H. Deng, Z. Li, Controlled Co-delivery of Growth Factors through Layer-by-Layer Assembly of Core-Shell Nanofibers for Improving Bone Regeneration, *ACS Nano*. 13 (2019) 6372–6382.

doi:10.1021/acsnano.8b06032.

- [334] B. Rai, S.H. Teoh, D.W. Hutmacher, T. Cao, K.H. Ho, Novel PCL-based honeycomb scaffolds as drug delivery systems for rhBMP-2, *Biomaterials*. 26 (2005) 3739–3748. doi:10.1016/j.biomaterials.2004.09.052.
- [335] B. Inanç, Y.E. Arslan, S. Seker, A.E. Elçin, Y.M. Elçin, Periodontal ligament cellular structures engineered with electrospun poly(DL-lactide-co-glycolide) nanofibrous membrane scaffolds, *J. Biomed. Mater. Res. - Part A*. 90 (2009) 186–195. doi:10.1002/jbm.a.32066.
- [336] M.C. Bottino, V. Thomas, G.M. Janowski, A novel spatially designed and functionally graded electrospun membrane for periodontal regeneration, *Acta Biomater*. 7 (2011) 216–224. doi:10.1016/j.actbio.2010.08.019.
- [337] S.G. Wise, M.J. Byrom, A. Waterhouse, P.G. Bannon, M.K.C. Ng, A.S. Weiss, A multilayered synthetic human elastin/polycaprolactone hybrid vascular graft with tailored mechanical properties, *Acta Biomater*. 7 (2011) 295–303. doi:10.1016/j.actbio.2010.07.022.
- [338] G. Cheng, X. Ma, J. Li, Y. Cheng, Y. Cao, Z. Wang, X. Shi, Y. Du, H. Deng, Z. Li, Incorporating platelet-rich plasma into coaxial electrospun nanofibers for bone tissue engineering, *Int. J. Pharm.* 547 (2018) 656–666. doi:10.1016/j.ijpharm.2018.06.020.
- [339] G. Cheng, J. Chen, Q. Wang, X. Yang, Y. Cheng, Z. Li, H. Tu, H. Deng, Z. Li, Promoting osteogenic differentiation in pre-osteoblasts and reducing tibial fracture healing time using functional nanofibers, *Nano Res.* 11 (2018) 3658–3677. doi:10.1007/s12274-017-1934-3.
- [340] E.J. Chong, T.T. Phan, I.J. Lim, Y.Z. Zhang, B.H. Bay, S. Ramakrishna, C.T. Lim, Evaluation of electrospun PCL/gelatin nanofibrous scaffold for wound healing and layered dermal reconstitution, *Acta Biomater*. 3 (2007) 321–330. doi:10.1016/j.actbio.2007.01.002.
- [341] J.S. Choi, K.W. Leong, H.S. Yoo, In vivo wound healing of diabetic ulcers using electrospun nanofibers immobilized with human epidermal growth factor (EGF), *Biomaterials*. 29 (2008) 587–596. doi:10.1016/j.biomaterials.2007.10.012.
- [342] Z. Cheng, S.H. Teoh, Surface modification of ultra thin poly ( $\epsilon$ -caprolactone) films using acrylic acid and collagen, *Biomaterials*. (2004). doi:10.1016/j.biomaterials.2003.08.038.

- [343] S. Miroshnichenko, V. Timofeeva, E. Permyakova, S. Ershov, P. Kiryukhantsev-Korneev, E. Dvořáková, D. Shtansky, L. Zajíčková, A. Solovieva, A. Manakhov, Plasma-Coated Polycaprolactone Nanofibers with Covalently Bonded Platelet-Rich Plasma Enhance Adhesion and Growth of Human Fibroblasts, *Nanomaterials*. (2019). doi:10.3390/nano9040637.
- [344] A.P. Hurt, G. Getti, N.J. Coleman, Bioactivity and biocompatibility of a chitosan-tobermorite composite membrane for guided tissue regeneration, *Int. J. Biol. Macromol.* (2014). doi:10.1016/j.ijbiomac.2013.11.020.
- [345] J. Mota, N. Yu, S.G. Caridade, G.M. Luz, M.E. Gomes, R.L. Reis, J.A. Jansen, X. Frank Walboomers, J.F. Mano, Chitosan/bioactive glass nanoparticle composite membranes for periodontal regeneration, *Acta Biomater.* (2012). doi:10.1016/j.actbio.2012.06.040.
- [346] J. Xue, M. He, Y. Liang, A. Crawford, P. Coates, D. Chen, R. Shi, L. Zhang, Fabrication and evaluation of electrospun PCL-gelatin micro-/nanofiber membranes for anti-infective GTR implants, *J. Mater. Chem. B*. (2014). doi:10.1039/c4tb00737a.
- [347] M. Kharaziha, M.H. Fathi, H. Edris, Development of novel aligned nanofibrous composite membranes for guided bone regeneration, *J. Mech. Behav. Biomed. Mater.* 24 (2013) 9–20. doi:10.1016/j.jmbbm.2013.03.025.
- [348] F.J. Bye, J. Bissoli, L. Black, A.J. Bullock, S. Puwanun, K. Moharamzadeh, G.C. Reilly, A.J. Ryan, S. MacNeil, Development of bilayer and trilayer nanofibrous/microfibrous scaffolds for regenerative medicine, *Biomater. Sci.* 1 (2013) 942–951. doi:10.1039/c3bm60074b.
- [349] L. Fu, Z. Wang, S. Dong, Y. Cai, Y. Ni, T. Zhang, L. Wang, Y. Zhou, Bilayer poly(Lactic-co-glycolic acid)/nano-hydroxyapatite membrane with barrier function and Osteogenesis promotion for guided bone regeneration, *Materials (Basel)*. 10 (2017) 257. doi:10.3390/ma10030257.
- [350] E.J. Lee, D.S. Shin, H.E. Kim, H.W. Kim, Y.H. Koh, J.H. Jang, Membrane of hybrid chitosan-silica xerogel for guided bone regeneration, *Biomaterials*. (2009). doi:10.1016/j.biomaterials.2008.10.025.
- [351] S.B. Qasim, R.M. Delaine-Smith, T. Fey, A. Rawlinson, I.U. Rehman, Freeze gelled porous membranes for periodontal tissue regeneration, *Acta Biomater.* 23 (2015) 317–328. doi:10.1016/j.actbio.2015.05.001.

- [352] L. Tayebi, M. Rasoulianboroujeni, K. Moharamzadeh, T.K.D. Almela, Z. Cui, H. Ye, 3D-printed membrane for guided tissue regeneration, *Mater. Sci. Eng. C.* 84 (2017) 148–158. doi:10.1016/j.msec.2017.11.027.
- [353] H.Y. Zhang, H.B. Jiang, J.-H. Ryu, H. Kang, K.-M. Kim, J.-S. Kwon, Comparing Properties of Variable Pore-Sized 3D-Printed PLA Membrane with Conventional PLA Membrane for Guided Bone/Tissue Regeneration, *Materials (Basel)*. 12 (2019) 1718. doi:10.3390/ma12101718.
- [354] D. Li, Y. Xia, Electrospinning of nanofibers: Reinventing the wheel?, *Adv. Mater.* (2004). doi:10.1002/adma.200400719.
- [355] Q.P. Pham, U. Sharma, A.G. Mikos, Electrospinning of polymeric nanofibers for tissue engineering applications: a review., *Tissue Eng.* 12 (2006) 1197–211. doi:10.1089/ten.2006.12.1197.
- [356] X. Qin, D. Wu, Effect of different solvents on poly( $\epsilon$ -caprolactone)(PCL) electrospun nonwoven membranes, *J. Therm. Anal. Calorim.* 107 (2012) 1007–1013. doi:10.1007/s10973-011-1640-4.
- [357] V. Beachley, X. Wen, Effect of electrospinning parameters on the nanofiber diameter and length, *Mater. Sci. Eng. C.* 29 (2009) 663–668. doi:10.1016/j.msec.2008.10.037.
- [358] S.H. Bahrami, A. Gholipour Kanani, Effect of changing solvents on poly( $\epsilon$ -Caprolactone) nanofibrous webs morphology, *J. Nanomater.* 2011 (2011) 1–10. doi:10.1155/2011/724153.
- [359] C. Langford, N. Cameron, *Materials for Tissue Engineering and 3D Cell Culture*, in: *Bio-Inspired Polym.*, 2016: pp. 460–480.
- [360] H. Zhang, A.I. Cooper, Synthesis and applications of emulsion-templated porous materials, *Soft Matter*. 1 (2005) 107–113. doi:10.1039/b502551f.
- [361] Z. Ma, W. He, T. Yong, S. Ramakrishna, Grafting of gelatin on electrospun poly( $\epsilon$ -caprolactone) nanofibers to improve endothelial cell spreading and proliferation and to control cell orientation, *Tissue Eng.* 11 (2005) 1149–1158. doi:10.1089/ten.2005.11.1149.
- [362] F.J.H. Abadi, M.A. Tehran, F. Zamani, M. Nematollahi, L.G. Mobarakeh, M.H. Nasr-Esfahani, Effect of nanoporous fibers on growth and proliferation of cells on electrospun poly ( $\epsilon$ -caprolactone) scaffolds, *Int. J. Polym. Mater. Polym. Biomater.*

(2013). doi:10.1080/00914037.2013.769248.

- [363] L.A. Bosworth, S. Downes, Acetone, a Sustainable Solvent for Electrospinning Poly( $\epsilon$ -Caprolactone) Fibres: Effect of Varying Parameters and Solution Concentrations on Fibre Diameter, *J. Polym. Environ.* (2012). doi:10.1007/s10924-012-0436-3.
- [364] M.I. Hassan, N. Sultana, Characterization, drug loading and antibacterial activity of nanohydroxyapatite/polycaprolactone (nHA/PCL) electrospun membrane, *3 Biotech.* (2017). doi:10.1007/s13205-017-0889-0.
- [365] M.I. Hassan, T. Sun, N. Sultana, Fabrication of nanohydroxyapatite/poly(caprolactone) composite microfibers using electrospinning technique for tissue engineering applications, *J. Nanomater.* (2014). doi:10.1155/2014/209049.
- [366] F.J. Bye, Development of composite electrospun scaffolds for tissue engineering, The University of Sheffield, 2014. [http://etheses.whiterose.ac.uk/5702/1/FBYE\\_Thesis\\_Library\\_edn.compressed.pdf](http://etheses.whiterose.ac.uk/5702/1/FBYE_Thesis_Library_edn.compressed.pdf).
- [367] A.J. Bullock, M.C. Higham, S. MacNeil, Use of human fibroblasts in the development of a xenobiotic-free culture and delivery system for human keratinocytes., *Tissue Eng.* 12 (2006) 245–255. doi:10.1089/ten.2006.12.245.
- [368] A.H. Fischer, K.A. Jacobson, J. Rose, R. Zeller, Hematoxylin and eosin staining of tissue and cell sections, *Cold Spring Harb. Protoc.* 3 (2008) 1–2. doi:10.1101/pdb.prot4986.
- [369] C. Gao, Polymeric biomaterials for tissue regeneration: From surface/interface design to 3D constructs, 2016. doi:10.1007/978-981-10-2293-7.
- [370] M. Mastrogiacomo, S. Scaglione, R. Martinetti, L. Dolcini, F. Beltrame, R. Cancedda, R. Quarto, Role of scaffold internal structure on in vivo bone formation in macroporous calcium phosphate bioceramics, *Biomaterials.* (2006). doi:10.1016/j.biomaterials.2006.01.031.
- [371] M. Marcacci, E. Kon, V. Moukhachev, A. Lavroukov, S. Kutepov, R. Quarto, M. Mastrogiacomo, R. Cancedda, Stem Cells Associated with Macroporous Bioceramics for Long Bone Repair: 6- to 7-Year Outcome of a Pilot Clinical Study, *Tissue Eng.* (2007). doi:10.1089/ten.2006.0271.
- [372] S.I. Somo, B. Akar, E.S. Bayrak, J.C. Larson, A.A. Appel, H. Mehdizadeh, A. Cinar, E.M. Brey, Pore Interconnectivity Influences Growth Factor-Mediated Vascularization in Sphere-Templated Hydrogels, *Tissue Eng. Part C Methods.* (2015).

- doi:10.1089/ten.tec.2014.0454.
- [373] A.J. Wright, M.J. Main, N.J. Cooper, B.A. Blight, S.J. Holder, Poly High Internal Phase Emulsion for the Immobilization of Chemical Warfare Agents, *ACS Appl. Mater. Interfaces*. (2017). doi:10.1021/acsami.7b09188.
- [374] M.P. Prabhakaran, J. Venugopal, C.K. Chan, S. Ramakrishna, Surface modified electrospun nanofibrous scaffolds for nerve tissue engineering, *Nanotechnology*. 19 (2008). doi:10.1088/0957-4484/19/45/455102.
- [375] K. Fujihara, M. Kotaki, S. Ramakrishna, Guided bone regeneration membrane made of polycaprolactone/calcium carbonate composite nano-fibers, *Biomaterials*. (2005). doi:10.1016/j.biomaterials.2004.09.014.
- [376] N.E. Zander, J.A. Orlicki, A.M. Rawlett, T.P. Beebe, Quantification of protein incorporated into electrospun polycaprolactone tissue engineering scaffolds, *ACS Appl. Mater. Interfaces*. (2012). doi:10.1021/am300045y.
- [377] L.A. Can-Herrera, A. Ávila-Ortega, S. de la Rosa-García, A.I. Oliva, J. V. Cauich-Rodríguez, J.M. Cervantes-Uc, Surface modification of electrospun polycaprolactone microfibers by air plasma treatment: Effect of plasma power and treatment time, *Eur. Polym. J.* (2016). doi:10.1016/j.eurpolymj.2016.09.060.
- [378] S.M. McGEE-RUSSELL, Histochemical methods for calcium, *J. Histochem. Cytochem.* (1958). doi:10.1177/6.1.22.
- [379] B. Bhaskar, R. Owen, H. Bahmaee, Z. Wally, P. Sreenivasa Rao, G.C. Reilly, Composite porous scaffold of PEG/PLA support improved bone matrix deposition in vitro compared to PLA-only scaffolds, *J. Biomed. Mater. Res. - Part A*. (2018). doi:10.1002/jbm.a.36336.
- [380] Z.J. Wally, A.M. Haque, A. Feteira, F. Claeysens, R. Goodall, G.C. Reilly, Selective laser melting processed Ti6Al4V lattices with graded porosities for dental applications, *J. Mech. Behav. Biomed. Mater.* (2019). doi:10.1016/j.jmbbm.2018.08.047.
- [381] M. Prideaux, N. Loveridge, A.A. Pitsillides, C. Farquharson, Extracellular matrix mineralization promotes E11/gp38 glycoprotein expression and drives osteocytic differentiation, *PLoS One*. (2012). doi:10.1371/journal.pone.0036786.
- [382] P. Mazón, P.N. De Aza, Porous scaffold prepared from  $\alpha'$ -L-Dicalcium silicate doped with phosphorus for bone grafts, *Ceram. Int.* (2018). doi:10.1016/j.ceramint.2017.09.208.

- [383] L. Tang, W. Wei, X. Wang, J. Qian, J. Li, A. He, L. Yang, X. Jiang, X. Li, J. Wei, LAPONITE® nanorods regulating degradability, acidic-alkaline microenvironment, apatite mineralization and MC3T3-E1 cells responses to poly(butylene succinate) based bio-nanocomposite scaffolds, *RSC Adv.* (2018). doi:10.1039/c7ra13452e.
- [384] I. Rajzer, A. Kurowska, A. Jabłoński, S. Jatteau, M. Śliwka, M. Ziąbka, E. Menaszek, Layered gelatin/PLLA scaffolds fabricated by electrospinning and 3D printing- for nasal cartilages and subchondral bone reconstruction, *Mater. Des.* (2018). doi:10.1016/j.matdes.2018.06.012.
- [385] S. Dikici, F. Claeysens, S. MacNeil, Decellularised baby spinach leaves and their potential use in tissue engineering applications: Studying and promoting neovascularisation, *J. Biomater. Appl.* 0 (2019) 1–14. doi:10.1177/0885328219863115.
- [386] R. Augustine, E.A. Dominic, I. Reju, B. Kaimal, N. Kalarikkal, S. Thomas, Investigation of angiogenesis and its mechanism using zinc oxide nanoparticle-loaded electrospun tissue engineering scaffolds, *RSC Adv.* 4 (2014) 51528–51536. doi:10.1039/c4ra07361d.
- [387] S. Singh, B.M. Wu, J.C.Y. Dunn, Delivery of VEGF using collagen-coated polycaprolactone scaffolds stimulates angiogenesis, *J. Biomed. Mater. Res. - Part A.* (2012). doi:10.1002/jbm.a.34010.
- [388] S.E.P. New, A. Ibrahim, L. Guasti, E. Zucchelli, M. Birchall, N.W. Bulstrode, A.M. Seifalian, P. Ferretti, Towards reconstruction of epithelialized cartilages from autologous adipose tissue-derived stem cells, *J. Tissue Eng. Regen. Med.* 11 (2017) 3078–3089. doi:10.1002/term.2211.
- [389] N.C. Rivron, J. Liu, J. Rouwkema, J. De Boer, C.A. Van Blitterswijk, Engineering vascularised tissues in vitro, *Eur. Cells Mater.* 15 (2008) 27–40. doi:vol015a03 [pii] ET - 2008/02/22.
- [390] J. Rouwkema, N.C. Rivron, C.A. van Blitterswijk, Vascularization in tissue engineering, *Trends Biotechnol.* 26 (2008) 434–441. doi:10.1016/j.tibtech.2008.04.009.
- [391] L.R. Madden, D.J. Mortisen, E.M. Sussman, S.K. Dupras, J.A. Fugate, J.L. Cuy, K.D. Hauch, M.A. Laflamme, C.E. Murry, B.D. Ratner, Proangiogenic scaffolds as functional templates for cardiac tissue engineering, *Proc. Natl. Acad. Sci.* (2010). doi:10.1073/pnas.1006442107.

- [392] S.C. Baker, G. Rohman, J. Hinley, J. Stahlschmidt, N.R. Cameron, J. Southgate, Cellular Integration and Vascularisation Promoted by a Resorbable, Particulate-Leached, Cross-Linked Poly( $\epsilon$ -caprolactone) Scaffold, *Macromol. Biosci.* 11 (2011) 618–627. doi:10.1002/mabi.201000415.
- [393] F.M. Klenke, Y. Liu, H. Yuan, E.B. Hunziker, K.A. Siebenrock, W. Hofstetter, Impact of pore size on the vascularization and osseointegration of ceramic bone substitutes in vivo, *J. Biomed. Mater. Res. - Part A.* 85 (2008) 777–786. doi:10.1002/jbm.a.31559.
- [394] N. Mangir, C.J. Hillary, C.R. Chapple, S. MacNeil, Oestradiol-releasing Biodegradable Mesh Stimulates Collagen Production and Angiogenesis: An Approach to Improving Biomaterial Integration in Pelvic Floor Repair, *Eur. Urol. Focus.* (2017). doi:10.1016/j.euf.2017.05.004.
- [395] M. Barbeck, J. Lorenz, A. Kubesch, N. Böhm, P. Booms, J. Choukroun, R. Sader, C.J. Kirkpatrick, S. Ghanaati, Porcine Dermis-Derived Collagen Membranes Induce Implantation Bed Vascularization Via Multinucleated Giant Cells: A Physiological Reaction?, *J. Oral Implantol.* (2014). doi:10.1563/aaid-joi-d-14-00274.
- [396] R.B. de Santana, C.M.L. de Mattos, C.E. Francischone, T. Van Dyke, Superficial Topography and Porosity of an Absorbable Barrier Membrane Impacts Soft Tissue Response in Guided Bone Regeneration, *J. Periodontol.* 81 (2010) 926–933. doi:10.1902/jop.2010.090592.
- [397] L. Moroni, R. Licht, J. de Boer, J.R. de Wijn, C.A. van Blitterswijk, Fiber diameter and texture of electrospun PEOT/PBT scaffolds influence human mesenchymal stem cell proliferation and morphology, and the release of incorporated compounds, *Biomaterials.* (2006). doi:10.1016/j.biomaterials.2006.05.027.
- [398] H. Fong, I. Chun, D.H. Reneker, Beaded nanofibers formed during electrospinning, in: *Polymer (Guildf.)*, 1999: pp. 4585–4592. doi:10.1016/S0032-3861(99)00068-3.
- [399] S. van der Wal, Low viscosity organic modifiers in reversed-phase HPLC, *Chromatographia.* (1985). doi:10.1007/BF02310382.
- [400] M.P. Zverev, P.I. Zubov, A.N. Barash, L.P. Nikonorova, L. V. Ivanova, The properties of solutions of polymers in good and poor solvents and of articles prepared from these solutions, *Polym. Sci. U.S.S.R.* 16 (1974) 589–598. doi:10.1016/0032-3950(74)90370-0.

- [401] A. Haider, S. Haider, I.K. Kang, A comprehensive review summarizing the effect of electrospinning parameters and potential applications of nanofibers in biomedical and biotechnology, *Arab. J. Chem.* (2018). doi:10.1016/j.arabjc.2015.11.015.
- [402] K.A.G. Katsogiannis, G.T. Vladisavljević, S. Georgiadou, Porous electrospun polycaprolactone (PCL) fibres by phase separation, *Eur. Polym. J.* (2015). doi:10.1016/j.eurpolymj.2015.01.028.
- [403] C.J. Luo, E. Stride, M. Edirisinghe, Mapping the influence of solubility and dielectric constant on electrospinning polycaprolactone solutions, *Macromolecules.* (2012). doi:10.1021/ma300656u.
- [404] M.A. Jahangir, T.M. Rumi, A. Wahab, M.A. Rahman, Z. Bin Sayed, Poly Lactic Acid (PLA) Fibres: Different Solvent Systems and Their Effect on Fibre Morphology and Diameter, *Am. J. Chem.* 2017 (2017) 177–186. doi:10.5923/j.chemistry.20170706.01.
- [405] Y. Zhu, Y. Cao, J. Pan, Y. Liu, Macro-alignment of electrospun fibers for vascular tissue engineering, *J. Biomed. Mater. Res. - Part B Appl. Biomater.* (2010). doi:10.1002/jbm.b.31544.
- [406] L. Du, H. Xu, Y. Zhang, F. Zou, Electrospinning of polycaprolactone nanofibers with DMF additive: The effect of solution properties on jet perturbation and fiber morphologies, *Fibers Polym.* 17 (2016) 751–759. doi:10.1007/s12221-016-6045-3.
- [407] C.M. Hsu, S. Shivkumar, N,N-dimethylformamide additions to the solution for the electrospinning of poly( $\epsilon$ -caprolactone) nanofibers, *Macromol. Mater. Eng.* 289 (2004) 334–340. doi:10.1002/mame.200300224.
- [408] N. Bölgen, Y.Z. Menceloğlu, K. Acatay, I. Vargel, E. Pişkin, In vitro and in vivo degradation of non-woven materials made of poly( $\epsilon$ -caprolactone) nanofibers prepared by electrospinning under different conditions, *J. Biomater. Sci. Polym. Ed.* 16 (2005) 1537–1555. doi:10.1163/156856205774576655.
- [409] Y.J. Lee, S.J. An, E. Bin Bae, H.J. Gwon, J.S. Park, S.I. Jeong, Y.C. Jeon, S.H. Lee, Y.M. Lim, J.B. Huh, The effect of thickness of resorbable bacterial cellulose membrane on guided bone regeneration, *Materials (Basel).* (2017). doi:10.3390/ma10030320.
- [410] M. Bubalo, Z. Lazic, S. Matic, Z. Tatic, R. Milovic, A. Petkovic-Curcin, D. Djurdjevic, S. Loncarevic, The impact of thickness of resorbable membrane of human origin on the ossification of bone defects: A pathohistologic study, *Vojnosanit. Pregl. Med. Pharm. J.*

- Serbia. (2012). doi:10.2298/vsp1212076b.
- [411] S. Liao, W. Wang, M. Uo, S. Ohkawa, T. Akasaka, K. Tamura, F. Cui, F. Watari, A three-layered nano-carbonated hydroxyapatite/collagen/PLGA composite membrane for guided tissue regeneration, *Biomaterials*. 26 (2005) 7564–7571. doi:10.1016/j.biomaterials.2005.05.050.
- [412] I. Yoshimoto, J.I. Sasaki, R. Tsuboi, S. Yamaguchi, H. Kitagawa, S. Imazato, Development of layered PLGA membranes for periodontal tissue regeneration, *Dent. Mater.* 34 (2018) 538–550. doi:10.1016/j.dental.2017.12.011.
- [413] S.B. Qasim, S. Najeeb, R.M. Delaine-Smith, A. Rawlinson, I. Ur Rehman, Potential of electrospun chitosan fibers as a surface layer in functionally graded GTR membrane for periodontal regeneration, *Dent. Mater.* 33 (2017) 71–83. doi:10.1016/j.dental.2016.10.003.
- [414] J.R. Rodrigues, N.M. Alves, J.F. Mano, Biomimetic polysaccharide/bioactive glass nanoparticles multilayer membranes for guided tissue regeneration, *RSC Adv.* 6 (2016) 75988–75999. doi:10.1039/c6ra14359h.
- [415] D. Anton, H. Burckel, E. Josset, G. Noel, Three-dimensional cell culture: A breakthrough in vivo, *Int. J. Mol. Sci.* 16 (2015) 5517–5527. doi:10.3390/ijms16035517.
- [416] C. Vaquette, J.J. Cooper-White, Increasing electrospun scaffold pore size with tailored collectors for improved cell penetration, *Acta Biomater.* (2011). doi:10.1016/j.actbio.2011.02.036.
- [417] T. Kodama, M. Minabe, T. Hori, Y. Watanabe, The Effect of Various Concentrations of Collagen Barrier on Periodontal Wound Healing, *J. Periodontol.* 60 (1989) 205–210. doi:10.1902/jop.1989.60.4.205.
- [418] P. Bunyaratavej, H.-L. Wang, Collagen Membranes: A Review, *J. Periodontol.* 72 (2001) 215–229. doi:10.1902/jop.2001.72.2.215.
- [419] Q.P. Pham, F.K. Kasper, A.S. Mistry, U. Sharma, A.W. Yasko, J.A. Jansen, A.G. Mikos, Analysis of the osteoinductive capacity and angiogenicity of an in vitro generated extracellular matrix, *J. Biomed. Mater. Res. - Part A.* 88 (2009) 295–303. doi:10.1002/jbm.a.31875.
- [420] P. Lichte, H.C. Pape, T. Pufe, P. Kobbe, H. Fischer, Scaffolds for bone healing: Concepts, materials and evidence, *Injury.* 42 (2011) 569–573. doi:10.1016/j.injury.2011.03.033.

- [421] W.S. Khan, F. Rayan, B.S. Dhinsa, D. Marsh, An osteoconductive, osteoinductive, and osteogenic tissue-engineered product for trauma and orthopaedic surgery: How far are we?, *Stem Cells Int.* 2012 (2012) 1–7. doi:10.1155/2012/236231.
- [422] J. Van Der Stok, K.A. Hartholt, D.A.L. Schoenmakers, J.J.C. Arts, The available evidence on demineralised bone matrix in trauma and orthopaedic surgery, *Bone Jt. Res.* 6 (2017) 423–432. doi:10.1302/2046-3758.67.BJR-2017-0027.R1.
- [423] U. Ranjan Dahiya, S. Mishra, S. Bano, Application of Bone Substitutes and Its Future Prospective in Regenerative Medicine, *Biomater. Tissue Reconstr. or Regen.* (2019). doi:10.5772/intechopen.85092.
- [424] K.S. Beebe, J. Benevenia, B.E. Tuy, C.A. Depaula, R.D. Harten, W.F. Enneking, Effects of a new allograft processing procedure on graft healing in a canine model: A preliminary study, *Clin. Orthop. Relat. Res.* 467 (2009) 273–280. doi:10.1007/s11999-008-0444-8.
- [425] D. Putzer, D.C. Huber, A. Wurm, W. Schmoelz, M. Nogler, The Mechanical Stability of allografts after a cleaning process: Comparison of two preparation Modes, *J. Arthroplasty.* 29 (2014) 1642–1646. doi:10.1016/j.arth.2014.03.028.
- [426] Medical Devices Directive (MDD), (1993). <https://eur-lex.europa.eu/LexUriServ/LexUriServ.do?uri=CELEX:31993L0042:EN:HTML> (accessed January 31, 2020).
- [427] J.P. Vacanti, Beyond Transplantation: Third Annual Samuel Jason Mixter Lecture, *Arch. Surg.* 123 (1988) 545–549. doi:10.1001/archsurg.1988.01400290027003.
- [428] R. Langer, J.P. Vacanti, Tissue engineering, *Science* (80-. ). 260 (1993) 920–926. doi:10.1126/science.8493529.
- [429] Y. Deng, W.Z. Yang, D. Shi, M. Wu, X.L. Xiong, Z.G. Chen, S.C. Wei, Bioinspired and osteopromotive polydopamine nanoparticle-incorporated fibrous membranes for robust bone regeneration, *NPG Asia Mater.* 11 (2019) 1–13. doi:10.1038/s41427-019-0139-5.
- [430] D.P. Bhattarai, L.E. Aguilar, C.H. Park, C.S. Kim, A review on properties of natural and synthetic based electrospun fibrous materials for bone tissue engineering, *Membranes* (Basel). 8 (2018) 1–24. doi:10.3390/membranes8030062.
- [431] S. Taherkhani, F. Moztarzadeh, Fabrication of a poly( $\epsilon$ -caprolactone)/starch nanocomposite scaffold with a solvent-casting/salt-leaching technique for bone tissue

- engineering applications, *J. Appl. Polym. Sci.* 133 (2016) 1–7. doi:10.1002/app.43523.
- [432] H.J. Park, O.J. Lee, M.C. Lee, B.M. Moon, H.W. Ju, J. min Lee, J.H. Kim, D.W. Kim, C.H. Park, Fabrication of 3D porous silk scaffolds by particulate (salt/sucrose) leaching for bone tissue reconstruction, *Int. J. Biol. Macromol.* 78 (2015) 215–223. doi:10.1016/j.ijbiomac.2015.03.064.
- [433] N. Sultana, M. Wang, PHBV/PLLA-based composite scaffolds fabricated using an emulsion freezing/freeze-drying technique for bone tissue engineering: Surface modification and in vitro biological evaluation, *Biofabrication.* 4 (2012) 1–14. doi:10.1088/1758-5082/4/1/015003.
- [434] X. Zhang, Y. Zhang, G. Ma, D. Yang, J. Nie, The effect of the prefrozen process on properties of a chitosan/hydroxyapatite/poly(methyl methacrylate) composite prepared by freeze drying method used for bone tissue engineering, *RSC Adv.* 5 (2015) 79679–79686. doi:10.1039/c5ra14549j.
- [435] S. Bose, S. Vahabzadeh, A. Bandyopadhyay, Bone tissue engineering using 3D printing, *Mater. Today.* 16 (2013) 496–504. doi:10.1016/j.mattod.2013.11.017.
- [436] J.R. Woodard, A.J. Hildore, S.K. Lan, C.J. Park, A.W. Morgan, J.A.C. Eurell, S.G. Clark, M.B. Wheeler, R.D. Jamison, A.J. Wagoner Johnson, The mechanical properties and osteoconductivity of hydroxyapatite bone scaffolds with multi-scale porosity, *Biomaterials.* 28 (2007) 45–54. doi:10.1016/j.biomaterials.2006.08.021.
- [437] B. Dhandayuthapani, Y. Yoshida, T. Maekawa, D.S. Kumar, Polymeric scaffolds in tissue engineering application: A review, *Int. J. Polym. Sci.* 2011 (2011) 1–19. doi:10.1155/2011/290602.
- [438] X. Liu, P.X. Ma, Polymeric scaffolds for bone tissue engineering, *Ann. Biomed. Eng.* 32 (2004) 477–486. doi:10.1023/B:ABME.0000017544.36001.8e.
- [439] T. Le Bao Ha, T. Minh, D. Nguyen, D. Minh, Naturally Derived Biomaterials: Preparation and Application, *Regen. Med. Tissue Eng.* (2013). doi:10.5772/55668.
- [440] E. Barua, A.B. Deoghare, P. Deb, S. Das Lala, Naturally derived biomaterials for development of composite bone scaffold: A review, *IOP Conf. Ser. Mater. Sci. Eng.* 377 (2018) 1–8. doi:10.1088/1757-899X/377/1/012013.
- [441] I.K. Jun, Y.H. Koh, S.H. Lee, H.E. Kim, Novel fabrication of a polymer scaffold with a dense bioactive ceramic coating layer, *J. Mater. Sci. Mater. Med.* 18 (2007) 1537–1542.

doi:10.1007/s10856-007-3057-y.

- [442] J.K. Carrow, A.K. Gaharwar, Bioinspired polymeric nanocomposites for regenerative medicine, *Macromol. Chem. Phys.* 216 (2015) 248–264. doi:10.1002/macp.201400427.
- [443] H. Shin, S. Jo, A.G. Mikos, Modulation of marrow stromal osteoblast adhesion on biomimetic oligo[poly(ethylene glycol) fumarate] hydrogels modified with Arg-Gly-Asp peptides and a poly(ethylene glycol) spacer, *J. Biomed. Mater. Res.* 61 (2002) 169–179. doi:10.1002/jbm.10193.
- [444] A.M. Wojtowicz, A. Shekaran, M.E. Oest, K.M. Dupont, K.L. Templeman, D.W. Hutmacher, R.E. Guldberg, A.J. García, Coating of biomaterial scaffolds with the collagen-mimetic peptide GFOGER for bone defect repair, *Biomaterials.* 31 (2010) 2574–2582. doi:10.1016/j.biomaterials.2009.12.008.
- [445] A.E. Hafeman, B. Li, T. Yoshii, K. Zienkiewicz, J.M. Davidson, S.A. Guelcher, Injectable biodegradable polyurethane scaffolds with release of platelet-derived growth factor for tissue repair and regeneration, *Pharm. Res.* 25 (2008) 2387–2399. doi:10.1007/s11095-008-9618-z.
- [446] W.L. Murphy, M.C. Peters, D.H. Kohn, D.J. Mooney, Sustained release of vascular endothelial growth factor from mineralized poly(lactide-co-glycolide) scaffolds for tissue engineering, *Biomaterials.* 21 (2000) 2521–2527. doi:10.1016/S0142-9612(00)00120-4.
- [447] T. Rozario, D.W. DeSimone, The extracellular matrix in development and morphogenesis: A dynamic view, *Dev. Biol.* 341 (2010) 126–140. doi:10.1016/j.ydbio.2009.10.026.
- [448] U. Hersel, C. Dahmen, H. Kessler, RGD modified polymers: Biomaterials for stimulated cell adhesion and beyond, *Biomaterials.* 24 (2003) 4385–4415. doi:10.1016/S0142-9612(03)00343-0.
- [449] Y. Kang, S. Kim, A. Khademhosseini, Y. Yang, Creation of bony microenvironment with CaP and cell-derived ECM to enhance human bone-marrow MSC behavior and delivery of BMP-2, *Biomaterials.* 32 (2011) 6119–6130. doi:10.1016/j.biomaterials.2011.05.015.
- [450] H.J. Kim, J.-S. Park, Usage of Human Mesenchymal Stem Cells in Cell-based Therapy: Advantages and Disadvantages, *Dev. Reprod.* 21 (2017) 1–10.

doi:10.12717/dr.2017.21.1.001.

- [451] N. Datta, H.L. Holtorf, V.I. Sikavitsas, J.A. Jansen, A.G. Mikos, Effect of bone extracellular matrix synthesized in vitro on the osteoblastic differentiation of marrow stromal cells, *Biomaterials*. 26 (2005) 971–977. doi:10.1016/j.biomaterials.2004.04.001.
- [452] Q.P. Pham, F. Kurtis Kasper, L. Scott Baggett, R.M. Raphael, J.A. Jansen, A.G. Mikos, The influence of an in vitro generated bone-like extracellular matrix on osteoblastic gene expression of marrow stromal cells, *Biomaterials*. 29 (2008) 2729–2739. doi:10.1016/j.biomaterials.2008.02.025.
- [453] R.A. Thibault, L. Scott Baggett, A.G. Mikos, F.K. Kasper, Osteogenic differentiation of mesenchymal stem cells on pregenerated extracellular matrix scaffolds in the absence of osteogenic cell culture supplements, *Tissue Eng. - Part A*. 16 (2010) 431–440. doi:10.1089/ten.tea.2009.0583.
- [454] N. Sadr, B.E. Pippenger, A. Scherberich, D. Wendt, S. Mantero, I. Martin, A. Papadimitropoulos, Enhancing the biological performance of synthetic polymeric materials by decoration with engineered, decellularized extracellular matrix, *Biomaterials*. 33 (2012) 5085–5093. doi:10.1016/j.biomaterials.2012.03.082.
- [455] G. Tour, M. Wendel, I. Tcacencu, Cell-derived matrix enhances osteogenic properties of hydroxyapatite, *Tissue Eng. - Part A*. 17 (2011) 127–137. doi:10.1089/ten.tea.2010.0175.
- [456] H. Lu, T. Hoshiba, N. Kawazoe, G. Chen, Comparison of decellularization techniques for preparation of extracellular matrix scaffolds derived from three-dimensional cell culture, *J. Biomed. Mater. Res. - Part A*. 100 A (2012) 2507–2516. doi:10.1002/jbm.a.34150.
- [457] K. Bush, A.A. Gertzman, Process Development and Manufacturing of Human and Animal Acellular Dermal Matrices, *Ski. Tissue Eng. Regen. Med.* (2016) 83–108. doi:10.1016/B978-0-12-801654-1.00005-X.
- [458] A. Gilpin, Y. Yang, Decellularization Strategies for Regenerative Medicine: From Processing Techniques to Applications, *Biomed Res. Int.* 2017 (2017) 1–13. doi:10.1155/2017/9831534.
- [459] P.M. Crapo, T.W. Gilbert, S.F. Badylak, An overview of tissue and whole organ decellularization processes, *Biomaterials*. 32 (2011) 3233–3243.

doi:10.1016/j.biomaterials.2011.01.057.

- [460] I. Perea-Gil, J.J. Uriarte, C. Prat-Vidal, C. Gálvez-Montón, S. Roura, A. Llucià-Valldeperas, C. Soler-Botija, R. Farré, D. Navajas, A. Bayes-Genis, In vitro comparative study of two decellularization protocols in search of an optimal myocardial scaffold for recellularization, *Am. J. Transl. Res.* 7 (2015) 558–573.
- [461] R.L. Barnhill, T.J. Ryan, Biochemical modulation of angiogenesis in the chorioallantoic membrane of the chick embryo, *J. Invest. Dermatol.* 81 (1983) 485–488. doi:10.1111/1523-1747.ep12522728.
- [462] G. Eke, N. Mangir, N. Hasirci, S. MacNeil, V. Hasirci, Development of a UV crosslinked biodegradable hydrogel containing adipose derived stem cells to promote vascularization for skin wounds and tissue engineering, *Biomaterials.* 129 (2017) 188–198.
- [463] S. Suvarnapathaki, M.A. Nguyen, X. Wu, S.P. Nukavarapu, G. Camci-Unal, Synthesis and characterization of photocrosslinkable hydrogels from bovine skin gelatin, *RSC Adv.* 9 (2019) 13016–13025. doi:10.1039/c9ra00655a.
- [464] D. Singh, A.J. Harding, E. Albadawi, F.M. Boissonade, J.W. Haycock, F. Claeysens, Additive manufactured biodegradable poly(glycerol sebacate methacrylate) nerve guidance conduits, *Acta Biomater.* 78 (2018) 48–63. doi:10.1016/j.actbio.2018.07.055.
- [465] J.W. Nichol, S.T. Koshy, H. Bae, C.M. Hwang, S. Yamanlar, A. Khademhosseini, Cell-laden microengineered gelatin methacrylate hydrogels, *Biomaterials.* 31 (2010) 5536–5544. doi:10.1016/j.biomaterials.2010.03.064.
- [466] D. Mondal, M. Griffith, S.S. Venkatraman, Polycaprolactone-based biomaterials for tissue engineering and drug delivery: Current scenario and challenges, *Int. J. Polym. Mater. Polym. Biomater.* 65 (2016) 255–265. doi:10.1080/00914037.2015.1103241.
- [467] Y. He, C.J. Tuck, E. Prina, S. Kilsby, S.D.R. Christie, S. Edmondson, R.J.M. Hague, F.R.A.J. Rose, R.D. Wildman, A new photocrosslinkable polycaprolactone-based ink for three-dimensional inkjet printing, *J. Biomed. Mater. Res. - Part B Appl. Biomater.* 105 (2017) 1645–1657. doi:10.1002/jbm.b.33699.
- [468] B.J. Green, K.S. Worthington, J.R. Thompson, S.J. Bunn, M. Rethwisch, E.E. Kaalberg, C. Jiao, L.A. Wiley, R.F. Mullins, E.M. Stone, E.H. Sohn, B.A. Tucker, C.A. Guymon, Effect of Molecular Weight and Functionality on Acrylated Poly(caprolactone) for

- Stereolithography and Biomedical Applications, *Biomacromolecules*. 19 (2018) 3682–3692. doi:10.1021/acs.biomac.8b00784.
- [469] C. Mendes-Felipe, J. Oliveira, I. Etxebarria, J.L. Vilas-Vilela, S. Lanceros-Mendez, State-of-the-Art and Future Challenges of UV Curable Polymer-Based Smart Materials for Printing Technologies, *Adv. Mater. Technol.* 4 (2019) 1–16. doi:10.1002/admt.201800618.
- [470] T. Matsuda, M. Mizutani, Liquid acrylate-endcapped biodegradable poly( $\epsilon$ -caprolactone-co-trimethylene carbonate). II. Computer-aided stereolithographic microarchitectural surface photoconstructs, *J. Biomed. Mater. Res.* 62 (2002) 395–403. doi:10.1002/jbm.10295.
- [471] A. Bagheri, J. Jin, Photopolymerization in 3D Printing, *ACS Appl. Polym. Mater.* 1 (2019) 593–611. doi:10.1021/acsapm.8b00165.
- [472] A. Einstein, Berichtigung zu meiner Arbeit: „Eine neue Bestimmung der Moleküldimensionen“, *Ann. Phys.* 339 (1911) 591–592. doi:10.1002/andp.19113390313.
- [473] P.T. Smith, A. Basu, A. Saha, A. Nelson, Chemical modification and printability of shear-thinning hydrogel inks for direct-write 3D printing, *Polymer (Guildf)*. 152 (2018) 42–50. doi:10.1016/j.polymer.2018.01.070.
- [474] Y. Zhang, W. Fan, Z. Ma, C. Wu, W. Fang, G. Liu, Y. Xiao, The effects of pore architecture in silk fibroin scaffolds on the growth and differentiation of mesenchymal stem cells expressing BMP7, *Acta Biomater.* 6 (2010) 3021–3028. doi:10.1016/j.actbio.2010.02.030.
- [475] K. Whang, D.R. Elenz, E.K. Nam, D.C. Tsai, C.H. Thomas, G.W. Nuber, F.H. Glorieux, R. Travers, S.M. Sprague, K.E. Healy, Engineering bone regeneration with bioabsorbable scaffolds with novel microarchitecture, *Tissue Eng.* 5 (1999) 35–51. doi:10.1089/ten.1999.5.35.
- [476] S.F. Hulbert, F.A. Young, R.S. Mathews, J.J. Klawitter, C.D. Talbert, F.H. Stelling, Potential of ceramic materials as permanently implantable skeletal prostheses, *J. Biomed. Mater. Res.* (1970). doi:10.1002/jbm.820040309.
- [477] A. Di Luca, B. Ostrowska, I. Lorenzo-Moldero, A. Lapedda, W. Swieszkowski, C. Van Blitterswijk, L. Moroni, Gradients in pore size enhance the osteogenic differentiation of

- human mesenchymal stromal cells in three-dimensional scaffolds, *Sci. Rep.* 6 (2016) 1–13. doi:10.1038/srep22898.
- [478] H.E. Götz, M. Müller, A. Emmel, U. Holzwarth, R.G. Erben, R. Stangl, Effect of surface finish on the osseointegration of laser-treated titanium alloy implants, *Biomaterials*. 25 (2004) 4057–4064. doi:10.1016/j.biomaterials.2003.11.002.
- [479] J. Kim, S. McBride, A. Donovan, A. Darr, M.H.R. Magno, J.O. Hollinger, Tyrosine-derived polycarbonate scaffolds for bone regeneration in a rabbit radius critical-size defect model, *Biomed. Mater.* 10 (2015). doi:10.1088/1748-6041/10/3/035001.
- [480] H. Lapczynya, L. Galea, S. Wüst, M. Bohner, S. Jerban, A. Sweedy, N. Doebelin, N. van Garderen, S. Hofmann, G. Baroud, R. Müller, B. von Rechenberg, Effect of grain size and microporosity on the in vivo behaviour of  $\beta$ -tricalcium phosphate scaffolds, *Eur. Cells Mater.* 28 (2014) 299–319. doi:10.22203/eCM.v028a21.
- [481] S.K. Lan Levensgood, S.J. Polak, M.B. Wheeler, A.J. Maki, S.G. Clark, R.D. Jamison, A.J. Wagoner Johnson, Multiscale osteointegration as a new paradigm for the design of calcium phosphate scaffolds for bone regeneration, *Biomaterials*. 31 (2010) 3552–3563. doi:10.1016/j.biomaterials.2010.01.052.
- [482] L.E. Rustom, T. Boudou, B.W. Nemke, Y. Lu, D.J. Hoelzle, M.D. Markel, C. Picart, A.J. Wagoner Johnson, Multiscale Porosity Directs Bone Regeneration in Biphasic Calcium Phosphate Scaffolds, *ACS Biomater. Sci. Eng.* 3 (2017) 2768–2778. doi:10.1021/acsbomaterials.6b00632.
- [483] M. Ellis, M. Jarman-Smith, J.B. Chaudhuri, Bioreactor systems for tissue engineering: A four-dimensional challenge, *Bioreact. Tissue Eng. Princ. Des. Oper.* (2005) 1–18. doi:10.1007/1-4020-3741-4\_1.
- [484] H. Yuan, K. Kurashina, J.D. De Bruijn, Y. Li, K. De Groot, X. Zhang, A preliminary study on osteoinduction of two kinds of calcium phosphate ceramics, *Biomaterials*. 20 (1999) 1799–1806. doi:10.1016/S0142-9612(99)00075-7.
- [485] J. Kim, M.H.R. Magno, H. Waters, B.A. Doll, S. McBride, P. Alvarez, A. Darr, A. Vasanji, J. Kohn, J.O. Hollinger, Bone regeneration in a rabbit critical-sized calvarial model using tyrosine-derived polycarbonate scaffolds, *Tissue Eng. - Part A*. 18 (2012) 1132–1139. doi:10.1089/ten.tea.2011.0582.
- [486] Y. Kato, A. Boskey, L. Spevak, M. Dallas, M. Hori, L.F. Bonewald, Establishment of an

- osteoid preosteocyte-like cell MLO-A5 that spontaneously mineralizes in culture, *J. Bone Miner. Res.* 16 (2001) 1622–1633. doi:10.1359/jbmr.2001.16.9.1622.
- [487] S. Akbari-Birgani, M.T. Birgani, H. Ansari, Generation of Organs Based on Decellularized Extracellular Matrix Scaffolds, *Stem Cells Biomater. Regen. Med.* (2019) 57–72. doi:10.1016/b978-0-12-812258-7.00005-8.
- [488] S.F. Badylak, D.O. Freytes, T.W. Gilbert, Reprint of: Extracellular matrix as a biological scaffold material: Structure and function, *Acta Biomater.* 23 (2015) S17–S26. doi:10.1016/j.actbio.2015.07.016.
- [489] L. Zilic, S.P. Wilshaw, J.W. Haycock, Decellularisation and histological characterisation of porcine peripheral nerves, *Biotechnol. Bioeng.* 113 (2016) 2041–2053. doi:10.1002/bit.25964.
- [490] C. Karlsson, K. Emanuelsson, F. Wessberg, K. Kajic, M.Z. Axell, P.S. Eriksson, A. Lindahl, J. Hyllner, R. Strehl, Human embryonic stem cell-derived mesenchymal progenitors- Potential in regenerative medicine, *Stem Cell Res.* 3 (2009) 39–50. doi:10.1016/j.scr.2009.05.002.
- [491] G.M. De Peppo, S. Svensson, M. Lennerås, J. Synnergren, J. Stenberg, R. Strehl, J. Hyllner, P. Thomsen, C. Karlsson, Human embryonic mesodermal progenitors highly resemble human mesenchymal stem cells and display high potential for tissue engineering applications, *Tissue Eng. - Part A.* 16 (2010) 2161–2182. doi:10.1089/ten.tea.2009.0629.
- [492] L.A. Hidalgo-Bastida, S.H. Cartmell, Mesenchymal stem cells, osteoblasts and extracellular matrix proteins: Enhancing cell adhesion and differentiation for bone tissue engineering, *Tissue Eng. - Part B Rev.* 16 (2010) 405–412. doi:10.1089/ten.teb.2009.0714.
- [493] A. Shekaran, A.J. García, Extracellular matrix-mimetic adhesive biomaterials for bone repair, *J. Biomed. Mater. Res. - Part A.* 96 A (2011) 261–272. doi:10.1002/jbm.a.32979.
- [494] H. Shin, K. Zygourakis, M.C. Farach-Carson, M.J. Yaszemski, A.G. Mikos, Attachment, proliferation, and migration of marrow stromal osteoblasts cultured on biomimetic hydrogels modified with an osteopontin-derived peptide, *Biomaterials.* 25 (2004) 895–906. doi:10.1016/S0142-9612(03)00602-1.
- [495] M. Baroncelli, B.C.J. Van Der Eerden, S. Chatterji, E. Rull Trinidad, Y.Y. Kan, M. Koedam,

- I.A.J. Van Hengel, R.D.A.M. Alves, L.E. Fratila-Apachitei, J.A.A. Demmers, J. Van De Peppel, J.P.T.M. Van Leeuwen, Human Osteoblast-Derived Extracellular Matrix with High Homology to Bone Proteome Is Osteopromotive, *Tissue Eng. - Part A*. 24 (2018) 1377–1389. doi:10.1089/ten.tea.2017.0448.
- [496] Y. Chen, K. Lee, N. Kawazoe, Y. Yang, G. Chen, PLGA-collagen-ECM hybrid scaffolds functionalized with biomimetic extracellular matrices secreted by mesenchymal stem cells during stepwise osteogenesis-: Co-adipogenesis, *J. Mater. Chem. B*. 7 (2019) 7195–7206. doi:10.1039/c9tb01959f.
- [497] Y. Deng, S. Wei, L. Yang, W. Yang, M.S. Dargusch, Z.G. Chen, A Novel Hydrogel Surface Grafted With Dual Functional Peptides for Sustaining Long-Term Self-Renewal of Human Induced Pluripotent Stem Cells and Manipulating Their Osteoblastic Maturation, *Adv. Funct. Mater.* 28 (2018) 1–17. doi:10.1002/adfm.201705546.
- [498] S. Lyu, C. Huang, H. Yang, X. Zhang, Electrospun fibers as a scaffolding platform for bone tissue repair, *J. Orthop. Res.* 31 (2013) 1382–1389. doi:10.1002/jor.22367.
- [499] Q. Yao, J.G.L. Cosme, T. Xu, J.M. Miszuk, P.H.S. Picciani, H. Fong, H. Sun, Three dimensional electrospun PCL/PLA blend nanofibrous scaffolds with significantly improved stem cells osteogenic differentiation and cranial bone formation, *Biomaterials*. 115 (2017) 115–127. doi:10.1016/j.biomaterials.2016.11.018.
- [500] S. Dikici, A.J. Bullock, M. Yar, F. Claeysens, S. MacNeil, 2-deoxy-d-ribose (2dDR) upregulates vascular endothelial growth factor (VEGF) and stimulates angiogenesis, *Microvasc. Res.* 131 (2020) 104035. doi:10.1016/j.mvr.2020.104035.
- [501] T.I. Valdes, D. Kreutzer, F. Moussy, The chick chorioallantoic membrane as a novel in vivo model for the testing of biomaterials, *J. Biomed. Mater. Res.* 62 (2002) 273–282. doi:10.1002/jbm.10152.
- [502] M.I. Santos, R.L. Reis, Vascularization in bone tissue engineering: Physiology, current strategies, major hurdles and future challenges, *Macromol. Biosci.* 10 (2010) 12–27. doi:10.1002/mabi.200900107.
- [503] M. Frohlich, W. Grayson, L. Wan, D. Marolt, M. Drobic, G. Vunjak- Novakovic, Tissue Engineered Bone Grafts: Biological Requirements, Tissue Culture and Clinical Relevance, *Curr. Stem Cell Res. Ther.* 3 (2008) 254–264. doi:10.2174/157488808786733962.

- [504] W. Wang, K.W.K. Yeung, Bone grafts and biomaterials substitutes for bone defect repair: A review, *Bioact. Mater.* 2 (2017) 224–247. doi:10.1016/j.bioactmat.2017.05.007.
- [505] S. Shafaat, N. Mangir, S.R. Regureos, C.R. Chapple, S. MacNeil, Demonstration of improved tissue integration and angiogenesis with an elastic, estradiol releasing polyurethane material designed for use in pelvic floor repair, *Neurourol. Urodyn.* 37 (2018) 716–725. doi:10.1002/nau.23510.
- [506] S. Dikici, F. Claeysens, S. MacNeil, Decellularised baby spinach leaves and their potential use in tissue engineering applications: Studying and promoting neovascularisation, *J. Biomater. Appl.* 34 (2019) 546–559. doi:10.1177/0885328219863115.
- [507] W. Zhang, C. Feng, G. Yang, G. Li, X. Ding, S. Wang, Y. Dou, Z. Zhang, J. Chang, C. Wu, X. Jiang, 3D-printed scaffolds with synergistic effect of hollow-pipe structure and bioactive ions for vascularized bone regeneration, *Biomaterials.* 135 (2017) 85–95. doi:10.1016/j.biomaterials.2017.05.005.
- [508] H. Ma, C. Feng, J. Chang, C. Wu, 3D-printed bioceramic scaffolds: From bone tissue engineering to tumor therapy, *Acta Biomater.* 79 (2018) 37–59. doi:10.1016/j.actbio.2018.08.026.
- [509] D. He, C. Zhuang, C. Chen, S. Xu, X. Yang, C. Yao, J. Ye, C. Gao, Z. Gou, Rational Design and Fabrication of Porous Calcium-Magnesium Silicate Constructs That Enhance Angiogenesis and Improve Orbital Implantation, *ACS Biomater. Sci. Eng.* 2 (2016) 1519–1527. doi:10.1021/acsbiomaterials.6b00282.
- [510] A. Bandyopadhyay, S. Bernard, W. Xue, S. Böse, Calcium phosphate-based resorbable ceramics: Influence of MgO, ZnO, and SiO<sub>2</sub> dopants, *J. Am. Ceram. Soc.* 89 (2006) 2675–2688. doi:10.1111/j.1551-2916.2006.01207.x.
- [511] J.M. Meseguer-Dueñas, J. Más-Estellés, I. Castilla-Cortázar, J.L. Escobar Ivirico, A. Vidaurre, Alkaline degradation study of linear and network poly( $\epsilon$ -caprolactone), *J. Mater. Sci. Mater. Med.* (2011). doi:10.1007/s10856-010-4182-6.
- [512] I. Castilla-Cortázar, J. Más-Estellés, J.M. Meseguer-Dueñas, J.L. Escobar Ivirico, B. Marí, A. Vidaurre, Hydrolytic and enzymatic degradation of a poly( $\epsilon$ -caprolactone) network, *Polym. Degrad. Stab.* (2012). doi:10.1016/j.polymdegradstab.2012.05.038.
- [513] M.A. Borkin, A.A. Vo, Z. Bylinskii, P. Isola, S. Sunkavalli, A. Oliva, H. Pfister, What makes

a visualization memorable, IEEE Trans. Vis. Comput. Graph. (2013). doi:10.1109/TVCG.2013.234.

[514] M.C. Brunet, H.T. Khuong, Entrapped ulnar nerve by flexor carpi ulnaris tendon: Case illustration, J. Neurosurg. (2019). doi:10.3171/2018.5.JNS172840.

[515] C. Mignot, Color (and 3D) for Scanning Electron Microscopy, Micros. Today. (2018). doi:10.1017/s1551929518000482.

[516] K.S. Sim, C.P. Tso, H.Y. Ting, Canny optimization technique for electron microscope image colourization, J. Microsc. (2008). doi:10.1111/j.1365-2818.2008.02103.x.

[517] K.S. Sim, H.Y. Ting, M.A. Lai, C.P. Tso, Improvement to the scanning electron microscope image colourization by adaptive tuning, J. Microsc. (2009). doi:10.1111/j.1365-2818.2009.03167.x.